Influence of initial soil state and installation parameters on the lateral behaviour of vibratory-driven monopiles in sand

By

Brice Dijksman

in partial fulfilment of the requirements for the degree of

Master of Science

in Civil Engineering

at the Delft University of Technology,

to be defended publicly on Thursday May 4, 2023 at 10:45 AM.

Supervisor:	Dr. A. P. Da Silva	Deltares
Thesis committee:	Dr. F. Pisanò,	TU Delft
	Dr. A. Tsouvalas,	TU Delft
	Ir. M. Post,	Deltares

An electronic version of this thesis is available at http://repository.tudelft.nl/.

Preface

This document is the product of my thesis, the final step of the study program for the obtention of a master's degree in the geotechnical track of Civil Engineering at the Technical University of Delft. The research carried out during this thesis has been executed in cooperation with Stichting Deltares in their Delft office under supervision of Dr. Anderson Peccin da Silva and Ir. Mark Post.

I would like to thank the people who have aided and supported me throughout this thesis, and whose help contributed greatly to this resulting report. Firstly, I would like to thank the members of my assessment committee.

I am extremely grateful to Dr. Anderson Peccin da Silva as well as Ir. Mark Post for their daily guidance, advice, and encouragement while I was working at the Deltares premises. I also thank them for giving me the opportunity to participate in the SIMOX laboratory experiments.

I am deeply thankful to Dr. Federico Pisanò for his detailed feedback and supervision as well as Dr. Apostolos Tsouvalas for his helpful exterior point of view.

Furthermore, I would like to offer my sincere thanks to Dr. Ahmed Elkadi from Deltares for helping me join such a pleasant working environment and assisting me with administrative matters at the company and Mario Martinelli for his help in processing the data.

Last but not least, I would like to give special thanks to my family, friends and partner Anran for supporting me along my journey to a master's degree.

Abstract

To support offshore wind turbines (OWT), monopiles are currently the most frequently used foundation method. These monopiles are open-ended steel tubes with a diameter of 5 - 12 m, which are most often installed in the seabed by means of hydraulic impact hammering usually mounted on a specialised ship. This method is produces high noise levels and releases shockwaves into the water, which can damage the sea life's hearing or even outright kill them. Additional measures can be taken to reduce noise emissions and adhere to strict environmental regulations written for marine biology protection, but they are costly and slow down projects significantly. There are other installation methods which have the potential to be more silent but are not well understood yet from a noise generation, driveability, and lateral behaviour point of view. These are aspects that will be investigated within the SIMOX Joint Industry Project (JIP). One of these methods is vibratory installation.

A monopile used as a foundation for an OWT will experience a multitude of loads during its service life, the most important of which are the lateral loads. While the behaviour of impact hammered piles under lateral loading has been researched extensively, the behaviour of vibratory driven piles is still relatively unknown. The influence of different parameters used during installation (frequency, penetration speed) and other conditions (wall thickness and soil conditions) on that behaviour must be understood to be able to accurately predict how a vibrated monopile will react to both cyclic and monotonic loading.

The present research explores the behaviour of monopiles under lateral loading and the impact different installation parameters have on it. To achieve this, a laboratory testing campaign was carried out with model piles. The purpose of these tests is to produce qualitative results to be used in following field-testing campaigns within SIMOX. Piles were installed with differing installation parameters in sand beds with different density. These piles were then subjected to initial monotonic loading, followed by cyclic loading, and then monotonic loading again. The data obtained during the experiments was then interpreted and analysed. By comparing the results as well as measurements taken during and after installation, conclusions are made concerning installation parameters and other factors that may play a role on the lateral behaviour of monopiles.

The interpretation focused mainly on pile head displacement during initial lateral loading depending on penetration speed and frequency. The loading tests have shown that impact hammered piles underwent lower displacements than vibrated piles after being loaded laterally. When solely considering vibrated piles, piles with a larger wall thickness showed lower displacements in general than thin-walled piles.

Frequency and penetration speed were found to play a role in the lateral behaviour of monopiles. In the experiments considered for this thesis, it seemed in dense sand crane-controlled piles showed lower displacements than free-hanging piles. In medium dense sand, lower penetration speed led to lower displacement during loading, but more research is needed on this topic to be able to formulate clear conclusions on the exact role of each installation parameters. The experiments also show an interesting phenomenon regarding measured soil elevation that might link compaction around the monopile to lower lateral displacements. The difference in elevation before and after installation seemed to correlate with

lateral displacements. In general, piles with larger compaction around the pile displaced less during initial loading.

In conclusion, this paper provides a range of observations regarding the impact of installation parameters and other conditions such as wall thickness and sand density on the behaviour of monopiles under lateral loading, as well as offering a comparison with impact hammered piles. Recommendations and suggestions are given for further research and for the field testing experiments, so that the analysis made here may be used to predict the lateral behaviour of vibrated monopiles more accurately.

Table of contents

Table of figures

1. Introduction

As demand for renewable energy increases, the amount of wind farms is set to rise in the near future. However, space on land in Europe is becoming increasingly limited, and projects often face strong resistance from the local population. A solution to this is constructing offshore wind farms.

Most offshore wind farms are currently installed in shallow and moderate water depths, up to 35 m. For these depths, monopiles are considered to be the most suitable foundation method for offshore wind turbine generators (WTG) and represented 75% of all installed foundations in Europe in 2018 (Wind Europe 2018). To install these monopiles, one commonly makes use of a hydraulic hammer driving the pile into the soil by means of several thousand hammer blows. The main problem with this method is the noise emission, which is high enough to kill or permanently injure marine life. To protect the wildlife, many countries have drafted restrictive legislation that regulates the maximum noise level measured at several points away from the installation location.

In order to comply with legislation and keep noise levels low, several noise mitigation measures must be taken during installation. These additional measures complicate the projects significantly with cost increases as a result. Despite all the efforts and measures taken during installation of monopiles, it is still difficult to comply with the prescribed noise emission limits.

As an alternative to the more standard impact hammering installation, monopiles may also be installed by vibratory driving. This driving method makes use of a hydraulic hammer vibrating the monopile in the vertical direction while lowering the pile into the sand. This process has considerable advantages when it comes to noise emission, as levels are considerably reduces compared to impact driving (Koschinksi & Lüdemann, 2013). However, before this method can be applied to projects in practice, the lateral behaviour of piles installed with a vibratory hammer must be understood in more detail as it governs the design and behaviour of monopiles in offshore wind applications (Byrne et al., 2020a). While offshore impact hammering is well-researched and understood, insight and experience are lacking with respect to the effect vibratory installation has on lateral behaviour of the monopile and the consequences of varying certain installation parameters. Only a handful of studies have been made regarding this (Achmus et al., 2020), (Labenski & Moormann, 2019), which will be discussed in chapter 2.

The Technical University of Delft and the Dutch research institute Deltares conceived an initiative involving several large companies from the offshore wind industry, i.e. the SIMOX project (Sustainable Installation of XXL Monopiles), to further investigate the behaviour of alternative installation methods, including vibratory-driven piles. As part of the SIMOX project, the Dutch research institute Deltares is performing a set of laboratory experiments in their Water-Soil Flume. The main goal of these experiments is to generate insights into the behaviour of vibratory driven (scaled) monopiles into sand compared to impact hammered piles. These laboratory experiments are a stepping stone towards large scale tests on monopiles in the field within the SIMOX project. The data generated by the laboratory experiments forms the basis for this thesis. This thesis report presents the generated data and the insights gained on the behaviour of vibrated piles compared to impact hammered ones, and what role certain installation parameters play in the lateral behaviour of vibrated monopiles as well as what the influence of the initial soil state is (dense and medium dense sand).

This thesis has been divided into eight chapters. The outline of the document is as follows. After this introductory chapter, the main question and problem statement will be presented. Thirdly, an overview of relevant works on the topic of vibratory installation of monopiles will be given. After that, the experiments carried out in the framework of this thesis will be explained and the followed programme will be detailed. Next, corrections applied to the data and a comparative finite element model are outlined. Following this, the results of the experiments will be presented in three sub-sections, each focusing on a different part of the experiments. In the next chapter, those results will be discussed and interpreted. Finally, the eight chapter summarises the conclusions made from the experiment results and gives recommendations for follow-up research.

2. Objective

This chapter contains the problem statement, the main research question as well as the sub-questions. Additionally, the objective of the thesis and the associated approach will also be explained.

2.1 Problem statement

Vibratory installation is a promising alternative to impact hammering for the installation of offshore monopiles, but the knowledge about the method and the effect of its installation on the lateral behaviour during the operational lifetime are not yet developed enough to be used in practice. There are very few comparisons with the more conventional impact hammering installation method, which is the standard installation method. The knowledge gaps which this thesis will aim to fill cover the lateral behaviour of monopiles in sand.

2.2 Research question and sub-questions

The main research question as well as the corresponding sub-questions for the thesis are as follows:

What is the influence of initial soil state and of installation parameters for vibratory installation on the lateral behaviour of monopiles in sand?

The main research question can be divided in the following sub-questions.

- What is the influence of installation parameters frequency, penetration speed and crane load on lateral stiffness and bearing capacity?
- What is the influence of initial soil density on lateral stiffness and bearing capacity?
- What is the relation between soil measurements, such as CPT and horizontal stress measurements, with lateral stiffness and bearing capacity?
- Which combination of installation parameters should be chosen to obtain the highest lateral bearing capacity?
- What kind of further research is needed to get a better understanding of the relation between installation parameters and lateral bearing capacity?

2.3 Objective and approach

This thesis aims to answer the research questions by analysing the data gathered during a series of scaled laboratory experiments within the context of the SIMOX project. To reach the objective, the following approach is taken:

1. Literature review.
2. Description of the scaled experiments.
3. Explanation of the necessary corrections applied to the data by the means of a finite element model.
4. Presentation of the corrected experiment results and associated measurements.

5. Interpretation and analysis of the results.
6. Main findings, conclusions, and recommendations for future research.

3. Literature study

This chapter will discuss the existing literature relevant to the thesis and the benefits the latter brings compared to existing research. Existing literature with different type of tests will be presented, namely large-scale field tests, reduced scale field tests as well as laboratory tests, and numerical studies. A selection of existing models will be explained, followed by the main observations and the difference between existing literature and the current research.

Section 3.1 describes relevant laboratory tests conducted on this topic in recent years. Section 3.2 showcases several field tests as well as their findings. After that, section 3.3 explains existing models and numerical studies. Section 3.4 sums up the main observations from all previously mentioned papers along different topics. Finally, section 3.5 highlights the difference between existing literature and the current research.

3.1 Laboratory tests

3.1.1 Labenski & Moormann (2019)

In the research of Labenski & Moormann (2019), a scaled model test is conducted with vibratory driven monopiles in dense sand. After installation, the lateral loading behaviour is investigated with a lateral load test and interpreted through a load-displacement curve. This experimental approach is then compared with the load-displacement curve obtained through an analytical model. They then propose a modified numerical approach to predict the lateral loading behaviour of vibratory driven monopiles. The main target of this research was to investigate the influence of installation parameters on the lateral load bearing capacity of vibrated monopiles. The detailed report of the experiments is in a document written in German (Labenski & Moormann, 2020).

A glass fibre reinforced pile was used to simulate the flexural rigidity of real piles. It had a diameter of 0.208m, a wall thickness of 3.2 mm and a length of 2 m. Its L/D ratio (ratio of embedded length to diameter) was 4.2 which is a typical figure for monopiles used in practice (Labenski & Moormann, 2019). The pile was installed in a concrete container with a diameter of 2 m. A sketch of the test setup is provided in Figure 3.1.

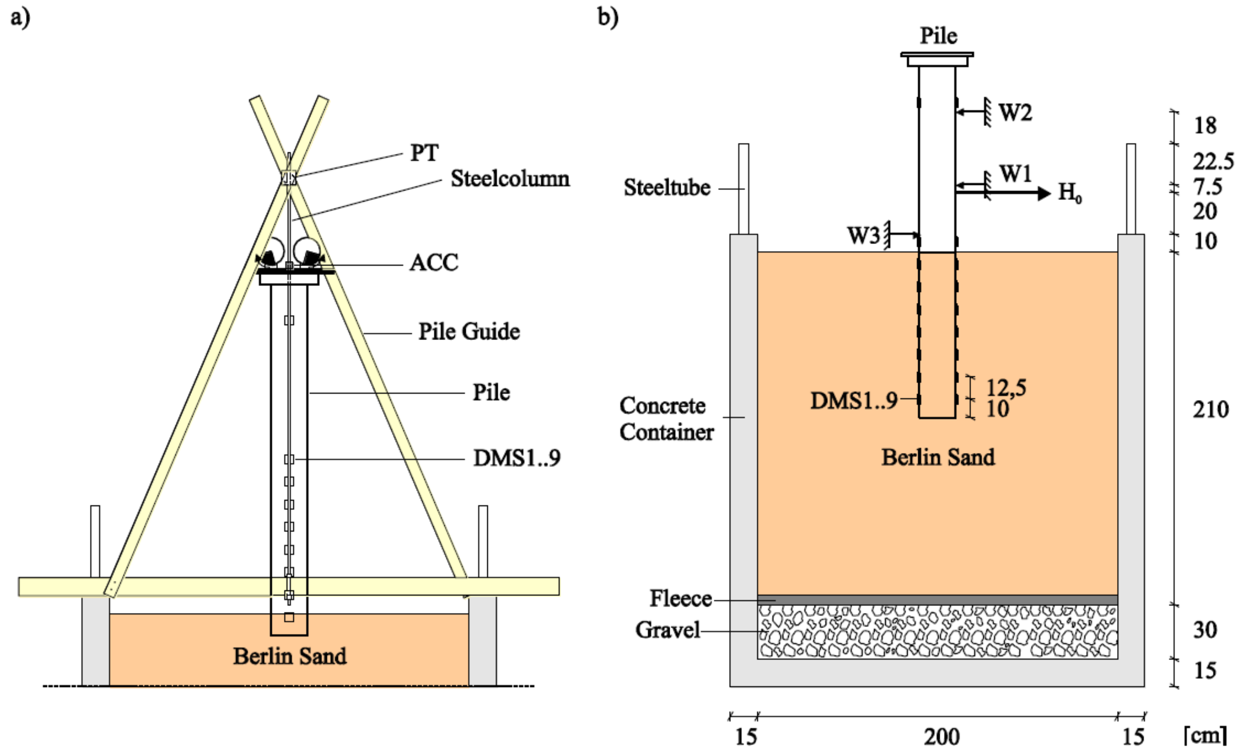

Figure 3.1: Model setup for pile installation (a) and for load test (b) (Labenski & Moormann, 2019)

During the scale model tests, multiple installation parameters were varied. The frequency, the static moment of the vibro-hammer and the sand density were all varied. The piles were first vibrated to their embedment depth with a frequency of up to 25 Hz, after which they were laterally loaded with a tension force. During the scale model tests, 33 vibratory driven piles were studied and 2 jacked piles for comparison.

According to Rodger (1980), there are two vibration modes that can occur during vibratory installation of monopiles: cavitational and non-cavitational. Figure 3.2 shows a simplification of the vibration process during both modes.

Two representative test results are presented, one where cavitational vibration occurred and one where non-cavitational vibration happened.

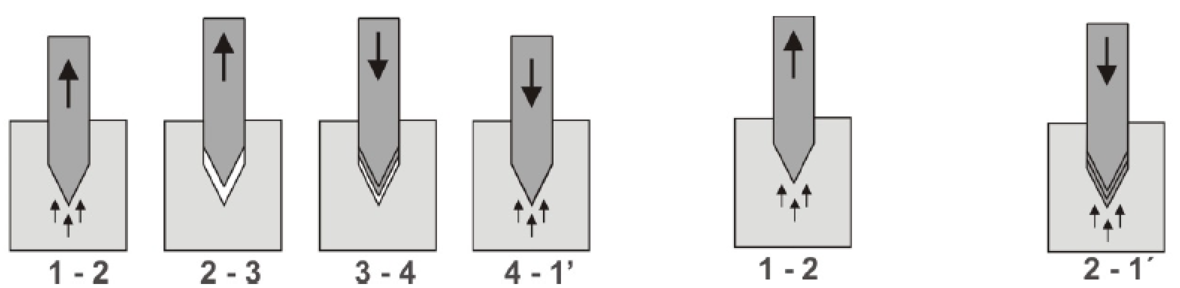

Figure 3.2: Schematisation of cavitational (left) and non-cavitational (right) vibration modes (Hoffmann et al., 2020)

The variation of installation parameters on the pile installation reveals that the pile installed in cavitational mode had a longer installation time than the non-cavitational one. The piles differed in their vertical displacements during vibrating, and Labenski & Moormann (2019) conclude that the difference in upward movement defines whether cavitational or non-cavitational mode occurs.

The results of the lateral load test showed that the pile installed in the cavitational vibration mode has a much larger lateral stiffness than the one installed with a non-cavitational vibration mode.

Labenski & Moormann conclude that load bearing behaviour is dependent on the vibration mode during installation. They also refer another paper and conclude that the standard method to calculate the load displacement curves does not fit the experimental data (Labenski & Moormann, 2018).

3.1.2 Hoffmann et al. (2020)

The conference paper by Hoffmann, Moormann, et al. (2020) describes an experimental study on the behaviour of vibrated monopiles in dense sand under cyclic lateral loading. The piles are vibrated in two different vibration modes, cavitational and non-cavitational. The results are also compared with an impact hammered pile to be able to relate them to a common monopile installation.

The same pile of diameter 0.208 m and 2 m length was used for all the tests. This gives a L/D ratio of 4.2 which is a representative number for monopiles. Its wall thickness was 3.2 mm. Fifty tests have been carried out with vibratory installation and two tests with impact driving.

Pore water pressure and total soil stress were measured during driving. During the lateral load tests, strain gauges measured the bending moment of the pile. Additionally, the pile head displacement was also measured. Load displacement curves and horizontal stresses are shown in Figure 3.3.

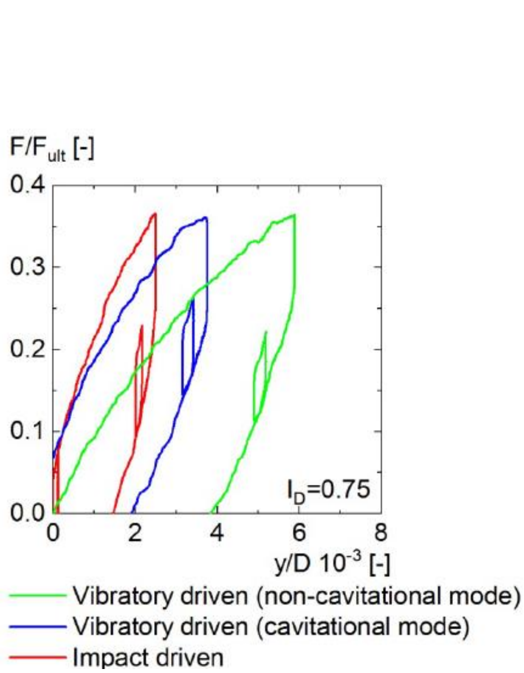

Figure 3.3: Load displacement curves for three installation modes (left) and horizontal stress ration over pile penetration depth (right) (Hoffmann et al., 2020)

Cyclic behaviour is also measured and shown in Figure 3.4. Interesting to note is that displacements as a result of cyclic loading converge after 100 cycles and are virtually similar at 1000 cycles, irrespective of the installation method.

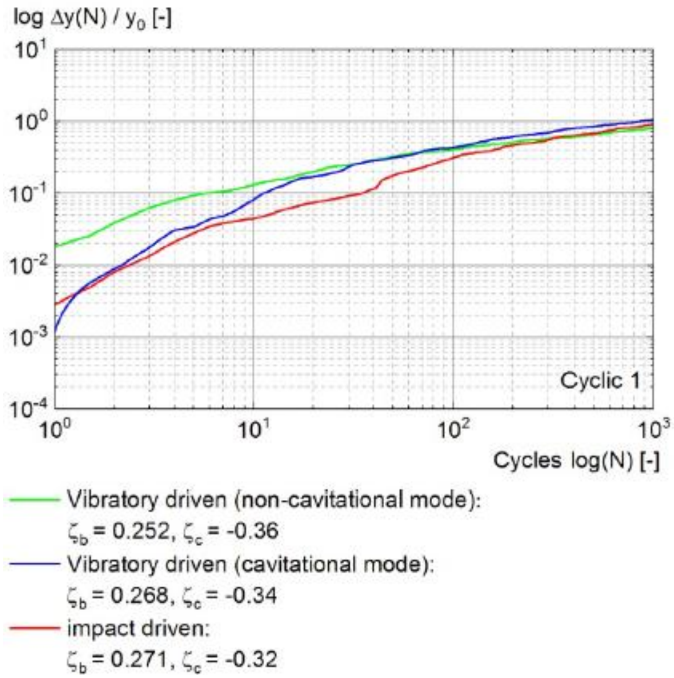

Figure 3.4: Accumulated lateral displacements under cyclic loading (Hoffmann et al., 2020)

As far as the observed horizontal stresses are concerned, the highest stresses were measured for piles installed with impact driving, then in cavitational mode, and then in non-cavitational vibration mode. The results of the lateral load tests show that the lateral stiffness exhibits the same classification order: highest is the impact pile, then the cavitational one, followed by the non-cavitational pile. This observation might be an indication that the lateral bearing behaviour of piles is related to the horizontal stresses in the soil around the pile after installation.

It is concluded that the installation method and differences in the same vibration method (cavitational or non-cavitational) influence the lateral capacity of the monopiles (Hoffmann et al., 2020).

3.1.3 Wang, Wang et al. (2021)

Wang, Wang, et al. (2021) carried out centrifuge experiments on slender large diameter piles, to compare the cyclic and monotonic lateral loading behaviour with slender small diameter piles. The lateral behaviours of the different piles can be compared, and the effect of diameter is assessed.

Two piles with different length to diameter ratios (L/D) are experimented upon. Both piles have a length of 60 m and diameters of 4 m and 6 m as well as wall thickness of 0.2 m in prototype scale. As this test is in a centrifuge, scaling laws are applied, and the actual pile dimensions are smaller. The centrifuge was subjected to an acceleration of 100 g. As a result, the model dimensions were 100 times smaller than the prototype. This means the piles had a length of 600 mm, diameters of 40 and 60 mm and wall thickness of 2 mm.

The piles were pre-fixed to the centrifuge boxed, after which it was filled with medium-dense sand. The piles were subjected to a loading eccentricity of 10 m above the surface. The monotonic loading was performed first, after which the piles were replaced with an identical set of piles. These were then subjected to cyclic loading.

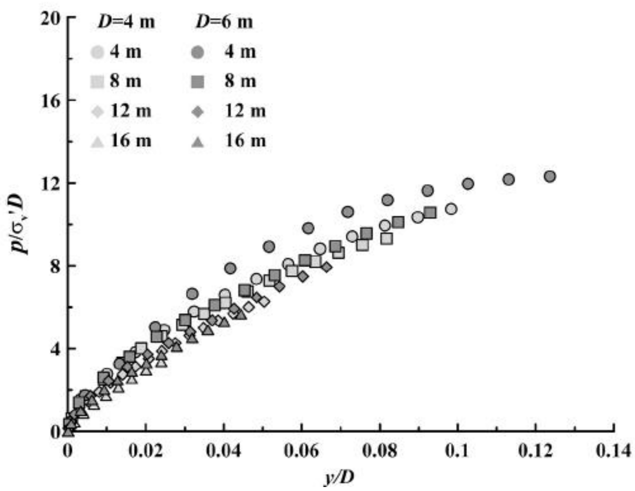

*Figure 3.5: Initial stiffness for piles of 4 and 6 m diameter (*Wang, Wang et al, 2021)

With the results from these experiments, Wang, Wang, et al. (2021) conclude that the effect of diameter on monotonic lateral load bearing is minimal as long as the relative pile-soil stiffness is the same, i.e. the lateral behaviour and failure mechanism of the pile is the same for rigid piles. The effect of diameter on cyclic behaviour seems limited as well.

3.1.4 Fan et al. (2021)

A centrifuge study is described in one paper by Fan et al. (2021a) which compares the lateral loading behaviour of monopiles installed with different methods, without stopping the centrifuge between installation and loading. This indicates that the installation induced effects in the centrifuge are not lost upon stopping the apparatus, and thus their effect on the stiffness of monopiles can be compared. This was then done with a numerical analysis in two companion papers (Fan et al., 2021c, 2021b).

Three tests were carried out with a single pile, two jacking tests and one impact hammering test. The model pile used in this test has a diameter of 50 mm, a thickness of 1 mm and a length of 500 mm giving it a L/D ratio of 10. The centrifuge tests are carried out at 100 g, which represents a prototype monopile with a diameter of 5 m and a wall thickness of 0.1 m (100 times larger than the model).

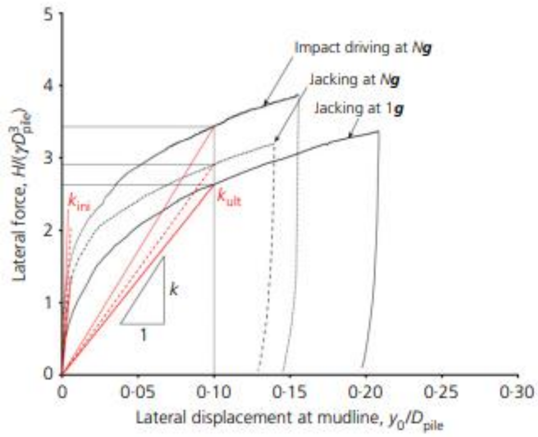

*Figure 3.6: Initial stiffness and load displacement of installed piles (*Fan et al., 2021a)

Results show that the stiffness of a monopile under monotonic lateral loading is significantly influenced by installation, and the impact of that on soil density is particularly noteworthy. The results of the centrifuge test are discussed, and a numerical model is built and addressed in the companion papers (Fan et al., 2021b, 2021c), which will be addressed on page 38.

3.1.5 Remspecher et al. (2019)

In an investigation by Remspecher et al. (2019), the changes in soil density around a monopile and the installation effects of vibrated piles were studied using an experimental model and image recording. The test is a symmetrical half-model. A halved pile was installed inside a frictionless glass wall container in such a way that the cut sections are against the glass. Zones with a density change during pile installation were then identified using particle image velocimetry (PIV).

One steel pile was installed, with an outer diameter of 20 cm, a wall thickness of 4 mm and achieving a penetration depth of 0.87 m. The pile was vibrated at a constant frequency of 23 Hz. During penetration, the sand movement was recorded from the other side of the glass panel.

The results of the PIV analysis are shown in Figure 3.7.

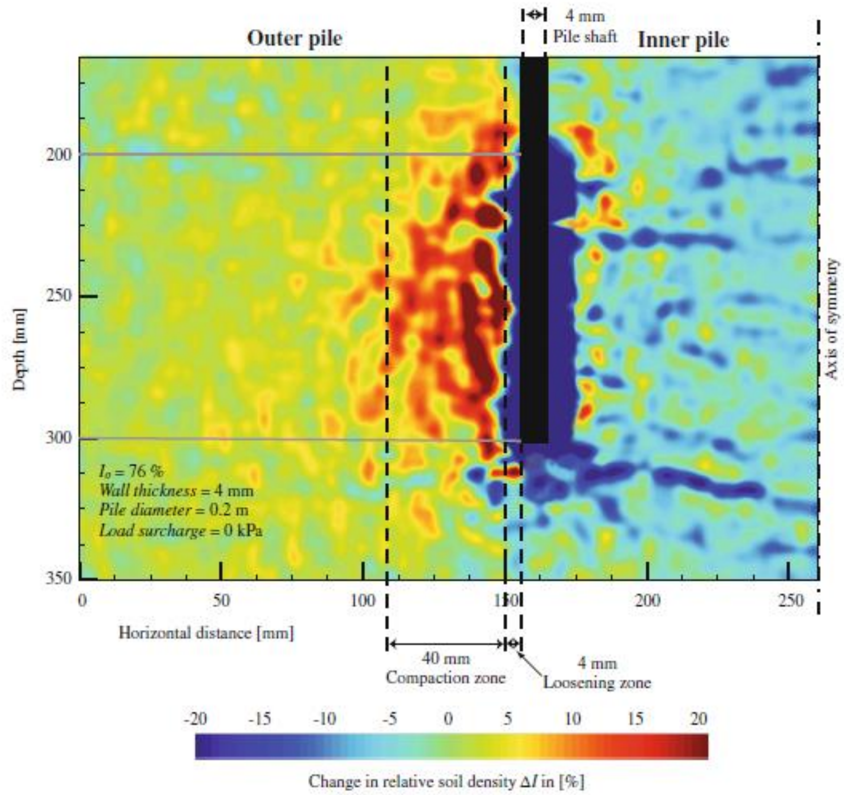

Figure 3.7: Plot showing the change in relative soil density around the pile wall with regards to the density at -0.2 m
(Remspecher et al., 2019)

These results show that during vibration installation of piles, there are clear loosening and compaction zones. Outside of the pile and nearest to the pile wall, there is a thin strip of loosening. Moving further away, we encounter a wider compaction zone. Inside of the pile. The soil becomes looser in general with the zone closes to the pile wall more strongly affected.

3.1.6 Stein et al. (2020)

The study by Stein et al. (2020), carried out as a part of the German Zyklamp project, was a large-scale model test in which the influence of installation method on the lateral bearing capacity of monopiles under cyclic and monotonic loading was investigated. Piles installed with vibratory methods were compared to impact hammered piles to understand whether they have a larger, smaller, or comparable lateral bearing capacity.

A pile with a length of 3 m, a diameter of 610 mm and a wall thickness of 3 mm was installed up to a depth of 2,4 m. This was done for two vibrated piles (slow and fast installation) as well as an impact hammered pile. Afterwards, the piles were tested under a monotonic loading regime and under a cyclic loading regime. During installation and loading, the radial stresses in the sand were measured. This resulted in differences between the two installation methods.

During installation, an increase in radial stresses around the pile toe was observed for the impact hammering method. The same was observed for vibrated piles, if they were installed with a larger frequency, although the measured stresses were quantitatively lower than for the impact hammered piles. However, vibrated piles installed at a lower speed do not show this effect.

Installationsvariante		$u(H)/u(H)_{geschlagen}$	
		H = 1 kN	**H = 15 kN**
geschlagen		100 %	100 %
vibriert	freireitend, hohes exzentrisches Moment, 'aggressive' Steuerung	85 %	104 %
	freireitend, niedriges exzentrisches Moment	82 %	98 %
	krangeführt, hohes exzentrisches Moment	70 %	106 %
	krangeführt, niedriges exzentrisches Moment	78 %	112 %

*Figure 3.8: Pile head displacement under different load levels for hammered (geschlagen) and vibrated (vibriert) piles (*Stein et al., 2020)

For the behaviour under monotonic loading, impact hammered piles showed a much stiffer behaviour with the smallest displacements. Both vibrated piles showed larger displacements, with a difference depending on the driving speed. The fast pile showed behaviour that is closer to the impact hammered pile, compared to the slow vibrated pile.

The cyclic behaviour was similar as well, with the same qualitative assessment. The stiffest pile was the impact hammered pile, followed by the faster vibrated pile, then the slower vibrated pile. All piles showed an increase in stiffness as the number of loading cycles increase.

3.1.7 Spill & Dührkop (2020)

In a study by Spill & Dührkop (2020), an experimental field test campaign was conducted to compare the lateral load-displacement behaviour of monopiles installed under different installation methods and with different diameters.

Piles with three different diameters were installed: 0.61 m, 0.914 m, and 1.22 m. The piles were installed at different embedment depths depending on the test procedures. The latter was divided into two parts: a first part where piles were installed by impact driving and the effect of diameter was studied, and a second part where the two largest piles were installed with vibratory installation at a frequency of 33 Hz. All the piles were laterally loaded with monotonic loading after installation and their behaviour was measured.

Results showed that vibratory-driven piles had a less stiff lateral behaviour than impact hammered piles. This paper also studies the accuracy of different models in predicting the behaviour under lateral loading.

It seems that the method proposed by the API (2011) tends to underestimate the initial stiffness. This is in accordance with Achmus et al. (2020).

3.1.8 Fischer & Stein (2022)

Fischer & Stein (2022) conducted a study on the difference in soil stresses due to the installation method between impact and vibratory driven piles. Variants with different pile diameters, soil parameters and installation methods were investigated by means of scale model tests.

A large-scale model testing facility was constructed to keep scaling effects as low as possible. The piles were installed in cylindrical containers with a diameter of 4 m and a height of 5 m. Two different soil densities were applied in two containers. One container had very loose sand and another dense sand. Three different pile diameters (0.36 m, 0.51m, 0.61m) as well as three installation methods were used. Those methods were impact driving, "free", and "crane-guided" vibratory driving. The difference between the last two was that during "crane-guided" driving, the installation assembly (including pile and vibratory hammer) was attached to the crane and pile penetration speed was dictated by the lowering speed of the crane. The pile was vibrated with a constant frequency high enough to drive it to depth. During "free" driving, the penetration speed was driven by the self-weight of the assembly and the frequency was increased manually to obtain a constant penetration speed. The combination of test conditions in indicated in Figure 3.9.

installation method	pile diameter	soil density	water content
impact	0.36 m 0.51 m	very loose dense	fully saturated
impact vibro (free) vibro (guided)	0.61 m	dense	fully saturated

Figure 3.9: Test conditions (Fischer & Stein, 2022)

During installation, total stress sensors and pore water pressure sensors were carrying out measurements at various depths along the penetration path. The radial effective stress was found to increase the most during impact driving, followed by free vibratory driving. Almost no increase in radial effective stress was measured during crane-guided vibratory driving.

Fischer & Stein concluded that vibratory-driven piles may attain similar load-bearing properties as impact-driven piles if the appropriate parameters are used (in this case, using installation parameters resembling "free" installation).

3.2 Field tests

In this section, a number of field-testing studies will be presented. These tests have been carried out with near-representative pile diameters in the field. The scale of the monopiles used in those tests is reduced compared to the current industry standards but offers insight on the behaviour of monopiles.

3.2.1 Achmus et al. (2020)

Achmus et al. (2020) conducted a field test with six piles in dense saturated soil to investigate the differences between impact-driven and vibrated piles regarding lateral load bearing behaviour. Load-displacement curves and CPTs were recorded and evaluated to gain insight on this. The piles had an outer diameter of 4.3 m and a total length of 21 m. The embedded length varied between 18.2 and 18.7 m. Horizontal loads were applied between 0.85 and 1.05 m above the surface. Figure 3.10 below shows a photograph of the test site.

Figure 3.10: Photograph of the test site (Achmus et al., 2020)

The pile pairs were installed and then loaded against each other horizontally by applying a tensile force (Achmus et al., 2020). CPTs were performed before and after the installation (prior to lateral loading) to assess the effects on the soil.

The vibrated piles were installed with a frequency of 12.5 Hz for the first 9 m, followed by 22.5 Hz for the rest of the embedment depth. One pile was the exception to this due to difficulties in the installation. Instead, the target frequency could not be reached, and the pile was driven at 15 Hz. The installation time for this pile was 16 minutes, compared to 4 and 3 minutes for the other vibrated piles.

Under primary loading, the vibrated piles showed a lower stiffness than the impact-driven pile. The reduction is different under different load levels. For pairing P4-P5, the ratio vibrated stiffness/hammered stiffness goes from 0.62 at 5MN to 0.76 at 15 MN. Under un- and reloading, it is even higher at 0.87 and 0.86 for 5 and 10 MN respectively. Interestingly, the first vibro-driven pile which was installed with deviating parameters showed a different behaviour than the other vibro-driven piles. The stiffness under primary loading had the same increasing trend as other piles, but it was only slightly weaker than the impact-hammered piles at 15 MN (ratio of 0.95). Under un- and reloading, the stiffness of this pile pairing was higher than that of the hammered pile at 1.13 and 1.04 for 5 and 10 MN respectively. The associated graphs are shown in Figure 3.11.

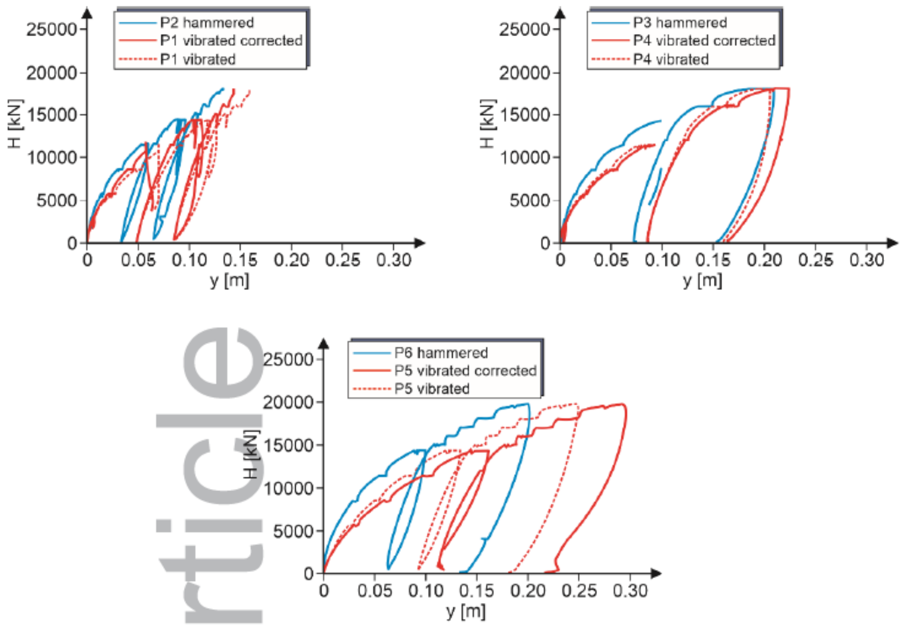

Figure 3.11: Comparison of the corrected load-displacement curves for the lateral load tests(Achmus et al., 2020)

Additionally, a comparison of CPT results from before and after the tests was done, resulting in generally lower cone resistance after installation. However, cone resistance after installation was less affected by impact driving than vibratory installation. The exception to this was again pile pairing P1-P2 where the cone resistance stayed constant. A comparison of the cone resistances is shown in Figure 3.12 below.

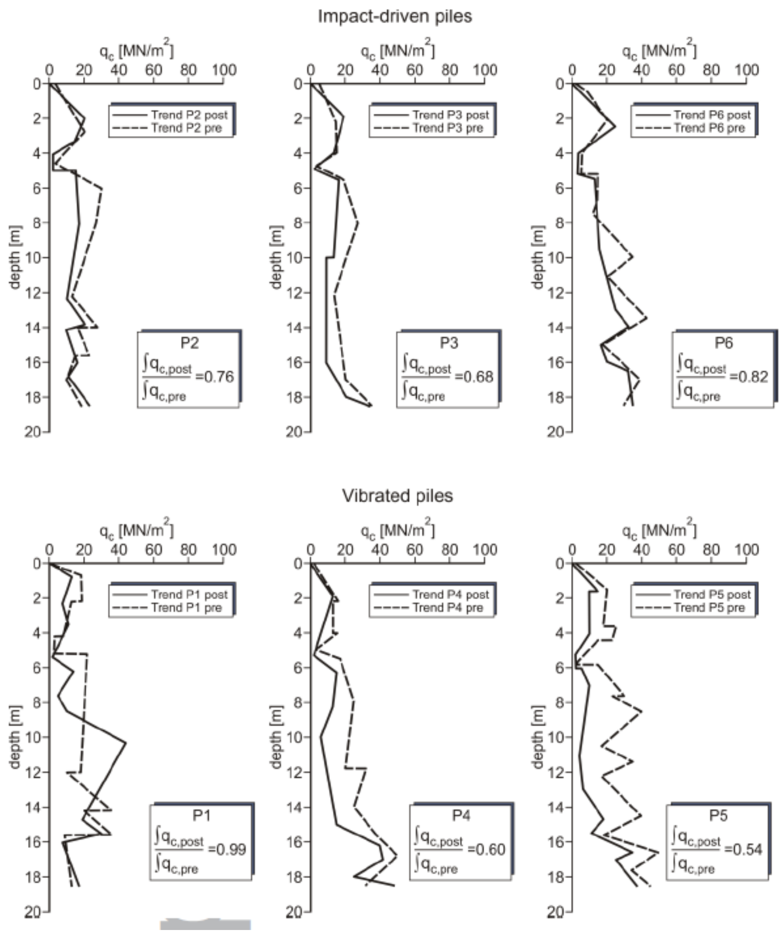

Figure 3.12: Comparison of pre- and post- installation trend functions of the cone resistance for impact hammered and vibrated piles(Achmus et al., 2020)

Achmus draws the conclusion that if a vibro-driven pile is installed in a controlled way to minimize loosening, it behaves similarly to an impact-driven pile.

3.2.2 El Kanfoudi (2016)

In the study by el Kanfoudi (2016), the field test results of 4 m outer diameter monopile driving were numerically investigated. Monopiles were installed with vibratory installation on the Maasvlakte in Rotterdam in dense to very dense sand to get insight on the effect of vibratory installation on soil conditions.

The piles had a wall thickness of 55 to 60 mm and a length of 26 m. All the parameters used for the finite element modelling of the pile behaviour are estimated based on CPT data. Pre and post installation logs near the piles were taken at different distances from the pile centre. It was found that installation effects are largest near the monopile and diminish with increasing distance from the pile. The most notable effect was an increase in cone resistance.

The pile was then loaded in a finite element model (FEM) using data from the CPT and the resulting p-y curve was compared to the API (2007) method. Results indicate showed discrepancies between both methods that increased with depth. The FEM showed a much lower stiffness which was attributed to several flaws in the API method. El Kanfoudi concluded that the discrepancies between current design methods and the FEM were much larger than could be justified by installation effects alone, but that the pile deflection results from the FEM were an accurate representation of reality.

3.2.3 Anusic et al. (2019)

Anusic et al. (2019) conducted field tests to determine the influence of installation method on the response of the pile. This was done in Western Australia, in medium dense sand to compare vibratory installation with two different impact hammering modes (air hammer and drop weight hammer)

Nine piles were installed, eight of which had a diameter of 0.165 m and one of them 0.127 m. The length of the eight larger piles was 4 m while the length of the last one was 1.5 m. Two piles were installed with a vibratory hammer, three with an air hammer and three with a drop weight hammer. The last pile was jacked with a CPT truck.

Lateral loading was then done on the pile pairs. Both piles were pushed away from each other by way of a hydraulic jack and displacements were measured to gain insight on the lateral loading capacity of the monopiles.

The results showed that the piles installed with an air hammer and by the drop weight method show similar load response. However, the vibrated piles show a much stiffer response than the impact hammered piles, by about 25%. The results of the lateral load-displacement tests are shown in Figure 3.13.

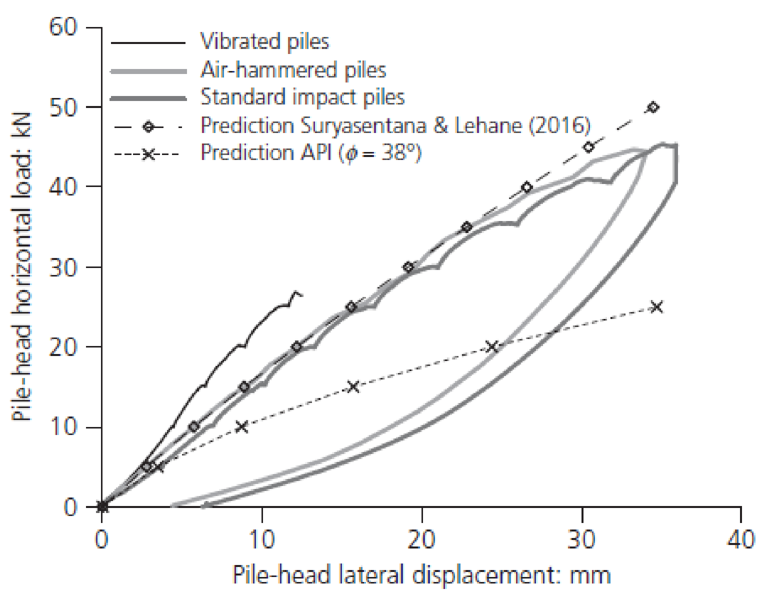

Figure 3.13: Lateral load-displacement behaviour for different pile installation types(Anusic et al., 2019)

This is interesting, as this study shows the opposite of Achmus' study described above. One point to note however, is that the piles used here had a diameter and a L/D ratio that are not representative of offshore piles. The L/D ratio here is much larger, causing the pile itself to be less stiff and to lean towards a predominantly bending behaviour whereas low L/D piles have a predominantly rotational behaviour.

Anusic relates the stiffer response and the lateral capacity to the installation frequency. It is concluded that the stiffer response of the vibrated piles possibly reflects compaction effects, which were not there during impact hammering (Anusic et al., 2019). Since this is the only study in medium-dense sand, this might mean that the soil density influences the post-installation behaviour of vibrated piles.

3.2.4 PISA project

The Pile Soil Analysis (PISA) project was a large research project with the goal of proposing a new framework for the design of large diameter monopiles by incorporating more parameters (Burd, Beuckelaers, et al., 2020; Zdravkovic, Jardine, et al., 2020). This resulted in a different model from all the existing ones, which was hoped to be more accurate for the use in offshore wind turbines (OWT) monopile foundations. To this end, field testing as well as three-dimensional finite element modelling have been used.

Two field tests have been conducted as part of the PISA project: one in stiff glacial clay till at Cowden, UK, and one in a dense marine sand in Dunkirk (Byrne et al., 2020a), (Byrne et al., 2020b). Twelve piles were installed, with three different diameters. 0.273 m, 0.762 m, and 2 m. The piles were divided in pairs with each pair having a different length. This means the L/D ratio varied between 3 and 10.

The piles were installed in two stages. They were vibrated until a stable depth between 1 and 1.5 m, followed by pile driving with a hydraulic hammer until reaching the target embedment. Piles were then monotonically loaded under a horizontal load, and the load displacement curves were studied. Each pile was loaded individually against a larger test pile.

The finite element modelling analysis was executed in two different papers (Taborda et al., 2020), (Zdravkovic, Taborda, et al., 2020).

The p-y model developed as a result of the PISA project and its application to marine sands are described in detail in multiple papers (Burd, Abadie, et al., 2020; Burd, Beuckelaers, et al., 2020; Burd, Taborda, et al., 2020; Byrne, Burd, Gavin, et al., 2019; Byrne, Burd, Martin, et al., 2019; Zdravkovic, Jardine, et al., 2020). The findings of the PISA project have been summarized in Byrne et al. (2017).

The model details will be explained further in section 3.3.

3.2.5 Kementztzidis et al. (2023)

Kementzetzidis et al. (2023) describes a field-testing experiment performed with medium-scale pipes at the Maasvlakte II site in Rotterdam, Netherlands. In this experiment, piles were installed under different installation methods. The goal of the paper was to investigate a different installation method using torsional movement (named GDP), but piles were also installed with impact hammering and vibratory hammering as in the SIMOX experiments of this thesis. Due to soil inhomogeneity, the results were calibrated using a 1-D FEM.

The piles used in that experiment had a length of 10 m (of which 8m were embedded), an outer diameter of 0.762 m and a wall thickness of 15.9 mm. They were loaded with the help of a reaction pile and a loading frame attached to said reaction pile. The piles underwent monontonic loading, followed by cyclic loading.

After analysis, differences caused by installation effects were found during initial monotonic loading, but also during cyclic loading. However, those differences seemed to gradually vanish with an increasing number of cycles. This would mean that process occur under cyclic loading that gradually erase the influence of installation parameters and methods.

3.3 Models and numerical studies

3.3.1 P-y methods

The p-y method is a way to model the behaviour of laterally loaded piles in soil. The "p" stands for the soil pressure per unit length and the "y" stands for the lateral displacement. The concept was first developed by (McClelland & Focht, 1956). Since then, it has been widely used by engineers for its simplicity. In a p-y method, the pile is modelled coupled to a series of lateral springs which represent the soil (*Http://Www.Findapile.Com/p-y-Curves*, n.d.). Figure 3.14 shows a diagram of the standard p-y method.

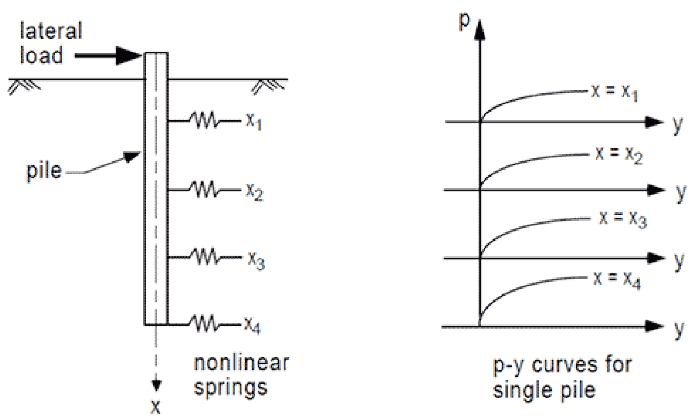

Figure 3.14: Schematisation of the standard p-y model (FHWA Manual, 2010)

A large number of different p-y models have been proposed for laterally loaded piles, though there is no single universally acknowledged p-y- model to date. The existing p-y model in the API code (API, 2007) has been safely used in oil and gas industry. The API are the most used guidelines to determine the lateral bearing capacity of offshore monopiles, but the model's reliability and applicability to monopile foundation for offshore wind turbines are questioned by researchers.

(I) Initial models

The first practical p-y model was proposed by Reese et al. (1974) is also the basis for the p-y model in the API. It is based on full scale field tests and the parameters were chosen empirically. The model (shown in Figure 3.15) consists of a straight line representing the initial elastic behaviour and a horizontal line representing the plastic behaviour. These two lines are connected by a parabola and an intermediate straight line.

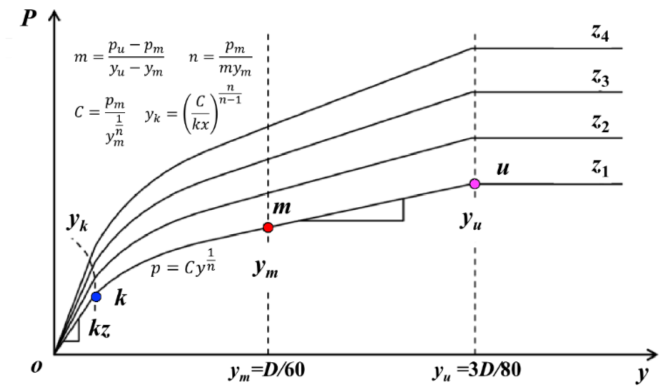

Figure 3.15: P-y model in Reese et al. (1974)

This model is developed upon by Bogard & Matlock (1980) and O'Neill & Murchinson (1983), the latter being the one used in the API guidelines. The reliability of these models is discussed and a few specific comments are presented below:

- The initial stiffness is purely empirical.
- This model was developed for a different type of piles, with a large L/D and flexible bending behaviour. Its application to piles with a different profile and different behaviour under loading is questionable.
- The value of certain parameters was assumed for the specific test locations and its applicability to other tests sites is questionable.
- The deflections and ultimate soil resistance are only for the tests by Reese et al. (1974) and their applicability to other test sites is questionable.
- The overall shape of the p-y curve might not be applicable to other tests with different relative densities and pile dimensions.

Except for models developed by Thieken et al. (2015) and Sorensen et al. (2010), these models are based on a slender and flexible pile with a small diameter. A different diameter pile will result in a different ultimate soil resistance.

(II) CPT-based models

Another group of p-y methods are CPT- based methods, developed after the methods addressed in the previous section. These can be subdivided into two groups. Papers by Novello (1999), Dyson & Randolph (2001) and Li et al. (2014) use power functions while Suryasentana & Lehane (2014) and Suryasentana & Lehane (2016) use the exponent function.

The power function papers are mainly proposed from centrifuge tests or field tests where limited deflection can be achieved. This is due to the limitations of the loading system or the yield strength of the pile used for the model. The exponent function papers are proposed based on numerical simulations in which a large deflection can be achieved. However, the deflection is still not enough to obtain the true ultimate soil resistance.

A few specific comments on these models are presented below:

- All the models except for Suryasentana & Lehane (2016) have no explicit initial stiffness and depend on the pile diameter.
- The power function has no limit, which is not realistic.
- The influence of a flexible or stiff failure mode is not reflected in these models.

To summarise, the p-y models all lack in one way or another and do not give a complete overview of lateral bearing behaviour of monopiles, while representing the situation in a simpler way than finite element models. While they improve on the basis of the API guidelines, researchers are still looking for more accurate models.

(III) Limitations of API method

The currently employed API p-y methodology has the advantage of being able to model the non-linearity of the soil with only a few input parameters and is fast to compute. However, it has shortcomings (Page et al., 2016) which are discussed below. In general, the method is inaccurate due to its simplicity and tends to underestimate the soil response.

The API method was developed for use in the oil and gas industry, where long and slender piles mainly designed to withstand vertical loads are used. The pile responds to applied loads mainly by bending. The piles used for the foundation of OWT have a lower L/D ratio (Doherty et al., 2011) and are under high horizontal load applied with an arm of 30 to 40 m which results in bending moments at the foundation. Piles used for offshore wind also show a more rigid behaviour (with rotation instead of bending) which means that ignoring some soil resistance components such as side and base shear can lead to inaccurate predictions (Page et al., 2016).

Cyclic loading and its long-term effect is not taken into account while it can cause accumulated displacements and a change in relative density of the soil around the pile. Cyclic loading is only addressed in a simplistic way by using a reduction in lateral capacity instead of focusing on the actual effects of cyclicity. This was done to obtain a conservative solution for the lateral capacity, which compromises accuracy (Page et al., 2016).

Soil damping is also not inherently included in the original API p-y curve formulation (Page et al., 2016). For soil damping, dynamic amplification was not a concern in oil and gas industry, hence the API not addressing it in detail. Its contribution can be relevant for OWT structures though and should be considered.

In the API method, the foundation stiffness cannot be accurately predicted under different loading conditions. OWT are subject to not only cyclic loading, but also extreme events. Fatigue is often a driver for the design of it and an inaccuracy in the stiffness can lead to differences in eigenfrequencies, which may negatively impact fatigue life (Page et al., 2016).

Lastly, gapping and accumulated deformations can affect the dynamic response of the OWT and the foundation stiffness (Page et al., 2016) and are also not taken into account in the p-y formulation from the API. However, those accumulated displacements can end up exceeding the maximum allowed for the serviceability limit state.

3.3.2 PISA model

The p-y model developed during the Pile Soil Analysis (PISA) project builds upon the API model by using lateral springs with a different mathematical formulation and adding three more springs, thus incorporating more parameters. In addition to that, the design approach consists of p-y curves calibrated with 3D FE analysis instead of standard values for the stiffness and the ultimate load as is the case in the API. This makes this model more accurate for the use in OWT monopile foundations.

The p-y curve is only part of the model proposed by the PISA model, which also takes into account shaft frictions, base shear force and base moment. To this end, three springs have been added on top of the lateral load spring present in the standard p-y model. A simple schematisation of the PISA project model is shown in Figure 3.16 below.

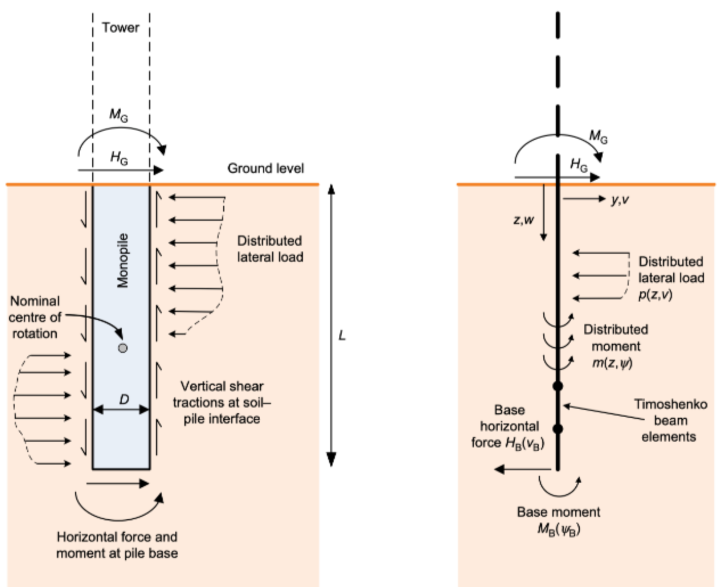

Figure 3.16: PISA project model (Burd, Abadie, et al., 2020)

The model uses a four-parameter conic function to determine the relation between soil resistance and deflection. The four parameters are the initial stiffness, the ultimate soil resistance, the deflection required to mobilize the ultimate soil resistance and the parameter that controls the nonlinearity of the p-y curve between initial and ultimate limit state. These extra springs and parameters make the model more flexible, more accurate and more adapted to OWT foundation monopiles, which are very stiff and have a large diameter.

According to the PISA project, the standard p-y method used in the API guidelines is unsatisfactory for use in the design of wind turbine monopile foundations, especially for the very stiff piles with a large diameter. Stiffness and capacity appear underpredicted in certain soil types (Byrne et al., 2017). The medium scale field testing campaign in the PISA project resulted in the development of an enhanced p-y approach. This approach retains the simplicity (and thus fast computing times) of the traditional p-y approach while reaching an accuracy close to the 3D finite element model. As a result, monopile designed with this model will be less conservative and thus cheaper, improving the economic viability of OWT.

This model is tested in two papers (Taborda et al., 2020; Zdravkovic, Taborda, et al., 2020) where results from a numerical analysis are compared to results predicted with the PISA model. The three-dimensional finite element analyses were performed before the field tests addressed previously and those show results that are in agreement with the measurements. The adequacy of the numerical model is addressed in these papers and the FE analyses are used to calibrate said model.

3.3.3 Wang et al. (2022)

Wang et al. (2022) conducted a numerical analysis on previously described centrifuge tests (Wang et al., 2021, see previous section 3.1.3). The centrifuge tests were modelled in a finite element software. In these finite-element simulations, pile diameter and load eccentricity have been varied to investigate their influence on the lateral capacity of piles.

Four different pile diameters (4 m, 6 m, 8 m, 10 m) and seven different load eccentricities (5, 10, 20, 40, 60, 80, 100 m) were studied, 28 different simulations in total. A typical finite element mesh for one of the piles is shown in Figure 3.17 below. Installation effects were not accounted for, the piles were wished in place.

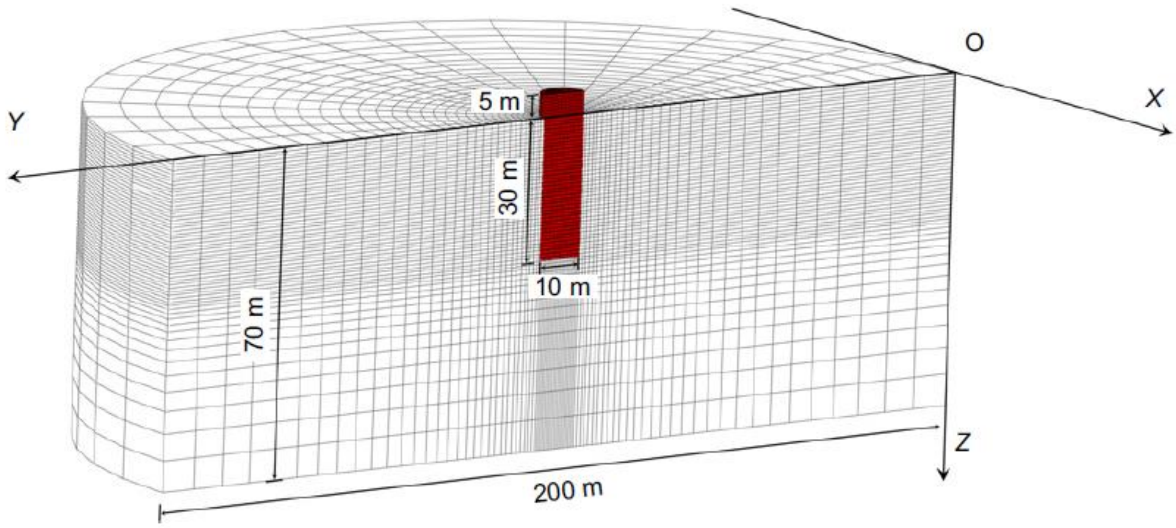

Figure 3.17: Typical finite element mesh for a pile of 10 m diameter (Wang et al., 2022)

The obtained p-y curves were normalized by diameter, and the results are presented in Figure 3.18. The results showed that for different diameters, the p-y curves are very similar after normalization. In the results comparing the p-y curves for piles under different loading eccentricity, the normalised curves also show very small differences. Wang et al. (2022) conclude that the p-y curves at any given depth are independent of the pile diameter and the loading eccentricity for a rigid pile.

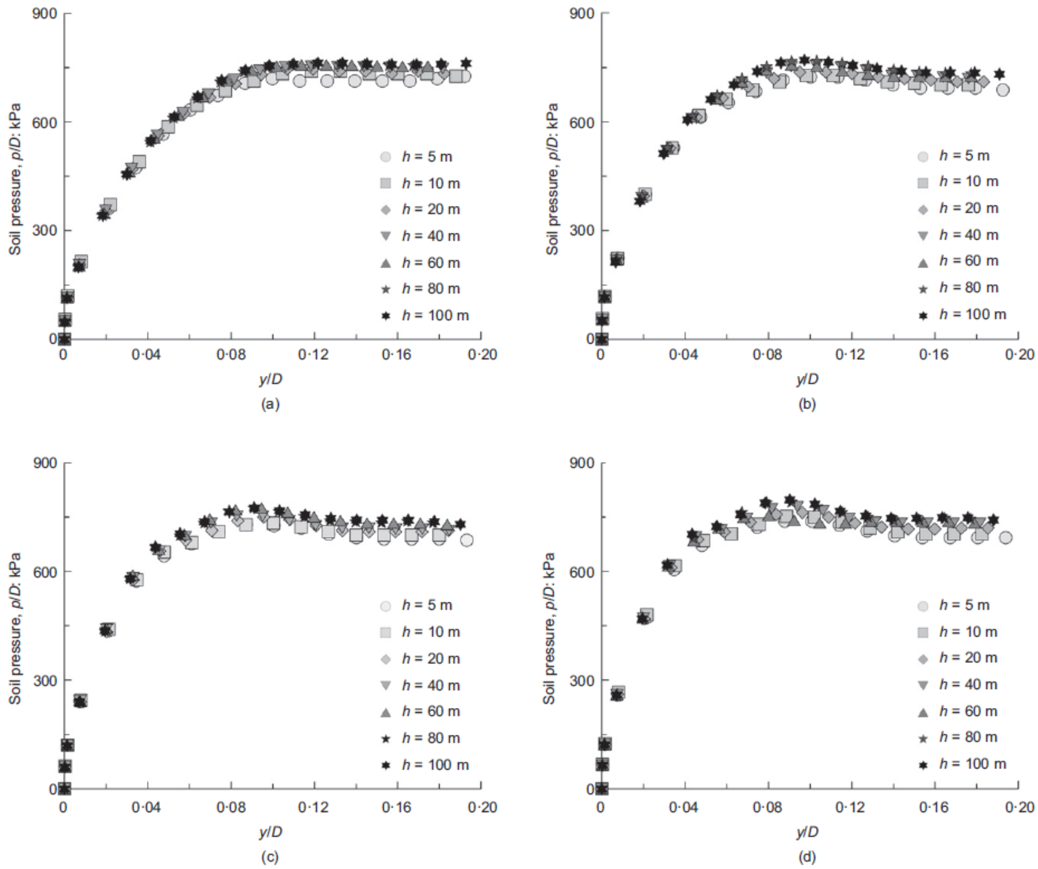

Figure 3.18: Soil reaction curves under different loading eccentricities of different diameter piles at 4.5 m below ground surface: (a) D=4 m; (b) D=6 m; (c) D=8 m; (d) D=10 m (Wang et al., 2022)

3.3.4 Fan et al. (2021)

In Fan et al. (2021a), a centrifuge study is described. Then the results of this centrifuge test are used to study the installation effects on lateral response during pile installation (Fan et al., 2021b) and during lateral loading (Fan et al., 2021c).

In Fan et al. (2021b), the soil state is analysed numerically. The numerical model is first validated against the earlier mentioned centrifuge tests, then used to quantify the installation effects. Three different initial sand densities were analysed: 38%, 60%, and 88%.

Two methods of installing the monopile were compared: impact driving and jacking. Results showed that there are differences in the effects of installation methods on void ratio, horizontal stress, plugging, and settlement. Inside of the pile impact driving led to densification of the sand while pile jacking led to loosening. Outside of the pile, the void ratio tended to reach the same value regardless of the installation method. Regarding horizontal stress, both methods caused an increase inside and outside of the pile, with the highest stress increasing as the initial relative density increases. Jacked piles had a higher tendency to show plugging, while soil settlement was much larger for impact hammered piles due to densification. This paper concludes that the impact of pile installation on the surrounding soil can be significant, with large densification occurring for impact driving and both methods leading to an increase in horizontal stresses.

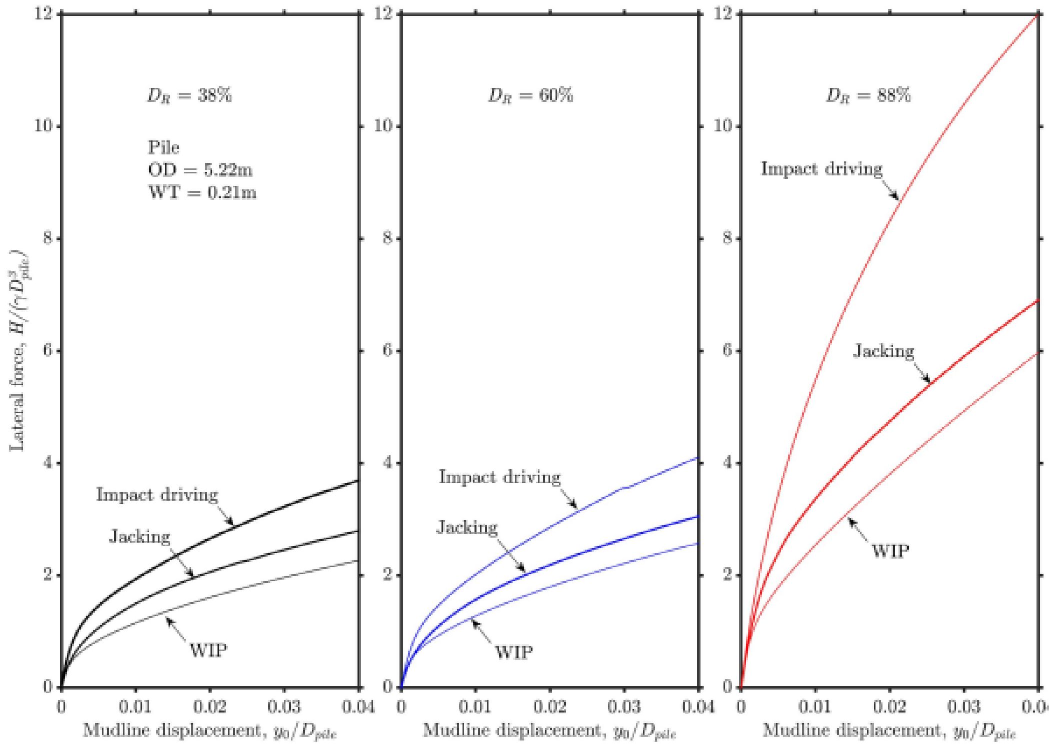

*Figure 3.19: Normalised load-displacement curves for piles in different soil densities (*Fan et al., 2021c)

In Fan et al. (2021c), the stiffness and lateral capacity of the monopiles are investigated. Results showed that piles installed with the impact driving method had a significantly higher lateral stiffness than jacked piles, which is consistent with the centrifuge tests. Different factors were explored to get more clarity on what influences and enhances the installation effects the most. Initial soil density, pile geometry, stress level and load eccentricity were all found to influence the lateral bearing behaviour of the pile. The paper stresses the importance of accounting for installation effects when modelling the lateral stiffness.

3.3.5 Gavin et al. (2020)

Gavin et al. (2020) explores the impact of installation method on load bearing behaviour of monopiles in sand. This was done by comparing full scale field tests from previous studies with a three-dimensional finite element model in PLAXIS. The model parameters were derived using CPT data from sand after installation with vibratory and impact driving.

The full-scale experimental tests were taken from the Cuxhaven project, which is mentioned in Achmus et al. (2020).

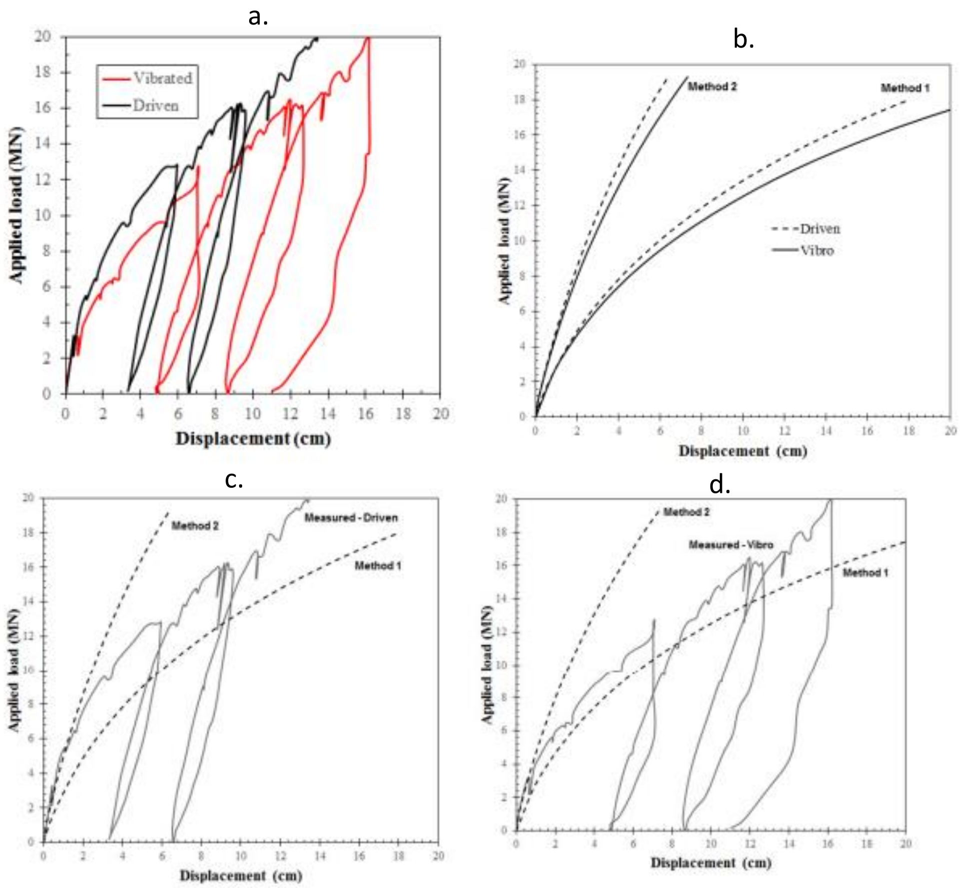

Figure 3.20: (a) Field measurement of the lateral load-displacement response of a driven and vibrated pile, (b) summary of FE analyses, (c) FE predictions for the driven pile, (d) FE predictions for the vibrated pile (Gavin et al., 2020)

The soil properties were determined by way of two different methods to evaluate the impact of installation effects on the lateral stiffness of the monopile. In both cases, the FE analyses showed relatively small effects of the different installation methods, whereas the field tests showed results that were not visible in the simulation result.

Since the field tests suggested that installation effects do impact the lateral load response and these were not visible in the model results, the authors concluded that using CPT data (as done in this study) may not be the most appropriate way to measure installation effects on the lateral load bearing behaviour (Gavin et al., 2020).

3.3.6 Staubach et al. (2022)

Staubach et al. (2022) explores the influence of vibratory or impact hammer installation of monopiles on the response of subsequent lateral cyclic loading. This behaviour was analysed numerically by simulating one million lateral load cycles using a so-called “high-cycle accumulation” (HCA) model. In addition to the installation method, pile drainage conditions during loading were also varied and compared.

This study gives insight on the effect on installation on the soil before and after loading. The analysis in dense sand indicated that the soil state in the direct vicinity of the pile is changed considerably. Impact hammered piles seemed to result in larger effective stress near the pile toe.

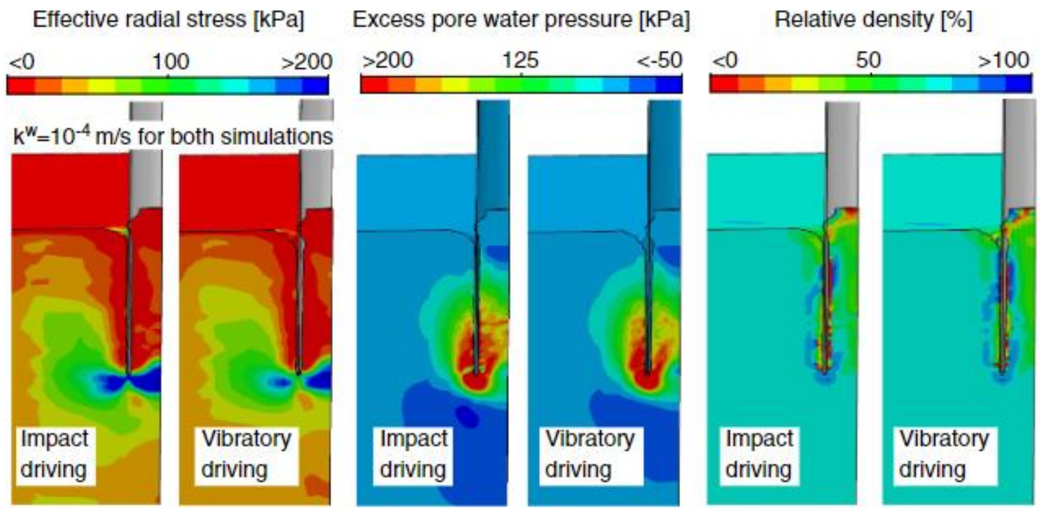

*Figure 3.21: Effective radial stress, excess pore water pressure and relative density at a pile penetration depth of 10 m (*Staubach et al., 2022)

During cyclic loading after installation, both vibratory and impact driven piles showed similar pile head displacement in partially drained conditions. However, if the situation was considered as ideal fully drained, the vibrated pile showed larger displacement. Staubach et al. (2022) conclude that better drainage during driving results in less pile head rotation during the following cyclic loading sequence.

3.4 Main observations

In this part of the report, the main takeaways from the previous sections will be addressed.

3.4.1 Installation method

Impact hammering and vibratory installation result in different lateral loading behaviour for monopiles, as it has been shown in many field and laboratory tests mentioned above. Piles installed via impact driving in dense sand have generally had a higher lateral stiffness than piles installed with a vibration hammer. However, studies have shown that there is some variety in the difference between the two installation methods, and that these depend on installation settings as well as initial soil density. This will be summarised in the following sections.

3.4.2 Vibration frequency

Vibration frequency is linked to penetration speed and impacts the soil state around the monopile. In general, vibrating piles at a low frequency, results in a slow penetration and a higher bearing capacity than a pile driven with a high frequency. The explanation given by Rainer Massarsch et al. (2022), in a paper that gives an overview of the existing literature on the topic, is that the optimal pile capacity is obtained when the pile is vibrated close to the resonance frequency, which is generally lower than the usual vibration frequencies that lead to an optimal penetration speed.

3.4.3 Penetration speed

In Achmus et al. (2020), the piles that were installed with a lower speed (which was a consequence of a lower installation frequency) lead to a higher lateral capacity, closer to the value obtained with impact driving. Results were similar in Hoffmann et al. (2020) and Labenski et al. (2019), where piles installed with a slower speed under vibratory installation behaved stiffer than piles installed with a higher speed.

However, the study of Stein et al. (2020) was the only study that showed opposite behaviour, where a vibrated pile with a high penetration speed had a lateral stiffness that was closest to the impact hammered pile.

3.4.4 Cavitational and non-cavitational driving

Two different vibration modes can occur during installation, and those seem to impact lateral bearing capacity differently. Depending on the interaction between the pile toe and the soil, one can have cavitational or non-cavitational installation. In non-cavitational mode, the pile toe stays in contact with the soil the entire time, which was shown to give a higher lateral bearing stiffness. This vibration mode is usually associated with high vibration frequencies and high penetration speeds but having such conditions does not necessarily produce a non-cavitational vibration mode, as this depends on a series of additional factors, such as displacement amplitude and ratio of dynamic force to static weight (Labenski et al., 2019). In cavitational mode, the pile toe loses contact with the soil, which results in a lower lateral bearing stiffness. This vibration mode is usually associated with low vibration frequencies and low penetration speeds but, once again, these conditions alone are not sufficient to produce a cavitational vibration.

In the study of Fischer & Stein (2022), the pile vibrated under a constant frequency and held back by the crane showed lower radial stresses due to installation than the pile which was installed under its own self-weight. The first pile could be categorised as cavitational, as it was held back by the crane and its tip was not in contact with the soil all the time. On the contrary, the pile installed under its own self-weight will have been in contact with the soil at all times, meaning it may have been installed under non-cavitational conditions. It was this latter pile that showed larger radial effective stresses due to installation, leading to believe that it could have a bearing capacity close to the impact hammered pile.

Labenski & Moormann (2019) measured the displacement of the pile itself, as well as the cavitation mode of the installation. This paper came to the opposite conclusion, where piles where a non-cavitational process was identified displayed larger displacements than piles identified as cavitational.

3.4.5 Initial soil density

While all other field tests were conducted in predominantly dense sand profile, Anusic et al. (2019) conducted field tests in medium sand. This study was also the only one that showed piles installed with vibratory installation as having a higher lateral resistance than impact hammering. The experiments in this paper were carried out in medium-dense sand and compared different methods of hammering (air-hammered and standard impact piles) and a vibrated pile. The different installation modes for hammered piles did not seem to affect the lateral capacity. However, vibrated piles showed a larger lateral bearing capacity and stiffness than impact hammered piles. This suggests that installation parameters are not the only aspects to play a role in lateral capacity of monopiles and that initial soil density influences lateral stiffness as well. One can derive from this paper that the lateral response of vibrated monopiles goes from softer than hammered to stiffer than hammered when the sand varies from dense to medium dense.

3.4.6 Soil measurements

Two different types of soil measurements are done in the discussed studies, CPT measurements and horizontal stress measurements.

Both El Kanfoudi (2016) as well as Achmus et al. (2020) did CPT testing on the soil before and after installation. El Kanfoudi (2016) found that closest to the pile wall, there was an increase in cone resistance after installation. In that study, only the installation effects after vibratory installation are considered. Achmus et al. (2020) compares CPT data from before and after installation for both methods, and finds that in almost in all cases, the cone resistance decreases after installation. In the paper by Gavin et al. (2020), the effects of installation are reproduced in PLAXIS by taking post-installation CPT data for impact-driven and vibrated piles and by deriving soil parameters from this CPT data using two interpretation methods. The impact of the installation method on the stiffness of the piles was relatively small, and the difference in stiffness between the method used to derive soil parameters has much more influence. This could mean that CPT tests alone may not give a full picture of the effects of installation.

In Hoffmann et al. (2020), horizontal stress sensors are used to monitor the forces in the ground as a result of different installation methods. The highest stresses were recorded for impact driving, then cavitational vibration, followed by non-cavitational vibration. The lateral load displacement behaviour had the same ranking with impact driving being the stiffest. This may suggest that horizontal stresses are positively correlated to lateral load bearing capacity (higher horizontal stresses will lead to lower displacement under loading) and are important to monitor during the testing campaign.

3.4.7 P-y methods

The p-y method is a method used to model the behaviour of laterally loaded piles in soil, where “p” stands for pressure per unit length and “y” for displacement. This concept was first developed by McClelland & Focht (1956)and is widely used by engineers nowadays due to its simplicity. After its original formulation, the p-y method has been the focus of many studies aiming to make it more accurate (Bogard & Matlock, 1980; O’Neill & Murchinson, 1983) or developed upon using CPTs as a base with a power or an exponential function (Dyson & Randolph, 2001; Suryasentana & Lehane, 2016).

Even then, this method has flaws which makes it poorly adapted for use in OWT monopiles. The main flaws are that the p-y method is not adapted for stiff and thick piles as used in OWT foundations as it was originally developed for thin and slender piles), and that in its simplicity the model does not take into account many other processes that happen when a monopile used for an OWT foundation is subjected to lateral loading (such as cyclic behaviour or gapping).

3.4.8 PISA project

The Pile Soil Analysis (PISA) project aimed to improve on the p-y method by incorporating more elements, thus potentially making it more accurate and more suitable for thicker piles as used in the offshore wind industry. Two field tests were done with piles installed and then monotonically loaded under a horizontal load. The piles used in the field test were close to representative. According to Byrne et al. (2020a), the configurations were chosen to obtain representative scaling of the key geometric aspects. The results were upscaled in a FEM. The L/D ratio remains in the same range as is used in practice.

The model developed after these tests uses a different mathematical formulation for the lateral springs, as well as adding three more springs. This incorporates more parameters in an effort to make the model more accurate than the standard p-y method. It uses a four-parameter conic function to determine the relation between soil resistance and deflection. The four parameters are the initial stiffness, the ultimate soil resistance, the deflection required to mobilize the ultimate soil resistance and the parameter that controls the nonlinearity of the p-y curve between initial and ultimate limit state. These parameters allow the model to reach an accuracy close to at 3D FE analysis while retaining the simplicity of the p-y model. This renders it fast to run and less conservative, resulting in cheaper monopiles and improving the economic viability of OWT.

3.4.9 Scaling effects

Two aspects of scaling effects are discussed, the L/D (embedded length to diameter ratio) and the load eccentricity. Wang et al. (2022) addresses both these effects in his research, where he compares the normalized p-y curves of piles with a different diameter as well as varying load eccentricities for each diameter. He concludes that the curves are extremely similar (Figure 3.18) and that the p-y curves at any given depth are independent of the pile diameter (as long as the L/D ratio remains the same) and the loading eccentricity for a rigid pile.

As discussed in the PISA project section, most of the tests in this literature study were scaled. Not all parameters can be scaled (for example the bending stiffness ratio of the pile to the soil), but if the key aspects of the problem can be accurately scaled, that is enough to give representative results. No attempt has been made to provide a fully scaled problem as that would require too much work for the added benefits.

3.5 Difference between existing literature and current research

The following differences between the thesis and the existing literature have been highlighted. These set this thesis apart from previous studies:

- In the SIMOX experiments, one batch will be carried out in medium-dense sand and three experiments will be carried out in dense sand. This will allow for a comparison of results and give insight on the influence of the soil properties. Anusic et al. (2019) is the only study in medium-dense sand, and all other literature addressed here studied dense sand. But none compared both sand densities. While Labenski & Moormann (2019) used different sand densities, the soil instrumentation was not as detailed as it will be during this thesis.

- In other studies with horizontal loading, soil conditions after the test were measured with CPT only. Apart from Stein et al. (2020) and Hoffmann et al. (2020), none measured the horizontal stresses in the soil. In the tests carried out during the thesis, horizontal stresses will be monitored with dedicated sensors instead of CPT.
- When horizontal stresses in the soil were being measured during installation (Fischer & Stein, 2022), this was not followed up by horizontal loading to verify assumptions about bearing capacity. In this study, stresses in the soil will be measured during installation and compared to load-displacement data to get a better picture of the influence of effective stress.
- In the tests carried out during the thesis, piles with two different wall thickness will be used. The impact of wall thickness on vibration installation has not been tested yet in previous studies.
- El Kanfoudi (2016) studies the impact that the vibratory installation process has on the cone resistance of CPT. Unlike this thesis, there is no comparison between this driving method and impact hammered piles.
- The differences in soil elevation in and around the pile will be compared during the experiments to gain a better understanding of what happens to the sand. Settlement after installation can be measured by doing that. This has not been done yet in other literature.

4. Experiments

In this chapter, the experiments conducted during the thesis will be explained. The experiments consist of four different batches where multiple piles are installed and subsequently loaded laterally. The details of each batch will be discussed in the corresponding sub-chapters. First, the timeline will be laid out. Secondly, the setup of the experiments will be shown. Then, the steps taken to preparation the tests will be discussed. After that, all four batches will be touched upon as well as their parameters and expectations.

4.1 Timeline

As the experiments carried out during this thesis were extensive and required thorough planning, the timeline for the experimental work will be explained below. Four different batches of experiments were conducted. Each batch was comprised of four different phases: filling, installing, loading, and emptying. These phases will be explained in detail in section 3.3. All in all, each batch required approximately three weeks to complete. The schedule of all the experiments is shown in Figure 4.1 below.

Actions	04-Jul	11-Jul	18-Jul	25-Jul	01-Aug	08-Aug	15-Aug	22-Aug	29-Aug	05-Sep	12-Sep	19-Sep	26-Sep	03-Oct	10-Oct
week	27	28	29	30	31	32	33	34	35	36	37	38	39	40	41
Batch 1															
Batch 2															
Batch 3															
Batch 4															

Figure 4.1: Test regime schedule

No work was carried out during weeks 30 to 33.

4.2 Setup

A general schematisation of the setup is given in Figure 4.2. This shows the pile positions in batches 2, 3 and 4 as well as the loading directions. The top figure shows an overhead view of the testing facility, with the locations of the piles marked as a circle and the distances between the pile centres and nearby walls/other piles indicated in centimetres. The loading direction in which the piles will be laterally loaded is indicated by two large arrows. The bottom right figure shows a front view, while the bottom left figure shows a side view. The nominal outer pile diameter for all piles was 32.29 cm.

Batch 1 differed from the other batches as it included installation only, i.e. the piles were not subjected to lateral loading. Hence, its results will not be covered in detail in this thesis. The different elements of the experiments will be discussed in this section, while the specific batches and their characteristics will be explained individually in section 4.3. All equipment specifications are presented in Appendix A.

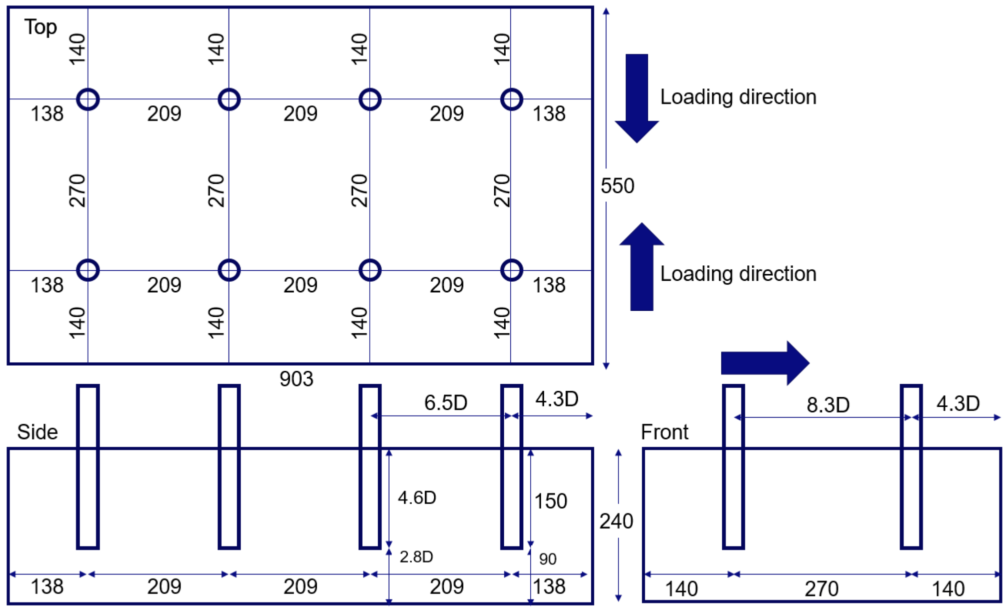

Figure 4.2: Schematisation of the experiment setup for batches 2, 3 and 4 (dimensions reported in cm)

4.2.1 Pile properties

Two different types of piles were used in the tests, with a total of eight piles. All the piles had a length of 2000 mm and a diameter of 323.9 mm (L/D ≈ 6). The piles differed in their wall thickness. Six piles had a wall thickness of 4 mm, and 2 piles (piles 3 and 8) had a wall thickness of 10 mm. The piles have all been measured to verify their dimensions. The measured pile dimensions are reported in Table 4-1.

Pile	Average diameter (mm)	Average thickness (mm)	Length (mm)
1	324	4.03	2030
2	324	3.65	2020
3	324	9.59	2031
4	324	3.72	2023
5	324	4.08	2026
6	324	3.60	2030
7	324	4.04	2028
8	324	9.61	2030

Table 4-1: Measured pile dimensions

On one end of the piles, a flange of 2 mm thickness has been welded to the pile to serve as an attachment point for the installation and loading devices. This flange is wider than the pile, with a diameter of 420 mm. This results in a pile geometry as shown in Figure 4.3.

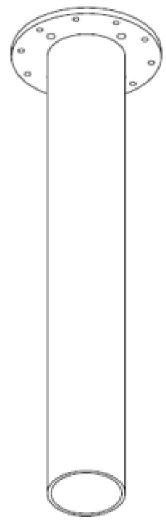

Figure 4.3: Pile geometry with flange

This flange was used to attach the vibratory hammer, a guidance system for impact hammering, as well as a plate through which lateral loading is carried out. These systems will be detailed in their respective sections below.

4.2.2 Testing facility

The tests have been carried out in the Deltares Water-Soil Flume (WSF) at its Delft location. The length of the testing pit was 9.03 m and its 5.50 m. The depth of the testing pit was 2.5 m. For this experiment, the testing pit was filled with sand up to a height of 2.4 m. A rolling wagon on rails above the testing pit was used for attaching the soil densification needles, CPT measurements, attachment point for the laser during driving and as attachment point for the loading device during lateral load testing. Pictures of the testing facility are shown below.

Figure 4.4: Testing pit before being filled with sand

Figure 4.5: Testing pit after being filled with sand and water

The sand used for the experiment was Sibelco S90 sand. This is a medium fine sand with a d_{50} of approximately 0.147 mm and a coefficient of uniformity c_u=1.6. The sand properties are indicated in Appendix B: Sand specifications. To produce medium dense testing conditions, the target relative density was between 40% and 60% and between 70% and 90% for dense sand conditions.

To construct the sand bed, the tank was first filled with water, after which the sand was deposited in layers. The layers were then vibrated with needles for densification. After skimming the tank with the needles, water was added, and another layer of sand deposited and densified. This process was repeated until the tank was filled. The preparations were different for each batch and will be explained in detail in section 4.3.

The WSF is equipped with a crane system spanning the entire length and width of the building. A crane on rails is situated overhead and enabled the transport of test elements such as wooden beams, a guidance frame, and the piles. This crane system was also used for vibratory driving, with the hammer being attached to the crane. Further details on the driving equipment and setup are discussed in 4.2.3. The crane has two possible lowering speeds: 110 mm/s and 10 mm/s. Both speeds were used during the experiments. Figure 4.6 showcases the lower part of the crane connected to the vibration hammer.

Figure 4.6: Crane with hammer and attached pile

4.2.3 Driving equipment

4.2.3.1 Vibratory driving

Vibratory driving was done with the help of an APE-23 hammer by CAPE Holland. The hydraulicly powered hammer has an eccentric moment of 1.3 kg*m. This figure was chosen after a driveability study conducted by CAPE. It was concluded that the standard eccentric moment of this hammer (2.3 kg*m) would be too strong for this pile and the expected soil profile. As a result, the hammer was modified to reach the figure of 1.3 kg*m.

The hammer was connected to the pile via an interface plate mounted on the flange. A picture of the mounting arrangement is shown below.

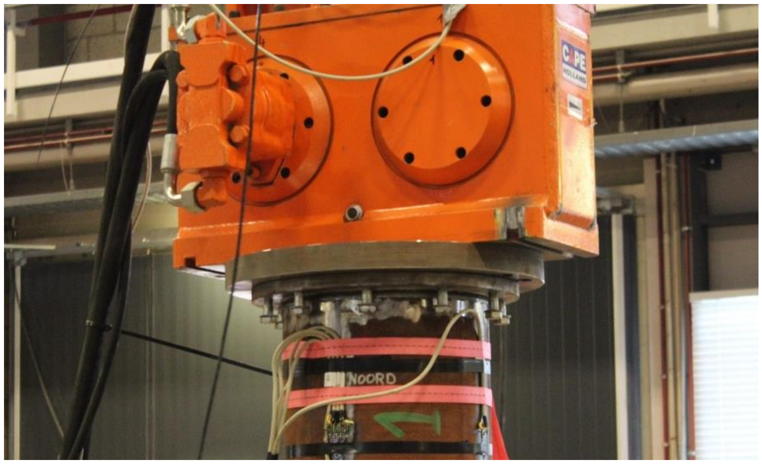

Figure 4.7: Close-up of hammer on the pile

As previously mentioned, the hammer was mounted on the overhead crane and had two possible lowering speeds: 110 mm/s and 10 mm/s. In addition to the flange on the pile, a steel guiding frame had been purpose-built for this experiment. The vibratory hammer was guided by sliding through the frame to prevent translation in one direction, as well as rotation.

Additionally, another guiding frame with wheels was placed between wooden beams. The hammer inside both guiding frames is shown in Figure 4.8 below. Figure 4.9 shows an overhead view of the guiding device placed between wooden beams.

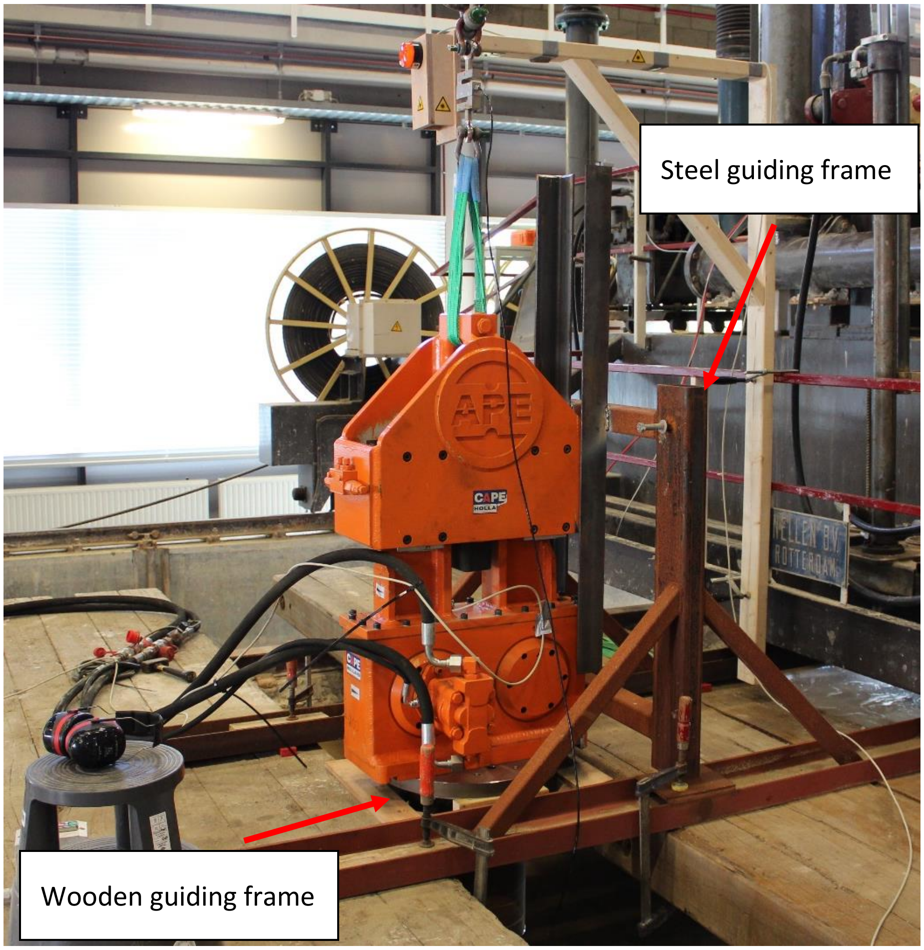

Figure 4.8: Hammer inside guiding frame

Figure 4.9: Overhead view of second (wooden) guiding device

4.2.3.2 Impact hammering

Impact hammering was done with a HL750 from VDB Funderingstechniek. The amount of falling weights, their weight and the falling height varied depending on the pile installation and are specified in section 4.3 for every batch. The hammer was rolled above the WSF onto wooden planks that cover it. A guiding tube for the falling weight was mounted above the pile to ensure it hit the pile centre and drove it straight into the ground. A simplified sketch of the hammering installation is shown in Figure 4.10.

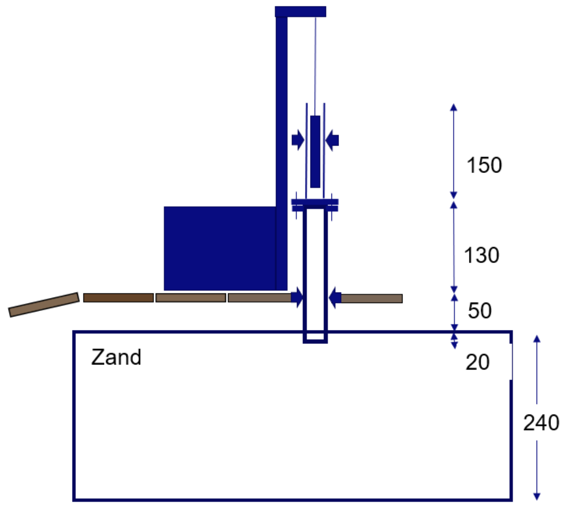

Figure 4.10: Impact hammer setup (dimensions reported in cm)

Figure 4.11: Impact hammer during installation

4.2.4 Loading equipment

After installation, the piles were loaded laterally with the use of a lateral loading device. The loading device was attached to the wagon, in a configuration schematized in Figure 4.12 below. Equipment specifications are provided in appendix A.

For loading, a MAC800 electric motor was combined with a gearbox and a spindle of 18 mm diameter. The theoretical maximum load of this combination was 316.2 kN and the theoretical maximum speed was 5 mm/s. However, the actual maximum applied load was 20 kN due to the chosen measuring equipment and its calibration range.

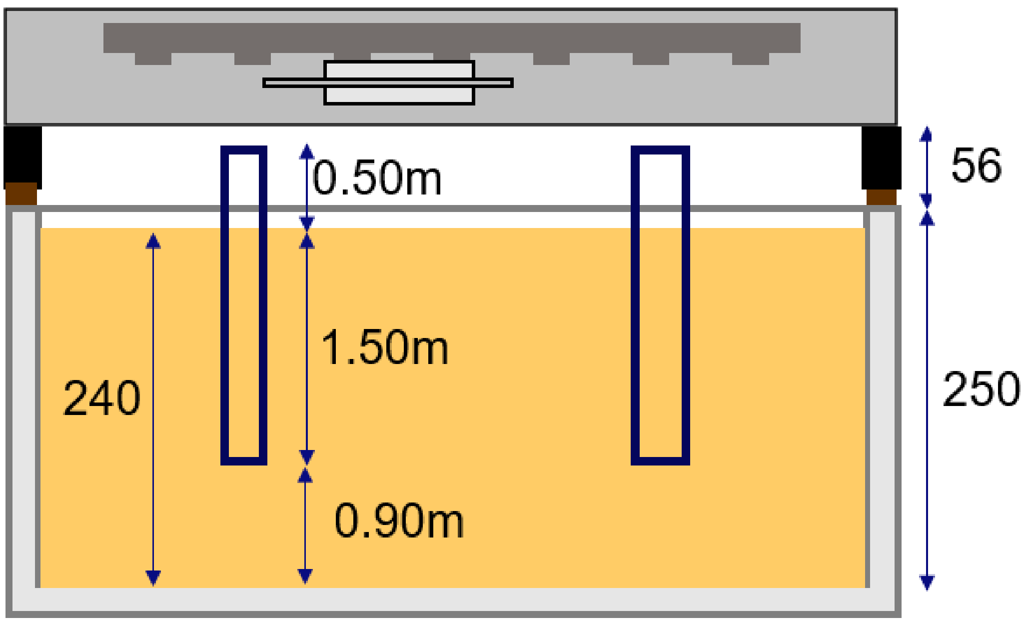

Figure 4.12: Configuration during loading

The loading device pulled the piles inwards, one pile at a time. The pile head was approximately 0.5m above ground level, with the exact height having been measured individually for all piles. The load application height was slightly above the pile head, see Figure 4.13. The exact load application point was 0.53m above the ground level. This load was transferred to the pile through a loading plate attached to the flange on top of it. The displacement was then measured through a ring on this same loading plate. This was done with a Temposonic magnetostrictive linear position sensor. Photos as well as a sketch of the loading plate and loading device are shown below.

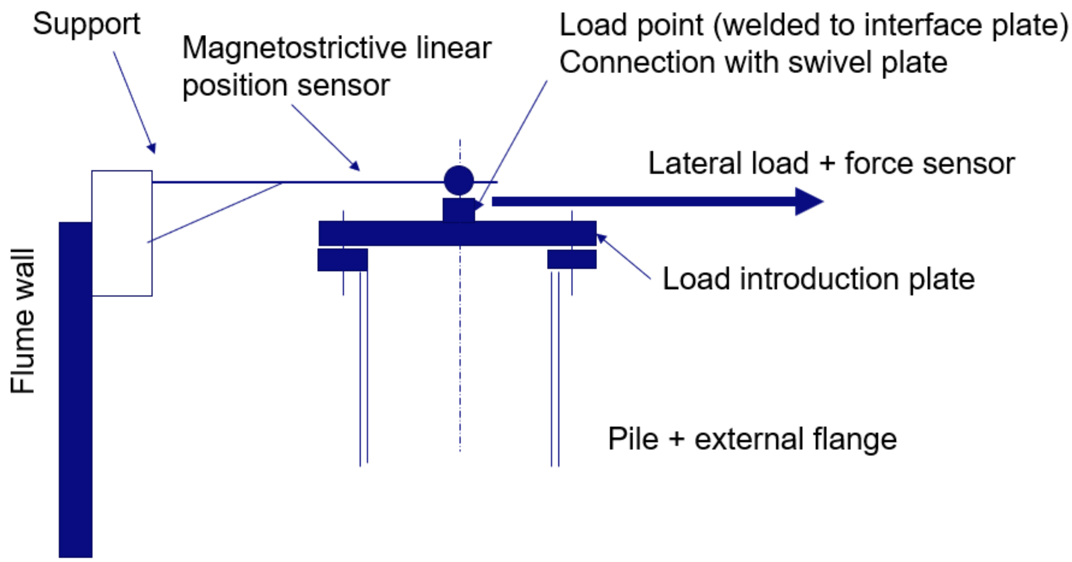

Figure 4.13: Sketch of the connection between pile and loading device

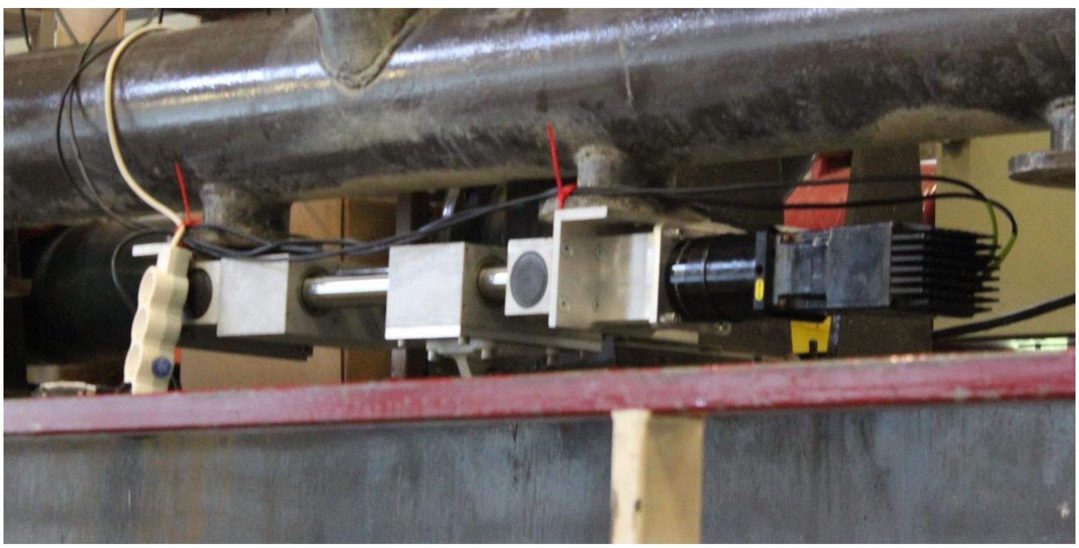

Figure 4.14: Loading device on wagon

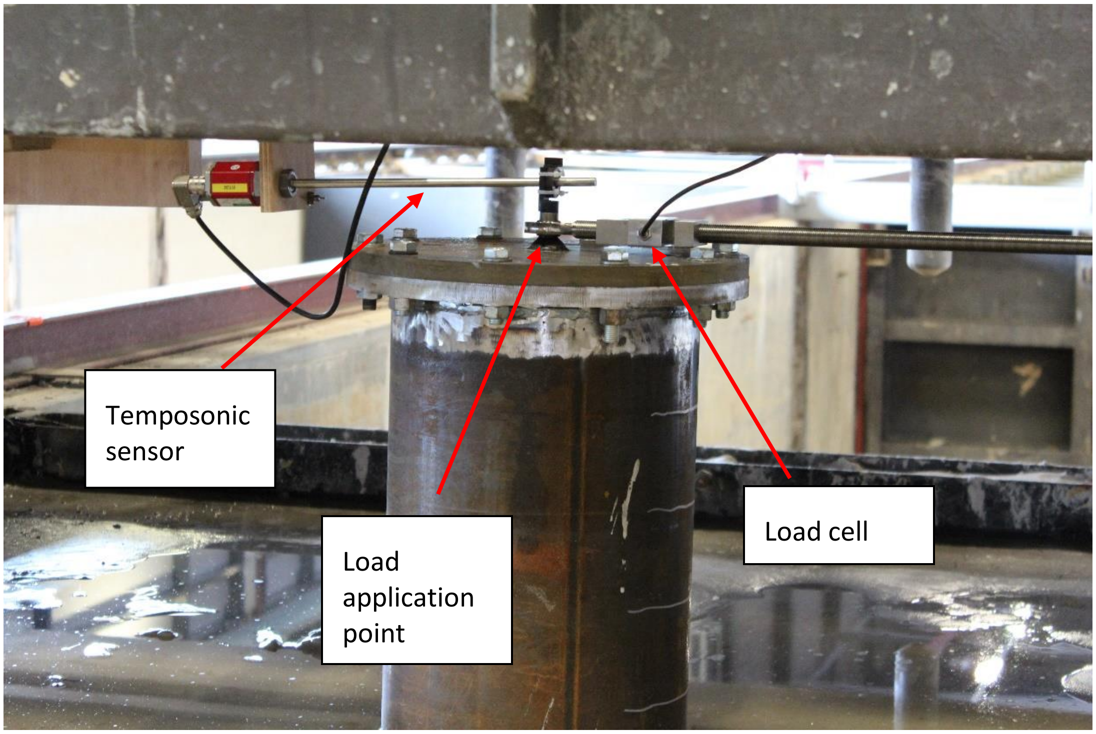

Figure 4.15: Connection between pile, loading device and sensor

4.2.5 Measuring equipment

Multiple sensors were used during the test. An overview of the various sensors, their positions, and their measuring windows is given in Table 4-2. Figure 4.16 presents a sketch of the different sensors and their locations in the experiment's setup. The specifications for all the equipment are presented in appendix A.

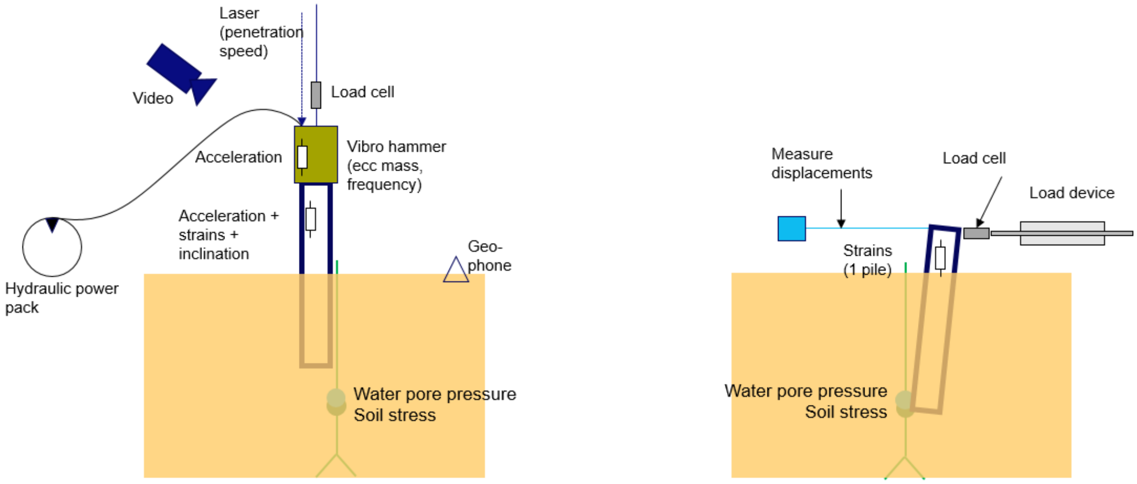

Figure 4.16: Sketch of the different sensors

The exact specifications of all the sensors are indicated in Appendix A.

Sensor	Position	Measuring during
Pore water pressure	In the soil, on the pile	Installation and loading
Total stress	In the soil, on the pile	Installation and loading
Frequency	On the vibro-hammer	Installation
Load cell	On the crane	Installation
Laser	On the pile	Installation
Strain gauge	On the pile	Installation and loading
Horizontal displacement	Attached to the wagon	Loading
Horizontal force	In the loading device	Loading

Table 4-2: Overview of used sensors

Based on this table, the sensors can be divided into three categories. The soil sensors, the pile and hammer sensors, and the loading sensors. These will be addressed separately below.

In addition to those sensors, an extensive cone penetration testing (CPT) campaign has been carried out during the entirety of the experiments. The details vary on a batch basis and will be explained in section 4.3.

4.2.5.1 Soil sensors

Two types of sensors were installed in the soil: pore water pressure sensors and total stress sensors. The pore water pressure sensors were mounted on the wall, to observe possible pore pressure build-up which could indicate liquefaction.

The total stress sensors were mounted onto a rod construction in the WSF before filling, at two positions near the piles on the East and West of the test basin. This rod was attached to the bottom of the tank. It consisted of a plate at a height of 1 m with a horizontal stress sensor as well as a pore water pressure sensor attached to it. The sensors were attached to a plate to ensure that there was no movement after filling the tank with sand. A PVC band was cut and placed around the edges of the total stress sensor to ensure a smooth stress distribution along the entire surface of the sensor. Without it, stress would accumulate on the edges of the total stress sensor. Photos of the sensor assembly are shown below.

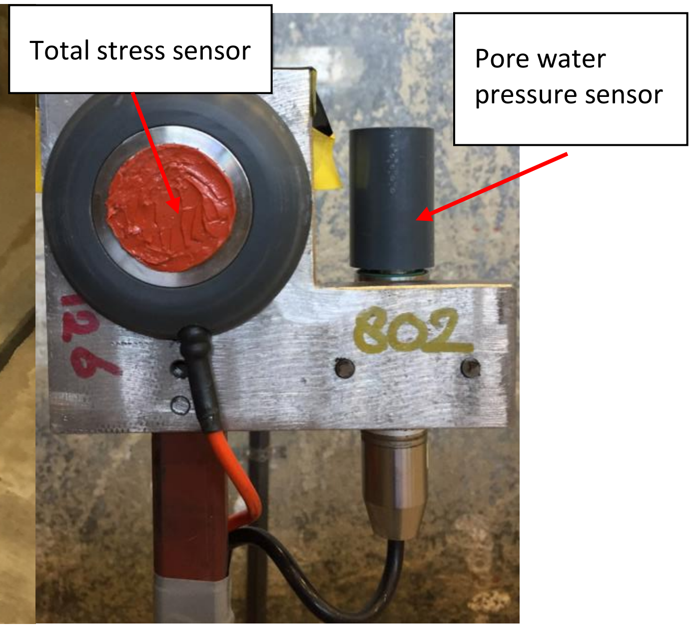

Figure 4.17: Sensor rod assembly *Figure 4.18: Close-up of the sensors on the plate*

Together with the horizontal stress sensors, pore water pressure sensors with a capacity of 5 bar were also mounted to the construction, both at a height of 1 m above the bottom of the WSF. Two other pore water pressure sensors were attached to opposing walls the location of the sensors as shown from above is demonstrated in Figure 4.19.

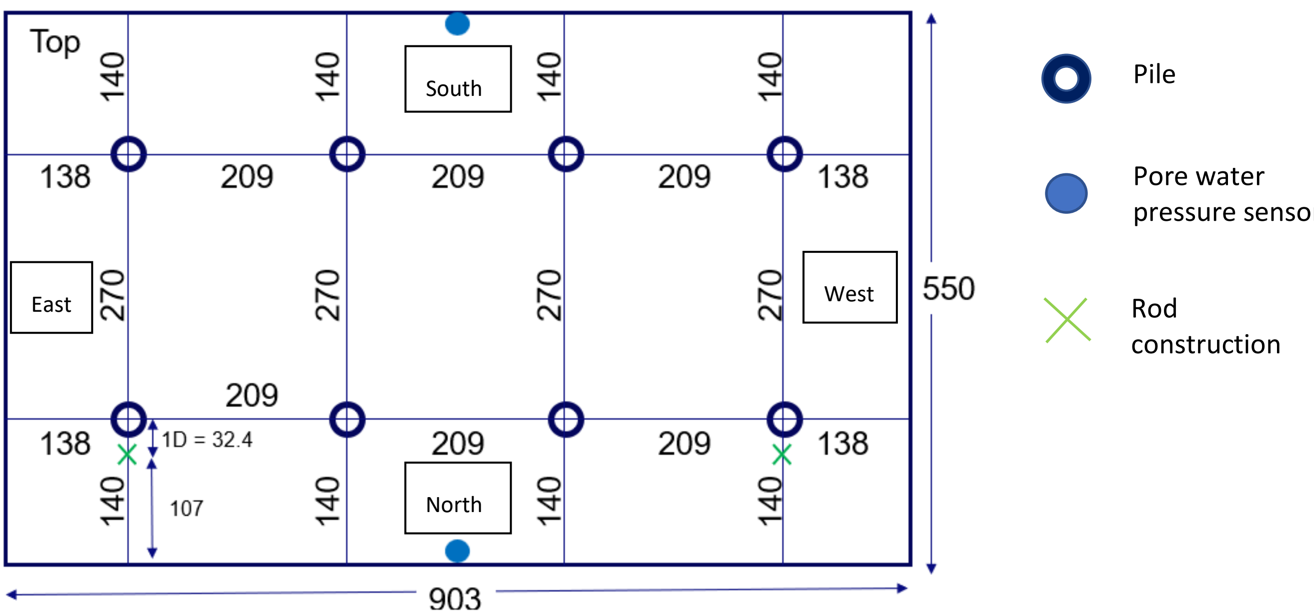

Figure 4.19: Location of soil sensors seen from above (distances in cm)

The total stress sensors used in the soil were Kulite LQ-080U stress sensors. The pore pressure sensors attached to the tank wall were ATM/N submersible transducers manufactured by STS.

4.2.5.2 Pile and hammer sensors

On the pile and the vibro-hammer, multiple sensors were installed and used during installation. The total pressure sensors attached to the pile wall were manufactured by Kyowa and were the PS-2KC and PS-10KC models with a capacity of 200 kPA and 1 MPa respectively. A close-up photograph is shown below. These sensors recorded the stress during installation only

Figure 4.20: Pore pressure sensor on pile wall

An accelerometer was placed on the vibratory hammer to measure the frequency. A load cell was placed on the crane to measure the weight of the system on the crane and detect when the pile is "standing" on the soil or if its weight is (partially) carried by the overhead crane. Mounted next to the pile, a laser measured the vertical displacement in order to compute the penetration speed and monitor the vertical movements of the pile during installation.

The load cell on the crane is a U9 load cell by Hottinger with a capacity of 20 kN. The laser was a Demetix DPE-30-500 Laser Distance Sensor.

These sensors measured data during installation of the pile to determine the installation parameters.

4.2.5.3 Loading sensors

During lateral loading of the pile, a magnetostrictive linear position sensor mounted on the wagon (see Figure 4.15) measured the displacement of the pile head. At the same time, the loading device was equipped with a load cell (the same model of load cell as on the crane during installation) measuring the force applied on the pile. A close-up picture of the sensors on the pile is shown in Figure 4.21.

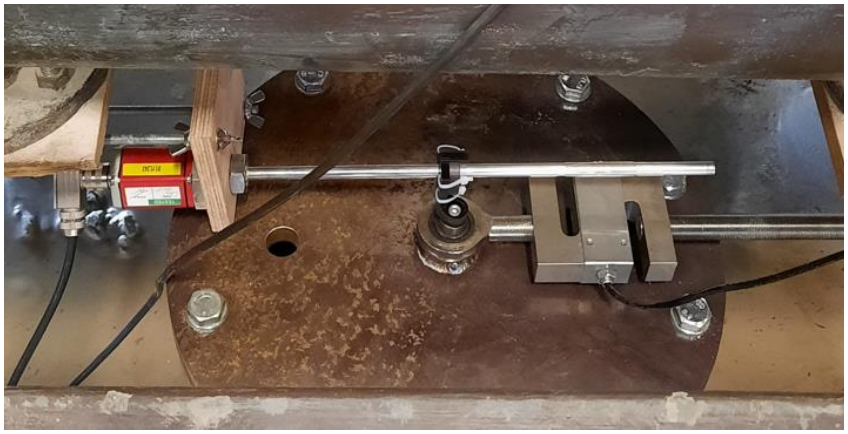

Figure 4.21: Top-down view of the loading sensor on the pile

Additionally, the ground sensors and some of the strain gauges on the piles were active during loading of certain piles to provide data if it was deemed interesting or useful.

4.2.5.4 CPT

In addition to the above sensors, the soil properties were measured at multiple moments throughout the experiments with a CPT rig mounted on the wagon. A photo of the CPT rig is shown in Figure 4.22. The details of the CPT, their locations and moment of measurement will be discussed per batch in section 4.3.

Figure 4.22: CPT rig mounted on wagon

4.2.5.5 Soil settlement measurements

In addition to all the above measurements, elevation measurements were carried out before and after installation with the help of a levelling instrument, shown in Figure 4.23. The measurement points were inside and outside of the pile.

Figure 4.23: Height measurement equipment

The measurements were read on a pole through the lens of the equipment in Figure 4.23. To interpret the readings, a reference reading was first taken on the corner of the tank (see Figure 4.24). This reference reading then allows a comparison with every subsequent reading, knowing the height of the corner of the tank compared to the sand surface. In the sketch below, a measurement taken before installation gave a reading of 1200 and a measurement taken after installation a reading of 1139.

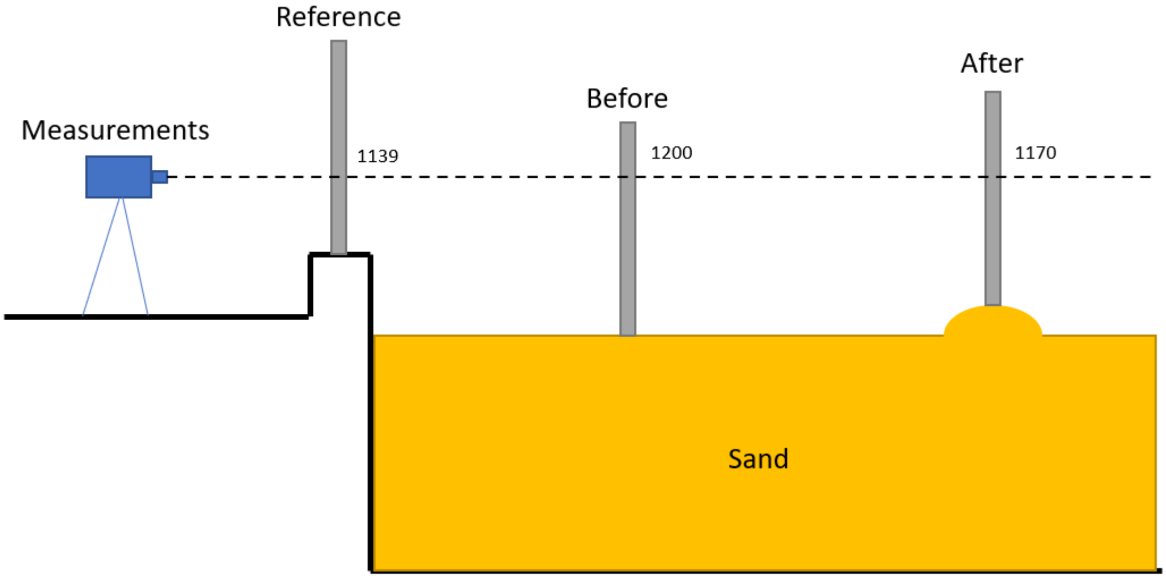

Figure 4.24: Sketch of the measuring equipment setup

4.3 Testing programme

The testing programme will be detailed for every batch. This included how many piles were installed, what installation parameters were used and what the loading regime was. The first batch was mainly used to test the equipment and determine which settings to use on the hammer and the loading device. All batches have been divided into preparation, installation, and loading. The logbook used for the duration of all experiments is presented in Appendix E: Experiment logbook.

4.3.1 Batch 1

4.3.1.1 Preparation

The sand in batch 1 was dense sand, with the aim of obtaining a relative density of 70% to 90%. CPT carried out after installation revealed a relative density of around 80%. The relative density calculations can be found in section 4.3.2.1. The tank was initially filled with 60 cm of water, after which a layer of 50 cm of sand was laid out with an excavator. The wagon with vibrated needles drove over the entire tank one way to densify the sand. This entire process was then repeated by adding 10 or 15 cm of water, 10 or 15 cm of sand and vibrating with the needles in the opposite way until reaching the full height of 2.4 m. The layering sequence is detailed in Figure 4.25, and the layer height in Table 4-3.

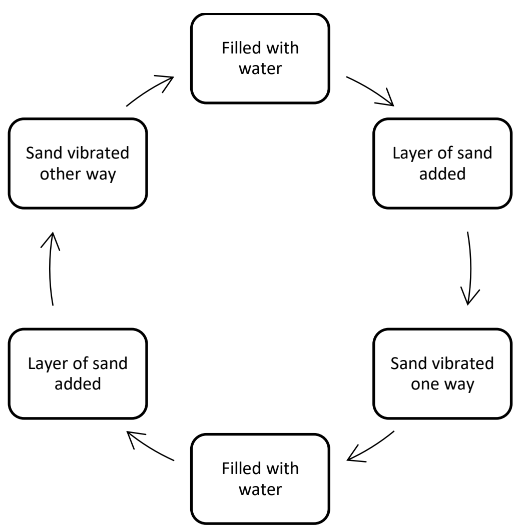

Figure 4.25: Layering sequence

Layer bottom [cm]	Layer top [cm]	Layer height [cm]
0	50	50
50	60	10
60	75	15
75	85	10

85	100	15
100	110	10
110	120	10
120	130	10
130	140	10
140	150	10
150	160	10
160	170	10
170	180	10
180	190	10
190	200	10
200	210	10
210	225	15
225	240	15

Table 4-3: Detailed layering sequence for batch 1

As shown in Figure 4.26, six needles were present on the wagon. The needles had a centre-to-centre distance of 78 cm, and 68 cm to the wall. Subsequent vibration drives were done in one direction, followed by the opposite direction to minimize the impact of driving in a single direction. The first layer was densified by needles moving from East to West, the next layer from West to East, etc.

Figure 4.26: Densification of the sand in progress

The result can be seen in Figure 4.5. The final sand depth was 2.4 m with a water table 5 cm higher than the sand surface.

4.3.1.2 Installation

As batch 1 was mostly used for testing of the equipment and the pile, more installations were planned during it than the other batches. In total, 14 installations were carried out with one instrumented pile (pile 1, see Figure 4.20) and one installation was carried out with a non-instrumented thick-walled pile. All piles were installed using the vibratory hammer. The piles in the last two positions were left in place to set up the loading device. The installation plan is shown below in Figure 4.27.

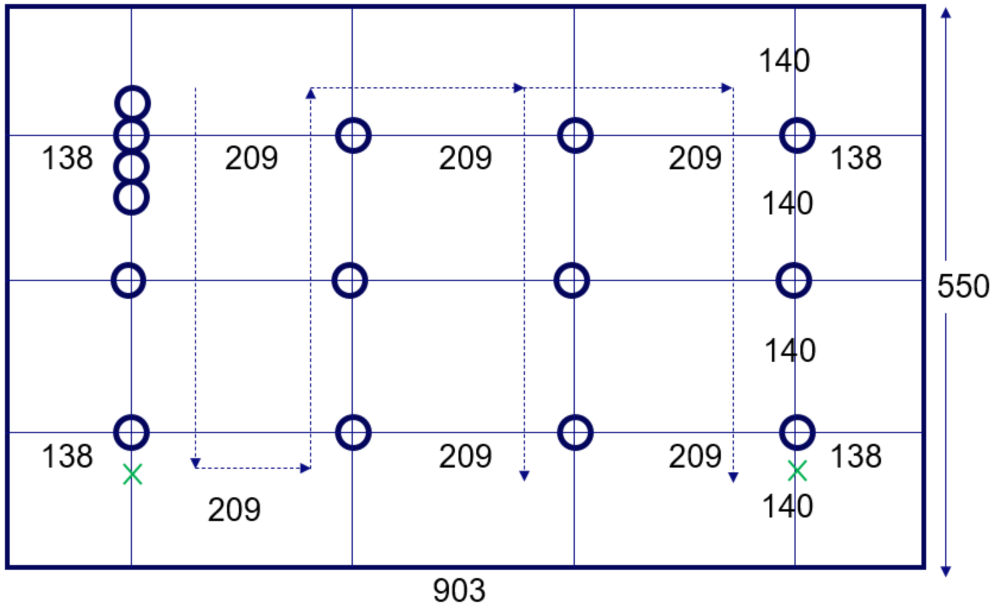

Figure 4.27: Installation plan of batch 1

The piles were installed to an embedded depth of 1.5 m. Figure 4.28 below shows a simple schematization of the cross-section of the WSF after installing the piles. This figure also shows the wooden beams going across the tank. These beams are used to provide support for the guiding frame and for the impact hammer.

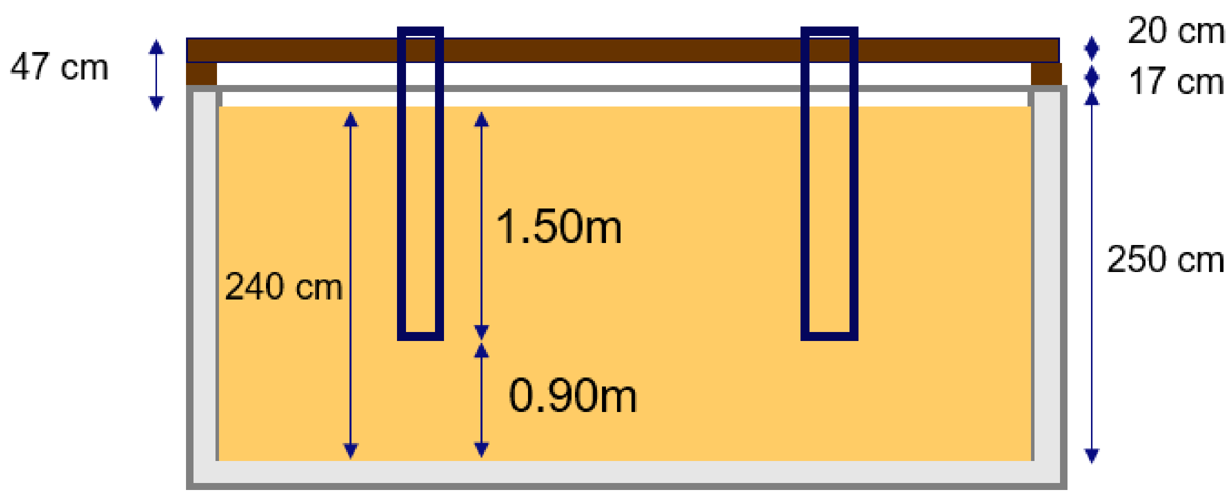

Figure 4.28: Schematisation of installed piles

4.3.1.3 Lateral loading

One pile was loaded at the end of batch 1 in order to test the loading device and tune the loading rate as well as generated feedback loops appropriately. This also allowed for identification of possible issues before the second batch. Both monotonic and cyclic loading tests were carried out.

After loading, the piles were extracted from the tank by attaching the vibratory hammer and operating it while pulling the piles out with the crane.

4.3.2 Batch 2

4.3.2.1 Preparation

The preparation of batch 2 was performed in a similar fashion as for batch 1.

As part of the preparation, CPT were carried out across the tank, as indicated in Figure 4.29. CPT were executed before, I between and after pile installations. After all pile installations, CPT were carried out right next to the pile flange, and others approximately 0.5D away from the pile wall. The results of those CPT are shown in Figure 4.30. During testing, the maximum cone penetration depth was 2.35 m (50 mm above the bottom of the tank).

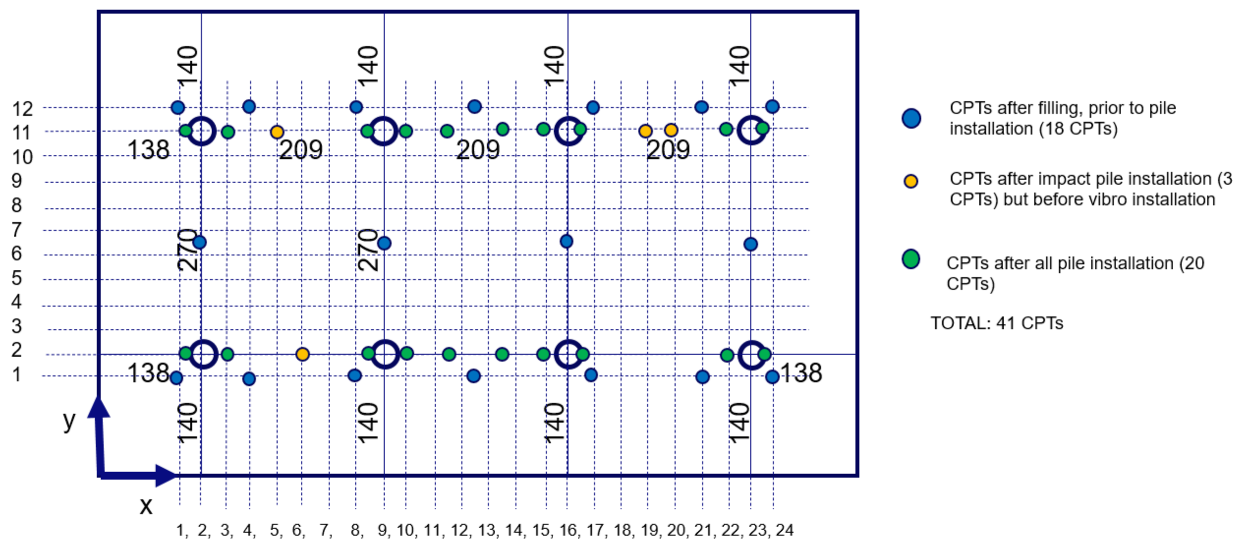

Figure 4.29: Cone penetration testing locations during batch 2

All CPT have an x and y location on the grid above. The grid has a spacing of 30 cm in the x direction and 30 cm in the y direction. The large circles indicate the pile positions.

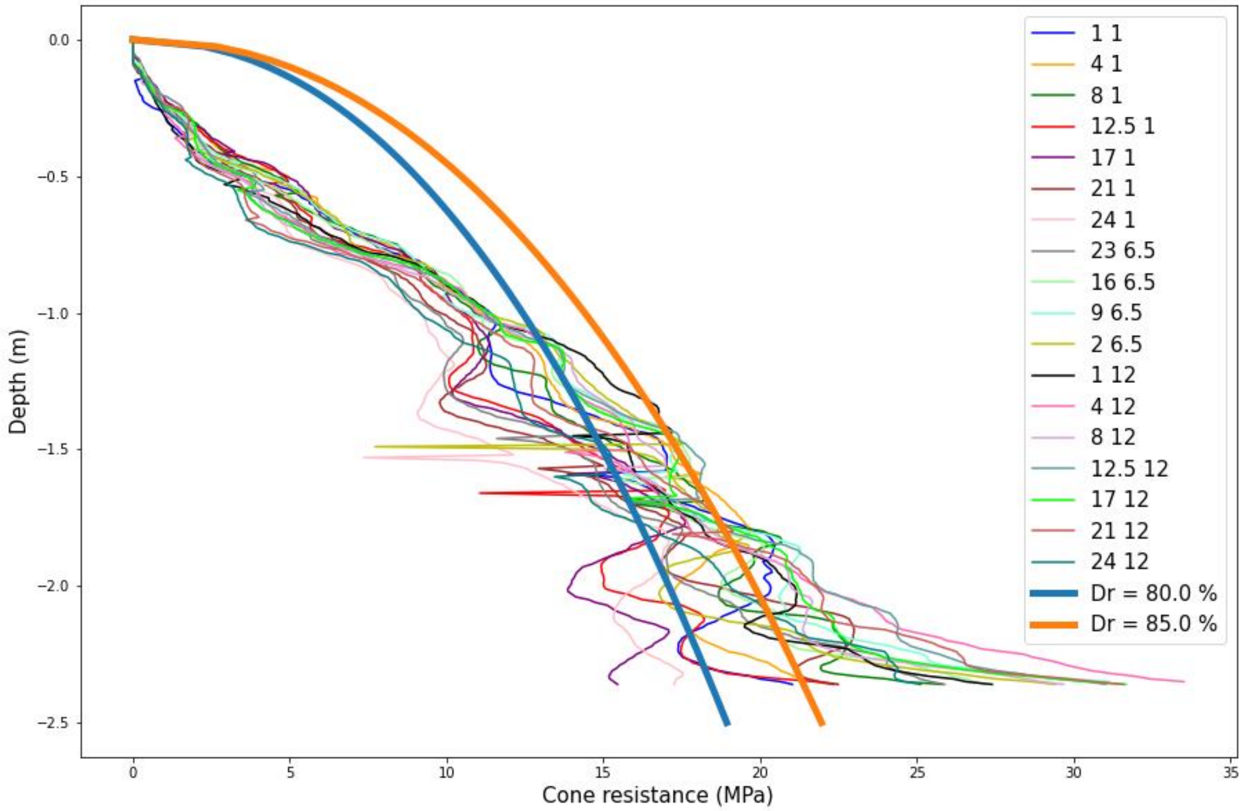

Figure 4.30: CPT results before installation

With the results from the CPT, it possible to estimate the actual relative density of the sand. For this, a study in shallow depth CPT was used (Krogh et al., 2022) as the depth of the sand bed in the experiments was 2.5 m. The following correlations for shallow depth CPT are used.

$$\sigma'_p = 0.33(q_t - \sigma_v)^{0.72}$$

$$OCR = \frac{\sigma'_p}{\sigma'_v}$$

$$K_0 = (1 - sin\varphi')OCR^{sin\varphi}$$

$$\sigma_m = \frac{\sigma'_v}{3}(1 + 2K_0)$$

$$RD = \frac{1}{2.96}\ln\left(\frac{q_c}{24.94\left({\sigma'_m}/{p_a}\right)^{0.46}}\right)$$

According to these equations, the CPT results above correspond to a relative density approximated to be between 80 and 85 %. The discrepancy in the top 1 m is due to a tendency of this method to obtain a curve that overestimates that layer, but it becomes accurate after that point. The last 0.2-0.5 m has an artificially high q_c value due to the concrete bottom of the tank creating a hard boundary.

4.3.2.2 Installation

During the second batch, eight piles have been installed at the same depth as during batch 1. Two thick-walled piles with a lower D/t, and six thin-walled piles. Three piles were installed using an impact hammer, and five with a vibratory hammer. Figure 4.31 shows the locations of the installed piles and Table 4-4 the installation methods and parameters for each pile. Green piles are impact hammered piles, and red piles are vibratory driven piles. The thick circles denote a thick pile (wall thickness of 10mm) while the thin circles denote a thin pile (wall thickness of 4mm).

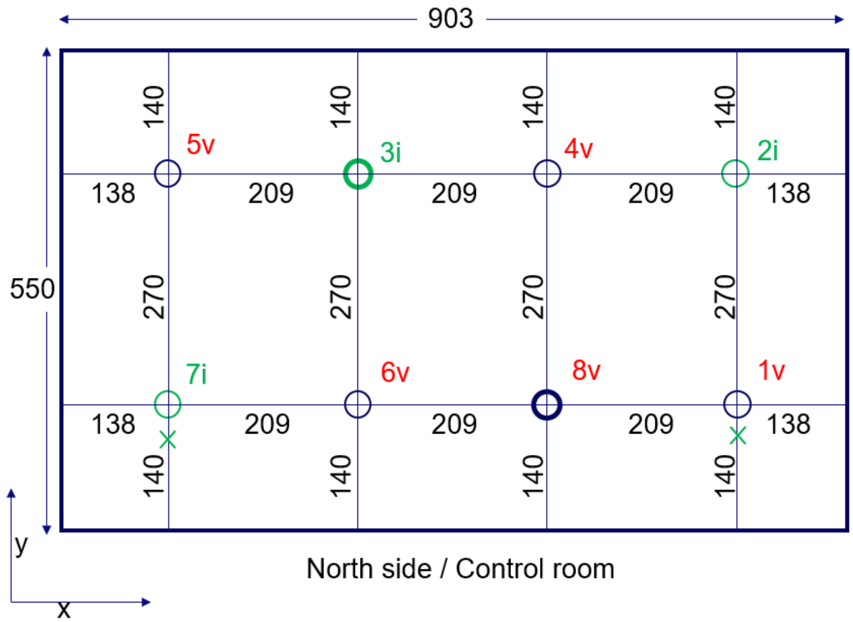

Figure 4.31: Pile locations for batch 2

Pile number	D/t	Impact Set 1	Impact Set 2	Speed	Frequency
1v	High	-	-	Low	Low
2i	Low	Low/High	-	-	-
3i	High	-	High/Low	-	-
4v	High	-	-	High	High
5v	High	-	-	High	Low
6v	High	-	-	Low	High
7i	High	-	High/Low	-	-
8v	Low	-	-	Low	High

Table 4-4: Installation parameters in batch 2

Piles installed at low frequency were vibrated around 20 Hz, while high frequencies corresponded to 35 Hz. Two different settings were used for the impact hammer. Set 1 used one falling weight of 285 kg with a falling height of 0.4 m. Set 2 used two falling weights of 285 kg with a falling height of 0.8 m. This was done to verify that the choice of setting did not have any influence on the lateral bearing capacity for impact hammered piles, as expected from the literature.

As indicated in Figure 4.29, CPT have also been carried out after installation to study the possible effects of installation on the soil density. The CPT after installation were carried 8 cm and 16 cm away from the pile wall. The results are shown in Appendix D: CPT results.

The CPT show an overall higher q_c after installation compared to before installation, although there is some scatter due to different installation methods and tests being taken at different distances from the piles. These results will be discussed in depth in chapter 5.

4.3.2.3 Lateral loading

All piles are first loaded monotonically until 4 kN, then subjected to a cyclic load between 0 and 4kN, and finally loaded monotonically up to 20 kN. The choice for 4 kN was made as that value is equal to 25% of the initially estimated lateral bearing capacity, the latter being the value at which the displacement is equal to 10% of the diameter, as obtained from a Plaxis 3D numerical model. The methodology for building this FEM model and its parameters is discussed in section 5.2.

Since this was the first batch with real loading, some adjustments still needed to be done to the loading device. Due to time constraints, some piles were subjected to only 100 cycles while others to 1000 cycles. After cyclic loading, all piles were subjected to a final monotonic loading phase. The magnitude of the load varied per pile, but the loading frequency was 0.1 Hz for all piles. As there were initially worries about excessive wear of the loading device, the choice was made to test with up to 12 kN at the first tests. The loading conditions for all piles are specified in Table 4-5.

Pile	Initial monotonic load (kN)	Cycles	Second monotonic load (kN)
1v	4	1000	20
2i	4	100	12
3i	4	100	12
4v	4	1000	12
5v	4	1000	12
6v	4	100	20

7i	4	1000	18
8v	4	100	20

Table 4-5: Loading conditions for all piles in batch 2

After loading, the piles were extracted from the tank by mechanical pull-out using the overhead crane. The extraction force was measured as well as the height of the sand present in the pile once extracted.

4.3.3 Batch 3

4.3.3.1 Preparation

For batch 3, the preparation was similar to that of batches 1 and 2. However, one densifying needle broke down, so the preparation process was slightly different in this regard. The remaining needles were spaced so that the centre-to-centre distance would be equal between all needles, and the distance to the wall remained the same.

The tank was initially filled with 60 cm of water, after which a layer of 50 cm of sand was placed with a crane. The wagon with vibrated needles drove over the entire tank one way to densify the sand. This process was then repeated by adding 10 or 15 cm of water, 10 or 15 cm of sand and vibrating with the needles in the opposite way until reaching the full height of 2.4 m. The layering sequence is detailed in Figure 4.32 and the layer height in Table 4-6.

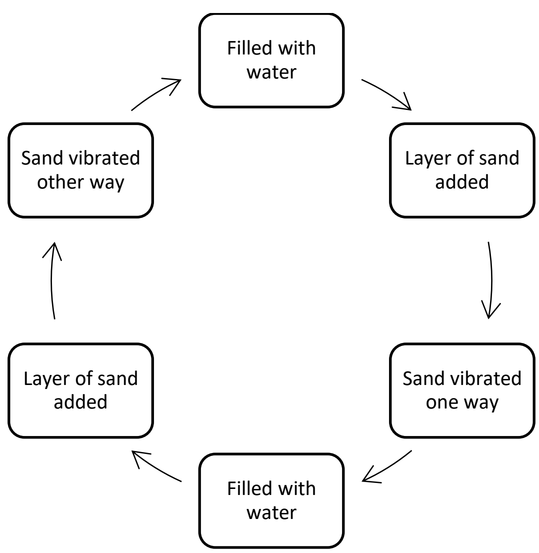

Figure 4.32: Layering sequence

Layer bottom [cm]	Layer top [cm]	Layer height [cm]
0	50	50
50	60	10

60	75	15
75	85	10
85	100	15
100	110	10
110	120	10
120	130	10
130	140	10
140	150	10
150	160	10
160	170	10
170	180	10
180	190	10
190	200	10
200	210	10
210	225	15
225	240	15

Table 4-6: Detailed layering sequence for batch 3

For this batch, five needles were present on the wagon due to a mechanical defect prior to the sand bed preparation. The needles had a centre-to-centre distance of 104 cm, and 68 cm to the wall. Subsequent vibration drives were done one way, then the other, to minimize the impact of driving in a single direction. The first height would for example be from East to West, then at the next height from West to East, etc.

As part of the preparation, CPT were carried out across the tank, as indicated in Figure 4.33. This figure also shows the locations of all other CPT that were carried out during the rest of the batch. The results of those CPT are presented in Figure 4.34. During testing, the cone penetration depth was 2.35 m (50 mm above the bottom of the tank).

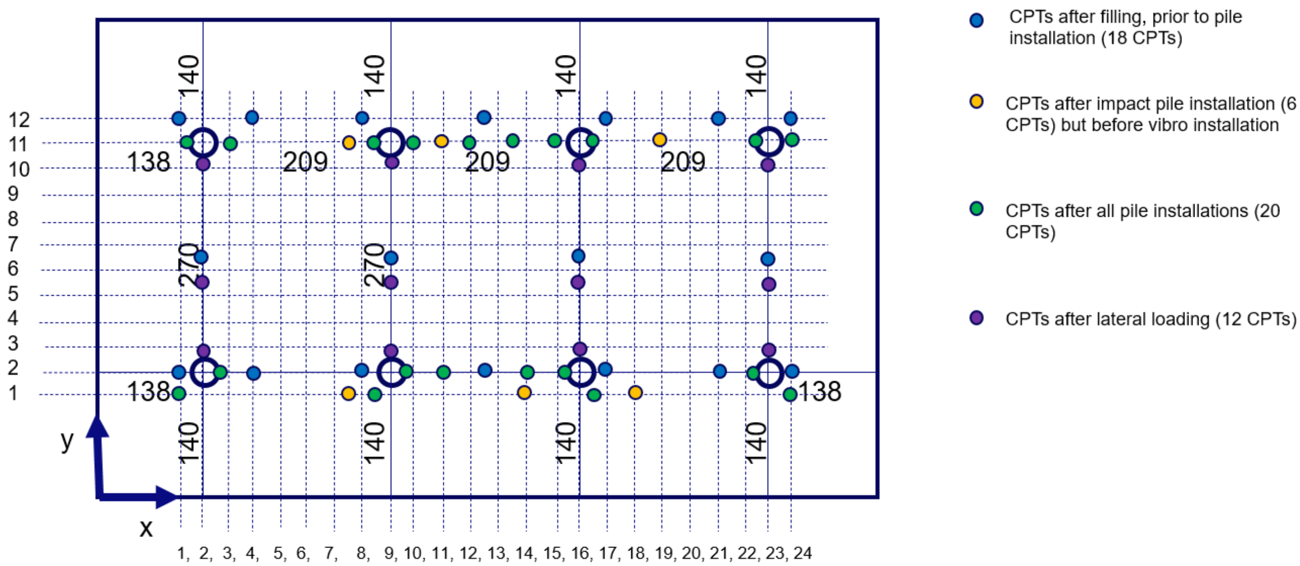

Figure 4.33: Cone penetration testing locations during batch 3

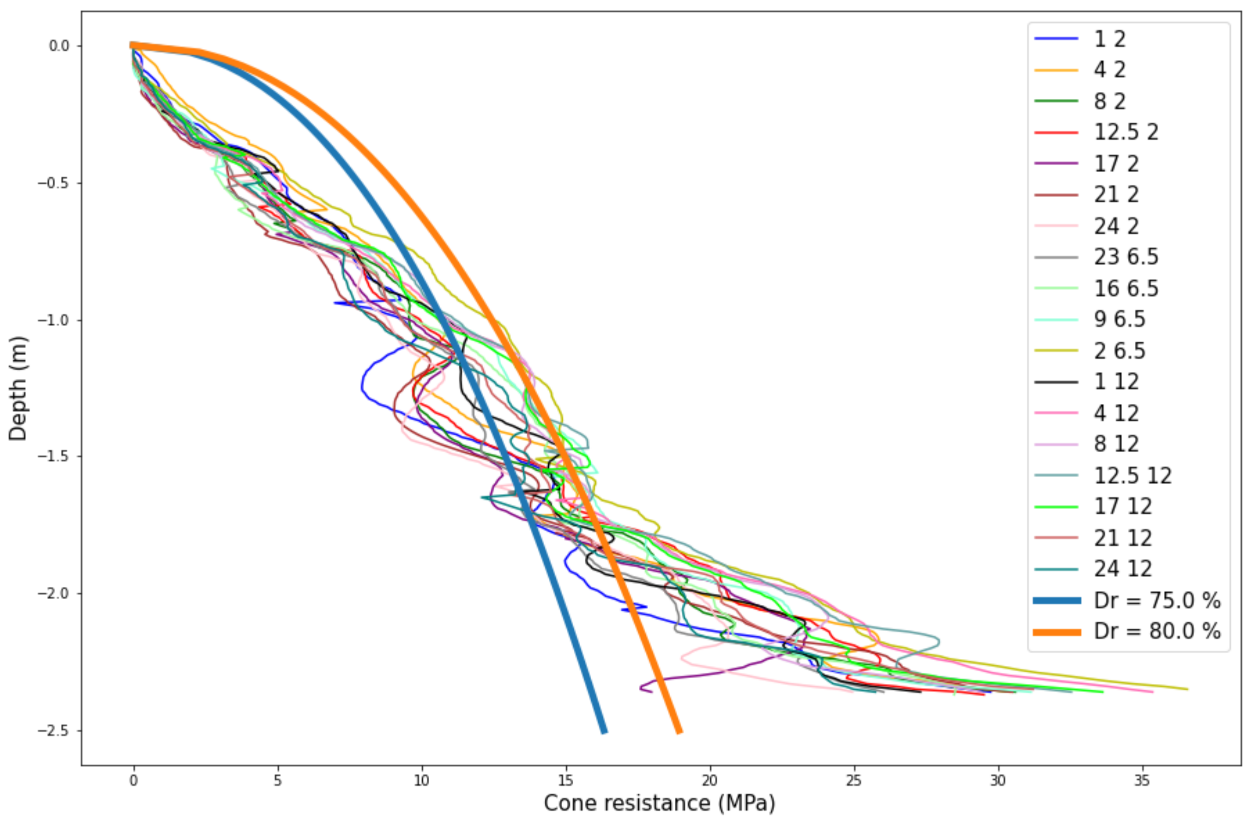

Figure 4.34: CPT results before installation

With the results from the CPT, it possible to estimate the actual relative density of the sand. For this, a study in shallow depth CPT was used (Krogh et al., 2022) as the depth of the sand bed in the experiments was 2.5 m. The same correlations are used as in batch 2.

According to these equations, the CPT results above correspond to a relative density approximated to be between 75 and 80 %. Overall, the sand in batch 3 was slightly looser than in batch 2. The discrepancy in the top 1 m is due to a tendency of this method to obtain a curve that overestimates that layer, but it becomes accurate after that point. The last 0.2-0.5 m has an artificially high q_c value due to the concrete bottom of the tank creating a hard boundary.

4.3.3.2 Installation

During the third batch, eight piles have been installed at the same depth as during batch 1 and 2. Two thick-walled piles with a lower D/t, and six thin-walled piles. Two piles were installed using an impact hammer, and five with a vibratory hammer. Figure 4.35 shows the locations of the installed piles and Table 4-7 the installation methods and parameters for each pile. Green piles are impact hammered piles, and red piles are vibratory driven piles. The thick circles denote a thick pile (wall thickness of 10mm) while the thin circles denote a thin pile (wall thickness of 4mm).

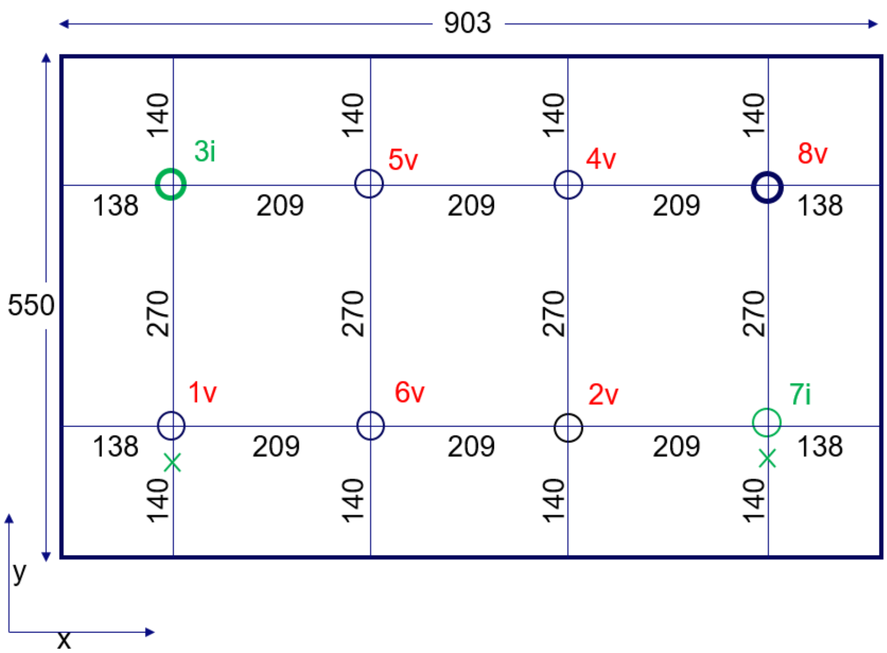

Figure 4.35: Pile locations for batch 3

Pile number	D/t	Impact Set 1	Impact Set 2	Speed	Frequency
1v	High	-	-	High	High
2v	Low	-	-	High	Low
3i	High	-	High/Low	-	-
4v	High	-	-	Free	Low

5v	High	-	-	Low	Low
6v	High	-	-	Low	High
7i	High	-	High/Low	-	-
8v	Low	-	-	Free	Low

Table 4-7: Installation parameters for batch 3

Piles installed at low frequency were vibrated around 20 Hz, while high frequencies corresponded to 35 Hz. Only one setting was used for the impact hammer. Set 1 used one falling weight of 285 kg with a falling height of 0.4 m. After having confirmed from batch 2 that installation settings for impact driving had no significant influence on the lateral stiffness, the choice was made for this more conventional method. Piles 4 and 8 were installed free hanging. This entails giving the belt between the pile and the vibratory hammer some slack before turning it on so that the driving speed is not influenced by technical restrictions of the crane's lowering speed.

As indicated in Figure 4.33, CPT have also been carried out after installation to study the possible effects of installation on the soil density. The CPT after installation were carried out 8 cm and 16 cm away from the pile wall. The results are shown in Appendix D: CPT results. These results will be presented in more detail in chapter 5.

4.3.3.3 Lateral loading

All piles are first loaded monotonically until 4 kN, then subjected to a cyclic load (1000 cycles) between o and 4kN, and finally loaded monotonically up to 20 kN. The choice for 4 kN was made as that value is equal to 25% of the lateral bearing capacity, the latter being the value at which the displacement is equal to 10% of the diameter, as obtained from a Plaxis 3D numerical model. The methodology for building this FEM model and its parameters is discussed in section 5.2.

Most pile were subjected to 1000 cycles, only pile 2v was subjected to 500 cycles due to time constraints. After cyclic loading, all piles were subjected to a final monotonic loading phase. The loading frequency for cyclic loading was 0.1 Hz.

Some CPT were also carried out after lateral loading to investigate the influence of loading on soil properties.

After loading, the piles were extracted from the tank by mechanical pull-out using the overhead crane. The extraction force was measured as well as the height of the sand present in the pile once extracted.

4.3.4 Batch 4

4.3.4.1 Preparation

For batch 4, the preparation was different from the previous batches to achieve a different sand density. The sand density was medium dense.

The desired sand density for this batch was dense. The tank was initially filled with 80 cm of water, after which a layer of 70 cm of sand was placed with a crane. The wagon with vibrated needles drove over the entire tank one way to densify the sand. For this batch, as the target density was lower than the previous batches, the needles only skimmed the surface. this can be seen in Figure 4.36. This entire process was then repeated, but less frequently than in previous batches. It was done at the following heights: 130 cm, 205 cm, 240 cm.

One of the needles still being defect, 5 needles were present on the wagon just as in batch 3. The needles had a center-to-center distance of 104 cm, and 68 cm to the wall. Subsequent vibration drives were done one way, then the other, to minimize the impact of driving in a single direction. The first height would for example be from East to West, then at the next height from West to East, etc.

Figure 4.36: Vibrating needles during installation of batch 4

As part of the preparation, CPT were carried out across the tank, as indicated in Figure 4.37. This figure also shows the locations of all other CPT that were carried out during the rest of the batch. The results of those CPT are shown in Figure 4.38. During testing, the cone penetration depth was 2.35 m (50 mm above the bottom of the tank).

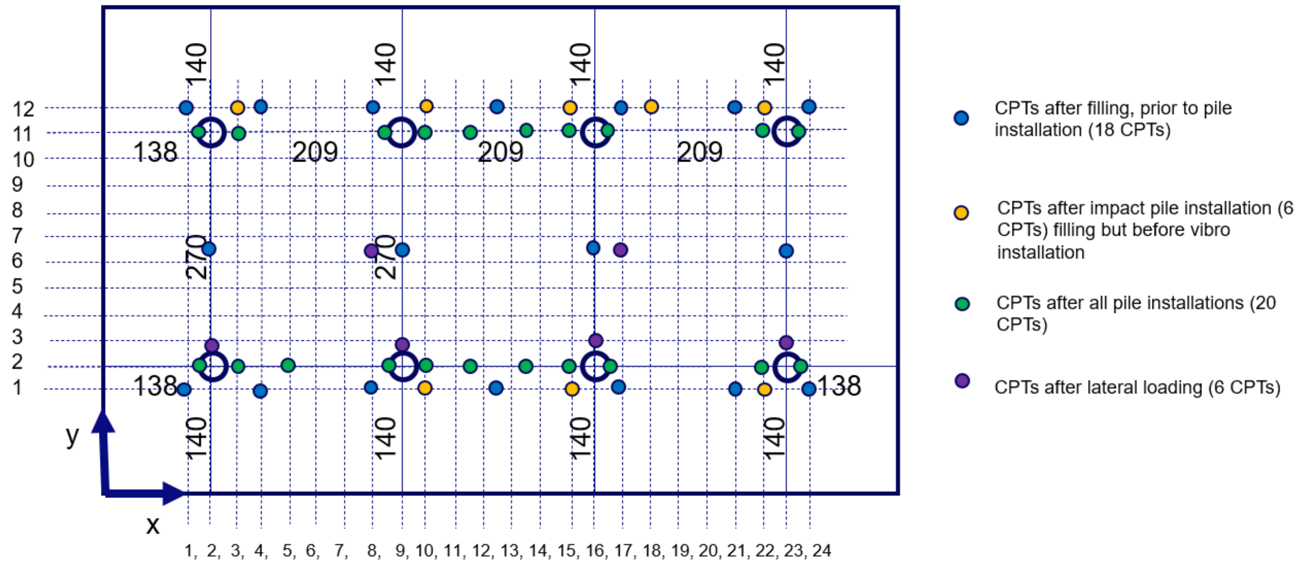

Figure 4.37: Cone penetration testing locations during batch 4

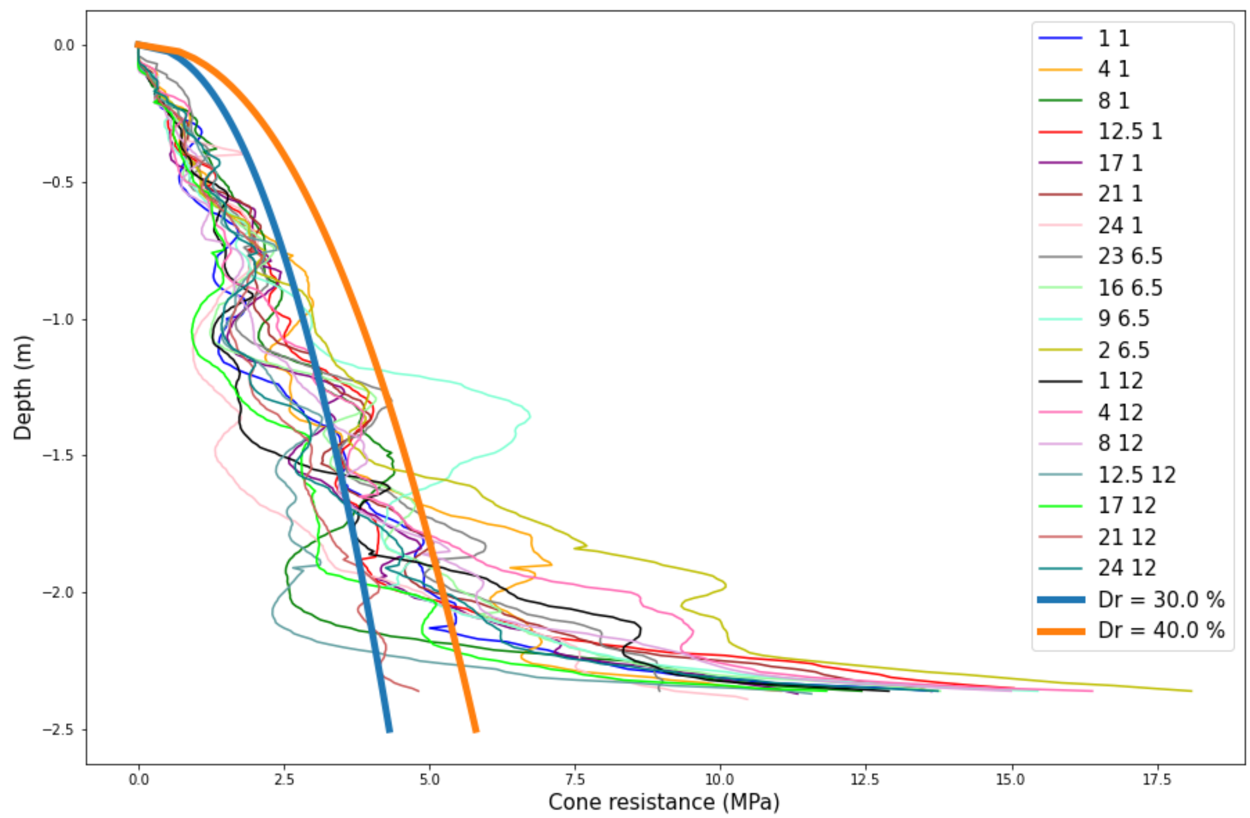

Figure 4.38: CPT results before installation for batch 4

With the results from the CPT, it possible to estimate the actual relative density of the sand. For this, a study in shallow depth CPT was used (Krogh et al., 2022) as the depth of the sand bed in the experiments was 2.5 m. The same correlations as in batches 2 and 3 are used. However, this method is less accurate in low consolidation sands. Using methods for more normally consolidated sands, the results might be slightly higher.

According to these equations, the CPT results above correspond to a relative density approximated to be between 30 and 40 %. The last 0.2-0.5 m has an artificially high q_c value due to the concrete bottom of the tank creating a hard boundary.

4.3.4.2 Installation

During the fourth batch, eight piles have been installed at the same depth as during batch 1 and 2. Two thick-walled piles with a lower D/t, and 6 thin-walled piles. Three piles were installed using an impact hammer, and five with a vibratory hammer. Figure 4.39 shows the locations of the installed piles and Table 4-8 the installation methods and parameters for each pile. Green piles are impact hammered piles, and red piles are vibratory driven piles. The thick circles denote a thick pile (wall thickness of 10mm) while the thin circles denote a thin pile (wall thickness of 4mm).

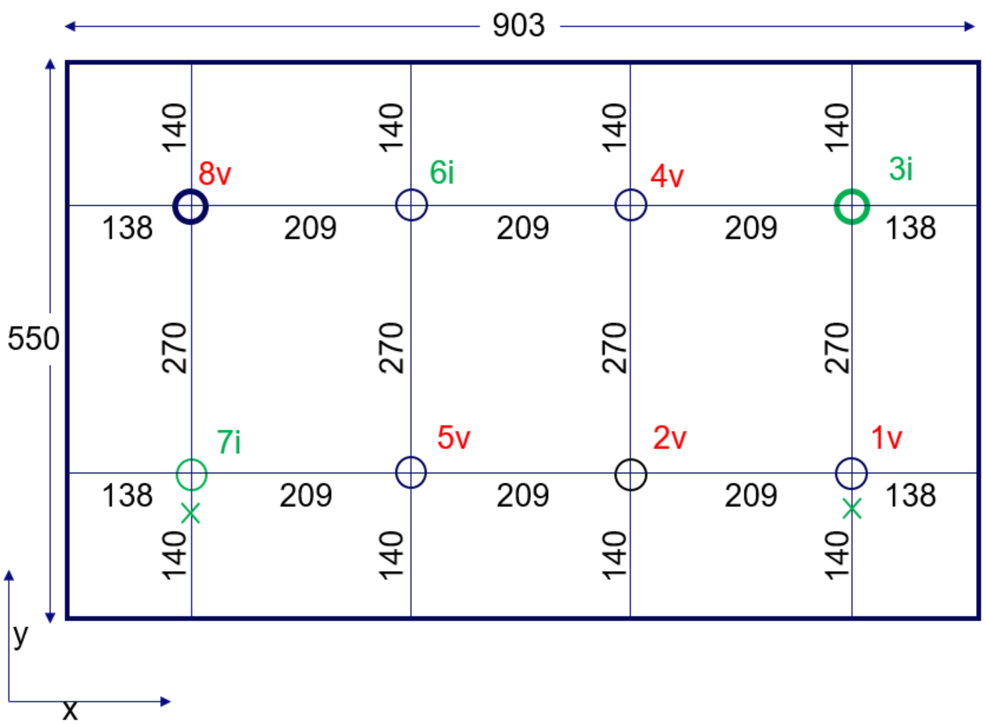

Figure 4.39: Pile locations for batch 4

Pile number	D/t	Impact Set 1	Impact Set 2	Speed	Frequency
1v	High	-	-	Low	23 Hz
2v	Low	-	-	High	23 Hz
3i	High	-	High/Low	-	-

4v	High	-	-	High	23 Hz
5v	High	-	-	Low	23 Hz
6i	High	-	High/Low	-	-
7i	High	-	High/Low	-	-
8v	Low	-	-	Low	23 Hz

Table 4-8: Installation parameters for batch 4

All piles were vibrated at 23 Hz for this batch because the hammer was expected to be too powerful with a higher frequency. The experience of the previous batches combined with the different sand density led to this conclusion. The chosen frequency of 23 Hz was the practical minimum frequency, as any lower frequency could lead to resonance in the crane and hammer system used for the SIMOX experiments. Additionally, since there was only one batch in medium-dense sand, it was deemed better to vary a single parameter in order to have more duplicates Only one setting was used for the impact hammer. Set 1 used one falling weight of 285 kg with a falling height of 0.1 m.

As indicated in Figure 4.37, CPT have also been carried out after installation to study the possible effects of installation on the soil density. The CPT after installation were carried out 8 cm and 16 cm away from the pile wall. The results are shown in Appendix D: CPT results.

4.3.4.3 Lateral loading

All piles were first loaded monotonically until 3 kN, then subjected to a cyclic load (1000 cycles) between 0 and 3 kN, and finally loaded monotonically up to 14 kN. The choice for 3 kN was made as that value is equal to 25% of the lateral bearing capacity, the latter being the value at which the displacement is equal to 10% of the diameter, as obtained from a Plaxis 3D numerical model. The methodology for building this FEM model and its parameters is discussed in section 5.2.

Most piles were subjected to 1000 cycles, only pile 3i was subjected to 500 cycles due to time constraints. After cyclic loading, all piles were subjected to a final monotonic loading phase. The loading frequency for all piles was 0.1 Hz. The loading conditions for all piles are specified in Table 4-9.

Pile	Initial monotonic load (kN)	Cycles	Second monotonic load (kN)
1v	3	1000	14
2v	3	1000	14

3i	3	500	14
4v	3	1000	12
5v	3	1000	14
6i	3	1000	14
7i	3	1000	14
8v	3	1000	14

Table 4-9: Loading conditions for all piles in batch 4

Some CPT were also carried out after lateral loading to investigate the influence of loading on soil properties.

After loading, the piles were extracted from the tank by mechanical pull-out using the overhead crane. The extraction force was measured as well as the height of the sand present in the pile once extracted.

Just as in any experimental process, some parts of the programme deviated from the aimed values inadvertently. Namely, there were variations in embedment depth and sand density. This is why, to ensure the experiment results are as accurate as possible and that the comparison is done under the same conditions for all piles, they must be corrected for some of these inaccuracies first. The following chapter will explain these corrections and discuss the effect of them.

5. Corrections and FE model

In this chapter, the methods and tools used for data interpretation will be explained. The finite element model will be addressed first, followed by an explanation of the applied corrections. The data interpretation computational work has been done with python.

5.1 Corrections

While the experiments happened in a controlled environment with very few varying conditions, there are some differences between piles that need to be accounted for and corrected to ensure that the comparison of results is done under the same conditions. The results have been corrected for three varying parameters: the cone resistance q_c of CPTs before pile installation, the pile embedment length, and the pile wall thickness. The procedure followed is similar to that in the work of Achmus et al. (2020).

Possible variations in cone resistance could be due to an uneven preparation of the sand bed. Pile embedment length varied in the order of centimetres throughout the experiments due to the difficulty of stopping the equipment at the exact final penetration when driving. The maximum difference in average q_c over the length of the pile in one batch was around 6.8 MPa (16.7 and 9.5 MPa).

Although an embedment length close to the desired length was achieved in most cases, there were some imprecisions when turning off the vibrating hammer that would result in differences of a few centimetres, especially for the piles driven at a high penetration speed. The largest difference between two piles in a single batch was found to be 8.9 cm (approximately 4.5% of the total pile length).

Finally, the pile wall thickness was measured before the experiment on the piles and was found to deviate slightly from the nominal thickness (in the order of tenths of millimetre). The largest deviation from the nominal value was 0.35 mm. This was on a pile (pile 2) with a nominal thickness of 4 mm, meaning this is a deviation of almost 9%. The actual pile wall thickness is presented in Table 4-1. To account for the effect such a difference could have, a correction was investigated by means of a 3D FE model.

5.1.1 CPT

To eliminate any possible effect of soil heterogeneity across the tank, data from CPT has been used to apply a correcting factor to the pile displacement. This factor was calculated individually for every pile in each batch.

To do this, the average q_c over the depth of the CPT (2.5 m) was calculated in three layers for every pile location prior to installation. A top layer from 0 to 1 m depth, a middle layer from 1 to 1.5 m depth, and a bottom layer from 1.5 to 2.5 m depth. Then, the finite element model (which consisted of applying lateral loading up to 3 or 4 kN, depending on the soil density) was run with input soil parameters of the HS Small model derived from correlations with the highest average q_c, as well as the lowest average q_c. The parameters were determined with correlations suggested by Brinkgreve et al. (2010). Details about this are described in section 5.2.2. Batches 2 and 3 had a negligible difference between both corrected displacements for extreme q_c values under a 4kN lateral point load (0.3% and 0.8% respectively). However, for batch 4 in medium dense sand, the difference in lateral displacement between two extreme average values of q_c was 5%. Hence, a CPT correction was only applied to the results from batch 4.

To calculate the value of the correction factor, the difference of each pile location with the highest q_c was calculated, which was then compared to the largest difference. The pile location with the lowest average q_c value has a correction factor of 5%, and every other pile is somewhere between 0 and 5%. This means that the following calculations were applied:

$$d = q_{c;max} - q_{c;n}$$

$$\alpha = \frac{d}{d_{max}} \times 0.05$$

For example, a pile location with a q_c exactly in the middle of the two extremes will have a correction factor α of 2.5%.

The pile displacement at the top of the pile during all loading phases was then multiplied by said factor during interpretation.

$$y_{cor} = y \times (1 + \alpha)$$

5.1.2 Pile embedment length

Ideally, each installed pile would have an embedment length of 1.5m, and the length above ground equals 0.5m. In practice, the measurements that have been carried out during the experiments show that most piles deviate slightly from this value, some of them having a shorter embedment length, others having a larger one with individual differences of up to 60 mm. This may lead to misinterpretation of the results, as piles with a larger embedment depth will mobilise a larger soil resistance than piles with a lower embedment. Because of this, results might be skewed in the favour of piles with a larger embedment length. To make sure that piles are not misinterpreted as stiffer simply because they are deeper into the sand, a correction factor must be applied to all piles. Additionally, this also affects the height of the load application point (load eccentricity).

Similarly to section 5.1.1 for the CPT correction, the pile embedment length correction was done by means of the finite element model. The model was run with two different embedment lengths: 1.50m and 1.55m. The displacement under a lateral load of 4 kN is compared for both cases, which gives a difference of 22% in batch 2 and 19% in batch 3. In the medium dense sand with a lateral load of 3 kN, this difference grew to 31%. Once this value is obtained, a correction factor is calculated following the same method as indicated in the previous section for the CPT correction.

The pile displacement during all loading phases was then multiplied by said factor during interpretation.

5.1.3 Wall thickness

As seen in 4.2.1, some piles deviate from the nominal wall thickness of 4 mm. The largest difference between two piles is between piles 5 and 6, where the difference is 0.5 mm. To ensure that differences in pile wall thickness do not affect the presented results, a verification was done similar to what was done in section 5.1.1 for the CPT data.

The finite element model was run with a pile thickness of 3.6 mm, followed by a computation for a wall thickness of 4.1 mm. Under a lateral point load of 4kN, the displacement for the thinnest pile is 1.2% larger than the displacement for the thinnest pile. For a wall thickness of 4.1 mm, the displacement was 1.598 mm while it was 1.629 mm for a thickness of 3.6 mm. In the medium dense sand and under a lateral load of 3 kN, this percentage was 2%. Since this is the largest difference and all others will be smaller, wall thickness variations are concluded to have no significant influence on the results of the lateral loading tests. As a result, no correction factor will be applied to the results for this.

5.1.4 Overview

The results presented later in the thesis will always be corrected, with an uncorrected figure in each batch to give insight on the magnitude of the corrections. In dense sand, the results will be corrected for embedment length only, while a CPT correction will be applied in the medium dense sand as well. The correction can make for large differences, which are almost entirely due to embedment length (5 - 30%). CPT based corrections are much smaller (0 – 2%) and only applied in batch 4. In some cases, piles that appeared to have a large displacement before correction were in fact not installed up to the entire desired embedment depth. This led to larger displacements which were corrected to compare them as if they were installed with a load application point.

There are points to remember about the corrections which have been applied to the results, and how they will be interpreted. Firstly, there was also a margin of error of 0.5 cm when carrying out the height and CPT measurements. Such a margin of error will be carried through the corrections and into the final corrected results. Secondly, the correction carried out during this thesis is a way to ensure more fairness when making comparisons between piles. There are inherent limitations to the corrections such as the accuracy of the input and limitations of the numerical model and the correlations used to obtain the soil parameters. As a result, the corrected values might still deviate from ideal values.

This needs to be considered when observing the results and making conclusions. Plots that are close to each other both before and after would still be considered within the margin of error of the corrections. Definitive conclusions about curves that are close together cannot be drawn. It can only be inferred that they are similar as they are within the margin of error of the corrections.

5.2 Finite element model

The finite element model (FEM) served as a reference calculation for applying a correction to the results obtained from the experiments. This model serves as an estimation of the behaviour of a wished-in-place pile with no installation effects. The finite element calculations were done in Plaxis 3D using the HSS (Hardening Soil Small) soil model. The choice for this soil model was made due to the sandy soil and the fact that the focus of the model was mostly to look at the behaviour of the pile under very small strains. The finite element model will be explained in this section, including model geometry, soil properties, and pile and load properties. Three different models were created, one for each batch. The geometry of the model did not change between batches, only the soil properties.

5.2.1 Model geometry

The model geometry was the same for all batches, and consisted of three elements: the soil, the pile, and the pile-soil interface. In this model, half of the situation was modelled to optimize computation time. This was possible due to the symmetry of the loading condition and material. Plaxis using x and y as horizontal coordinates and z as vertical coordinates, the model dimensions can be described as having a length in x direction of 5 m, a depth in y direction of 2.5 m, and a height in z direction of 2.4 m.

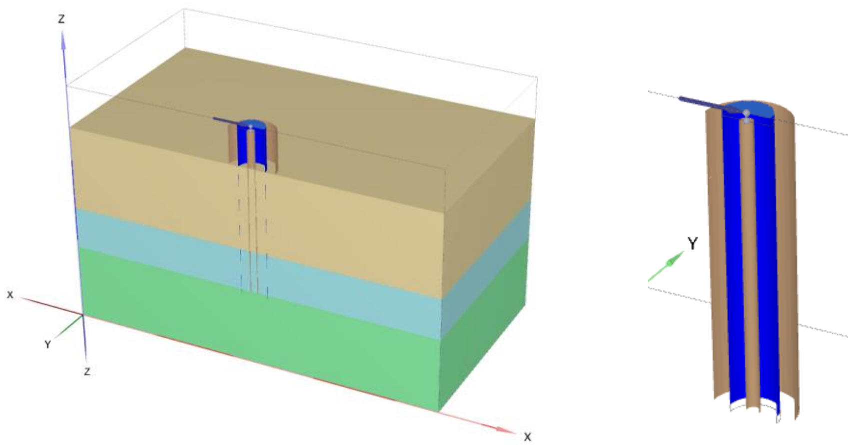

Figure 5.1: (right) Plaxis model geometry and (left) monopile plate elements and interface

Figure 5.1 depicts a general view of the model as well as the pile (blue) and interface (brown) elements. The soil was divided in three layers: a top layer of 1 m thickness, a middle layer of 0.5 m thickness, and a bottom layer of 0.9 m thickness. The soil properties will be adressed in section 5.2.2. The pile was modelled as a half-cyllinder with a length of 2 m, of which 1.5 m is embedded into the soil. The pile had a closed top part which represents the top plate used in the experiments for load application. The load application point was in the centre of the plate.

The model was designed in a way that allows the comparison of two piles: one with the desired embedment length, and another with a larger embedment. To achieve this, the pile was cut into surfaces and interfaces that can be activated depending on the desired scenario. One phase of the model had the pile embedded 1.5 m into the sand, another phase had the pile embedded 1.55 m into the sand. This will be explained in further detail in section 5.2.3.

5.2.2 Soil properties

The soil properties in the model were calculated with the method of Brinkgreve et al. (2010) as done in Gavin et al. (2020). This method takes as input the relative density RD and outputs parameters used by the HSS soil model in Plaxis. The correlations used are shown below, where RD is expressed as a percentage and the reference pressure is p_{ref} = 100 kN/m^2.

$$\gamma_{unsat} = 15 + 4.0RD/100\ [kN/m^3]$$

$$\gamma_{sat} = 19 + 1.6RD/100\ \ [kN/m^3]$$

$$E_{50}^{ref} = 60RD/100\ \ [MN/m^2]$$

$$E_{oed}^{ref} = 60RD/100\ \ [MN/m^2]$$

$$E_{ur}^{ref} = 180RD/100\ \ [MN/m^2]$$

$$G_0^{ref} = 60 + 68RD/100\ \ [MN/m^2]$$

$$m = 0.7 - RD/320\ \ [-]$$

$$\gamma_{0.7} = (2 - RD/100) \cdot 10^{-4}\ \ [-]$$

$$\varphi' = 28 + 12.5RD/100\ \ [°]$$

$$\psi = -2 + 12.5RD/100\ \ [°]$$

$$R_f = 1 - RD/800\ \ [-]$$

The relative density was calculated with the help of relations suitable for shallow CPT (Krogh et al., 2022).

$$\sigma'_p = 0.33(q_t - \sigma_v)^{0.72}$$

$$OCR = \frac{\sigma'_p}{\sigma'_v}$$

$$K_0 = (1 - sin\varphi')OCR^{sin\varphi}$$

$$\sigma_m = \frac{\sigma'_v}{3}(1 + 2K_0)$$

$$RD = \frac{1}{2.96}\ln\left(\frac{q_c/p_a}{24.94\left(\sigma'_m/p_a\right)^{0.46}}\right)$$

Where σ'_v is the lateral effective stress, φ' is the critical state friction angle, and p_a is the atmospheric pressure (100 kPa) For these relations, the average q_c within a layer was used. The sand was divided into three layers (bottom layer between z = 0 and z = 0.9, middle layer between z = 0.9 and z = 1.5, top layer between z = 1.5 and z = 2.5) all having a different q_c and thus different soil parameters. The soil parameter values changed per batch as well and are shown in Table 5-1. For batches 2 and 3, all layers had a saturated unit weight of γ_{sat} = 20 kN/m^3 and an unsaturated unit weight of γ_{unsat} = 18 kN/m^3. For batch 4, the unsaturated unit weight was γ_{unsat} = 17 kN/m^3.

	E_{50} (MPa)	E_{oed} (MPa)	E_{ur} (MPa)	m (-)	Φ' (°)	ψ(°)	R_f (-)	e_{init} (-)
Batch 2, top	48	48	144	0.45	38.84	8	0.9	0.5
Batch 2, middle	48	47	144	0.45	42.07	8	0.9	0.5
Batch 2, bottom	48	45	144	0.45	43.25	8	0.9	0.5
Batch 3, top	48	48	144	0.45	40.20	8	0.9	0.5
Batch 3, middle	48	47	144	0.45	41.96	8	0.9	0.5
Batch 3, bottom	48	45	144	0.45	43.72	8	0.9	0.5
Batch 4, top	24	24	72	0.58	28.67	3	0.9	0.5
Batch 4, middle	24	24	72	0.58	34.21	3	0.9	0.5
Batch 4, bottom	24	24	72	0.58	38.45	3	0.9	0.5

Table 5-1: Parameters for the HS Small model

5.2.3 Pile and load properties

The pile was modelled as a half-cylinder with a diameter of 324 mm and a length of 2 m. The pile embedment depth and location in the model differed depending on the phase of the model. The comparison between both cases is shown in Figure 5.3. Building the model this way allowed for a comparison of two scenarios without having to run the model twice. This was achieved with the phases indicated below.

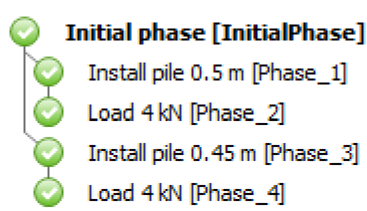

Figure 5.2: Phases used for the FEM

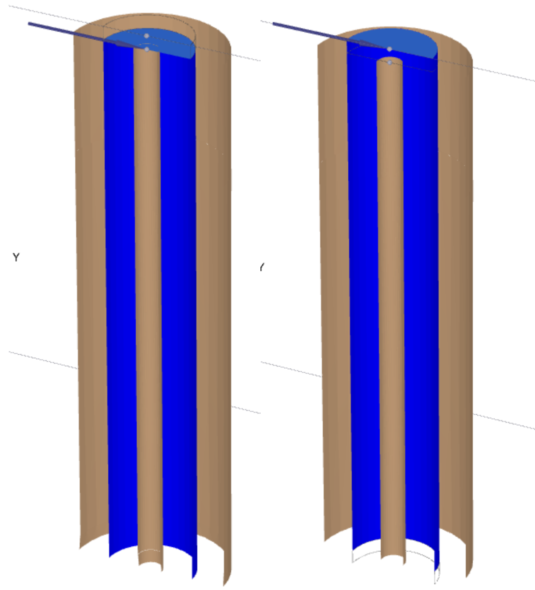

Figure 5.3: (left) Pile embedded 1.55m into the sand and (right) pile embedded 1.5 m into the sand

The plate elements used for the pile walls were made of an isotropic and linear material with the properties of steel. The plate on top of the pile was assumed to be rigid and was modelled as such. This allowed the horizontal forces to be distributed evenly on the pile, which is close to reality where the plate was bolted to the pile flange. The material properties of both plates are shown in Table 5-2. The interface properties were taken from the adjacent soil, which is discussed in the previous section.

Plate	γ (kN/m³)	E (kN/m²)	ν	d (mm)	G (kN/m²)
Pile wall	78.50	210×10^6	0.2	4	87.50×10^6
Pile head	0	210×10^6	0	4	105×10^6

Table 5-2: Plate properties

The load was modelled as a point load in the x direction in the FEM. The load application point on the pile was the centre of the top plate, at the y = 0 coordinate. The z coordinate of this point load changed depending on the pile embedment length, as can be seen in Figure 5.3. Since the pile was modelled as a half-cylinder here, the value of the load applied in the model must be equal to half the actual load. This means that in the batches where the initial monotonic load was 4 kN, the value of the load in the model must be 2 kN. In batch 4, where the load during the experiments was 3 kN, the load in the model was 1.5 kN.

6. Results

In this chapter, the experiment results will be presented and discussed. When presenting results, pile names will often be indicated as “Pile n x” where *n* is a number from 1 to 8, and *x* is either “v” or “i”. The number denotes the number that was painted on the pile, used for organisation purposes and to keep track of the piles. The letter following that gives information on how each pile was installed. A “v” signifies a vibratory installation, whereas a “i” means an impact hammer installation.

6.1 Installation

Installation data consists of data from the total stress sensors in the soil, the pore water pressure sensors in the soil, the strain gauges near the tip of the piles, the load on the crane, and the frequency measured on the vibro-hammer. These were measured as a function of time and pile penetration, the latter provided by the laser present near the pile. For all the batches, the figures showing pile penetration as a function of time are presented in appendix B.

6.1.1 Batch 2

Table 6-1 presents the installation parameters for all piles in batch 2. As a reminder, set 1 used one falling weight of 285 kg with a falling height of 0.4 m. Set 2 used two falling weights of 285 kg with a falling height of 0.8 m. High speed corresponded to a crane lowering speed of 110 mm/s whereas low speed corresponded to a crane lowering speed of 10 mm/s. High frequency was roughly equal to 35 Hz and low frequency was roughly equal to 20 Hz.

Pile number	D/t	Impact Set 1	Impact Set 2	Speed	Frequency
1v	High	-	-	Low	Low
2i	High	-	X	-	-
3i	Low	X	-	-	-
4v	High	-	-	High	High
5v	High	-	-	High	Low
6v	High	-	-	Low	High
7i	High	X	-	-	-
8v	Low	-	-	Low	High

Table 6-1: Installation parameters for batch 2

6.1.1.1 Total stress sensors

Two total stress sensors were installed into the ground, and piles 1v and 7i were installed right next to those sensors. As such, these two piles were the most relevant when looking at total stress sensor data. The data from those sensors collected during the installation of both piles is shown in Figure 6.1.

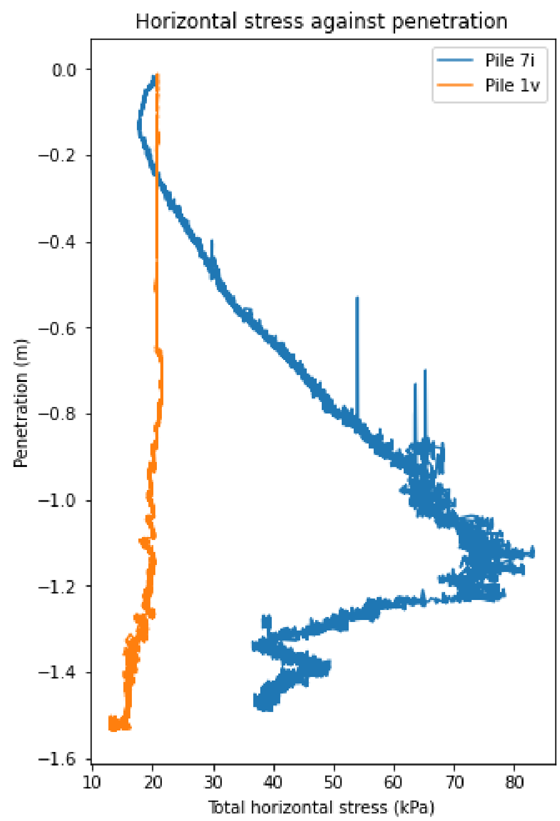

Figure 6.1: Total horizontal stress as a function of penetration for batch 2

During the installation of pile 1v, the total horizontal stress in the soil decreased slightly, while it increased during the installation of pile 7i (going from a base of 25 kPa to 750 kPa the moment the pile toe passes the location of the sensor).

Additionally, stress sensors were placed on the pile wall and recorded the horizontal stress during installation. The results shown in Figure 6.2 present the total stress on the exterior pile wall for the same two piles as previously. The sensors with a denomination code beginning by B1 are the sensors on the vibrated pile (1v) and the ones starting by B2 were placed on the impact hammered pile (7i).

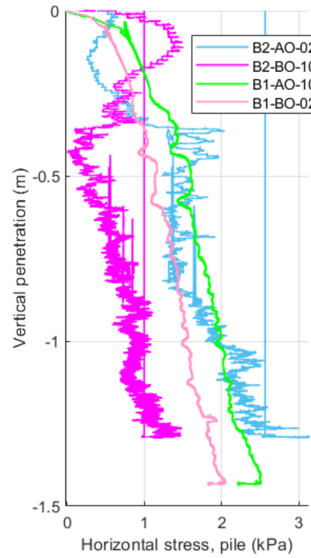

Figure 6.2: Total stress sensors on the pile wall during installation in batch 1

This figure shows that the stress on the pile wall is very similar for both methods. This confirms that the stress increase seen in figure 6.1 is present at the toe of the pile, but not directly adjacent to the pile wall. The installation method does not seem to influence total stress on the outer pile wall. Unfortunately, almost all sensors situated on the pile wall failed after batch 2, resulting in a lack of results to compare figure 6.2 with.

6.1.1.2 Pore water pressure sensors

During installation, the pore water pressure sensors next to the wall did not register any significant increase in pore water pressure. These sensors were used to monitor possible liquefaction of the sand bed. Liquefaction did not happen during batch 2. While some oscillations were present in the readings from the sensors near the pile when driving the pile, no increase of the mean pore water pressure was recorded. This was the case for all installed piles in batch 2. All pore water pressure plots are present in Appendix C: Installation results. In the figures, the pore pressure sensors are referred to with their position on the four cardinal coordinates. Figure 4.19 shows the position of all the sensors in the soil as well as which sensor corresponds to which direction.

6.1.1.3 Strain gauges

Strain gauges were installed on pile 1v. The two strain gauges near the toe are referred to as C1 and C2 and are placed diametrically opposite of each other on the outside of the pile wall. The measurements taken during installation are shown in Figure 6.3.

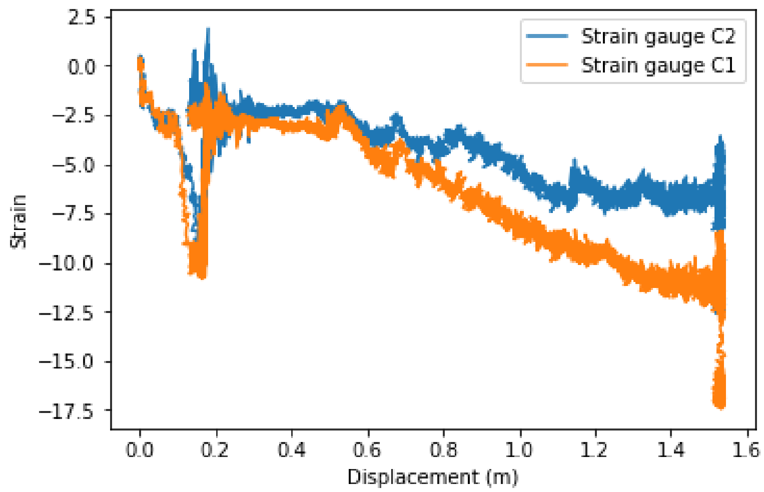

Figure 6.3: Strains on pile 1v during installation

From this figure, it can be seen that the strain on the pile wall increased during installation of pile 1v. This is expected as the pile is penetrating deeper into the soil and encountering stiffer soil.

6.1.1.4 Load cell

Due to technical difficulties with the frequency sensors and the measured data, frequency could not be plotted in the figures for this batch. Although information regarding the actual frequency was not available during installation, the input parameters of the vibratory hammer give a reasonable estimation for the actual frequency. As such, a differentiation between high and low frequency will be sufficient for analysis purposes in following chapters.

During the vibratory installations, a load cell on the crane measured the load of the pile + hammer system. Two results are presented below: pile 1v and pile 4v. All other crane load plots are shown in Appendix C: Installation results. Pile 1v was installed at a low frequency and a low speed, while pile 4v at a high frequency and a high speed. Both piles had opposite installation parameters and yield different results.

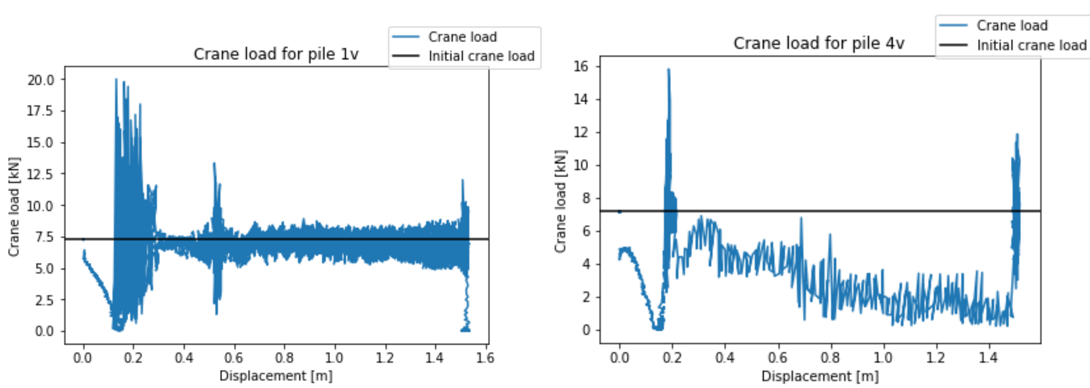

Figure 6.4: Crane load during installation of pile 1v (left) and pile 4v (right)

During installation of pile 1, the load on the crane remained constant and equal to the starting value. This means that the crane supported the entire system. During the installation of pile 4, the load on the crane diminished during the installation, from 500 kg to 200 kg. This means that the soil supported part of the system weight during installation of pile 4. All piles in batch 2 have been divided in the two categories presented in the figure below.

Fully crane-controlled installation	Partially crane-controlled installation
1, 6	4, 5, 8

Table 6-2: Overview of load cell data from batch 2

6.1.1.5 Soil settlement measurements

Height measurements were taken before and after installation. These were taken with the help of the levelling instrument shown in Figure 4.23. The measurement process is explained in section 4.2.5.5. The reference level (situated on the wall of the tank) of the measurements was 1139 mm. The measurements taken outside of the pile were taken on the side of the pile subjected to passive loading, meaning in the loading direction. The values of the measurements themselves matter less than the difference found between the two measurements. Table 6-3 shows the height measurements taken before and after installation. The measurements were done outside of the pile (average of two measurements) and inside the pile. A negative value in the "*Difference*" column indicates a decrease in soil elevation, a positive value signifies an increase.

Pile number	Before (outside)	After (outside)	Difference	Before (inside)	After (inside)	Difference
1	1196	1206	-10	1196	1140	56
2	1203	1234	-31	1208	1274	-66
3	1219	1250	-40	1216	1263	-56
4	1210	1219	-9	1207	1173	34
5	1214	1228	-14	1214	1253	-39
6	1210	1216	-6	1210	1160	50
7	1222	1245	-23	1219	1244	-25
8	1199	1200	-1	1197	1083	14

Table 6-3: Height measurements in batch 2 (measurements in mm)

Pile number (increasing difference outside the pile)	Pile number (increasing difference inside the pile)	Pile number (increasing displacement)
3	2	8
2	3	3
7	5	2
5	7	7
1	8	4
4	4	6
6	6	5
8	1	1

Table 6-4: Overview of soil elevation difference and pile displacement order in batch 2

Table 6-4 shows an overview of the order of piles when ranking them from smallest to largest displacement, and when ranking them from smallest to largest difference in soil elevation measurement difference. Although the order is not the exact same (as expected since there are other factors that influence the displacement), the general order of the piles shows a lot of similarities. For example, piles 2v and 3i are in the top 3 for all columns. Similarly, the placement of piles 4v and 6v is noted. Pile 8v seems to be an exception. This table seems to show that differences in soil elevation measurements might be correlated to pile lateral stiffness, but a conclusion can only be made after observing the results from the other batches.

6.1.2 Batch 3

Table 6-5 presents the installation parameters for all piles in batch 3. As a reminder, set 1 used one falling weight of 285 kg with a falling height of 0.4 m. Set 2 used two falling weights of 285 kg with a falling height of 0.8 m. High speed corresponded to a crane lowering speed of 110 mm/s whereas low speed corresponded to a crane lowering speed of 10 mm/s. High frequency was roughly equal to 35 Hz and low frequency was roughly equal to 20 Hz.

Pile number	D/t	Impact Set 1	Impact Set 2	Speed	Frequency
1v	High	-	-	High	High
2v	High	-	-	High	Low
3i	Low	X	-	-	-

4v	High	-	-	Free	Low
5v	High	-	-	Low	Low
6v	High	-	-	Low	High
7i	High	X	-	-	-
8v	Low	-	-	Free	Low

Table 6-5: Installation parameters for batch 3

6.1.2.1 Total stress sensors

Two total stress sensors were installed into the ground, and piles 1v and 7i were installed right next to those sensors. As such, these two piles are the most relevant when looking at total stress sensor data. The data from those sensors collected during the installation of both piles is shown in Figure 6.5.

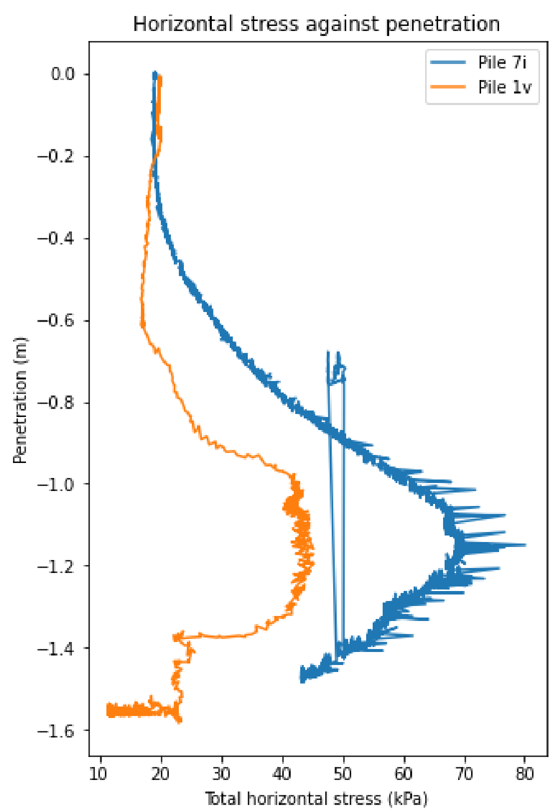

Figure 6.5: Total horizontal stress as a function of penetration for batch 3

During the installation of both piles, the total stress recorded by the sensors increased and peaked when the pile toe passed the sensor depth. This increase was larger for pile 7, which is the impact hammered pile. Compared to batch 2, the increase for the impact hammered pile is the same, but the stress around the vibratory driven pile increases instead of decreasing. The two piles had different installation parameters: high frequency and high speed for batch 2, low frequency and low speed for batch 3.

The stress sensors on the pile wall broke during batch 2, so no results are available regarding that data.

6.1.2.2 Pore water pressure sensors

During installation, the pore water pressure sensors next to the wall did not register any significant increase in pore water pressure. These sensors were used to monitor possible liquefaction of the sand bed. Liquefaction did not happen during batch 3. The largest pore water pressure increase recorded near the pile during installation was for pile 1. This pile was installed in the East corner of the tank nearest to the sensor, which explains the observed reaction. All pore water pressure plots are present in Appendix C: Installation results. In the figures, the pore pressure sensors are referred to with their position on the four cardinal coordinates. Figure 4.19 shows the position of all the sensors in the soil as well as which sensor corresponds to which direction.

6.1.2.3 Strain gauges

Strain gauges were installed on pile 1v. The two strain gauges near the tip are referred to as C1 and C2 and are placed diametrically opposite of each other on the outside of the pile wall. The measurements taken during installation are shown in Figure 6.6.

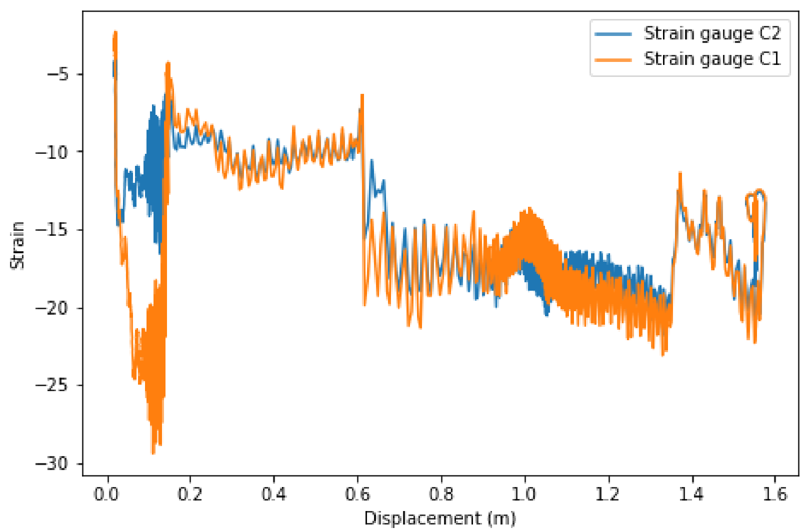

Figure 6.6: Strains on pile 1v during installation

From this figure, it can be seen that the strain on the pile wall increased during installation of pile 1v. This is expected as the pile was penetrating deeper into the soil and encountering stiffer soil.

6.1.2.4 Load cell and frequency

During the vibratory installations, a load cell on the crane measured the load of the pile and hammer system. All results are shown in Appendix C: Installation results. Two results are plotted below: pile 4v and pile 6v.

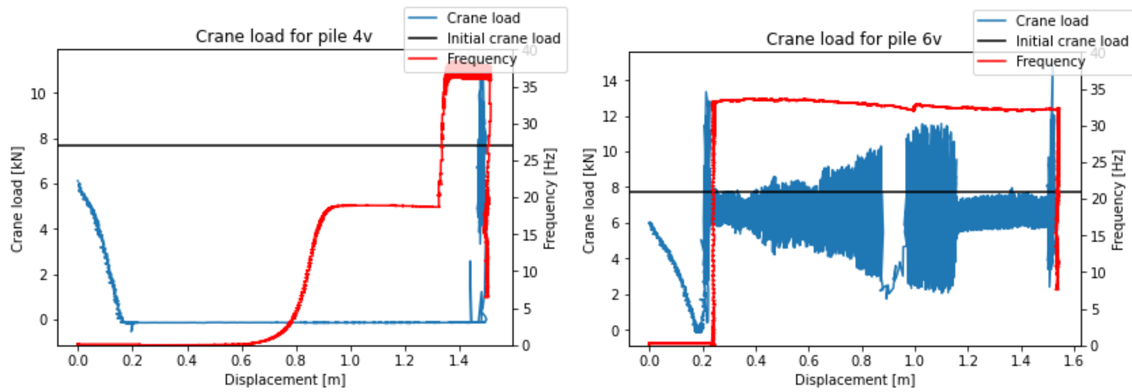

Figure 6.7: Crane load and frequency during installation of pile 4v (left) and pile 6v (right)

Figure 6.7 shows two different behaviours, which can be found in all the other pile installation plots. On the left, the load on the crane decreased and was supported by the soil. For most of the installation, there was no load on the crane at all indicating that the pile rested fully on the sand (this is referred to as a free hanging pile). This was the case for piles 1, 4 and 8. All these piles were installed with a high lowering speed.

On the other side, piles 5 and 6 showed a behaviour similar to the right plot, where the load on the crane did not decrease during installation and stayed constant during the entire installation (this is referred to as a crane-controlled pile). Both piles were installed at low speed. All piles in batch 3 have been divided in the two categories in the figure below.

Fully crane-controlled installation	Partially crane-controlled installation	Fully free-hanging
5, 6	1, 2	4, 8

Table 6-6: Overview of load cell data from batch 3

Comparing these two responses, piles installed with a high installation speed seem to show a behaviour where the soil supports the pile. This did not seem to happen at low speed. This indicates that installation speed could play a role in whether the pile installation was free-hanging or crane-controlled.

6.1.2.5 Soil settlement measurements

Height measurements were taken before and after installation. These were taken with the help of the levelling instrument shown in Figure 4.23. The measurement process is explained in section 4.2.5.5. The reference level (situated on the wall of the tank) of the measurements was 1139 mm. The measurements taken outside of the pile were taken on the side of the pile subjected to passive loading, meaning in the loading direction. The values of the measurements themselves matter less than the difference found between the two measurements. Table 6-7 shows the height measurements taken before and after installation. The measurements were taken outside of the pile (average of two measurements) and inside the pile. A negative value in the "*Difference*" column indicates a decrease in soil elevation, a positive value signifies an increase.

Pile number	Before (outside)	After (outside)	Difference	Before (inside)	After (inside)	Difference
1	1178	1178	0	1171	1093	78
2	1217	1229	-12	1226	1203	23
3	1180	1197	-17	1189	1237	-48
4	1231	1235	-4	1232	1266	-34
5	1214	1217	-3	1222	1172	50
6	1213	1218	-5	1222	1203	19
7	1181	1212	-31	1184	1204	-20
8	1197	1196	1	1197	1105	92

Table 6-7: Height measurements in batch 3 (measurements in mm)

Pile number (increasing difference outside the pile)	Pile number (increasing difference inside the pile)	Pile number (increasing displacement)
7	3	3
3	4	2
2	7	7
6	6	6
4	2	5
5	5	4
1	1	1
8	8	8

Table 6-8: Overview of soil elevation difference and pile displacement order in batch 3

Table 6-8 shows an overview of the order of piles when ranking them from smallest to largest displacement, and when ranking them from smallest to largest difference in soil elevation measurement difference. Although the order is not the exact same (as expected since there are other factors that influence the displacement), the general order of the piles shows a lot of similarities. The similarities have been reported in batch 2 (section 6.1.1.5) as well but are more striking here. The difference in soil elevation measurements outside of the pile shows the almost exact same order as the pile displacement. Additionally, piles 1v and 8v make up the bottom 2 in all cases. This seems to show that piles where a decrease in soil elevation (compaction) happened are the piles that also show the least displacement under monotonic loading. With the results of batch 2 and 3, this phenomenon is consistent across dense sand. To verify whether this is also the case in medium dense sand, results from batch 4 will be verified.

6.1.3 Batch 4

Table 6-10 presents the installation parameters for all piles in batch 4. As a reminder, set 1 used one falling weight of 285 kg with a falling height of 0.4 m. Set 2 used two falling weights of 285 kg with a falling height of 0.8 m. High speed corresponded to a crane lowering speed of 110 mm/s whereas low speed corresponded to a crane lowering speed of 10 mm/s.

Pile number	D/t	Impact Set 1	Impact Set 2	Speed	Frequency
1v	High	-	-	Low	23 Hz
2v	High	-	-	High	23 Hz
3i	Low	X	-	-	-
4v	High	-	-	High	23 Hz
5v	High	-	-	Low	23 Hz
6i	High	X	-	-	-
7i	High	X	-	-	-
8v	Low	-	-	Low	23 Hz

Table 6-9: Installation parameters for batch 4

6.1.3.1 Total stress sensors

Two total stress sensors were installed into the ground, and piles 1v and 7i were installed right next to those sensors. As such, these two piles are the most relevant when looking at total stress sensor data. The data from those sensors collected during the installation of both piles is shown in Figure 6.8.

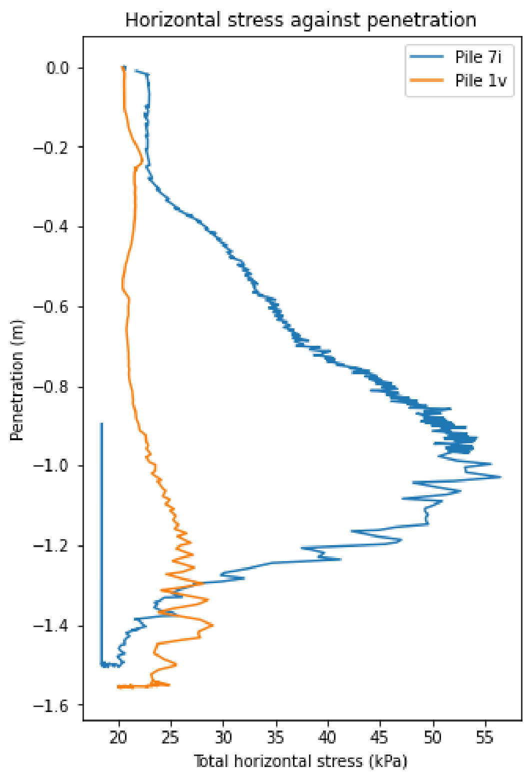

Figure 6.8: Total horizontal stress as a function of penetration for batch 4

The total stress recorded during installation increased for both piles, but the increase was much larger for pile 7i. Similar to previous batches, the increase occurred when the pile toe passed the sensor depth. The increase was approximately 5 kPa for the vibrated pile, 30 kPa for the impact hammered pile.

The stress sensors on the pile wall broke during batch 2, so no results are available regarding that data.

6.1.3.2 Pore water pressure sensors

During installation, the pore water pressure sensors next to the wall did not register any significant increase in pore water pressure. These sensors were used to monitor possible liquefaction of the sand bed. Liquefaction did not happen during batch 4. While some oscillations were present in the readings from the sensors near the pile when driving the pile, no increase of the mean pore water pressure was recorded except for pile 1v, situated near the pore pressure sensor. All pore water pressure plots are present in Appendix C: Installation results. In the figures, the pore pressure sensors are referred to with their position on the four cardinal coordinates. Figure 4.19 shows the position of all the sensors in the soil as well as which sensor corresponds to which direction.

6.1.3.3 Strain gauges

Strain gauges were installed on pile 1v. The two strain gauges near the tip are referred to as C1 and C2 and are placed diametrically opposite of each other on the outside of the pile wall. The measurements taken during installation are shown in Figure 6.9.

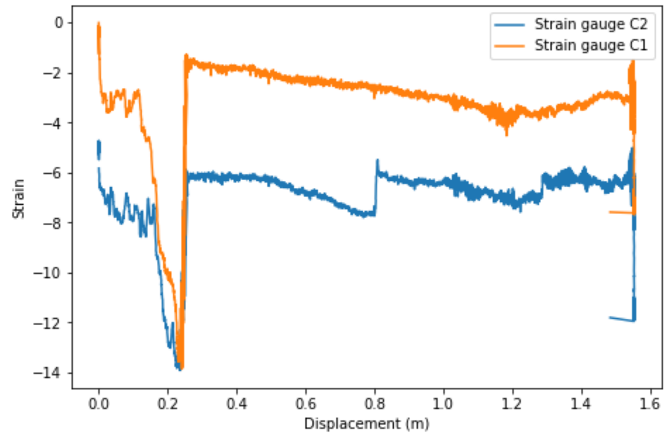

Figure 6.9: Strains on pile 1v during installation

Though the strains seem to increase during installation as in the previous batches, the rate of increase is lower than in batch 2 and 3.

6.1.3.4 Load cell and frequency

During the vibratory installations, a load cell on the crane measured the load of the pile + hammer system. In this batch, the sampling frequency was accidentally changed to 1 Hz. This caused the oscillations in the crane load to not be fully captured. All results are shown in Appendix C: Installation results. In this batch, all crane load plots showed the same behaviour. Pile 1v is shown below as representative of all piles in this batch.

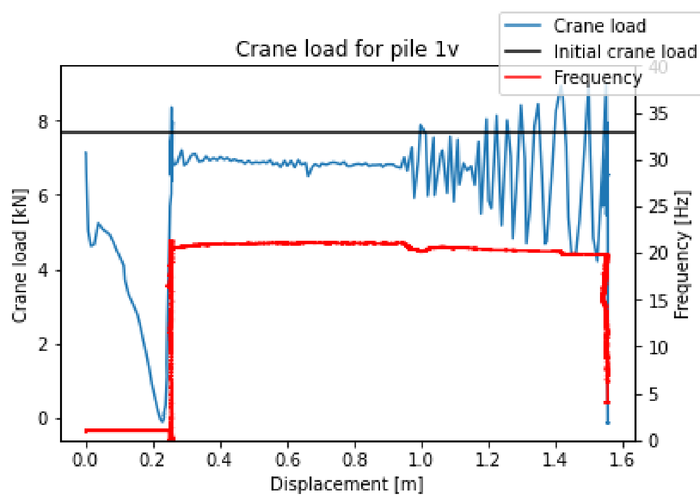

Figure 6.10: Crane load and frequency during installation of pile 5v

All the piles showed a load on the crane that did not decrease during installation and remained equal to the starting value. This indicates that during batch 4, all vibratory installations were crane controlled.

6.1.3.5 Soil settlement measurements

Height measurements were taken before and after installation. These were taken with the help of the levelling instrument shown in Figure 4.23. The measurement process is explained in section 4.2.5.5. The reference level (situated on the wall of the tank) of the measurements is 1139 mm. The measurements taken outside of the pile were taken on the side of the pile subjected to passive loading, meaning in the loading direction. The values of the measurements themselves matter less than the difference found between the two measurements. Table 6-10 shows the height measurements taken before and after installation. The measurements were done outside of the pile (average of two measurements) and inside the pile. A negative value in the "*Difference*" column indicates a decrease in soil elevation, a positive value signifies an increase.

Pile number	Before (outside)	After (outside)	Difference	Before (inside)	After (inside)	Difference
1	1202	1224	-22	1202	1292	-90
2	1235	1246	-11	1240	1248	-8
3	1211	1246	-35	1212	1333	-121
4	1233	1248	-15	1242	1252	-10
5	1218	1235	-17	1227	1294	-67
6	1255	1290	-35	1254	1370	-16
7	1220	1259	-39	1220	1317	-97
8	1208	1225	-17	1216	1258	-42

Table 6-10: Height measurements in batch 4 (measurements in mm)

Pile number (increasing difference outside the pile)	Pile number (increasing difference inside the pile)	Pile number (increasing displacement)
7	7	7
6	1	5
1	5	1
5	8	8
8	6	6
4	4	4
2	2	2

Table 6-11: Overview of soil elevation difference and pile displacement order in batch 4

Table 6-11 shows an overview of the order of piles when ranking them from smallest to largest displacement, and when ranking them from smallest to largest difference in soil elevation measurement difference. Although the order is not the identical, since other factors also influence the displacement, the general order of the piles shows a lot of similarities. Pile 3i was removed from this table due to its displacement during initial monotonic loading not being measured. Just as in batches 2 and 3 and as discussed in section 6.1.2.5, the difference in soil elevation measurements shows almost the same order as the pile displacement, showing that this phenomenon is not limited to dense sand. Pile 7i is the pile where the most compaction happens, and it is also the pile with the least displacement. Conversely, piles 4v and 2v are the piles with the least compaction in and around the pile, and the piles with the highest displacement.

6.2 CPT data

In this section, CPT data from before and after installation will be presented for each pile. This will give an overview of the effect installation had on the soil near the pile. With the data, a possible correlation between post-installation CPT results and initial stiffness of the load-displacement curve can be investigated. The CPT coordinates are given according to the grid in section 4.3 (Figure 4.29, Figure 4.33 and Figure 4.37) in the form of “x/y”.

6.2.1 Batch 2

The coordinates of the CPT before and after installation for batch 2 are presented in Table 7-1. Figure 4.29 shows the locations of all CPT taken during batch 2. The post-installation CPT were taken approximately 10 cm away from the pile wall.

Pile	Installation speed	Frequency	Before	After
1v	Low	Low	24/1	23.5/2
2i	-	-	24/12	23.5/11
3i	-	-	8/12	8.5/11
4v	High	High	17/12	16.5/11
5v	High	Low	1/12	1.5/11
6v	Low	High	8/1	8.5/2
7i	-	-	1/1	1.5/2
8v	Low	High	17/1	16.5/2

Table 6-12: CPT locations before and after installation for batch 2

For all piles except pile 1, the CPT yielded higher q_c after installation than before installation. In general, this increase was larger for impact hammered piles (such as 2i and 7i). Figure 6.11 shows an example result, for pile 6 where an increase of approximately 20% is seen. The figures for all the piles are present in Appendix D: CPT results.

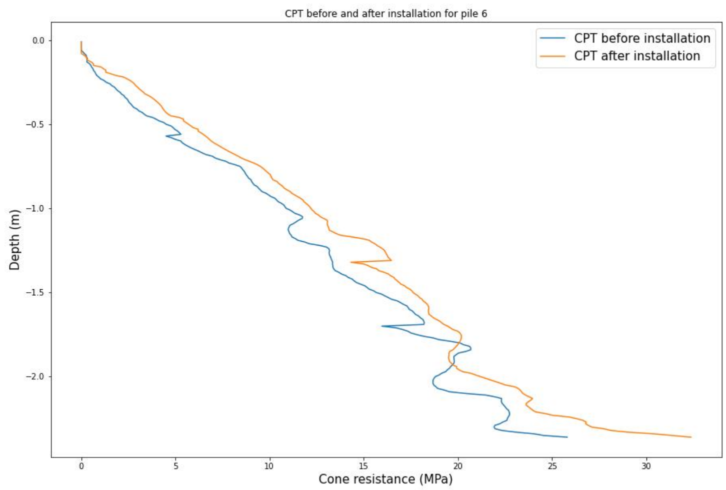

Figure 6.11: CPT results before and after installation at the location of pile 6 in batch 2

6.2.2 Batch 3

The coordinates of the CPT before and after installation for batch 2 are presented in Table 6-13. Figure 4.33 shows the locations of all CPT taken during batch 2.

Pile	Installation speed	Frequency	Before	After
1v	High	High	1/2	2.5/2
2v	High	Low	17/2	15.5/2
3i	-	-	1/12	1.5/11
4v	Free	Low	17/12	16.5/11
5v	Low	Low	8/12	8.5/11
6v	Low	High	8/2	9.5/2
7i	-	-	24/2	22.5/2
8v	High	Low	24/12	23.5/11

Table 6-13: CPT locations before and after installation for batch 3

Overall, the CPT yielded higher or similar q_c after installation compared to before the pile was installed. Impact hammered piles showed a clear increase, while all the vibrated piles showed curves that were similar to prior installation. Figure 6.12 shows an example result, for pile 6. The figures for all the piles are present in Appendix D: CPT results.

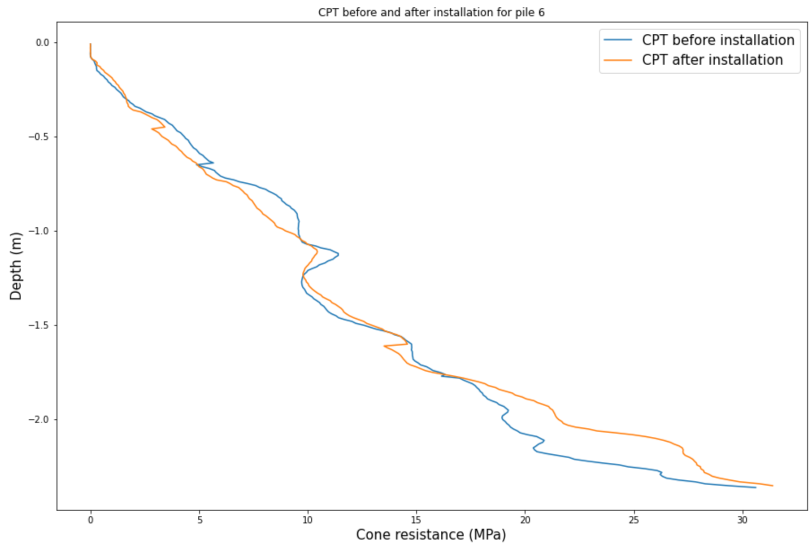

Figure 6.12: CPT results before and after installation at the location of pile 6 in batch 3

6.2.3 Batch 4

The coordinates of the CPT before and after installation for batch 2 are presented in Table 6-14. Figure 4.37 shows the locations of all CPT taken during batch 2.

Pile	Installation speed	Frequency	Before	After
1v	Low	23	24/1	23.5/2
2v	High	23	17/1	16.5/2
3i	-	23	24/12	23.5/11
4v	High	23	17/12	16.5/11
5v	Low	23	8/1	8.5/2
6i	-	23	8/12	8.5/11
7i	-	23	1/1	1.5/2
8v	Low	23	1/12	1.5/11

Table 6-14: CPT locations before and after installation for batch 4

For all piles, the CPT yielded higher q_c after installation than before installation. This increase was large for the impact hammered piles (3i, 6i and 7i) than for the vibrated piles. Figure 6.13 shows an example result, for pile 6 where an increase of approximately 100% over most of the depth can be seen. The figures for all the piles are present in Appendix D: CPT results.

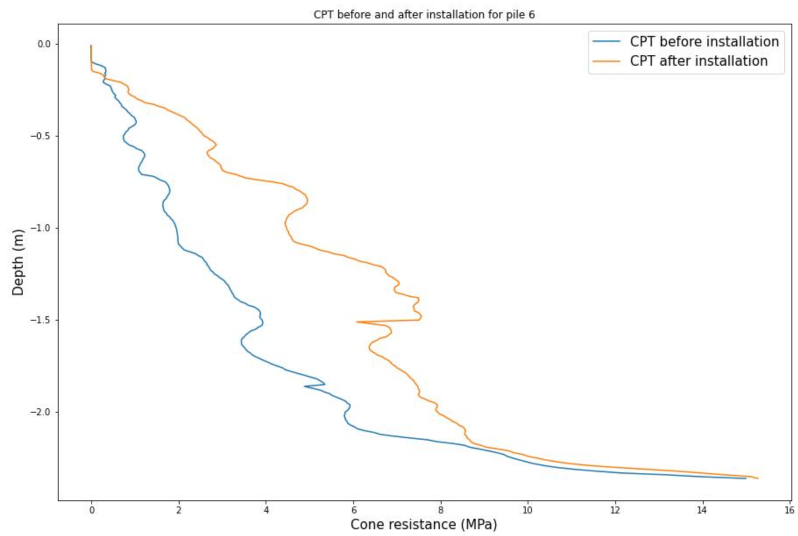

Figure 6.13: CPT results before and after installation at the location of pile 6 in batch 4

6.3 Loading

The results from the loading tests are presented in three subdivisions: the initial monotonic loading (3 or 4 kN), the subsequent cyclic loading (up to 1000 cycles of the same load, with a frequency of 0.1 Hz), and the second monotonic loading (14, 18 or 20 kN). All the values have been corrected according to the process described in 5.1.

6.3.1 Batch 2

6.3.1.1 Initial monotonic loading

In batch 2, five piles were installed using a vibratory hammer, and three piles using an impact hammer. The installation parameters of the vibrated pile are indicated in Table 6-15. A thin-walled pile had a wall thickness of 4 mm, while a thick-walled pile had a diameter of 10 mm. Low speed corresponded to a crane lowering speed of 10 mm/s, while high speed corresponded to 110 mm/s. Piles installed at low frequency were vibrated around 20 Hz, while high frequencies corresponded to 35 Hz. The exact values can be found in appendix C.

Pile	Thick/thin walled	Speed	Frequency
1v	Thin	Low	Low
2i	Thin	-	-

3i	Thick	-	-
4v	Thin	High	High
5v	Thin	High	Low
6v	Thin	Low	High
7i	Thin	-	-
8v	Thick	Low	High

Table 6-15: Pile installation characteristics for batch 2

Below, the effect of all applied corrections is visible when comparing two figures in the same batch. Figure 6.14 shows the uncorrected curves for initial monotonic loading and Figure 6.15 shows the corrected curves.

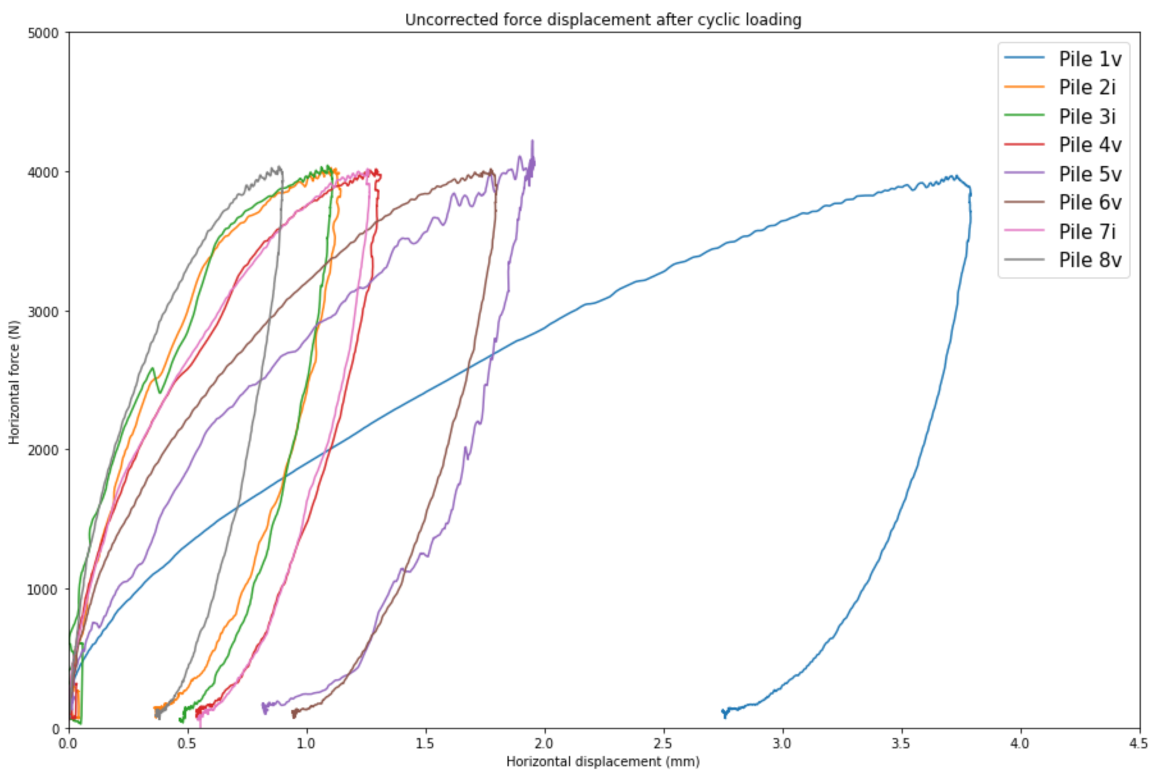

Figure 6.14: Uncorrected displacement during initial monotonic loading for all piles in batch 2

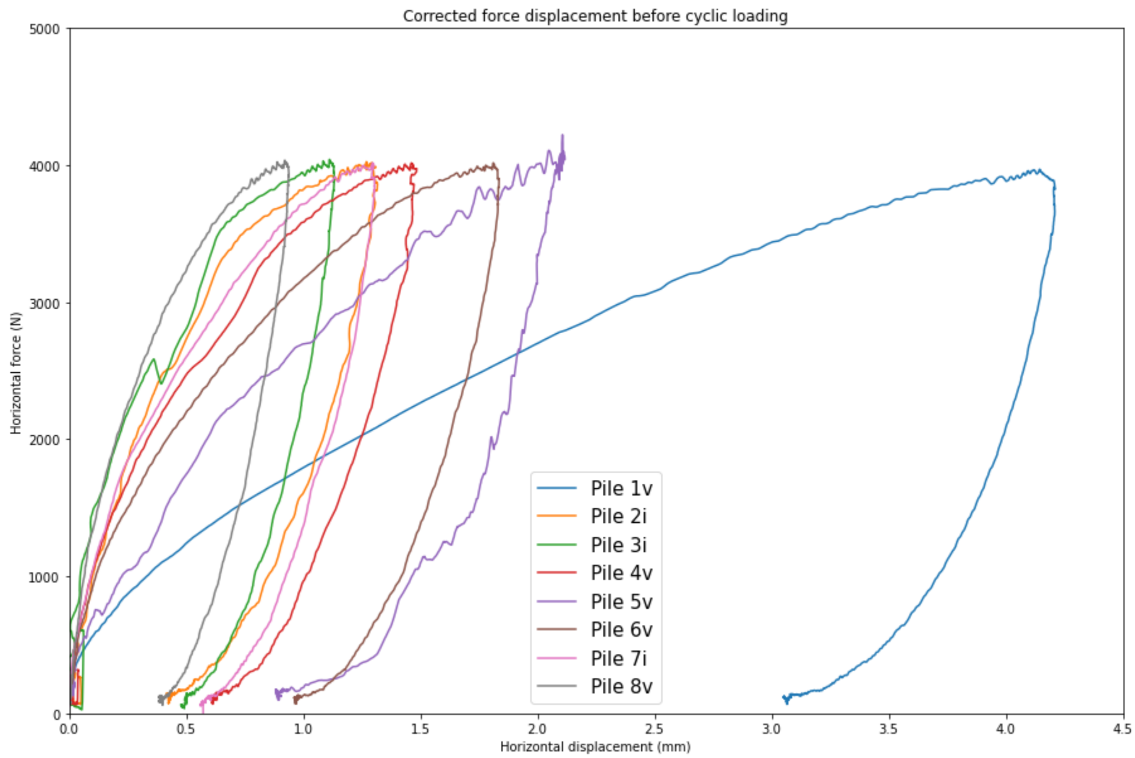

Figure 6.15: Corrected displacement during initial monotonic loading for all piles in batch 2

According to Figure 6.15, the piles showing the lowest displacements were the thick-walled pile and the impact hammered piles. The stiffest thin-walled vibratory driven pile was pile 4v, which was driven under high speed and with a high frequency. A human mistake occurred before loading pile 1v during the loading equipment set-up, the pile was accidentally loaded up to 2.5 kN in the opposite direction and then brought back to zero. This means the result for pile 1 in the figure above is not representative.

Figure 6.16 below shows the horizontal stresses recorded by the total stress sensors near piles 1 and 7 (see section 4.2.5). The sensors were place in the sand, half a diameter away from the pile wall in the loading direction. In the figure, the stresses are plotted on the y-axis, as a function of the load applied on the pile. One can see that the stresses increase as the lateral load increases, decreasing again during unloading. The values for pile 1v are below those of pile 7i at all times, as the stress level before loading is larger for the impact driven pile. This reflects the observations of Figure 6.1 and the fact that the displacement of pile 1v was larger than pile 7i during this loading step.

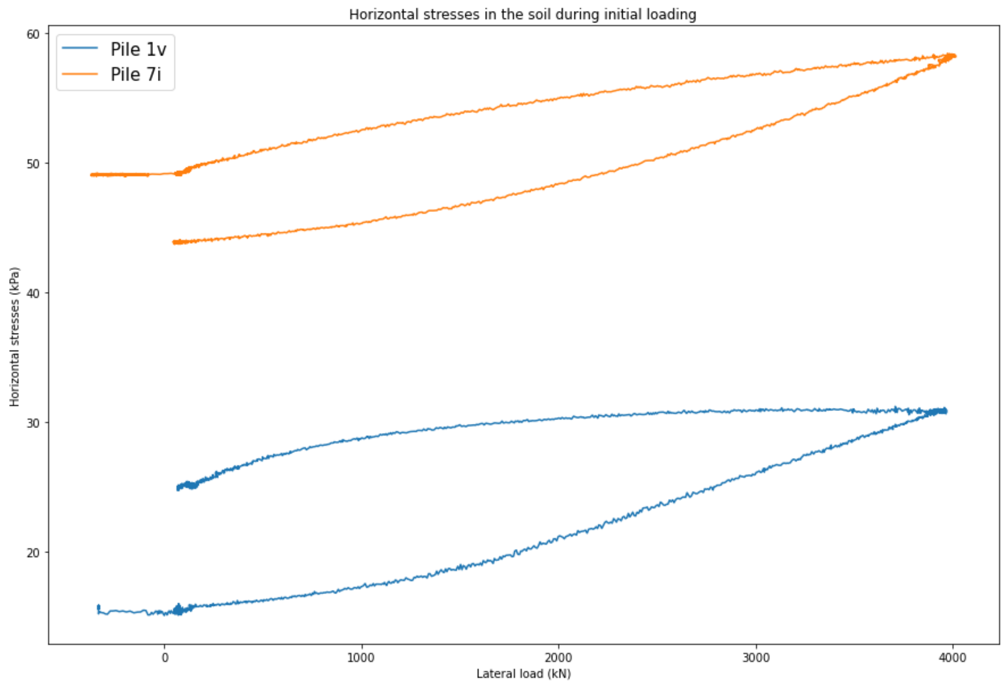

Figure 6.16: Horizontal stresses measured in the soil during initial loading, batch 2

6.3.1.2 Cyclic loading

Displacement maxima for every cycle during cyclic loading have been plotted in Figure 6.17 below. Most piles were subjected to 1000 cycles, but some were only loaded 100 cycles due to time constraints. Pile 2i was not subjected to cyclic loading due to software issues.

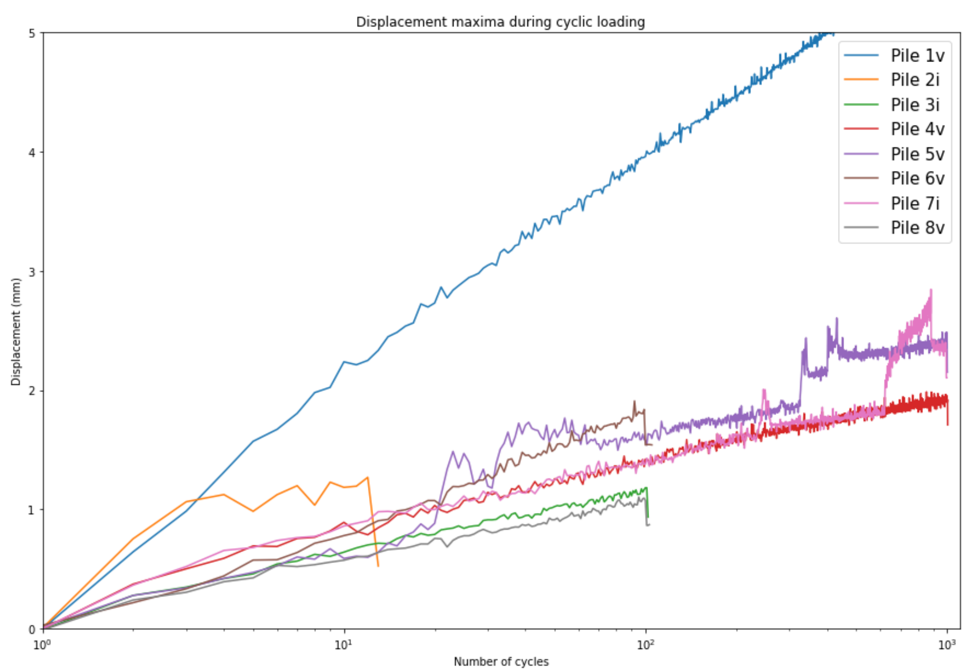

Figure 6.17: Peak displacement according to the number of cycles in batch 2

The order of the piles remained the same as during initial monotonic loading, with very few differences.

The rotation during cyclic loading has also been calculated. This was done according to the method of LeBlanc et al. (2010). This paper studies the response of stiff piles to cyclic loading in sand. This method consists of first calculating the stiffness with the use of pile rotation. The rotation is equal to:

$$\frac{\Delta\theta(N)}{\theta_s} = \frac{\theta_N - \theta_0}{\theta_s}$$

Where θ_s is the rotation for the initial monotonic test, θ_0 is the initial rotation (rotation after the first cycle) and θ_N is the rotation at cycle N. To calculate the rotation at any moment one must use:

$$\theta = \arctan\left(\frac{x}{L_R}\right)$$

Where x is the horizontal displacement and L_R is the length of the rotation arm. This length was chosen as the sum of 0.76 times the embedment length (1.5 m) according to Wang et al. (2022) and the height of the load application point above the ground level (0.53 m). This gives:

$$L_R = 0.76 \times 1.5 + 0.53 = 1.67\ m$$

The result of the rotation calculations is shown in Figure 6.18. The first few cycles show some oscillations due to inaccuracies with the loading device, especially for pile 2 which was the first cyclic load test of the experiments. However, later pile tests show much clearer trends. Compared to the figures in LeBlanc et al. (2010), the curves also show a constant slope, albeit less steep that in that paper. This difference may be caused by the sand density, as the sand used by LeBlanc et al. was very loose, compared to medium dense here.

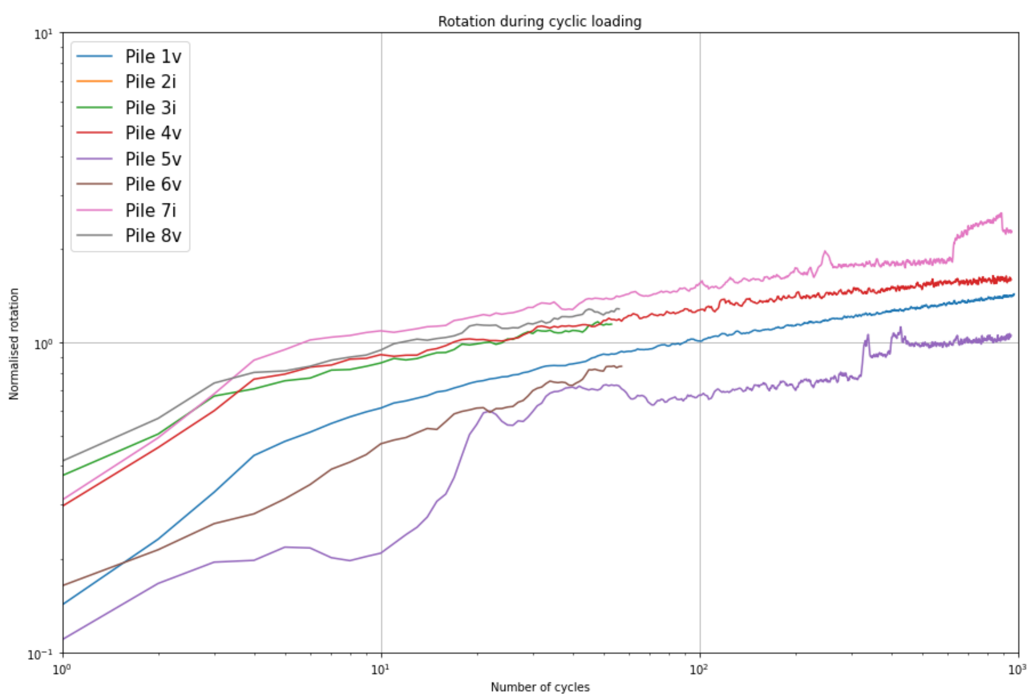

Figure 6.18: Rotation during cyclic loading in batch 2

The secant stiffness of the piles was calculated by dividing the peak load (4 kN) by the amplitude of the displacement during one cycle. The results are shown in the figure below.

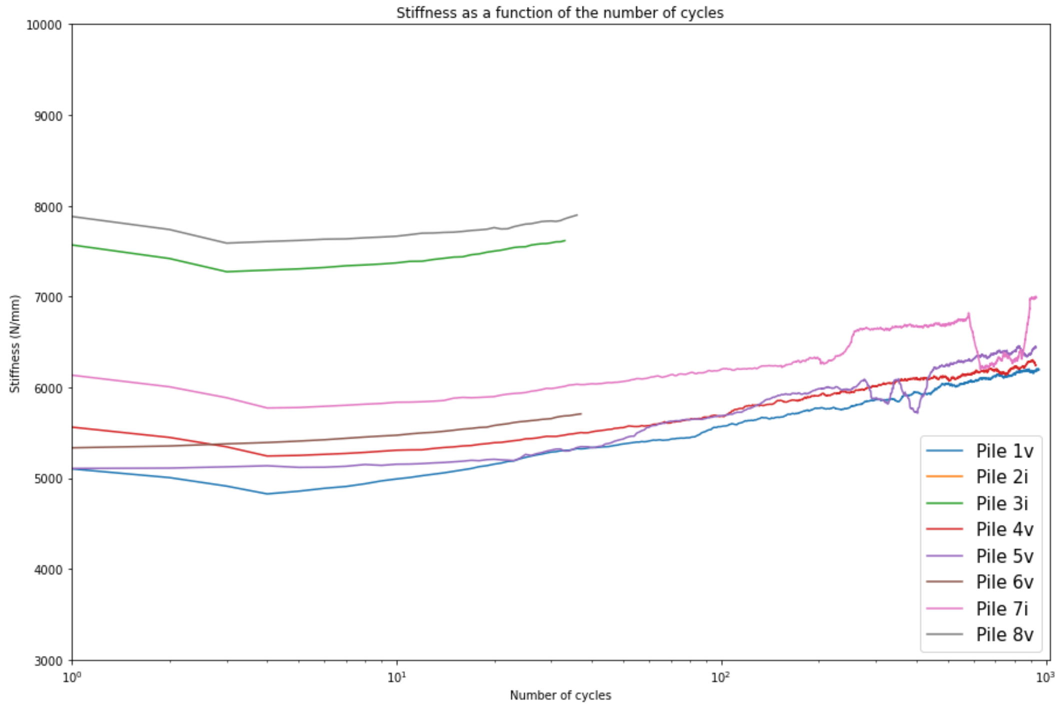

Figure 6.19: Stiffness under cyclic loading in batch 2

When looking at the stiffness of the piles under cyclic loading, the same order as in Figure 6.15 is observed where pile 1v which had the highest displacements shows the lowest stiffness, and piles 3i and 8v showed the highest stiffness and had the lowest displacement. The stiffness tended to increase with the number of cycles.

6.3.1.3 Second monotonic loading

After the initial monotonic load and the cyclic loading period, the pile was loaded monotonically again. Batch 2 being the first batch where the loading device was used, this was first done to 12.5 kN, then 20 kN as the loading device needed to be set up properly. Figure 6.20 shows the force-displacement curves for the piles under this load. Figure 6.21 is on the same scale as in Figure 6.15 to give a better comparison. In this figure, the effect the first two loading phases have had on the piles is visible, as the differences in displacement between piles were negligible up to the load level of 4kN. After that point, the piles undergo virgin loading so the differences become more pronounced and the order of strength of the piles changed.

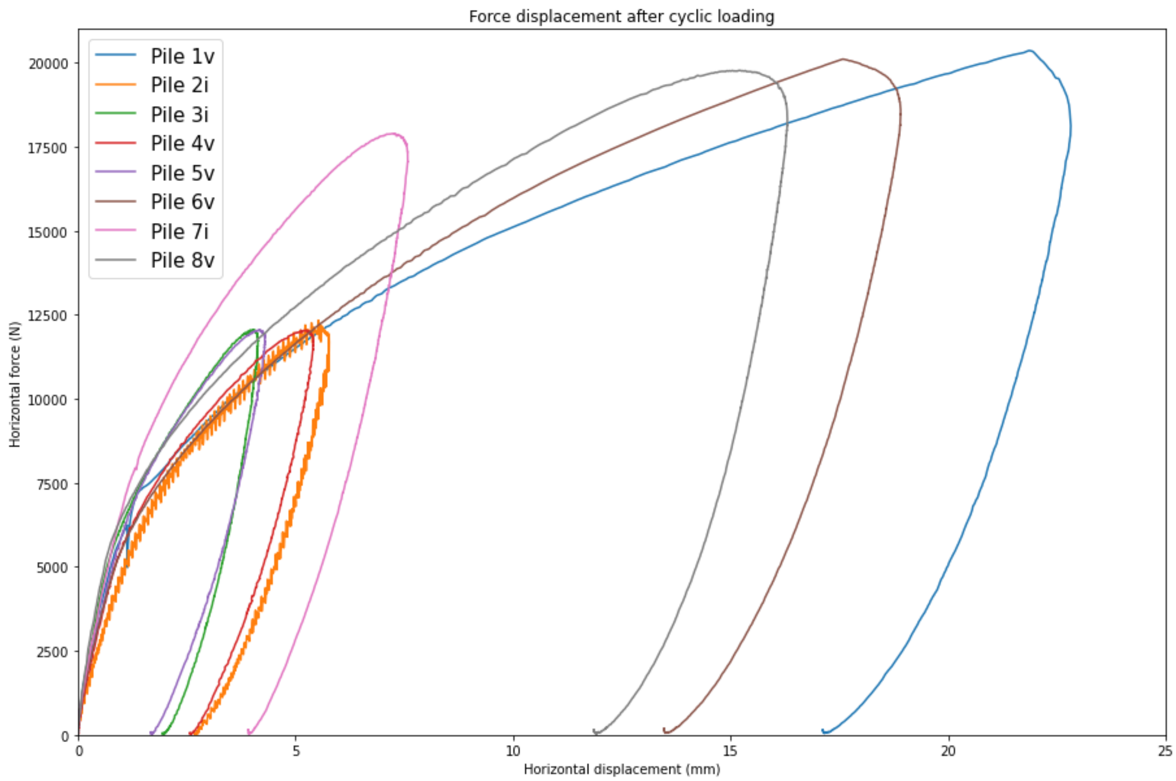

Figure 6.20: Displacement during secondary monotonic loading in batch 2

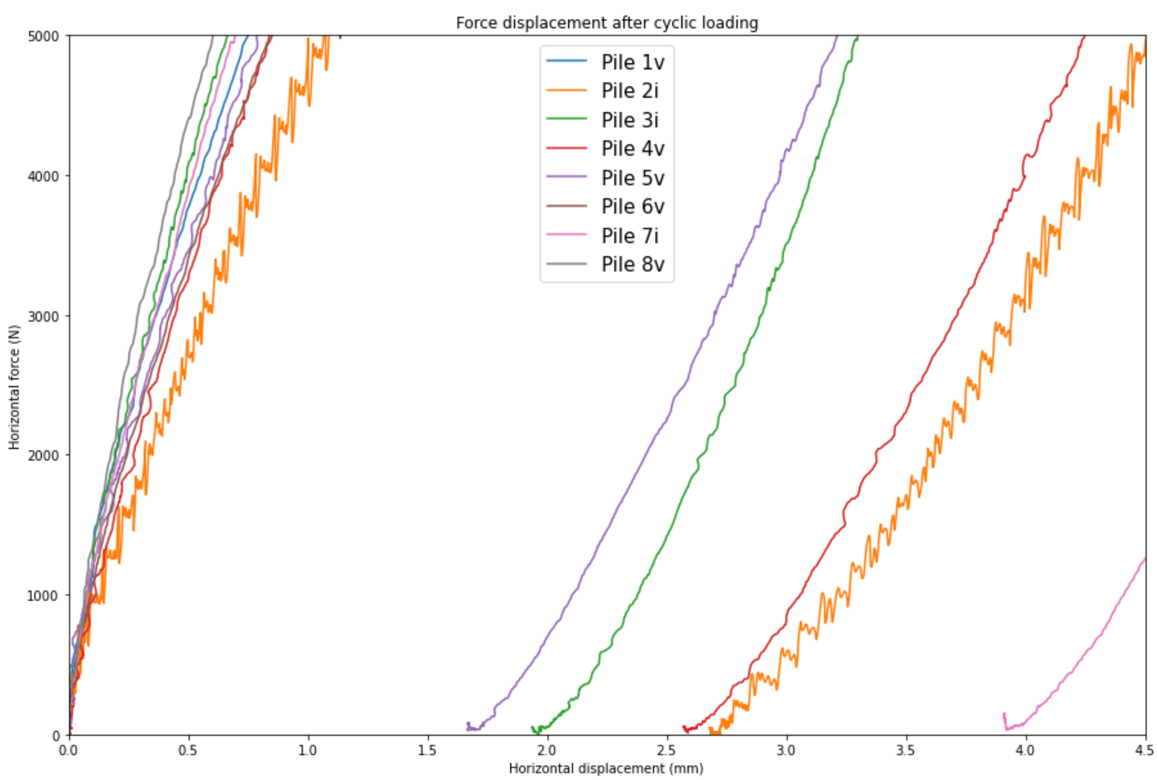

Figure 6.21: Displacement during secondary monotonic loading in batch 2, at the same scale as Figure 6.15

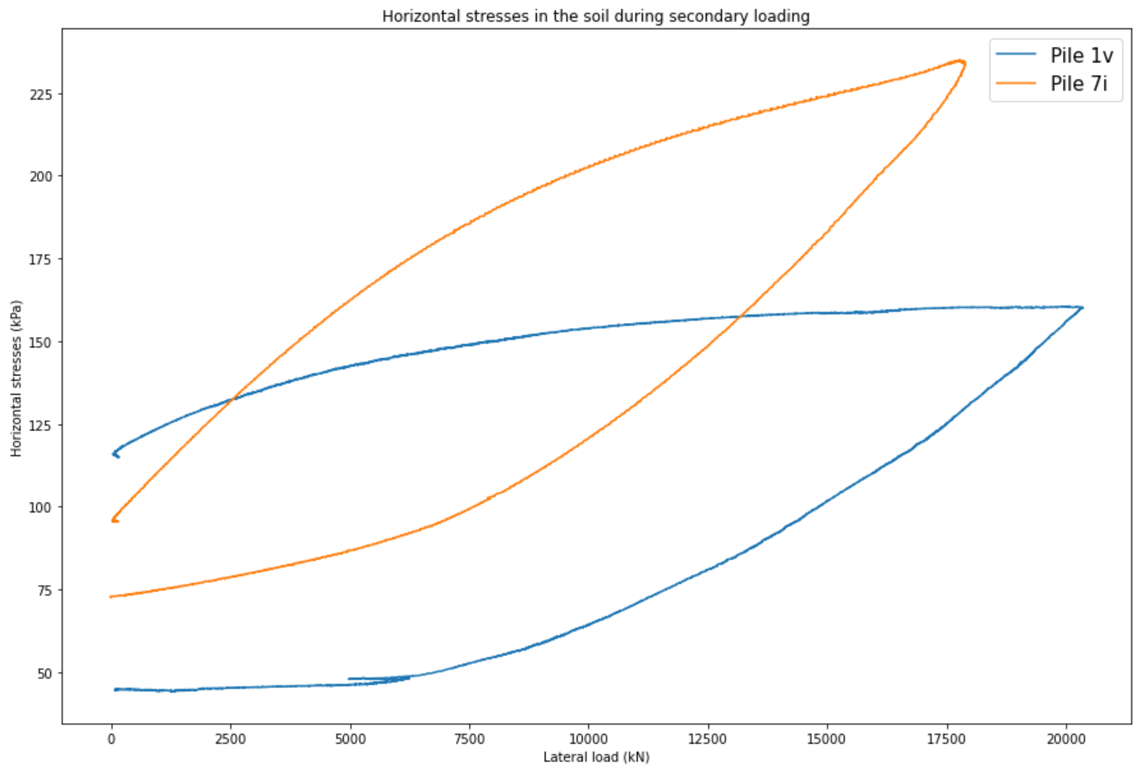

Figure 6.22: Horizontal stresses measured in the soil during secondary loading, batch 2

The stresses in the soil near the pile were also measured during secondary loading, just as during initial monotonic loading. Comparing Figure 6.22 to Figure 6.16, one can see that the initial stress values are higher during this loading step than during the initial loading step, and that both piles are proportionally closer. The stress level in the soil increased during the cyclic loading test. Just like during initial monotonic loading, larger stresses are recorded around pile 7i than around pile 1v. This correlates with the displacement here as well, as a larger displacement was observed for pile 1v in this phase in Figure 6.20.

6.3.2 Batch 3

6.3.2.1 Initial monotonic loading

In batch 3, six piles were installed using a vibratory hammer, and two piles using an impact hammer. The installation parameters of the vibrated pile are indicated in Table 6-16. A thin-walled pile had a wall thickness of 4 mm, while a thick-walled pile had a diameter of 10 mm. Low speed corresponded to a crane lowering speed of 10 mm/s, while high speed corresponded to 110 mm/s. Piles installed at low frequency were vibrated around 20 Hz, while high frequencies corresponded to 35 Hz. The exact values can be found in appendix C. Piles 4 and 8 were installed free hanging. This entailed giving the rope some slack before turning on the vibratory hammer so that the driving speed was not influenced by technical restrictions of the crane speed. For these piles, the lowering speed was faster than 110 mm/s.

Pile	Thick/thin walled	Speed	Frequency
1v	Thin	Free	High
2v	Thin	High	Low
3i	Thick	-	-
4v	Thin	Free	Low
5v	Thin	Low	Low
6v	Thin	Low	High
7i	Thin	-	-
8v	Thick	Free	Low

Table 6-16: Pile installation characteristics for batch 3

Below, the effect of all the applied corrections is visible when comparing two figures in the same batch. Figure 6.23 shows the uncorrected curves for initial monotonic loading and Figure 6.24 shows the corrected curves.

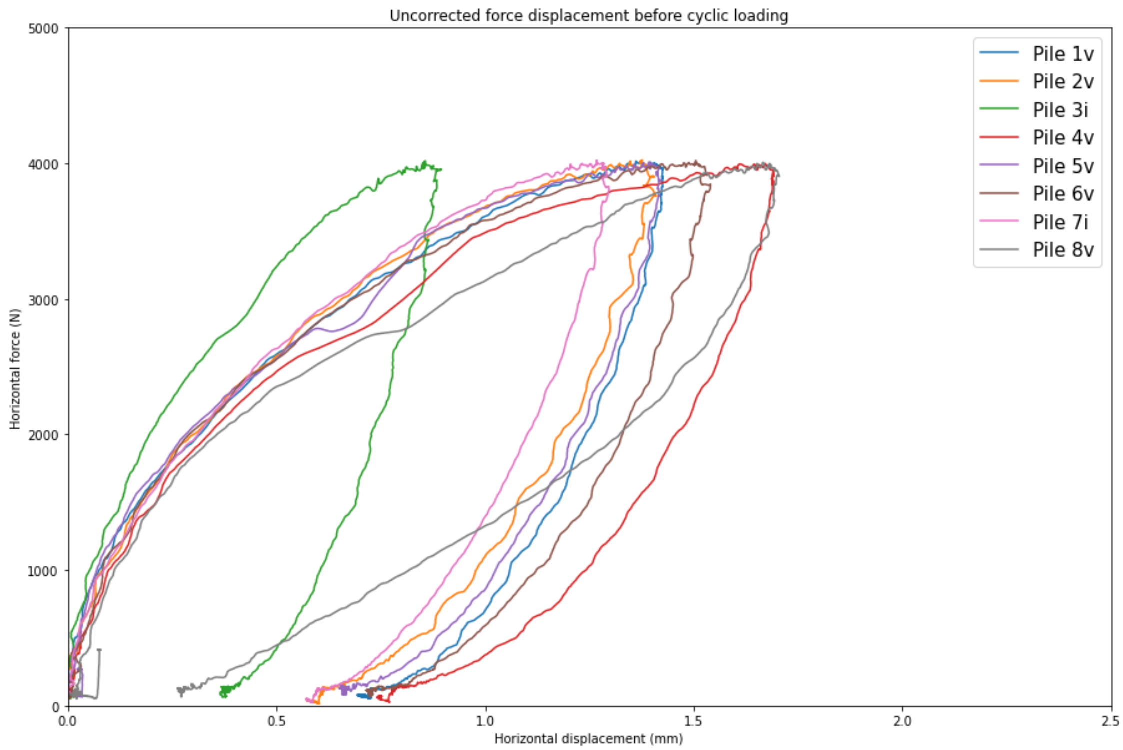

Figure 6.23: Uncorrected displacement during initial monotonic loading for all piles in batch 3

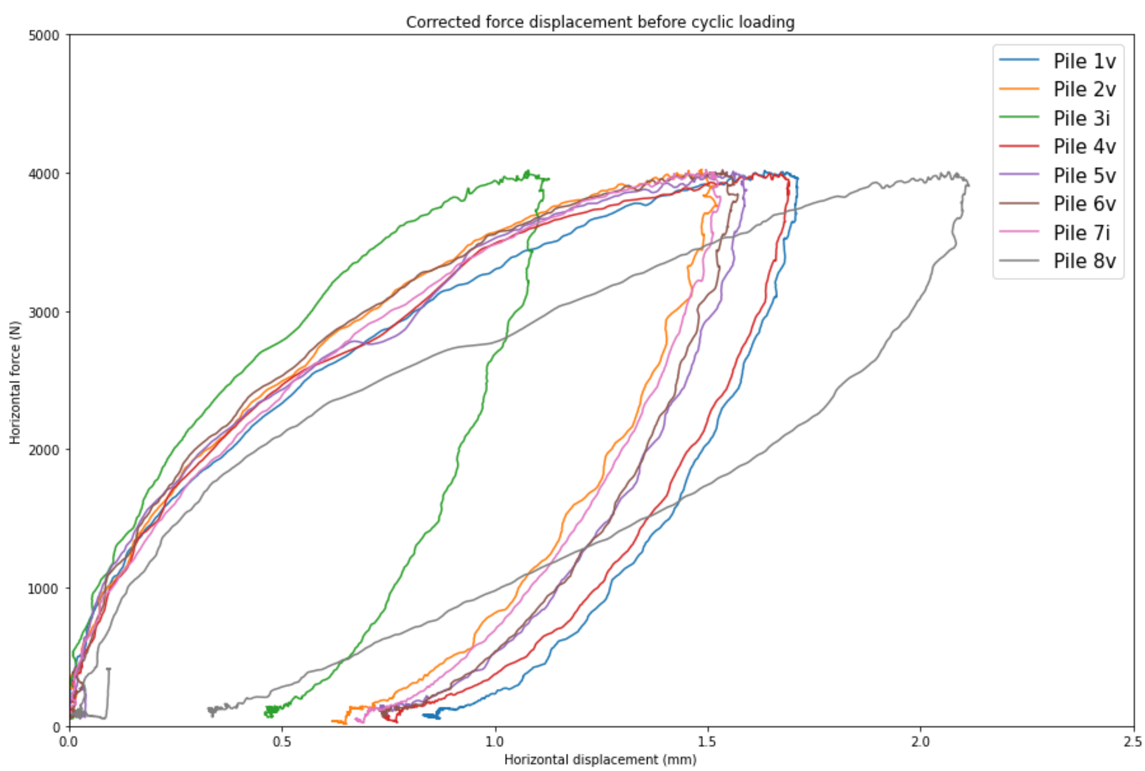

Figure 6.24: Displacement during initial monotonic loading for all piles in batch 3

According to Figure 6.21, the lowest displacement piles were the impact hammered piles, as well as one vibrated pile (2v) which was driven under high speed and low frequency. The two thin-walled piles 1v and 4v showed similar behaviour despite being installed with different frequencies. This indicates that frequency alone does not indicate their lateral behaviour. This is confirmed by piles 5v and 6v also showing similar behaviour despite being installed at different frequencies.

Additionally, piles 1v, 4v, and 8v were installed free-hanging and were also the piles with the largest displacements. This could indicate that lack of crane control results in larger displacement than for crane-controlled piles.

Pile 8v showed behaviour much different from other vibratory piles, which could be due to pile 8v being a thick-walled pile. This might mean it was heavier and sank into the sand much faster. The effects of free-hanging installation such as lack of stability would then have been amplified.

Figure 6.25 shows the horizontal stresses recorded in the soil near piles 1v and 7i. The sensors were place in the sand, half a diameter away from the pile wall in the loading direction. In the figure, the stresses are plotted on the y-axis, as a function of the load applied on the pile. Pile 1 sees an increase in stress as the load increases, whereas this increase is lower for pile 7. The horizontal stresses around pile 7 were higher than around pile 1 during the entire loading phase. The results here are similar to those of batch 2, where the stresses around the impact hammered pile (which has a lower lateral displacement) are higher than those around the vibrated pile.

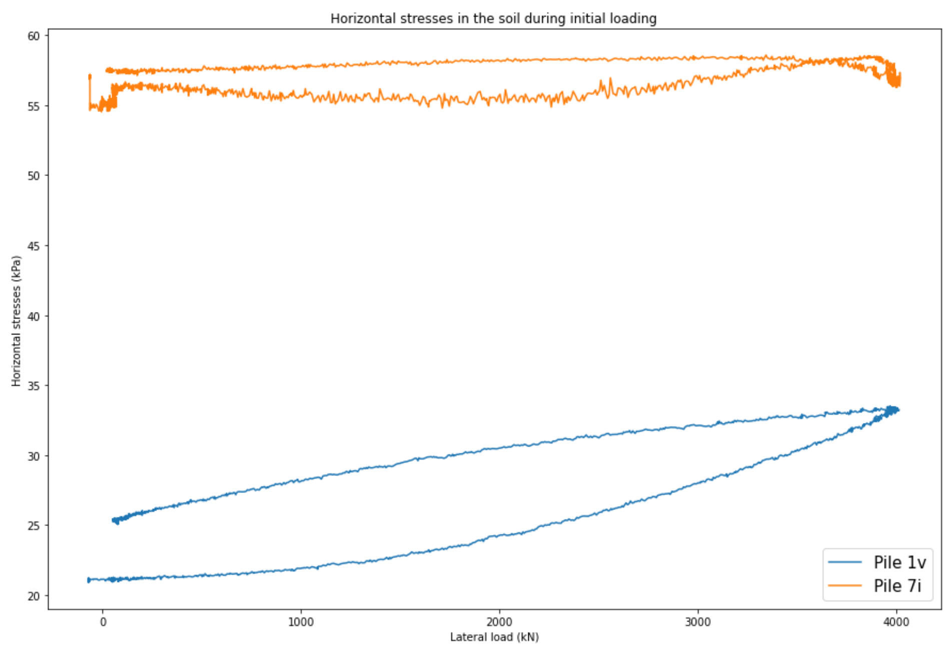

Figure 6.25: Horizontal stresses measured in the soil during initial loading, batch 3

6.3.2.2 Cyclic loading

Displacement maxima for every cycle during cyclic loading were plotted in Figure 6.26 below. All piles were subjected to 1000 cycles with a load of 4 kN each, except for pile 2v due to time constraints.

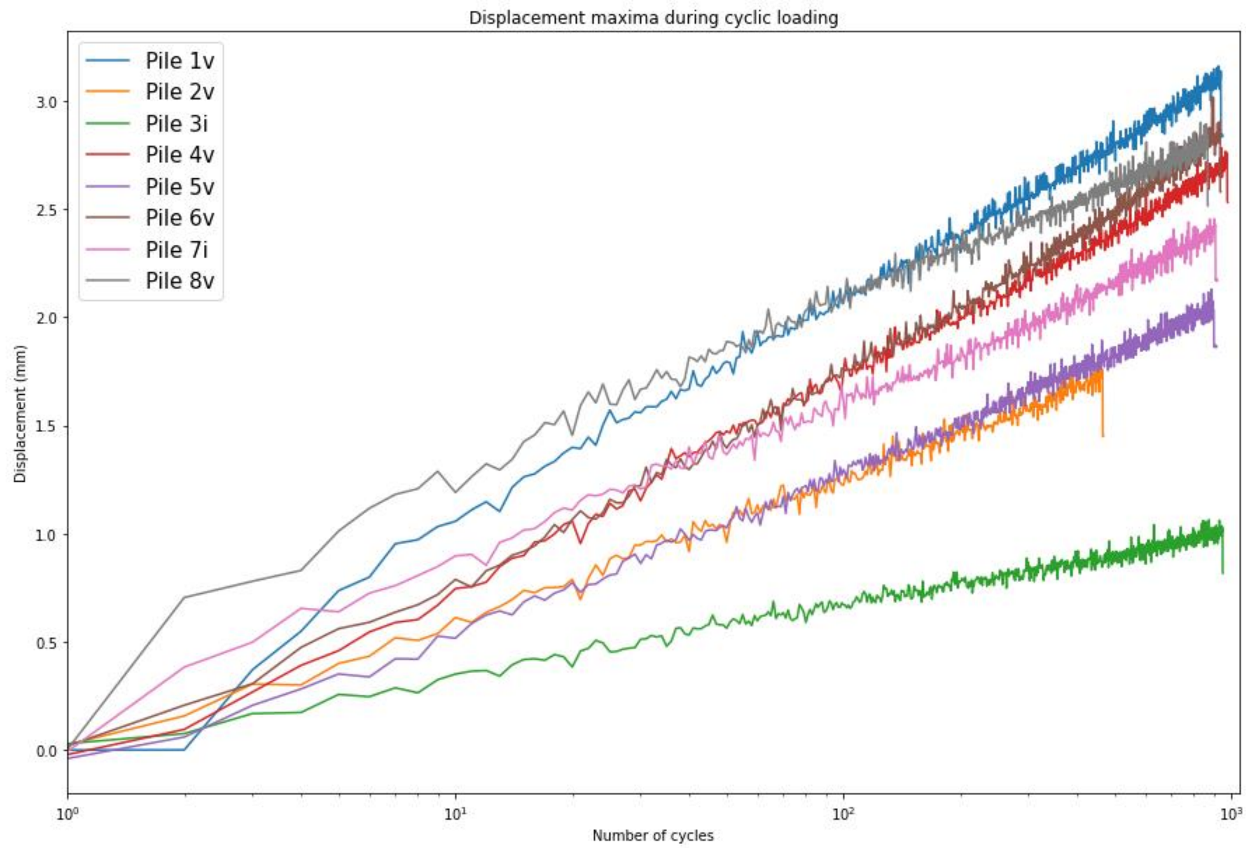

Figure 6.26: Peak displacement according to the number of cycles in batch 3

The order of the piles remained the same as during initial monotonic loading, with very few differences.

The rotation during cyclic loading was also calculated. This was done according to the method of LeBlanc et al. (2010). This paper studies the response of stiff piles to cyclic loading in sand. The steps taken to calculate the rotation have been explained in section 6.3.1.2. The result of the rotation calculations is shown in Figure 6.27. Compared to the figures in LeBlanc et al. (2010), the curves also show a constant slope, albeit less steep that in that paper. This difference may be caused by the sand density, as the sand used by LeBlanc et al. was very loose, compared to medium dense here.

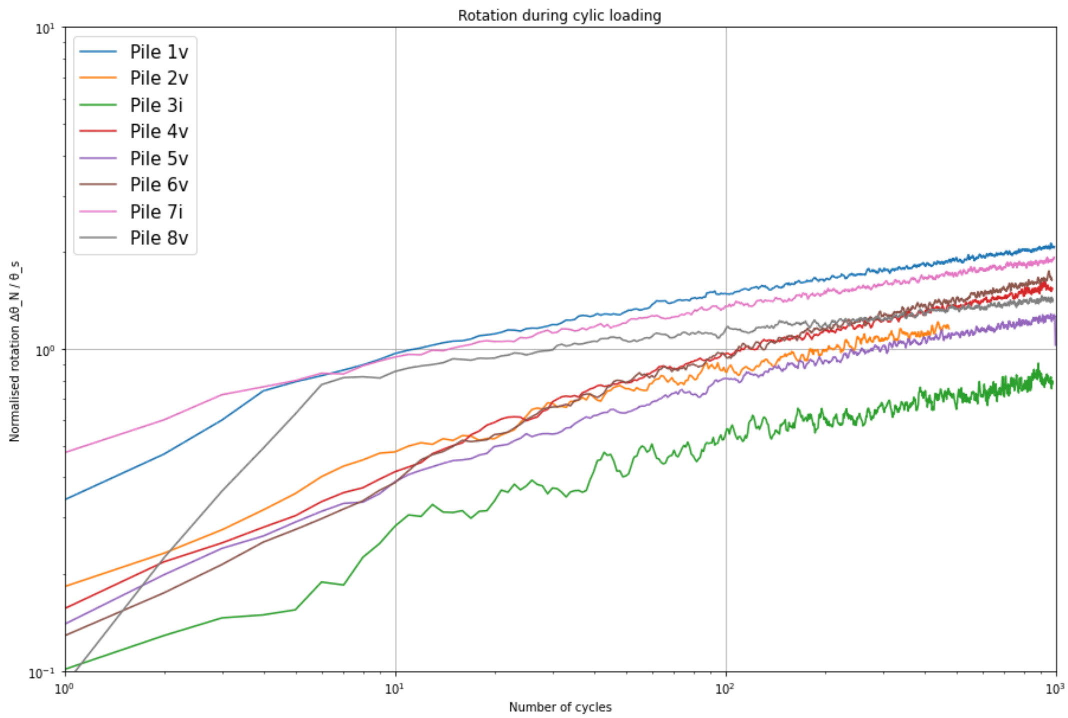

Figure 6.27: Rotation during cyclic loading in batch 3

The secant stiffness of the piles was calculated by dividing the peak load (4 kN) by the amplitude of the displacement during one cycle. The results are shown in the figure below. The curves for all piles except 3i and 8v were parallel to each other. These two exceptions are the two thick-walled piles.

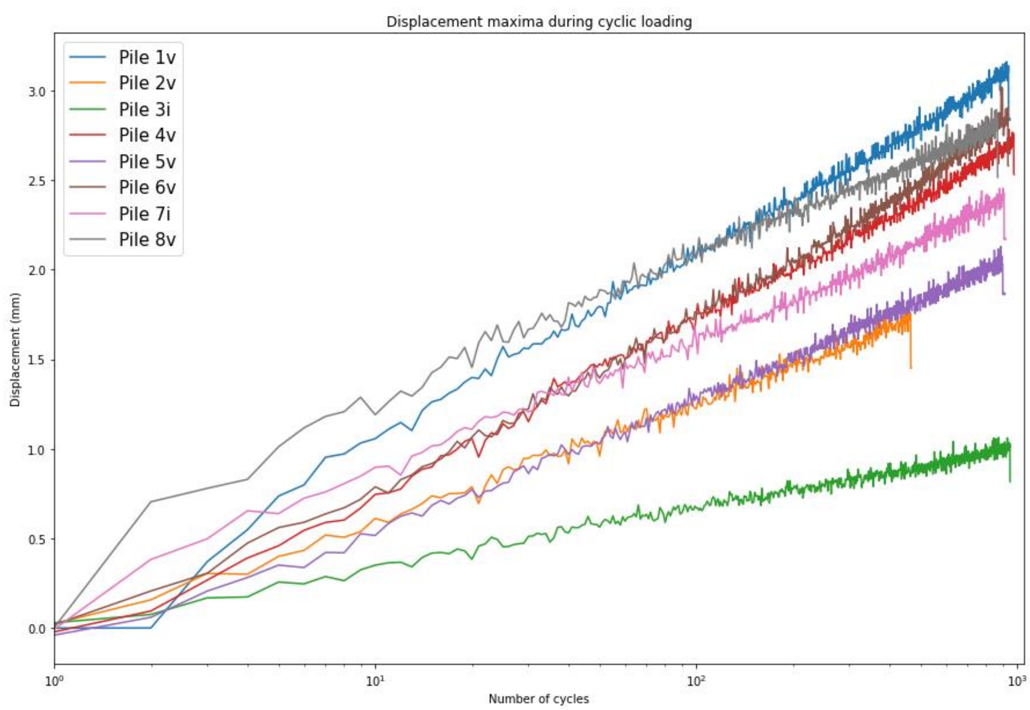

Figure 6.28: Stiffness under cyclic loading in batch 3

When looking at the stiffness of the piles under cyclic loading, the stiffness of pile 3i is markedly higher than the other piles, reflecting the difference in displacement observed in Figure 6.24 and Figure 6.26. Pile 8v, which was installed free-hanging and displayed large displacements during initial monotonic loading, also started with a stiffness much lower than other piles, only to get close to other vibratory piles halfway through cyclic loading.

6.3.2.3 Second monotonic loading

After the initial monotonic load and the cyclic loading period, the pile was loaded monotonically again. All piles were loaded to 20 kN. Figure 6.29 shows the force-displacement curves for the piles under this load. Figure 6.30 is on the same scale as in Figure 6.24 to give a better comparison. In this figure, the effect the first two loading phases had on the piles is visible, as the differences between piles were much smaller up to the load level of 4 kN. After that point, the piles undergo virgin loading so the differences become more pronounced. However, the piles were still divided in the same two groups as during initial loading, which means the qualitative assessment remains the same.

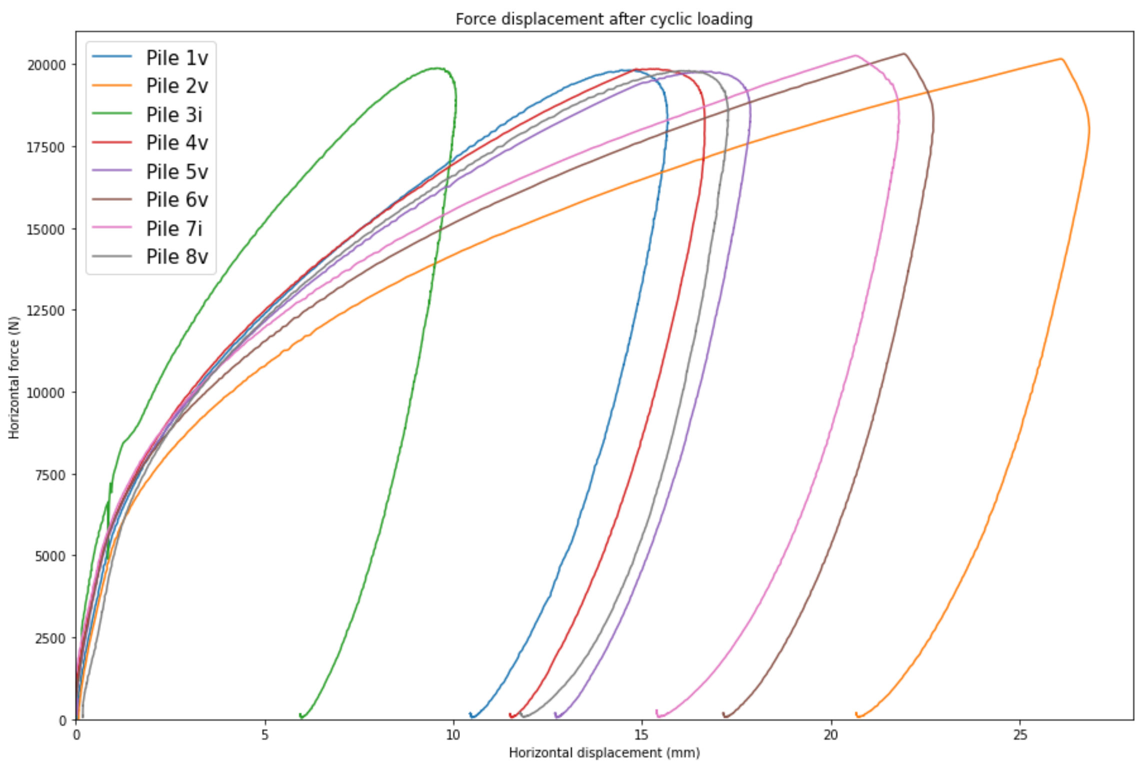

Figure 6.29: Displacement during secondary monotonic loading in batch 3

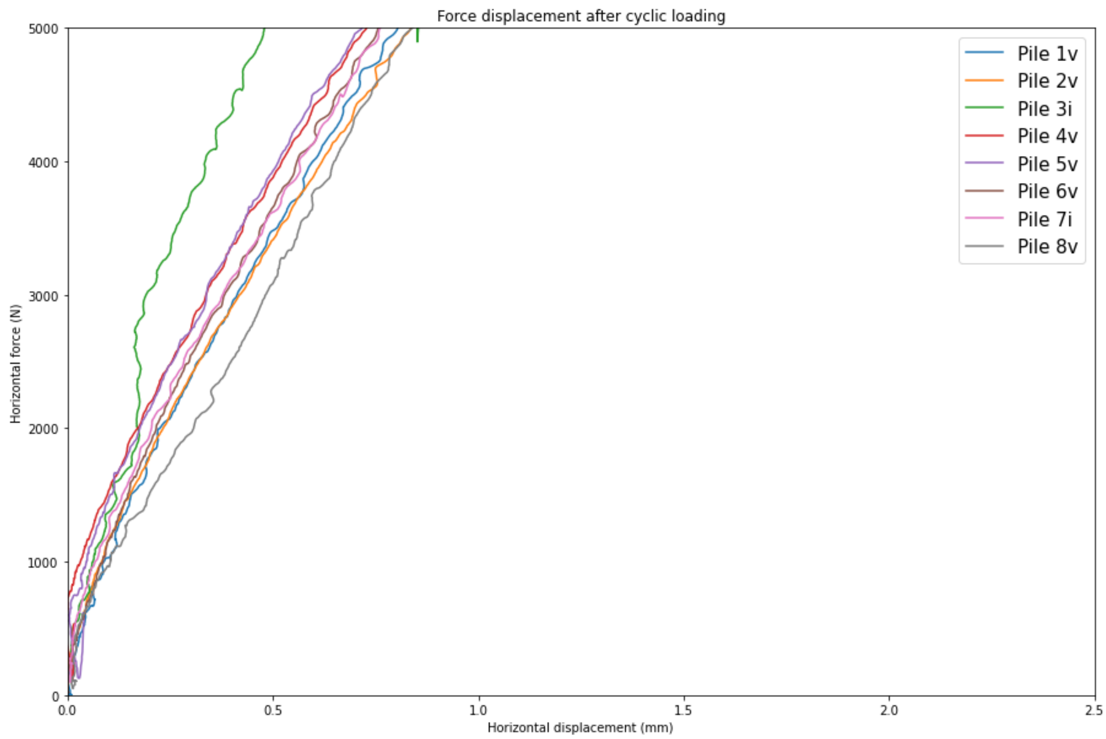

Figure 6.30: Displacement during secondary monotonic loading in batch 3, at the same scale as Figure 6.24

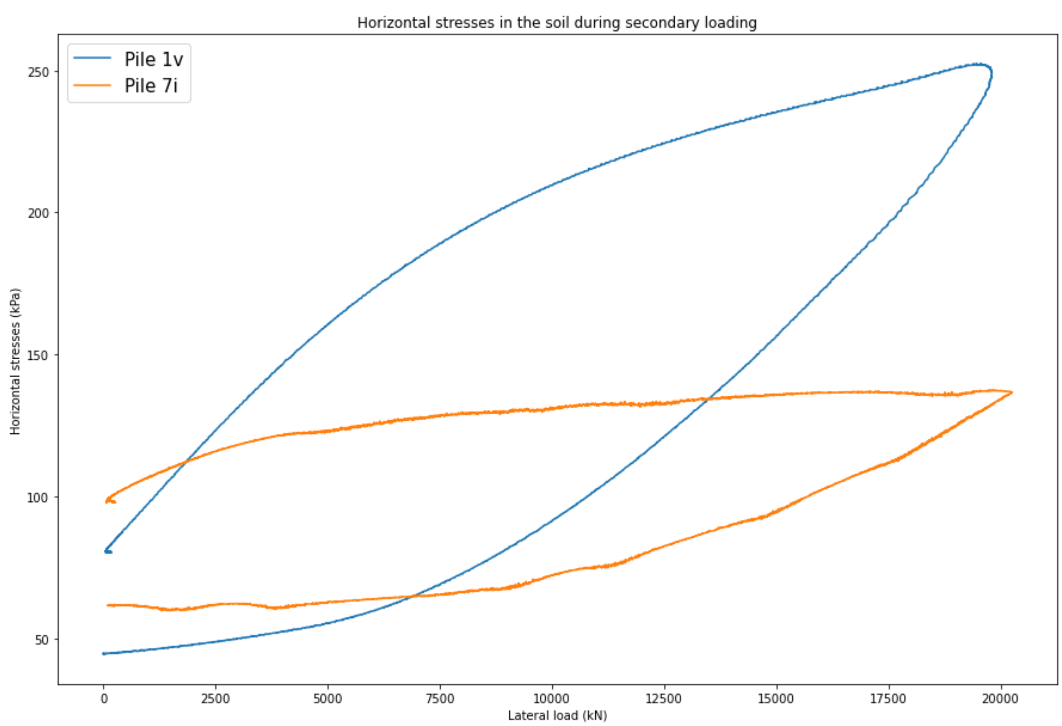

Figure 6.31: Horizontal stresses measured in the soil during secondary loading, batch 3

The stresses in the soil near the pile were also measured during secondary loading, just as during initial monotonic loading. Comparing Figure 6.31 to Figure 6.25, one can see that the initial stress values are higher during this loading step than during the initial loading step, and that the stress levels around both piles are proportionally closer to each other. The stresses around pile 7i barely increased, while those around 1v did. While the vibrated pile initially has lower stresses, it surpasses the impact hammered pile around a lateral load of 7 kN and peaks at 250 kPa, compared to the 175 kPa of the impact hammered pile. Just as in batch 2, the pile where the higher lateral stresses were measured showed lower displacement under loading.

6.3.3 Batch 4

6.3.3.1 Initial monotonic loading

In batch 4, five piles were installed using a vibratory hammer, and three piles using an impact hammer. The installation parameters of the vibrated pile are indicated in Table 6-17. A thin-walled pile had a wall thickness of 4 mm, while a thick-walled pile had a diameter of 10 mm. Low speed corresponded to a crane lowering speed of 10 mm/s, while high speed corresponded to 110 mm/s.

Pile	Thick/thin walled	Speed	Frequency
1v	Thin	Low	23 Hz
2v	Thin	High	23 Hz
3i	Thick	-	-
4v	Thin	High	23 Hz
5v	Thin	Low	23 Hz
6i	Thin	-	-
7i	Thin	-	-
8v	Thick	Low	23 Hz

Table 6-17: Pile installation characteristics for batch 4

Below, the effect of all the applied corrections is visible when comparing two figures in the same batch. Figure 6.32 shows the uncorrected curves for initial monotonic loading and Figure 6.33 shows the corrected curves.

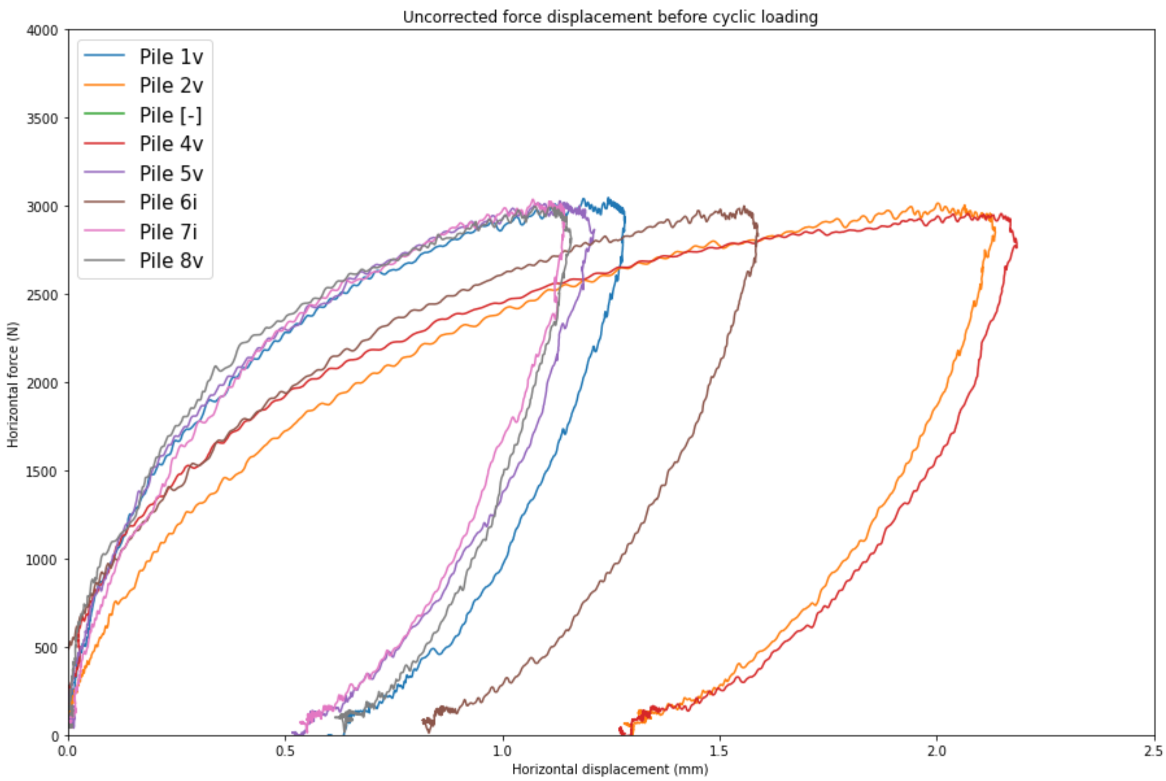

Figure 6.32: Uncorrected displacement during initial monotonic loading for all piles in batch 4

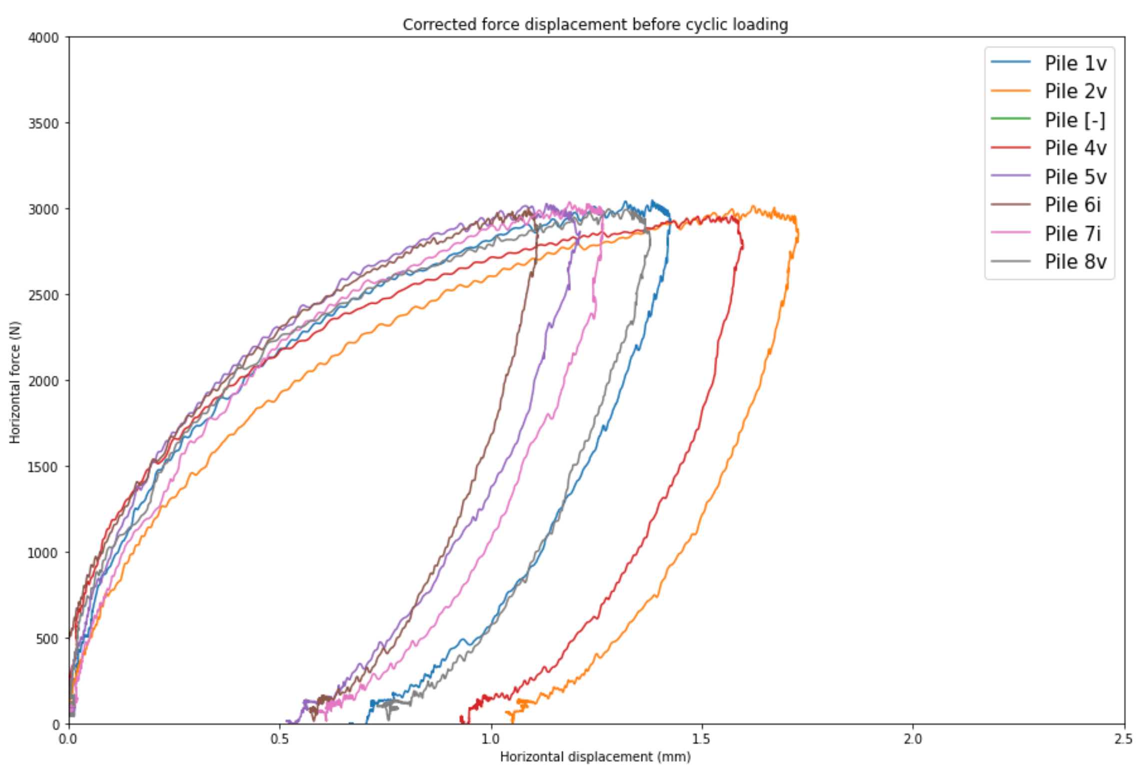

Figure 6.33: Displacement during initial monotonic loading for all piles in batch 4

As can be seen in Figure 6.33, the lowest displacement pile was the impact hammered pile 6i. Interestingly, pile 5v (low speed) showed displacement close to the value of the impact hammered pile 7i. The displacement of pile 3i was not measured during the initial loading phase due to technical issues with the recording equipment. However, other loading phases may give an indication as to how it compares to other piles. The next lowest displacement among the thin-walled vibrated piles is 1v, also a low-speed pile. The two weakest piles, 2v and 4v, were both installed with a high penetration speed.

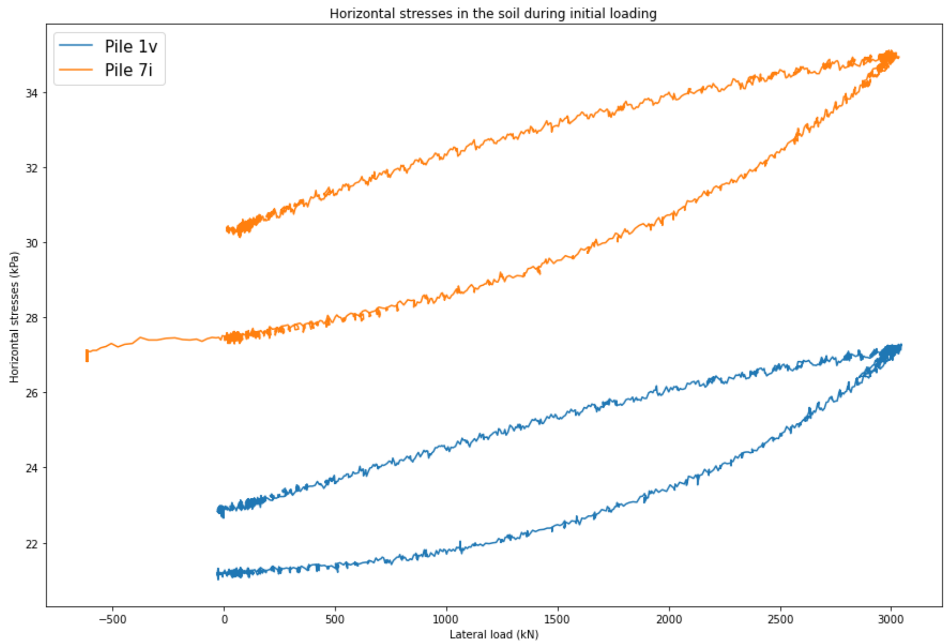

Figure 6.34: Horizontal stresses measured in the soil during initial loading, batch 4

Figure 6.34 shows the horizontal stresses recorded in the soil near piles 1v and 7i. The sensors were place in the sand, half a diameter away from the pile wall in the loading direction. In the figure, the stresses are plotted on the y-axis, as a function of the load applied on the pile. The sensors near both piles recorded an increase in horizontal stress as load is applied to the pile, and the horizontal stresses around pile 7 were higher than around pile 1 during the entire loading phase. This is similar to the previous two batches, where the stresses for the pile with the lowest displacement (7i) were higher than the stresses around the pile with the highest displacement of the two.

6.3.3.2 Cyclic loading

Displacement maxima for every cycle during cyclic loading were plotted in Figure 6.35 below. All piles were subjected to 1000 cycles with a load of 3 kN each, except for the thick-walled pile 3i due to time constraints.

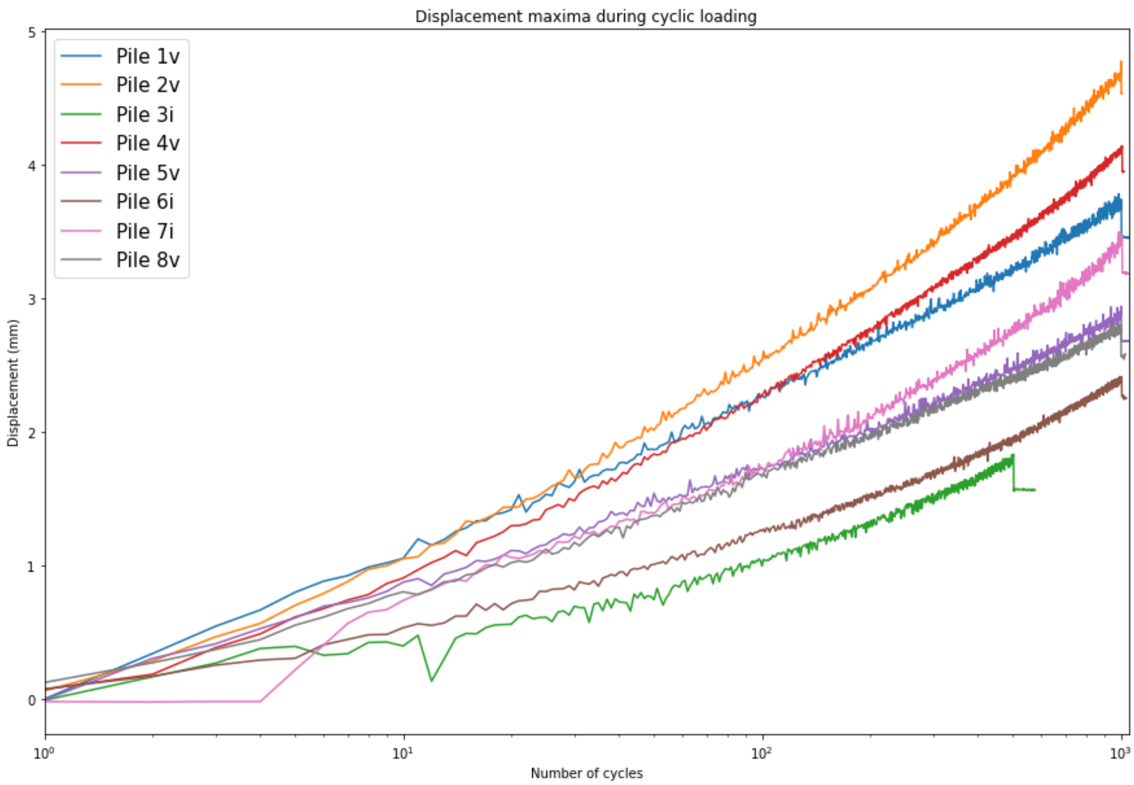

Figure 6.35: Peak displacement according to the number of cycles in batch 4

The order of the piles remains the same as during initial monotonic loading, with very few differences. Pile 3i seems to show the lowest accumulated displacements.

The rotation during cyclic loading was also calculated. This was done according to the method of LeBlanc et al. (2010). This paper studies the response of stiff piles to cyclic loading in sand. The steps taken to calculate the rotation have been explained in section 6.3.1.2. The result of the rotation calculations is shown in Figure 6.36. Compared to the figures in LeBlanc et al. (2010), the curves also show a constant slope, albeit less steep that in that paper. This difference may be caused by the sand density, as the sand used by LeBlanc et al. was very loose, compared to medium dense here.

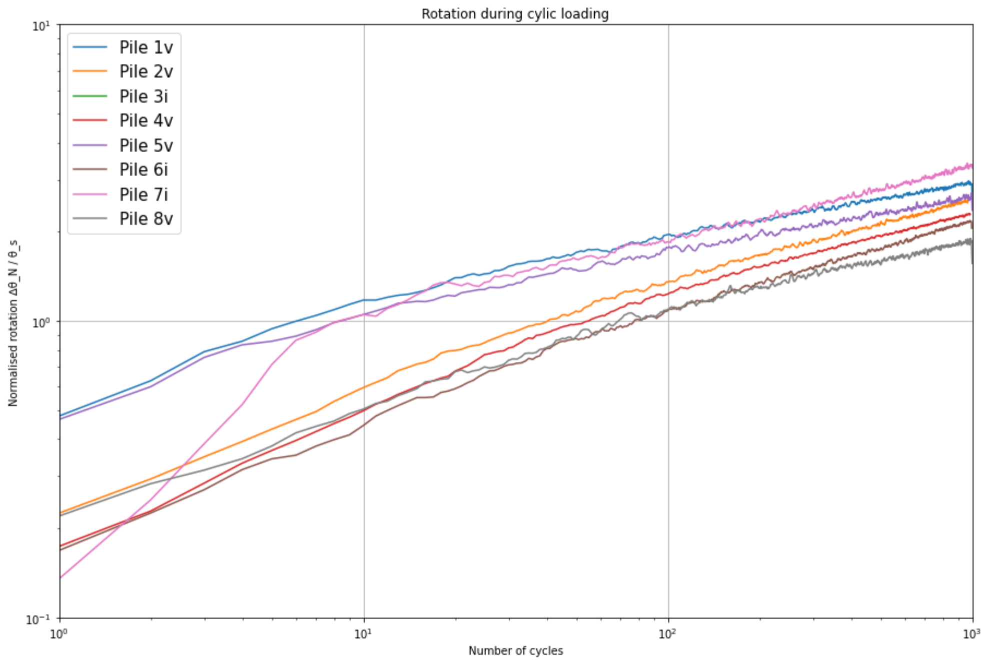

Figure 6.36: Rotation during cyclic loading in batch 4

The secant stiffness of the piles was calculated by dividing the peak load (3 kN) by the amplitude of the displacement during one cycle. The results are shown in the figure below.

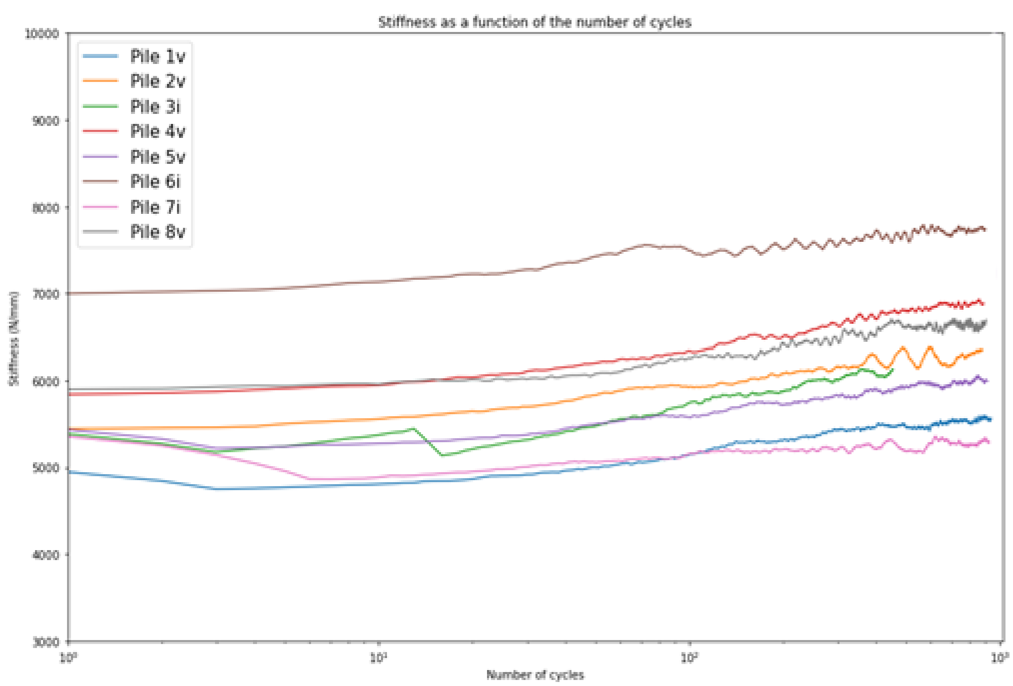

Figure 6.37: Stiffness under cyclic loading in batch 4

When looking at the stiffness of the piles under cyclic loading, pile 6i showed a large stiffness compared to other piles. This difference was not as marked during initial loading. In general, the order of stiffness is not the same. For example, piles 1v and 7i have the lowest stiffness during cyclic loading, but have high or medium initial stiffness during monotonic loading. Similarly, pile 5v which had largest displacement during initial loading and average stiffness compared to other piles.

6.3.3.3 Second monotonic loading

After the initial monotonic load and the cyclic loading period, the pile was loaded monotonically again. All piles were loaded to 12 or 14 kN. Figure 6.38 shows the force-displacement curves for the piles under this load. Figure 6.39 is on the same scale as in Figure 6.33 to give a better comparison. In this figure, the effect the first two loading phases had on the piles is visible, as the differences between piles were almost non-existent up to the load level of 3 kN. After that point, the piles undergo virgin loading, so the differences become more pronounced and the order of strength of the piles changes.

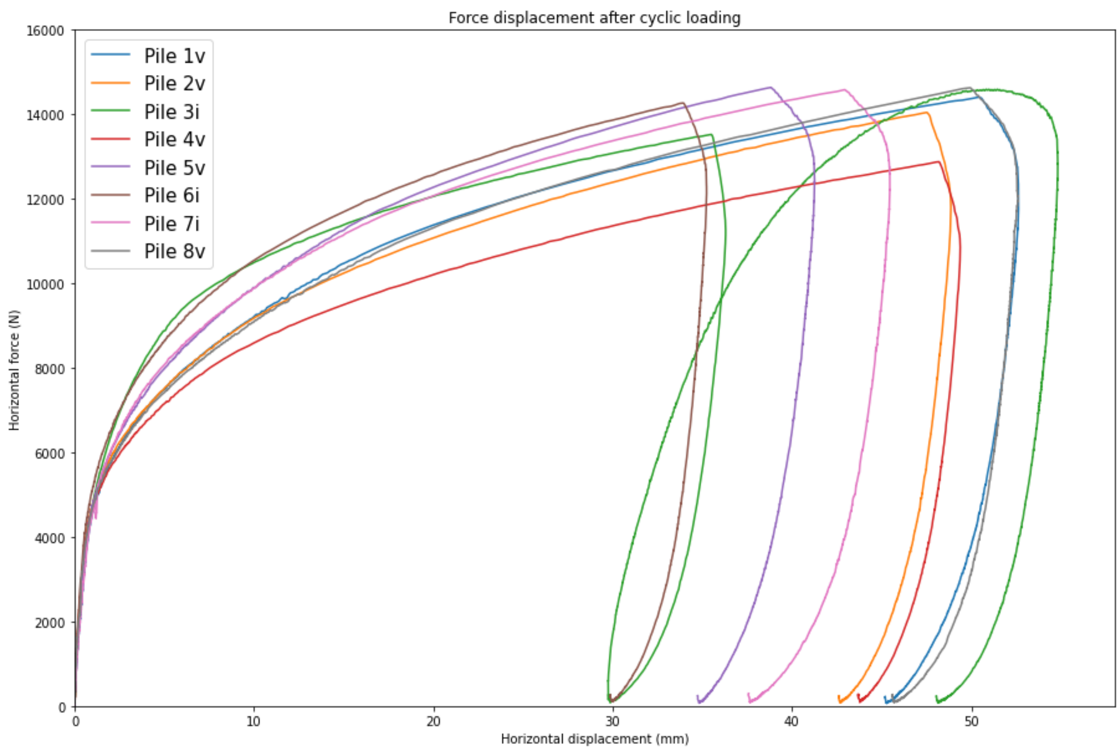

Figure 6.38: Displacement during secondary monotonic loading in batch 4

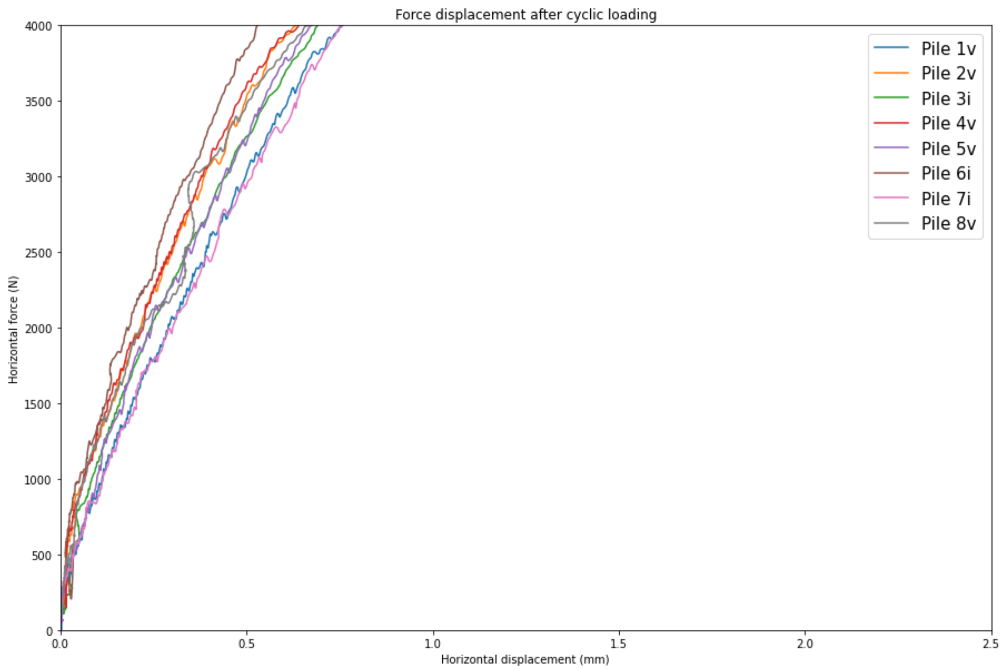

Figure 6.39: Displacement during secondary monotonic loading in batch 4, at the same scale as Figure 6.33

Following cyclic loading where 6i was stiffer than other piles, the pile also shows less displacement in this load phase when looking at both figures above. This shows that the behaviour recorded in Figure 6.37 is in line with observations from the cyclic loading phase and reinforces the indication that the initial monotonic response was likely due to local effects. During cyclic and post-cyclic loading, this pile behaved stiffer. The results during the latter two phases may be more representative as a larger portion of the soil is mobilized compared to during initial monotonic loading.

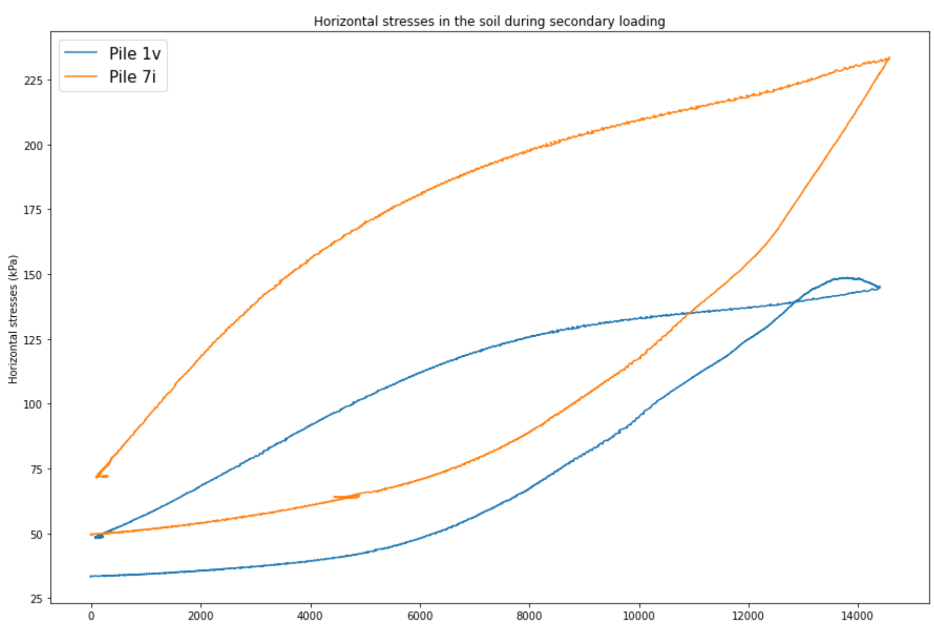

Figure 6.40: Horizontal stresses measured in the soil during secondary loading, batch 4

The stresses in the soil near the pile were also measured during secondary loading, just as during initial monotonic loading. Comparing Figure 6.40 to Figure 6.34, one can see that the initial stress values are higher during this loading step than during the initial loading step. Just as during initial monotonic loading, larger stresses were recorded around pile 7 than pile 1. The same phenomenon is observed here as for batches 2 and 3, where the pile with the lowest displacement during loading also has the highest lateral stresses.

7. Interpretation

In this chapter, the experiment results will be interpreted and some possible explanations for the pile behaviour will be given. This will be done by analysing the results of the loading experiments across both monotonic phases and the cyclic phase, and the data collected during installation. The observed results will be compared to existing literature. For reference, batches 2 and 3 were carried out with dense sand. Batch 4 was carried out with medium dense sand. First, the behaviour of the piles across all loading stages will be analysed, followed by the influence of several installation parameters. After that, other possible factors affecting the lateral behaviour will be mentioned. Next, the use of CPT to predict this behaviour will be discussed. Finally, the soil settlement measurements carried out during the testing campaign will be addressed.

7.1 Behaviour across all loading stages

The experiments in this thesis conclude that the influence of the installation process is not visible anymore after cyclic loading up to the load level the piles had been subjected to in previous phases (4 kN and 3 kN). The load displacement curves of the second monotonic loading phase are very similar for all piles up to that point. This could be due to an accumulation of the strains on the soil. Once the load level exceeds that point and the soil is subjected to virgin loading, differences emerge again. The order of stiffness of the piles is inverted compared to the first two loading phases.

Additionally, the influence of installation effects is reduced as the number of cycles increases. One can infer that from the figures presenting rotation and stiffness. After approximately 100 cycles, the lines almost all piles run parallel to each other meaning the piles experience a similar increase in stiffness/rotation. This has been observed in literature by LeBlanc et al. (2010) or Kementzetzidis et al, (2023). The horizontal stresses measured near an impact hammered and vibrated piles during both monotonic loading stages show that the proportional difference between the piles is lower after cyclic loading. In batch 3, the pile with the lower stress during initial loading is even the pile with the higher recorded stress during secondary monotonic loading. This may be another indicator of the reduction or disappearance of installation effects.

One can combine this with the knowledge from Stein et al. (2020) who observed total stresses around the pile during monotonic and cyclic loading. The experiments in that paper are very similar to the ones described in this thesis. Stein measured larger total stresses around piles with a lower lateral displacement during monotonic loading. During cyclic loading, stresses around the pile were redistributed in that experiment between both sides of the pile on the load axis. This may be the cause for the reduced installation effects discussed above.

7.2 Influence of installation method

When looking solely at installation method among all the thin-walled piles, impact hammered piles showed a lower displacement than vibrated piles in both batches with dense sand. This behaviour was seen across the initial monotonic loading phase, as well as the cyclic loading phase. The final monotonic loading phase until failure did not show this behaviour as discussed above.

In batch 2, the impact hammered piles 2i and 7i underwent lower displacements than thin-walled vibrated piles during initial loading (see Figure 6.24). In batch 3, pile 7i was the impact hammered thin-walled pile. It showed virtually identical horizontal displacement as a thin-walled vibrated pile: 2v (high speed, low frequency, partly crane-controlled).

In batch 4, which was carried out with medium-dense sand, pile 7i undergoes higher displacements than other vibrated piles. In that batch, the lowest displacement piles were low-speed vibrated piles. The results are not clear enough to be able to conclude whether impact hammered piles or low-speed vibrated piles are stiffer under lateral loading in medium dense sand.

When comparing the thin-walled piles individually, impact hammered piles perform better than vibrated piles and have a lower initial displacement. The impact hammered pile is always either the stiffest pile, or among the two stiffest. When looking at medium dense sand however, one can observe that the behaviour of the vibrated pile with the least initial displacement is close to the impact hammered pile in certain cases. In batch 4, the displacement of the stiffest vibrated pile is roughly 10% larger than the impact hammered one. In batches 2 and 3, this number is close to 75%. This means that, provided the installation parameters are chosen correctly, vibrated piles can get close to impact hammered piles in terms of stiffness. These precise parameters are discussed in further sections below. This behaviour does not characterise the piles as a whole, but rather is an observation of the extremes for both methods.

This is in accordance with the paper from Hoffmann et al. (2020) where vibratory driven piles with different installation parameters were compared to impact hammered piles. Impact hammered piles showed lower displacement during initial loading, and the magnitude of the displacement for the vibrated piles depended in installation factors. The same conclusion was also made in Stein et al. (2020) and Spill & Dührkop (2020).

7.3 Influence of wall thickness

During the experiments, two piles with a wall thickness of 10 mm were used, and 6 piles with a wall thickness of 4 mm. In all batches, the pile with the least displacement during the initial loading phase was one with the largest wall thickness (except batch 4 where pile 3i was not measured due to technical issues). During the cyclic loading phase, the piles with higher wall thickness were also stiffer and showed lower displacements than the thin-walled piles. However, this apparent stiffer behaviour is not always true. By looking at initial loading during batch 3, one can see that pile 8v (thick-walled) was the pile with the highest displacement. Not only was its displacement higher than pile 4v which was driven with the same parameters, but it was also higher than all the other vibrated piles. This indicates that even with the additional stiffness provided by the thicker wall, optimal installation parameters are still necessary to obtain low displacements. Based on the observations from pile 8v, free hanging installation may lead thick-walled piles to a lower stiffness than thin-walled piles.

The effect of wall thickness was not broadly analysed in literature. Zdravković et al. (2015) analysed the effect of wall thickness, but in clay and through a numerical model. In that study, it was concluded that wall thickness did not make a difference as piles with two D/t ratios of 110 and 80 showed the same horizontal displacement. Byrne et al. (2020a) uses piles with different wall thicknesses, but the differences are small (5 mm, D/t of 54 and 40) and the influence of that was found to be negligible in those tests. Those were also impact piles, compared to the vibrated piles used here. In this thesis, the difference in D/t ratio is larger (81 and 32) and the results show that when subjected to optimal driving parameters, piles with a larger wall thickness (by extension, a lower D/t ratio) are stiffer and undergo less displacements during initial monotonic and cyclic loading in most cases. In practice however, piles with a higher D/t are used, the value of which corresponds better to the thin-walled piles used in this test.

The results in controlled installations are expected, as thicker pile will innately provide a larger bending stiffness than the thin-walled piles, regardless of soil interaction. This difference in structural stiffness may explain the gap between 4 mm piles and 10 mm piles. Additionally, thicker piles may transfer more energy into the ground during installation (due to their larger weight), which might be the cause of the higher stiffness. On the other hand, they may also accentuate the effects of uncontrolled installation, explaining their behaviour during free-hanging installation.

7.4 Influence of frequency

Vibratory installation in batches 2 and 3 was conducted with different frequencies, but all piles in batch 4 were installed with the same frequency (23 Hz).

In batches 2 and 3, piles installed with the same parameters except for frequency showed similar load-displacement curves. Examples of that are pairs 1v/4v and 5v/6v in batch 3. These two pairs consist of vibrated piles with high speed and low speed respectively. The frequency changed between the pairs which did not influence the load-displacement curves.

In batch 4, all piles are installed at a frequency of 23 Hz. This is lightly higher than what is called “low” frequency in previous batches (which is around 20 Hz). A frequency of 23 Hz is the value usually used in offshore installation (Achmus et al., 2020). Having the same frequency for all vibrated piles allows for an observation of the effect of other installation factors. In that batch, differences in displacement were just as present for piles with the same frequency. Identical piles with the same installation parameters (1v and 5v) even showed different displacements, meaning other installation or soil parameters are the cause of this difference.

7.5 Influence of penetration speed

As explained earlier, batches 2 and 3 had piles installed with varying penetration speed and frequency, but batch 4 only varied penetration speed. While it may be tempting to consider only batch 4 when analysing penetration speed only, one must remember that the soil conditions in batch 4 were medium dense. The dense sand in batches 2 and 3 is closer to North Sea applications, the most relevant environment for this research.

In both batches 2 and 3, the piles with the lowest displacement during initial loading (among all vibrated thin-walled piles) are the piles installed with a high penetration speed. However, an interesting observation in both batches is that when disregarding frequency, there is no logical order to the piles when comparing displacement (as was the case when taking only frequency into account in the previous section). Although it seems that high penetration speed is necessary to install a pile which will have low displacements, but that alone is no guarantee. In batch 3 for example, pile 1v (high speed/high frequency) has much larger displacements than pile 2v (high speed/low frequency) when both are installed with high speed. It is therefore clear from this and the previous chapter that in dense sand, a combination of both parameters dictates the pile behaviour under lateral loading.

Some piles in batch 3 were installed in a way that penetration speed would not be limited by the crane lowering speed. This was done by giving the rope some slack before starting the installation. Those piles are called “free hanging”. The free hanging piles were installed at high speed, and all had a load displacement curve in the initial monotonic phase that is less stiff than the other piles. Despite two thin walled free-hanging piles having different frequency, both showed very similar displacement during initial loading meaning penetration speed plays an important role in the lateral behaviour of piles.

While high speed can result in stiffer piles (like pile 2v), it can also result in large displacements if the speed is not controlled (in this case by a crane). Lack of crane control during installation clearly influences the lateral behaviour of the piles. This could be due to the presence of a non-cavitational environment, which has been identified in the literature study as resulting in piles with higher displacement. This is supported by the results of Labenski & Moormann (2019) where piles installed in a non-cavitational way also resulted in larger displacements.

In batch 4, installation speed was the only varying parameters between thin-walled vibrated piles and all piles were crane-controlled. The frequency was kept at 23 Hz for all piles. In that case, as can be seen in Figure 6.33, the piles with the lowest displacement during initial loading were the two piles installed with a low penetration speed. These piles (1v and 5v) are within 10% lateral displacement of the thin-walled impact hammered pile. Meanwhile, the two piles installed with a high penetration speed show the same force-displacement curve, with more than twice the displacement of the “slow” piles. This shows that, when choosing a low frequency of 23 Hz, a low installation speed is necessary to obtain piles that will have the lowest displacement under lateral loading in medium dense sand. This is in contrast with batches 2 and 3, where the opposite effect was observed. One can conclude that soil density has a role in shaping the effects of installation speed on pile behaviour under loading. A low installation speed might compact the medium dense sand (resulting in higher stiffness piles) more than the dense sand.

The results in existing literature also showed a difference in behaviour depending on initial sand density. Labenski & Moormann (2019) reach the conclusion that piles installed with a lower speed show lower displacement under monotonic loading. The study was using medium dense sand in their experiments, with properties close to batch 4 here. The results from the literature line up with the results from that batch. On the other hand, studies in dense sand such as Stein et al. (2020) showed the opposite behaviour: piles with a higher penetration speed (not including the free hanging piles) had an initial stiffness closest to the impact hammered piles. The circumstances correspond to batch 2 and 3: Both these batches were executed in a higher sand density. Although in the thesis’ experiments, the piles with the least displacement were also piles installed at high speed, the rest of the pile loading tests do not provide enough evidence to make a definitive conclusion.

7.6 Influence of horizontal stresses in the sand

The findings from the literature study and the conclusion from previous papers (Hoffmann et al., 2020), (Remspecher et al., 2019), (Stein et al., 2020) indicate changes in the horizontal stresses during and after pile installation. Hoffmann correlates the increase of horizontal stresses in the sand near the pile wall during installation with the horizontal displacement during monotonic loading, stating that piles showing a larger increase of horizontal stresses had lower displacements. Remspecher measures the soil density around the pile with help of particle image velocimetry and observes notable changes close to the pile wall. Because of this, horizontal stresses in the soil during installation were believed to be of interest and were measured in the SIMOX experiments. Horizontal stresses were measured on two piles every batch: one vibratory driven pile (1v) and one impact hammered pile (7i). The measurements were recorded during installation and loading with the presence of a sensor in the soil at a depth of 1.4 m and are presented in section 6.1.

7.6.1 During installation

The horizontal stresses during the installation of the impact hammered pile were the same during batch 2 and 3, with a peak of 75 kPa at the sensor depth. In both cases, the installation parameters were also the same. The horizontal displacement during initial loading was very similar as well, around 1.10 mm. In batch 4, which consisted of medium dense sand, the lateral stresses peaked lower at 50 kPa but the horizontal displacements remained approximately the same as in previous batches.

When looking at the horizontal stresses measured near the vibrated pile, there is a noticeable increase (20 kPa) during installation in batch 3, but almost no increase (2.5 kPa) in batch 4 and even a decrease (2.5 kPa) in batch 2. However, the large increase in batch 3 was barely present anymore by the time the installation was finished (30 kPa) with the end value being slightly higher than the other batches (around 25 kPa). A likely explanation for this is that the peak in stress is present around the pile toe, as it is also observed when the pile passes the sensor. This exact behaviour can also be seen clearly in Stein et al. (2020).

The only difference between the installations in batches 2 and 3 were the installation parameters: batch 2 was done with low speed and low frequency, whereas batch 3 was done with high speed and high frequency. This seems to show that either installation speed, frequency, or possibly both influence the soil which can be observed in the form of horizontal stresses. It is important to note that this increase happening in batch 3 might also happen during the installations of batch 2 and 4, but at a reduced distance from the pile which cannot be captured by the sensors.

In this experiment, horizontal stresses were measured in the soil at a certain distance of the pile wall, and are most present close to the pile toe as can be seen in Figure 6.1 and Figure 6.5. This is also observed by Fischer & Stein (2022): multiple stress sensors were placed at different depths along the pile installation path, and a peak was visible on each sensor the moment the pile toe passed the sensor depth. Fischer & Stein (2022) observed an increase in horizontal stresses in the soil during installation as well, as multiple sensors were placed at different depths of the pile penetration path. In the case of impact hammered installation and free hanging vibratory installation, an increase was measured as the pile toe passed by the sensor. This was not measured during crane-controlled installation. This result is very similar to what was observed in this thesis' experiments where all impact piles saw an increase as well as pile 1 in batch 3 (a partially free hanging pile) but crane controlled vibrated piles saw no increase.

Although higher horizontal stresses around the pile toe are measured during installation for impact hammered piles and free hanging piles, this does not necessarily translate into lower lateral displacements. Free hanging piles had notably large displacements during monotonic loading, but their installation resulted in higher horizontal stresses in the soil compared to crane guided vibrated piles. More piles would need to be instrumented during installation to be able to compare more results, especially more vibrated piles.

7.6.2 During loading

During both monotonic loading phases, the total horizontal stresses in the soil were measured near two piles: an impact hammered pile (7i) and a pile installed by vibratory driving (1v). The same piles were studied for all the batches. The stresses on the pile wall were also measured, but almost all sensors failed during the first installation which makes it impossible to compare the data obtained.

In all the batches and for all the piles, the pile with the lower displacement between 1v and 7i showed the larger horizontal stresses in the soil. In batch 3 where pile 1v shows a higher displacement during initial loading than pile 7i but a lower displacement during secondary loading, the inversion is also visible in the horizontal stresses.

These observations seem to indicate a link between horizontal stresses around the pile and lateral displacements during loading. However, there seems to be a difference in which stresses play a role in the lateral behaviour of the pile. During installation, the stresses that were recorded were the ones around the pile toe. These were discussed in the previous section and did not seem to impact lateral stiffness. The stresses recorded during loading were further away from the toe (0.5 m, one third of the embedment length) and did seem to have an impact.

7.7 Other possible parameters

Outside of all the installation parameters and factors mentioned in the previous sections of this chapter, there might be other factors that influence the lateral load bearing capacity of monopiles. The factors mentioned in this section have not been investigated during this thesis because of time constraints or because the experiments did not allow for accurate interpretation. However, they will still be mentioned here.

Results have been obtained and conclusions have been made using data from batch 4, where the sand is medium dense. This is in contrast with batches 2 and 3 where the sand was dense. However, there exists the possibility that the same set of installation factors yields qualitatively different results in dense and medium dense sand. Due to the difference in initial density, different phenomenon (such as densification and loosening) could happen even though the same penetration speed and frequency are used. The influence of the initial sand density has been explored during the literature study in section 3.4.5 where it was found to matter. The SIMOX experiments confirm the results from Anusic et al. (2019) where vibrated piles in medium dense sand behaved stiffer in comparison with impact hammered piles than in dense sand. Additionally, different interpretations can be made about the role of penetration speed in dense and medium dense sand (see section 7.5).

Another possible factor for the behaviour of piles under lateral loading, is the stability, or inclination, of the piles during installation. In batch 3, the 3 piles with the highest displacements were piles that were either fully or partially free hanging during installation (piles 1v, 4v and 8v). Since the movement of those piles was not restricted by the crane, incidental inclination of the pile when driving may have been larger compared to impact driving or crane-controlled vibratory installation. Although no measurements were made concerning this, variations in inclination were visually observed during the installation of the free hanging piles. This could be a reason for the larger displacements during lateral loading and might also give a possible explanation as to why pile 8v has significantly larger displacements than piles 1v and 4v. Since 8v was a heavier pile, controlling the inclination was more challenging when installing it free hanging.

7.8 Use of CPT to predict lateral load resistance

The data obtained from cone penetration tests (CPT) showed the difference in cone resistance (q_c) before and after installation at every pile location. Below, an overview is given of the results from CPT after installation compared to the pile displacement during initial loading.

To investigate the relevance of CPT data. The CPT have been ordered from highest q_c to lowest q_c after installation, next to a list of piles from lowest to highest lateral displacement during loading (see 6.3). Average q_c was calculated over the top 1.5 m. The CPT data has been plotted previously and is available in Appendix D: CPT results. For batch 2, this results in the following order.

Pile number (decreasing q_c after installation)	Pile number (increasing displacement)
7i, impact hammered	8v, low speed, high frequency, crane controlled
5v, high speed, low frequency, crane-controlled	3i, impact hammered
3i, impact hammered	2i, impact hammered
4v, high speed, high frequency, crane-controlled	7i, impact hammered
6v, low speed, high frequency, crane-controlled	4v, high speed, high frequency, crane-controlled
8v, low speed, high frequency, crane controlled	6v, low speed, high frequency, crane-controlled
1v, low speed, low frequency, crane-controlled	5v, high speed, low frequency, crane-controlled
2i, impact hammered	1v, low speed, low frequency, crane-controlled

Table 7-1: Comparison of CPT results and loading results for batch 2

For batch 3, this results in the following order.

Pile number (decreasing q_c after installation)	Pile number (increasing displacement)
3i, impact hammered	3i, impact hammered
4v, low frequency, free hanging	2v, high speed, low frequency, crane-controlled
1v, high frequency, partially free hanging	7i, impact hammered
8v, low frequency, free hanging	6v, low speed, high frequency, crane controlled
7i, impact hammered	5v, low speed, low frequency, crane-controlled
5v, low speed, low frequency, crane-controlled	4v, low frequency, free hanging
6v, low speed, high frequency, crane controlled	1v, high frequency, partially free hanging
2v, high speed, low frequency, crane-controlled	8v, low frequency, free hanging

Table 7-2: Comparison of CPT results and loading results for batch 3

For batch 4, this results in the following order. All vibrated piles in this batch were installed at a hammer frequency of 23 Hz.

Pile number (decreasing q_c after installation)	Pile number (increasing displacement)
3i, impact hammered	7i, impact hammered
6i, impact hammered	5v, low speed, crane-controlled
7i, impact hammered	1v, low speed, crane-controlled
5v, low speed, crane-controlled	8v, low speed, crane-controlled
8v, low speed, crane-controlled	6i, impact hammered
4v, high speed, crane-controlled	4v, high speed, crane-controlled
2v, high speed, crane-controlled	2v, high speed, crane-controlled
1v, low speed, crane-controlled	3i, impact hammered

Table 7-3: Comparison of CPT results and loading results for batch 4

When comparing both columns, no consistency in the order of the piles is apparent. Average q_c after installation cannot be correlated to pile displacement during initial loading. As q_c values after installation are not related to the displacements under initial monotonic loading, CPT testing cannot be used as the only tool cannot to predict the lateral behaviour of monopiles since they do not capture all installation effects. Multiple studies in the past have tried and failed to correlate post-installation CPT with lateral stiffness. These studies followed the same process of using post-installation CPT data to derive soil parameters for a 3D finite element model. Gavin et al. (2020) particularly studied the accuracy of the CPT method in predicting the behaviour of a laterally loaded pile in sand and came to the conclusion that CPT data are not the most appropriate to observe installation effects. El Kanfoudi (2016) built a FEM using CPT data taken after installation, which turned out to be unreliable in predicting those same effects. Achmus et al. (2020) compared CPT before and after installation and concluded that it did not capture all installation effects.

7.9 Interpretation of soil settlement measurements

In section 6.1, the soil settlement measurements have been compared to the pile displacement during initial monotonic loading. This was done by means of a table ranking the piles in the order of smallest to largest difference in measurements before and after loading (outside and inside of the pile) and in the order of smallest to largest displacements. Although the order is not the exact same, the general order of the piles shows a lot of similarities in all batches. The piles with the smallest difference (the largest negative difference, meaning the largest decrease in soil elevation) are also the piles who show the least displacement during initial monotonic loading. This phenomenon is present in dense and medium dense sand.

The overview of the soil settlement measurements as presented in chapter 6 are given below. For batch 2 in dense sand, this results in the following:

Pile number (increasing difference outside the pile)	Pile number (increasing difference inside the pile)	Pile number (increasing displacement)
3	2	8
2	3	3
7	5	2
5	7	7
1	8	4
4	4	6
6	6	5
8	1	1

Table 7-4: Overview of soil elevation difference and pile displacement order in batch 2

For batch 3 in dense sand, this results in the following:

Pile number (increasing difference outside the pile)	Pile number (increasing difference inside the pile)	Pile number (increasing displacement)
7	3	3
3	4	2
2	7	7
6	6	6
4	2	5
5	5	4
1	1	1
8	8	8

Table 7-5: Overview of soil elevation difference and pile displacement order in batch 3

For batch 4 in medium dense sand, this results in the following:

Pile number (increasing difference outside the pile)	Pile number (increasing difference inside the pile)	Pile number (increasing displacement)
7	7	7
6	1	5
1	5	1
5	8	8
8	6	6
4	4	4
2	2	2

Table 7-6: Overview of soil elevation difference and pile displacement order in batch 4

As the soil inside of the pile is not mobilised during lateral loading, it has less effect on lateral movement in a stiff pile than the soil outside of the pile. The measurements outside will be considered for the interpretation. When looking at all piles across all batches, impact hammered piles compact more than vibrated piles. In fact, vibrated piles compact very little or not at all in dense sand, the compaction is only significant in batch 4 (the experiment with medium dense sand. The reason for this might be a lower compaction potential in dense sand as a result of vibrations. It may be that with these vibration forces and this soil density, the sand is close to the critical state line. However, in medium dense sand, the soil has room to compact and does so when installing vibrated piles. This compaction happening in medium dense sand might be why vibrated piles show similar lateral displacements under initial monotonic loading as impact hammered piles in batch 4.

This supports the hypothesis that lateral stiffness of monopiles in sand is linked with stresses in the soil after installation. This might mean that the parameters needed to achieve a higher lateral stiffness are similar to those used for the piles showing a large elevation difference. There are no conclusions about this phenomenon in literature, but it seems like soil elevation measurements before and after installation may be used to predict the general order of pile displacement under monotonic loading.

A decrease in soil elevation in and around the pile could be explained by compaction of the sand in the vicinity of the pile wall, which results in a pile with a higher pile initial stiffness. The research by Remspecher et al. (2019) proves the existence of such a zone, and the observations made during the SIMOX experiments regarding horizontal stresses around the pile point towards this zone potentially playing a role in the lateral behaviour of piles.

8. Conclusion

The main objective of this study is to investigate the lateral behaviour of monopiles under monotonic and cyclic loading. This was done by means of a laboratory testing campaign as a part of the SIMOX project in the Deltares Water-Soil Flume (WSF). The WSF tests were a stepping stone towards a large-scale testing campaign within the SIMOX project. The insight obtained from the WSF are valuable input for this follow up.

Piles of 324 mm diameter and 2000 mm length (of which 1500 mm embedded) were installed into the soil. The installation method and factors varied by pile: some piles were installed with an impact hammer, others with a vibratory hammer. For the piles that were vibrated into the ground, the frequency and installation were different depending on the pile. Measurements were carried out during installation and loading of the piles, and the results were interpreted with the goal of finding the correlation between installation parameters and lateral stiffness. In total, four batches of eight piles were installed, with the piles from three batches being loaded laterally. The piles were loaded in three phases: an initial monotonic load until 25% of the initially estimated lateral bearing capacity, a cyclic loading phases with 1000 cycles between 0 and the previous value, followed by a second monotonic loading phase until the estimated lateral bearing capacity. During all the loading phases, the pile head displacement was measured with the help of a displacement sensor. In chapter 7, the results have been interpreted in detail. This chapter highlights the conclusions that can be inferred from the interpretation.

On average, the impact hammered piles showed less displacement in dense sand during initial loading than the vibrated piles. In medium dense sand, both impact hammered and vibrated piles with a low penetration speed showed comparable displacements. These displacements were lower than vibrated piles installed with a high penetration speed.

Pile behaviour across batches varies: during the initial monotonic loading phase and the cyclic loading phase, the order of stiffness of the piles remains roughly the same. After cyclic loading, the order is reversed. This happens during the secondary monotonic loading, after the load level has passed the load level of the previous phases. This level corresponds to the moment that the soil is subjected to virgin loading, which may be the reason for this change in behaviour.

When comparing piles of different wall thickness, it is concluded that thick-walled piles displace less than thin-walled piles in crane-controlled installations. During both initial and cyclic loading, thick-walled piles underwent lower displacements and were stiffer than their thin-walled counterparts. This conclusion was valid for all installation parameters and for both impact hammered as well as vibrated piles. However, the increased wall thickness has the opposite effect on lateral displacement in the case of free-hanging installation.

Conclusions can be made regarding penetration speed. It seems that piles installed with a low penetration speed show lower displacement during loading than pile installed with a high penetration speed in medium dense sand. The same conclusion cannot be made in dense sand. It is impossible to make a confident conclusion about the role of penetration speed in dense sand as the results are not conclusive enough.

From comparing the results of free hanging piles with the piles that had their penetration speed controlled by the crane, lack of crane control could be identified as a factor resulting in higher displacements. This is valid for piles with both wall thicknesses. The exact cause of this phenomenon is not clear, but it could be that the cavitational or non-cavitational installation mode (as identified in Labenski & Moormann (2019)) could play a role here.

Pile inclination after installation was investigated to determine whether this conclusion about free-hanging piles was due to that, but no link between the final inclination angle of the pile and lateral behaviour could be observed.

Furthermore, it is concluded that cone penetration testing (CPT) is not an accurate tool to predict lateral behaviour after installation. An extensive CPT campaign was carried out during this thesis, in order to investigate a possible correlation between CPT results and loading test results, but none was found. The results from this experiment seem to confirm the ones from literature in that CPT alone is not sufficient to obtain an accurate prediction of the lateral behaviour of monopiles.

However, soil elevation measurements carried out before and after installation depicted the relative order of displacement among the piles during initial monotonic loading relatively accurately. The difference between measurements before and after installation show compaction in all cases, but the sand around some piles compacted more than others. Piles with a larger compaction showed lower displacements and higher initial stiffness. This compaction of the sand was largest in medium dense sand, which has more potential to compact than dense sand. Piles with the lowest displacements were the piles with the largest compaction around the pile. Combined with the observations made in Remspecher et al. (2019), it seems possible that a zone of compaction around the exterior of the pile wall may the lateral behaviour of monopiles.

Horizontal stresses in the soil during loading seemed to be related to pile displacement during the loading step as they were measured near two piles and the pile with the higher stresses showed the lowest displacement. This was consistent for all batches and for both monotonic loading phases. Using the measurements, one could conclude the stresses around the pile wall were responsible for this behaviour and not the stresses around the pile toe.

Horizontal stresses around the pile seemed to influence the displacement of the pile under lateral loading. Soil sensors measured the total stresses around the pile during both monotonic loading phases, and the pile that showed the lowest displacement was always the one with the highest peak stress during loading. While the stresses were also recorded during installation and higher stresses were recorded around the pile toe during impact hammering, no conclusion could be made linking stresses at the toe of the pile with lateral behaviour.

9. Recommendations

Many aspects of the experiments from this thesis require further research. In order to guide possible future experiments, this chapter provides recommendations based on the experience gained from the current study. Two types of recommendations will be made: recommendations for the next phase of the SIMOX project (field testing) and recommendations for further research independent of this project.

From the point of view of the SIMOX project, the purpose of the testing campaign conducted during this thesis is to provide guidance for field testing. Following the conclusions made in the previous chapter, the following recommendations can be made regarding the field-testing campaign:

- Pile inclination during and after installation should also be measured to investigate any possible effect on lateral behaviour.
- Horizontal stresses should be measured on more piles than during the laboratory experiments, to measure the horizontal stress in the soil during installation and loading. In this thesis, two piles per batch were instrumented, but more instrumented piles will allow for more comparisons and give a better overview of the role of horizontal stresses on lateral behaviour. Additionally, extra sensors are recommended
- As concluded in this thesis, cone penetration testing (CPT) did not give an accurate estimation of the lateral behaviour of monopiles. Future experiments may use less CPT than during the laboratory experiments, as their use for predicting the lateral behaviour of piles is limited.
- The process used in batch 4, where different penetration speeds were tested without varying the vibration frequency, yielded insights on the role of penetration speed in medium dense sand. Such a process should be repeated with a fixed penetration speed and different frequencies to obtain information regarding the influence of frequency on lateral behaviour of monopiles. It is recommended to choose a low penetration speed.
- Similarly, this setup could be used for dense sand as well. This would also allow for a comparison between two sand densities in addition to giving insight on the role of other installation parameters.
- It is recommended to install more piles in free-hanging conditions during the SIMOX onshore tests than during the laboratory tests. The results of those tests combined with the results from the experiments carried out during this thesis could help clarify the processes occurring during installation and complement existing literature.
- It is recommended to use a crane with more than two possible lowering speeds. During the WSF experiments, the crane could be lowered at two different speeds. A crane with more options will allow to experiment with more options.

Additionally, further study focusing solely on the free hanging piles could give a better understanding of the processes that happen during installation and during loading. To do that, more research could be carried out on cavitational and non-cavitational installation, building on the research of Labenski (2019).

The compaction zone around the pile could be investigated as well in a study of its own. In the previous chapter, this was identified as potentially playing a role in the lateral behaviour of monopiles in sand, but little is known about its relation to the installation parameters. A PIV study such as the one by Remspecher et al. (2019) could be done using different installation methods and parameters.

10. References

Achmus, M., Schmoor, K. A., Herwig, V., & Matlock, B. (2020). Lateral bearing behaviour of vibro- and impact-driven large-diameter piles in dense sand. *Geotechnik*, *43*(3), 147–159. https://doi.org/10.1002/gete.202000006

Anusic, I., Lehane, B. M., Eiksund, G. R., & Liingaard, M. A. (2019). Influence of installation method on static lateral response of displacement piles in sand. *Geotechnique Letters*, *9*(3), 193–197. https://doi.org/10.1680/jgele.18.00191

API. (2007). *Recommended Practice for Planning, Designing and Constructing Fixed Offshore Platforms-Working Stress Design API RECOMMENDED PRACTICE 2A-WSD (RP 2A-WSD) TWENTY-FIRST EDITION, DECEMBER 2000 ERRATA AND SUPPLEMENT 1, DECEMBER 2002 ERRATA AND SUPPLEMENT 2, SEPTEMBER 2005 ERRATA AND SUPPLEMENT 3, OCTOBER 2007*.

Bogard, D., & Matlock, H. (1980). Simplified calculation of p-y curves for laterally loaded piles in sand. *Earth Technology Corporation*.

Brinkgreve, R. B. J., Engin, E., & Engin, H. K. (2010). Validation of empirical formulas to derive model parameters for sands. *Numerical Methods in Geotechnical Engineering - Proceedings of the 7th European Conference on Numerical Methods in Geotechnical Engineering*, 137–142. https://doi.org/10.1201/b10551-27

Burd, H. J., Abadie, C. N., Byrne, B. W., Houlsby, G. T., Martin, C. M., McAdam, R. A., Jardine, R. J., Pedro, A. M. G., Potts, D. M., Taborda, D. M. G., Zdravkovic, L., & Andrade, M. P. (2020). Application of the PISA design model to monopiles embedded in layered soils. *Geotechnique*, *70*(11), 1067–1082. https://doi.org/10.1680/jgeot.20.PISA.009

Burd, H. J., Beuckelaers, W. J. A. P., Byrne, B. W., Gavin, K. G., Houlsby, G. T., Igoe, D. J. P., Jardine, R. J., Martin, C. M., McAdam, R. A., Muirwood, A., Potts, D. M., Gretlund, J. S., Tabord, D. M. G., & Zdravkovic, L. (2020). New data analysis methods for instrumented medium-scale monopile field tests. *Geotechnique*, *70*(11), 961–969. https://doi.org/10.1680/jgeot.18.PISA.002

Burd, H. J., Taborda, D. M. G., Zdravkovic, L., Abadie, C. N., Byrne, B. W., Houlsby, G. T., Gavin, K. G., Igoe, D. J. P., Jardine, R. J., Martin, C. M., McAdam, R. A., Pedro, A. M. G., & Potts, D. M. (2020). PISA design model for monopiles for offshore wind turbines: Application to a marine sand. *Geotechnique*, *70*(11), 1048–1066. https://doi.org/10.1680/jgeot.18.P.277

Byrne, B. W., Burd, H. J., Gavin, K. G., Houlsby, G. T., Jardine, R. J., McAdam, R. A., Martin, C. M., Potts, D. M., Taborda, D. M. G., & Zdravkovic, L. (2019). PISA: Recent developments in offshore wind turbine monopile design. In *Lecture Notes in Civil Engineering* (Vol. 18, pp. 350–355). Springer. https://doi.org/10.1007/978-981-13-2306-5_48

Byrne, B. W., Burd, H. J., Martin, C. M., McAdam, R. A., Potts, D. M., & Taborda, D. M. (2019). *OTC-29373-MS PISA Design Methods for Offshore Wind Turbine Monopiles*. http://onepetro.org/OTCONF/proceedings-pdf/19OTC/1-19OTC/D011S005R002/1986257/otc-29373-ms.pdf/1

Byrne, B. W., McAdam, R. A., Burd, H. J., Beuckelaers, W. J. A. P., Gavin, K. G., Houlsby, G. T., Igoe, D. J. P., Jardine, R. J., Martin, C. M., Muirwood, A., Potts, D. M., Gretlund, J. S., Taborda, D. M. G., & Zdravkovic, L. (2020a). Monotonic laterally loaded pile testing in a dense marine sand at Dunkirk. *Geotechnique*, *70*(11), 986–998. https://doi.org/10.1680/jgeot.18.PISA.004

Byrne, B. W., McAdam, R. A., Burd, H. J., Beuckelaers, W. J. A. P., Gavin, K. G., Houlsby, G. T., Igoe, D. J. P., Jardine, R. J., Martin, C. M., Muirwood, A., Potts, D. M., Gretlund, J. S., Taborda, D. M. G., & Zdravkovic, L. (2020b). Monotonic laterally loaded pile testing in a stiff glacial clay till at Cowden. *Geotechnique*, *70*(11), 970–985. https://doi.org/10.1680/jgeot.18.PISA.003

Byrne, B. W., Mcadam, R., Burd, H., & Houlsby, G. T. (2017). *PISA: New Design Methods for Offshore Wind Turbine Monopiles PISA Project View project Tunnels, Excavations, Settlements and Buildings View project OFFSHORE SITE INVESTIGATION AND GEOTECHNICS SMARTER SOLUTIONS FOR FUTURE OFFSHORE DEVELOPMENTS*. https://www.researchgate.net/publication/320863997

Doherty, P., Gavin, K., & Casey, B. (2011). *The Geotechnical Challenges Facing the Offshore Wind Sector*. 162–171. https://doi.org/10.1061/41165(397)18

Dyson, G. J., & Randolph, M. F. (2001). Monotonic Lateral Loading of Piles in Calcareous Sand. *Journal of Geotechnical and Geoenvironmental Engineering*, *127*(4), 346–352. https://doi.org/10.1061/(asce)1090-0241(2001)127:4(346)

El Kanfoudi, N. (2016). *ON MODELLING THE LATERAL BEHAVIOUR OF VIBRATORY DRIVEN MONOPILE FOUNDATIONS FOR OFFSHORE WIND TURBINES*.

Fan, S., Bienen, B., & Randolph, M. F. (2021a). Centrifuge study on effect of installation method on lateral response of monopiles in sand. *International Journal of Physical Modelling in Geotechnics*, *21*(1), 40–52. https://doi.org/10.1680/jphmg.19.00013

Fan, S., Bienen, B., & Randolph, M. F. (2021b). Effects of Monopile Installation on Subsequent Lateral Response in Sand. I: Pile Installation. *Journal of Geotechnical and Geoenvironmental Engineering*, *147*(5), 04021021. https://doi.org/10.1061/(asce)gt.1943-5606.0002467

Fan, S., Bienen, B., & Randolph, M. F. (2021c). Effects of Monopile Installation on Subsequent Lateral Response in Sand. II: Lateral Loading. *Journal of Geotechnical and Geoenvironmental Engineering*, *147*(5), 04021022. https://doi.org/10.1061/(asce)gt.1943-5606.0002504

Fischer, J., & Stein, P. (2022). *Impact and vibratory driven pipe piles: the difference in soil stresses and bearing capacities due to the installation method*.

Gavin, K., Blok, S. D., & Eiksund, G. R. (2020). *The Impact of Installation Method on Monotonic Loading of Monopiles in Sand*. https://www.openaccess.nl/en/you-share-we-take-care

Hoffmann, B., Moormann, C., & Labenski, J. (2020). *Effects of Vibratory Driving of Monopiles on Soil Conditions and Their Cyclic Lateral Load Bearing Behavior Static lateral bearing behaviour of vibratory-driven monopiles View project Liquefaction modelling using Material Point Method View project*. https://www.researchgate.net/publication/344390418

http://www.findapile.com/p-y-curves. (n.d.).

Kementzetzidis, E., Pisano, F., Tsetsas, A., & Metrikine, A. V. (2023). Gentle Driving of Piles (GDP) at a sandy site combining axial and torsional vibrations: quantifying the influence of pile method on lateral behaviour. *Journal of Geoenvironmental and Geotechnical Engineering*, *under review*. https://doi.org/10.4233/uuid:36b8a133-2a5a-49b3-9701-f75f102bbe3d

Koschinksi, S., & Lüdemann, K. (2013). *Development of Noise Mitigation Measures in Offshore Wind Farm Construction*. www.riffgat.de

Krogh, L., Quinteros, S., Engin, H. K., & Lunne, T. (2022). Revisiting interpretation of relative density from shallow depth CPTs in sand. *Canadian Geotechnical Journal*, *59*(6), 808–826. https://doi.org/10.1139/cgj-2021-0200

Labenski, J., & Moormann, C. (2018). *Experimental Investigations on the Lateral Bearing Behaviour of Vibratory-Driven Open Steel Pipe Piles*.

Labenski, J., & Moormann, C. (2019). Lateral bearing behaviour of vibratory-driven monopiles: A modified p-y approach based on experimental observations of scaled model tests. *17th European Conference on Soil Mechanics and Geotechnical Engineering, ECSMGE 2019 - Proceedings*, *2019-September*. https://doi.org/10.32075/17ECSMGE-2019-0350

Labenski, J., & Moormann, C. (2020). *Untersuchungen zum Einbringverhalten und dem lateralen Tragverhalten unter monotoner Einwirkung von in nichtbindigen Böden vibrierend installierten Monopiles*.

LeBlanc, C., Houlsby, G. T., & Byrne, B. W. (2010). Response of stiff piles in sand to long-term cyclic lateral loading. *Geotechnique*, *60*(2), 79–90. https://doi.org/10.1680/geot.7.00196

Li, W., Igoe, D., & Gavin, K. (2014). Evaluation of CPT-based p–y models for laterally loaded piles in siliceous sand. *Géotechnique Letters*, *4*(2), 110–117. https://doi.org/10.1680/geolett.14.00021

McClelland, B., & Focht, Jr. (1956). Soil Modulus for Laterally Loaded Piles. *Journal of the Soil Mechanics and Foundations Division*, *82*(4). https://doi.org/10.1061/JSFEAQ.0000023

Novello, E. A. (1999). From static to cyclic p-y data in calcareous sediments. *Proc. 2nd Int. Conf. on Engineering for Calereous Sediments*, 17–27.

O’Neill, M. W., & Murchinson, J. M. (1983). *An evaluation of p-y relationships in sands*. University of Houston.

Page, A. M., Eiksund, G. R., Schafirt, S., Skau, K. S., & Jostad, H. P. (2016). *Alternative Numerical Pile Foundation Models for Integrated Analyses of Monopile-based Offshore Wind Turbines*. https://www.researchgate.net/publication/319262514

Rainer Massarsch, K., Wersäll, C., & Fellenius, B. H. (2022). Vibratory driving of piles and sheet piles-state of practice. *Proceedings of the Institution of Civil Engineers: Geotechnical Engineering*, *175*(1), 31–48. https://doi.org/10.1680/jgeen.20.00127

Reese, L. C., Cox, W. R., & Koop, F. D. (1974). Analysis of laterally loaded piles in sand. *Proceedings of the Annual Offshore Technology Conference*, *1974-May*, 473–480. https://doi.org/10.4043/2080-ms

Remspecher, F., Le, V. H., Rackwitz, F., Herwig, V., & Matlock, B. (2019). Vibratory driven installation of monopiles – An experimental investigation of the soil-pile interaction. In *Lecture Notes in Civil Engineering* (Vol. 18, pp. 171–176). Springer. https://doi.org/10.1007/978-981-13-2306-5_22

Rodger, A. A. (1980). *A study of vibratory driving in granular soils* (Vol. 30, Issue 3).

Sorensen, S. P. H., Ibsen, L. B., & Augustesen, A. H. (2010). *Effects of diameter on initial stiffness of p-y curves for large-diameter piles in sand*. CRC Press.

Spill, S., & Dührkop, J. (2020). *COMPARISON OF P-Y METHODS WITH LARGE-SCALE TESTS OF IMPACT- AND VIBRATORY-DRIVEN PILES*.

Staubach, P., Machaček, J., Bienen, B., & Wichtmann, T. (2022). Long-Term Response of Piles to Cyclic Lateral Loading Following Vibratory and Impact Driving in Water-Saturated Sand. *Journal of*

Geotechnical and Geoenvironmental Engineering, *148*(11), 4022097. https://doi.org/10.1061/(ASCE)GT.1943-5606.0002906

Stein, P., Gattermann, J., Daumlechner, E., Hinzmann, N., & Stahlmann, J. (2020). *ZykLaMP Großmaßstäbliche Modellversuche zur lateralen Tragfähigkeit offener Stahlrohrpfähle unter zyklischer Belastung bei verschiedenen Einbringverfahren*.

Suryasentana, S. K., & Lehane, B. M. (2014). Numerical derivation of CPT-based p–y curves for piles in sand. *Géotechnique*, *64*(3), 186–194. https://doi.org/10.1680/geot.13.P.026

Suryasentana, S. K., & Lehane, B. M. (2016). Updated CPT-based p–y formulation for laterally loaded piles in cohesionless soil under static loading. *Géotechnique*, *66*(6), 445–453. https://doi.org/10.1680/jgeot.14.P.156

Taborda, D. M. G., Zdravkovic, L., Potts, D. M., Burd, H. J., Byrne, B. W., Gavin, K. G., Houlsby, G. T., Jardine, R. J., Liu, T., Martin, C. M., & McAdam, R. A. (2020). Finite-element modelling of laterally loaded piles in a dense marine sand at Dunkirk. *Geotechnique*, *70*(11), 1014–1029. https://doi.org/10.1680/jgeot.18.PISA.006

Thieken, K., Achmus, M., & Lemke, K. (2015). A new static p-y approach for piles with arbitrary dimensions in sand. *Geotechnik*, *38*(4), 267–288. https://doi.org/10.1002/gete.201400036

Wang, H., Bransby, F. M., Lehane, B. M., Wang, L., & Hong, Y. (2022). Numerical investigation of the monotonic drained lateral behaviour of large diameter rigid piles in medium dense uniform sand. *Geotechnique*. https://doi.org/10.1680/jgeot.21.00149

Wang, H., Wang, L., Hong, Y., Mašín, D., Li, W., He, B., & Pan, H. (2021). Centrifuge testing on monotonic and cyclic lateral behavior of large-diameter slender piles in sand. *Ocean Engineering*, *226*. https://doi.org/10.1016/j.oceaneng.2020.108299

Zdravkovic, L., Jardine, R. J., Taborda, D. M. G., Abadias, D., Burd, H. J., Byrne, B. W., Gavin, K. G., Houlsby, G. T., Igoe, D. J. P., Liu, T., Martin, C. M., McAdam, R. A., Muirwood, A., Potts, D. M., Gretlund, J. S., & Ushev, E. (2020). Ground characterisation for PISA pile testing and analysis. *Geotechnique*, *70*(11), 945–960. https://doi.org/10.1680/jgeot.18.PISA.001

Zdravkovic, L., Taborda, D. M. G., Potts, D. M., Abadias, D., Burd, H. J., Byrne, B. W., Gavin, K. G., Houlsby, G. T., Jardine, R. J., Martin, C. M., McAdam, R. A., & Ushev, E. (2020). Finite-element modelling of laterally loaded piles in a stiff glacial clay till at Cowden. *Geotechnique*, *70*(11), 999–1013. https://doi.org/10.1680/jgeot.18.PISA.005

Zdravković, L., Taborda, D. M. G., Potts, D. M., Jardine, R. J., Sideri, M., Schroeder, F. C., Byrne, B. W., McAdam, R., Burd, H. J., Houlsby, G. T., Martin, C. M., Gavin, K., Doherty, P., Igoe, D., Muirwood, A., Kallehave, D., & Skov Gretlund, J. (2015). Numerical modelling of large diameter piles under lateral loading for offshore wind applications. *Frontiers in Offshore Geotechnics III - Proceedings of the 3rd International Symposium on Frontiers in Offshore Geotechnics, ISFOG 2015*, 759–764. https://doi.org/10.1201/b18442-105

11. Appendix

Appendix A: Equipment specifications

STS
global.sensor.excellence

Submersible Transmitter

ATM/N - Analog Level Transmitter

CUSTOMER BENEFITS

- Fast customization thanks to configurable product design
- Titanium version with PTFE cable available for use in aggressive media
- Available with overvoltage protection
- Compact design requires minimal space

Release: 10.80.0529.A - 2019.06
www.stssensors.com 1

Technical Specifications

PRESSURE MEASURING RANGE (MH20)

	1 ... 5, (1)	> 5 ... 20	> 20 ... 250
Overpressure	3 bar	3 x FS (≥ 3 bar)	3 x FS
Burst pressure, (2)	> 200 bar	> 200 bar	> 200 bar
Accuracy, (3) (± % FS)	≤ 0.5 / ≤ 0.25	≤ 0.5 / ≤ 0.25 / ≤ 0.1	≤ 0.5 / ≤ 0.25 / ≤ 0.1
Thermal shift, (± % FS/°C)			
Zero point -5 ... 50°C	≤ 0.06	≤ 0.03	≤ 0.015
Span -5 ... 50°C	≤ 0.015	≤ 0.015	≤ 0.015
Response time, (typ.)	< 1ms / 10 ... 90% FS	< 1ms / 10 ... 90% FS	< 1ms / 10 ... 90% FS
Long term stability, (4)	< 0.5% FS / < 4 mbar	< 0.2% FS / < 4 mbar	< 0.1% FS / < 0.2% FS

(1) 0.5 mH2O on request
(2) Transducer
(3) Zero based accuracy according to DIN-16086, incl. hysteresis and repeatability at ambient temperature
(4) 1 year (typ. / max.), the long term stability can be improved by ageing (burn-in) the sensor

TEMPERATURE RANGE

Operating temperature	-5 ... 80°C (1)
Process temperature	-5 ... 80°C (1)
Storage temperature	-10 ... 80°C

(1) For operating temperatures > 50°C, please use PE or FEP cable

ELECTRICAL SPECIFICATIONS

	4 ... 20 mA	0 ... 20 mA	0 ... 5 V / 0 ... 10 V
Power supply	9 ... 33 VDC	9 ... 33 VDC	15 ... 30 VDC
Supply influence	< 0.1% FS	< 0.1% FS	< 0.1% FS
Current consumption			3 mA
Circuit diagram	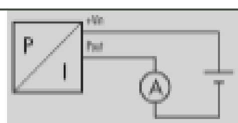	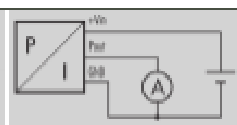	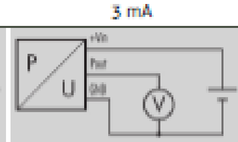
Load resistance	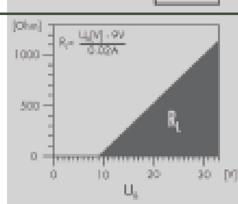	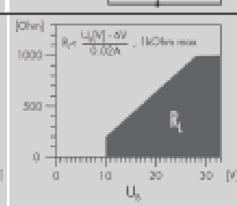	R_L > 10kOhm
Load influence	< 0.1% FS	< 0.1% FS	< 0.1% FS

QUALIFICATIONS

	Description	Level	Typical interferences
EN 61000-4-2	Electrostatic discharge	4 kV contact / 8 kV air	
EN 61000-4-3	Irradiated RF	10 V/m (0.08 ... 1 GHz)	Radio sets, wireless phones
EN 61000-4-4	Transients (burst)	2 kV	Motors, valves
EN 61000-4-5, (1)	Surge	10 kA (8 / 20 µs)	Overvoltage
EN 61000-4-6	Conducted RF	10 V (0.15...80 MHz)	Frequency converters

(1) Only with optional overvoltage protection

PHYSICAL SPECIFICATIONS

Materials	
Transducer	Stainless steel (316L / 1.4435), titanium (Gr. 2)
Housing	Stainless steel (316L / 1.4404), titanium (Gr. 2)
Seals	Viton (Standard), EPDM, Kalrez, NBR
Cable	PUR, FEP, PE, PVC
Weight (1)	108 g

(1) Specification for a ATM/N, closed, without cable

Equipment

OVERVIEW

10.00.0091	Accessories overview

Additional documents

OPERATING AND SAFETY INSTRUCTIONS

	Article number
10.88.0092	DMM029

Ordering information

			X.	XXXX.	XXXX.	XX.	XXX
Type							
	ATM/N	24					
Pressure type							
	Gauge		1				
	Absolute (vacuum)		2				
Pressure measuring range							
	50 mbar ...< 100 mbar			XX			
	100 mbar ... 25 bar			XX			
	Offset, special adjustment			99			
Process connection							
	Closed, (Fig. 1)			55			
	Closed, 1.4435 (7) (8), (Fig. 1)			59			
	Open, (Fig. 2)			56			
	G 1/4 M, (Fig. 3)			11			
	G 1/2 M, (Fig. 3)			13			
	Customized connections available			99			
Electrical connection							
	PE cable, IP 68, black (4) (5)				13		
	PUR cable, IP 68, black (4) (6)				15		
	FEP cable, IP 68, black (4)				21		
	PVC cable, blue, IP 68, (4) (7)				14		
	Connectable version, IP 68, M12x1, (Fig. 4), (3)				07		
	Customized				99		
Output signal							
	0 ... 5 VDC				46		
	0 ... 10 VDC				47		
	0 ... 20 mA				00		
	4 ... 20 mA				05		
	4 ... 20 mA with overvoltage protection				08		
	0 ... 10 VDC with overvoltage protection				49		
	0 ... 5 VDC with overvoltage protection				50		
	Customized				99		
Accuracy							
	≤ ± 0.5 % FS					0	
	≤ ± 0.25 % FS					1	
	≤ ± 0.1 % FS					2	
Temperature range							
	-5 ... 50°C compensated (allowed process temperature: -5 ... 50°C)					4	
	-5 ... 80°C compensated (allowed process temperature: -5 ... 80°C)					5	
Option 1							
Option 2							
	Electronics packed in gel: Gauge pressure						C
	Electronics packed in gel: Absolute pressure						D
Option 3							
	Ballast weight 1.4435						B

Version titanium (without ballast weight)	K
Seals: Viton (standard)	U
Seals: EPDM	S
Seals: Kalrez (Level)	T
Seals: NBR (7)	H
Humidity filter element for gauge versions (only for PUR and PE cable)	Z
Separate electronic (2 tube housings)	Y

(3) Connector with required cable has to be ordered separately (KART100)

(4) Please specify the required cable length and medium

(5) Suitable for drinking water (food approved)

(6) For operating temperature > 50°C, PE or FEP cable must be used

(7) Recommended for drinking water applications

(8) With stainless steel cap

Dimensions

Fig. 1: Closed version

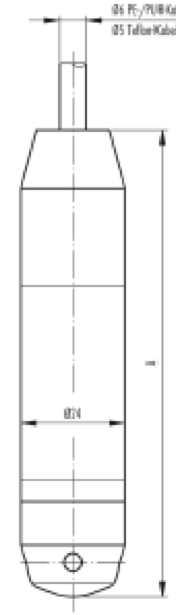

Fig. 2: Open version

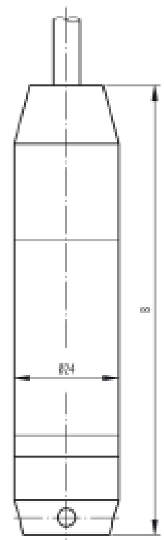

Fig. 3: with process connection

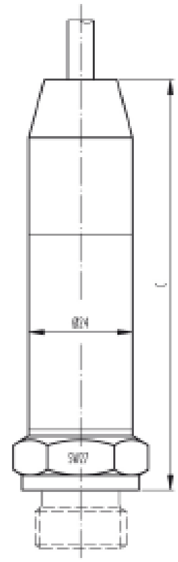

Fig. 4: Electrical connection, connectable

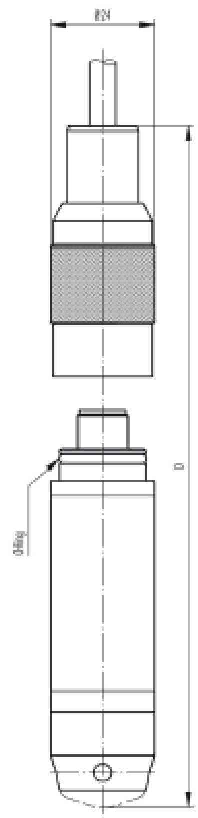

Standard	A [mm]	B [mm]	C [mm]	D [mm]	Weight[g]
without ballast weight	108	104	on request*	on request*	approx. 160
with ballast weight	195	191	on request*	on request*	approx. 420

*C: Depending on process connection

*D: Depending on process connection or version

Version with surge (lightning) protection	A [mm]	B [mm]	C [mm]	D [mm]	Weight [g]
without ballast weight	157	153	on request	on request	approx. 200
with ballast weight	244	240	on request	on request	approx. 460

Colour	2-Wire	3-Wire
white	+Vin	+Vin
yellow	Pout	GND
brown		Pout

Laser Distance Sensors D-Series

Type DPE-30-500

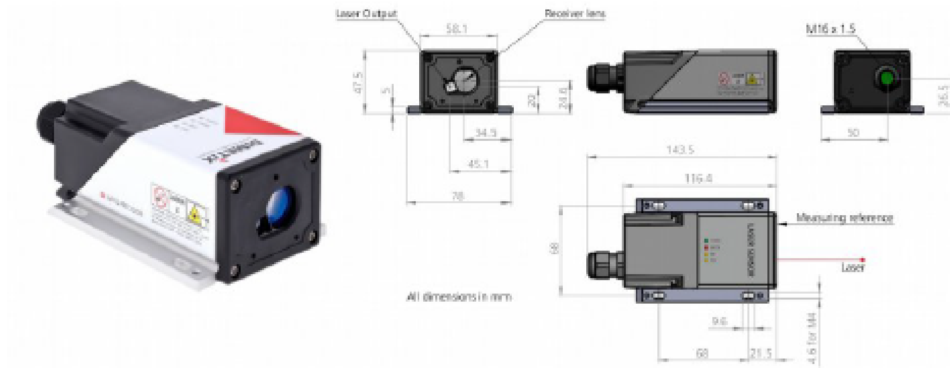

Part No. 500636

SPECIFICATION	
Typical accuracy @ ±2σ (@ ±1σ)	±3 (±1.5) mm
Typical repeatability @ ±2σ (@ ±1σ)	±0.7 (±0.35) mm
Measuring range on natural surfaces	0.05...~100 m
Measuring range on reflective foil	~0.5...500 m
Max. measuring rate	250 Hz
Max. output rate	1 kHz
Operating temperature	-40...+60°C
Degree of protection	IP65
Power supply	12...30 VDC (0.5A @ 24 VDC)
Laser red, visible (Laser Class 2, <1mW)	✓
Typical diameter of laser dot @ 10, 50, 100 m	7 x 3 mm; 28 x 13 mm; 55 x 30 mm
Dimension (L x W x H)	140 x 78 x 48 mm
Weight	350 g

INTERFACES	
Analog output, programmable	0/4...20 mA
Max. error analog output	±0.1 %
Digital input, programmable	1
Digital output, programmable / error display (Type: NPN, PNP, Push-Pull)	2 / 1
Serial Interfaces: RS-232, RS-422 / RS-485, SSI	✓
USB, only for configuration	✓
Optional: PROFIBUS (external) / PROFINET / EtherNet/IP / EtherCAT	✓

CONNECTION	
Internal screw terminals	✓

LASER 2

Technical Data

GENERAL		All data are specified for the MAC400-3000 motor only, i.e. without any expansion module mounted.				
Technology		AC-servomotor with built-in 2000 PPR encoder, hall sensor and 3 phase servo amplifier/controller.				
Controller Type		MAC400-D2 and D3	MAC400-D5 and D6 w. brake	MAC402-D2 and D3	MAC402-D5 and D6 w. brake	MAC800-D2 and D3
Controller capacity	Rated output @ 3000RPM	400W (0.54hp)	400W (0.54hp)	400W (0.54hp)	400W (0.54hp)	750W (1.00hp)
	Rated Torque RMS	1.28Nm (181.26oz-in)	1.28Nm (181.26oz-in)	1.28Nm (181.26oz-in)	1.28Nm (181.26oz-in)	2.38Nm (337.04oz-in)
	Peak Torque	3.8Nm (538.13oz-in)	3.8Nm (538.13oz-in)	3.8Nm (538.13oz-in)	3.8Nm (538.13oz-in)	6.8Nm (962.96oz-in)
	Inertia ($kgcm^2$)/($oz\text{-}in\text{-}s^2$)	0.34/0.004815	0.36/0.005098	0.34/0.004815	0.36/0.005098	0.91/0.01289
	Max. angular acceleration	-rad/sec^2	-rad/sec^2	-rad/sec^2	-rad/sec^2	40000rad/sec^2
	Length	191mm (7.52")	225mm (8.86")	191mm (7.52")	225mm (8.86")	174mm (6.85") / 202mm (7.95")
	Weight (without expansion module)	2.3kg (5.11lb)	2.8kg (6.17lb)	2.3kg (5.11lb)	2.8kg (6.17lb)	3.5kg (7.716lb)
	Audible noise level (measured in 30cm distance)	-	(to be defined) dB(A)	-	(to be defined) dB(A)	-
	Backlash (when brake is activated)	-	<±1 degree	-	<±1 degree	
Controller Type		MAC800-D5 and D6 w. brake	MAC1500-D2 and D3	MAC1500-D5 and D6 w. brake	MAC3000-D2 and D3	MAC3000-D5 and D6 w. brake
Controller capacity	Rated output @ 3000RPM	750W (1.00hp)	1500W (2.04hp)	1500W (2.04hp)	3000W (4.08hp)	3000W (4.08hp)
	Rated Torque RMS	2.38Nm (337.04oz-in)	5.0Nm (708,06oz-in)	5.0Nm (708,06oz-in)	9.55Nm (1352.39oz-in)	9.55Nm (1352.39oz-in)
	Peak Torque	6.8Nm (962.96oz-in)	15.0Nm (2124.18oz-in)	15.0Nm (2124.18oz-in)	28.7Nm (4064.26oz-in)	28.7Nm (4064.26oz-in)
	Inertia ($kgcm^2$)/($oz\text{-}in\text{-}s^2$)	1.13/0.016	13.96/0.198	14.10/0.200	27.83/0.394	27.98/0.396
	Max. angular acceleration	40000rad/sec^2	40000rad/sec^2	40000rad/sec^2	40000rad/sec^2	40000rad/sec^2
	Length	209mm (8.23") / 234mm (9,21")	250mm (9.84")	305.86mm (12.04")	312mm (12.28")	366mm (14.44")
	Weight (without expansion module)	4.3kg (9.48lb)	10.95kg (24.14lb)	13.15kg (28.99lb)	13.2kg (29.10lb)	17.1kg (37.70lb)
	Audible noise level (measured in 30cm distance)	65 dB(A)	-	65 dB(A)	-	65 dB(A)
	Backlash (when brake is activated)	<±1 degree	-	<±1 degree	-	<±1 degree
Speed range for MAC400-402		0-3000RPM with full torque. (Max 3500 RPM shortterm.) Overspeed protection trips at >4300RPM. Motor will shut down				
Speed range for MAC800-3000		0-3000RPM with full torque. Max 3500 RPM. Overspeed protection if speed>3600=motor will go in passive mode				
Amplifier control system		MAC400-800: Sinusoidal wave PWM control. 20kHz switching. MAC1500-3000: Sinusoidal wave PWM control. 5kHz switching.				
Filter:		6th order filter with only one inertia load factor parameter to be adjusted. Expert tuning also available for professionals				
Feedback. Standard incremental:		MAC400, MAC402, MAC1500 and MAC3000 : Incremental A and B encoder 8192 CPR. (Physical 2048 PPR) MAC800: Incremental A and B encoder 8000CPR (Physical 2000PPR)				
Optional absolute multiturn encoder:		Encoder 65535 CPR and 4096 rev.				
Input power supply for MAC400		115/230/240VAC (±10%) for main power circuit. 18-32VDC for control circuit. Consumption at 115-240VAC - see power supply section. Control circuitry consumption: MAC400D1, 2 and 3 (wo/brake) = Typical 0.22A @ 24VDC(5.3W). Control circuitry consumption: MAC400D4, 5 and 6 (w/brake) = Typical 0.58A @ 24VDC(14W).				
Input power supply for MAC402		Nominal 12-48VDC (±10%) for main power circuit. Recommended also for 12V battery applications. Consumption at 12-48VDC - see power supply section. 18-32VDC for control circuit. Control circuitry consumption: MAC400D1, 2 and 3 (wo/brake) = Typical 0.22A @ 24VDC(5.3W). Control circuitry consumption: MAC400D4, 5 and 6 (w/brake) = Typical 0.58A @ 24VDC(14W).				
Input power supply for MAC800		115/230/240VAC (±10%) for main power circuit. 18-32VDC for control circuit. Consumption at 115-240VAC - see power supply section. Control circuitry consumption: MAC800D1, 2 and 3 (wo/brake) =0.25A @ 24VDC(6W). Control circuitry consumption: MAC800D4, 5 and 6 (w/brake) =0.75A @ 24VDC(18W).				
Input power supply for MAC1500 and 3000		3 phase supply 400 to 480AC for driver circuit. Absolute max 550VAC ! 18-32VDC for control circuit. Control circuitry consumption: MAC1500 and 3000-D1, 2 and 3 (wo/brake) =0.3A @ 24VDC(8W). Control circuitry consumption: MAC1500 and 3000-D4, 5 and 6 (w/brake) =1.2A @ 24VDC(24W).				
Control mode		* ±10V Speed and Torque. A+B encoder outputs * Pulse/direction and 90° phase shifted A+B (Incremental). * RS422 or RS232 (5V) position and parameter commands * Gear mode with analog input speed offset + various options. * Sensor zero search or mechanical zero search.				
Flange and shaft dimension MAC400 and 402: MAC800: MAC1500 and 3000		 Front: 60x60mm. Rear 63x115mm. Shaft Ø14mm Front: 80x80mm. Rear: 80x113mm. Shaft Ø19mm Front: 130x130mm. Rear: 130x203mm (excl. connectors). Shaft Ø24.0mm +0/-0.013mm				

Technical Data (continued)

POSITION (pulse inputs)			
Command input pulse	Pulse/direction or 90° phase shifted A+B. RS422		
Input frequency	0-8 MHz. 0-1MHz with input filter		
Electronic gear	A/B: A= -10000 to 10000, B=1 to10000. Simulation of all step resolutions.		
Follow error register	32 bit		
In position width	0-32767 pulse		
Position range	32 bit. Infinity, Flip over at $\pm 2^{31}$ pulses.		
POSITION (serial communication)			
Communication facility	From PLC, PC etc via RS422 or asynchronous serial port RS232 with special cable. MacTalk JVL commands, special commands with high security.		
Communication baud rate	19200 bit/sec (19.2kBaud)		
Position range	±67 000 000		
Speed range	0-3000 RPM.		
Digital resolution	0.3606 RPM		
Acceleration range	250 - 444675 RPM/sec		
Addressing	Point to point on RS422. Up to 32 units on the same serial RS232/RS485 interface with built-in expansion module. Address range 1-254		
Speed variance	Max ±4 RPM variance between command and actual speed.		
SPEED/ TORQUE			
Analogue speed/torque input	11bit + sign. Nom. input voltage ±10V. 10kOhm input resistance. Voltage range max. -10 to +32VDC. Offset typical ±50mV.		
Sampling rate at analogue input	750 Hz		
Encoder output signals	A+, A-, B+, B-, RS422. Line driver 5V outputs (SN75176). 90° Phase shifted.		
Analogue speed input	+voltage -> CW rotation. Shaft view		
Zero speed determination.	0 - rated speed.		
Speed variance at rated speed	Initial error @20°C: ±0,0%	Power Supply: ±10%: 0.0%	
	Load 0-300%: ±0.0%	Ambient temperature 0-40°C: ±0,0005% (±50ppm)	
Torque limit in speed mode	0-300% by parameter		
Analogue torque input	+voltage (positive torque) -> CW rotation. Shaft view		
Torque control accuracy	±10% @ 20°C (Reproducibility)		
VARIOUS			
Electromechanical brake	Optional feature. The brake is activated automatically when an unrecoverable error situation occur.		
Regenerative	Integrated power dump. External attachment is possible		
Protective functions.	Error trace back. Overload I²t, follow error, function error, regenerative overload (over voltage), software position limit. Abnormality in flash memory, under voltage, over current, temperature too high.		
LED functions	Power (Green LED), Error (Red LED). Note that the LED's are only visible when no module is mounted.		
Output signals	3 general purpose NPN 30V/25 mA outputs. Error and In position.		
Zero search	1: Automatic zero search with sensor connected to input (2 formats) 2: Mechanical zero search without sensor. (Torque controlled)		
Shaft load maximum MAC400 and 402: MAC800: MAC1500 and 3000:	Radial load: 24.5kg (13.5mm from flange). Axial load: 9.8kg. Radial load: 18kg (20mm from flange). Axial load: 11kg Radial load: xxN (xxmm from flange). Axial load: xxkg.		
Optional brake (-D5 or D6) MAC400-800 MAC1500-3000	Controlled automatic or from input. 3.25Nm, inertia 0.22cm2, turn on time: 50ms, turn off time: 15ms Controlled automatic or from input. xxNm, turn on time: 50ms, turn off time: 15ms		
Rated power rate. (motor)	MAC400 and 402: 50.0 kW/s	MAC800: 62.8 kW/s	MAC1500-3000: xxx kW/s
Mechanical time constant. (motor)	MAC400 and 402: 0.59±10% ms	MAC800: 0.428±10% ms	MAC1500-3000: ?
Electrical time constant. (motor)	MAC400 and 402: 3.5±10% ms	MAC800: 4.122±10% ms	MAC1500-3000: ?
Standards	MAC400 and 402: CE approved/UL pending MAC800: CE approved/UL recognized file number E254947 MAC1500: CE approved/UL recognized file number E254947 - 20120725 Pending MAC3000: CE approved/UL recognized file number E254947 - 20130524 Pending		
Protection	MAC400: IP55 and IP65 MAC402: IP55 (IP65 on request) MAC800: IP55 (IP42 and IP67 on request) MAC1500 and 3000: IP55 (-D2 or D5 version). IP67 (D3 or D6 version)		
Usage / Storage Temperature	Ambient 0 to +40°C (32-104°F)/ Storage (power not applied): -20 to +85°C (-4 to 185°F) (Humidity 90%). Temperature warning is given before reaching max. Temperature shut down and error message generated at 84°C (183F). The heatsink fan in MAC800-3000 starts at 55°C (131F).		

Mechanical dimensions MAC400

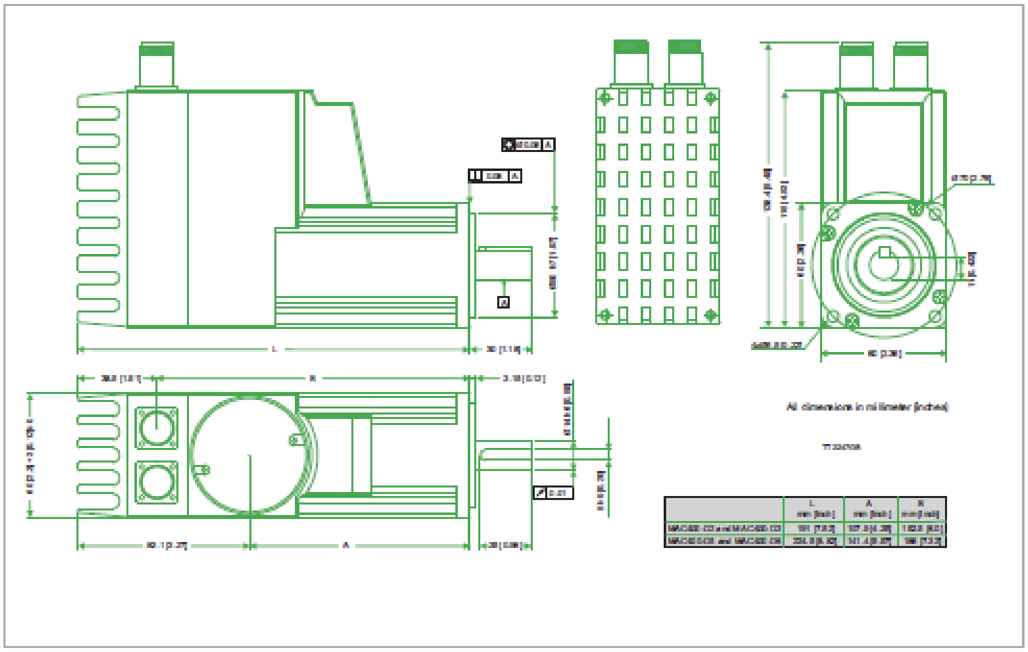

Mechanical dimensions MAC402

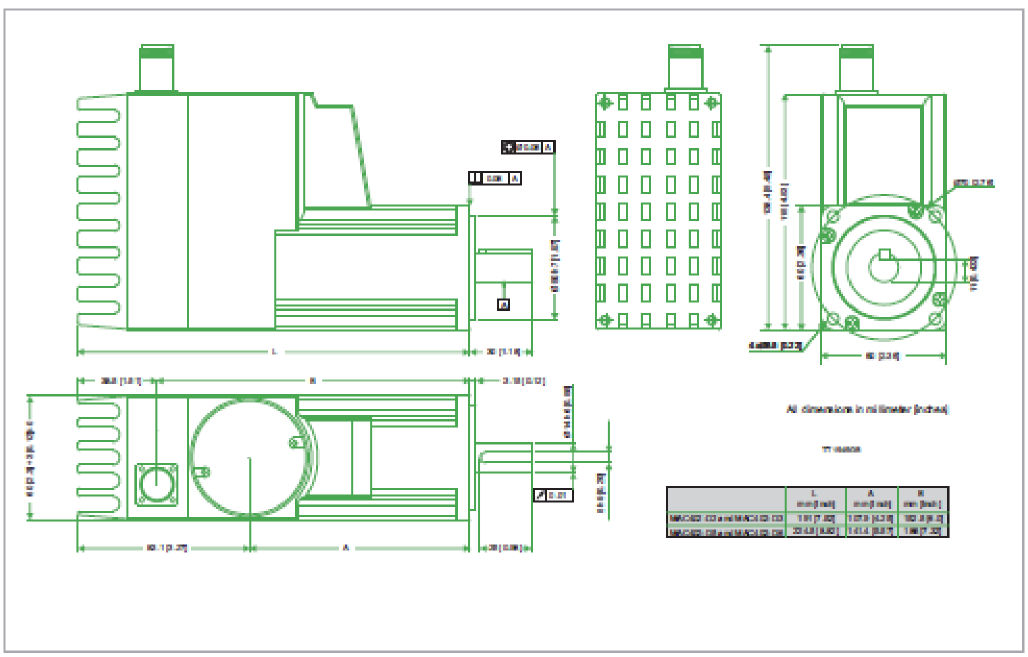

Mechanical dimensions MAC800

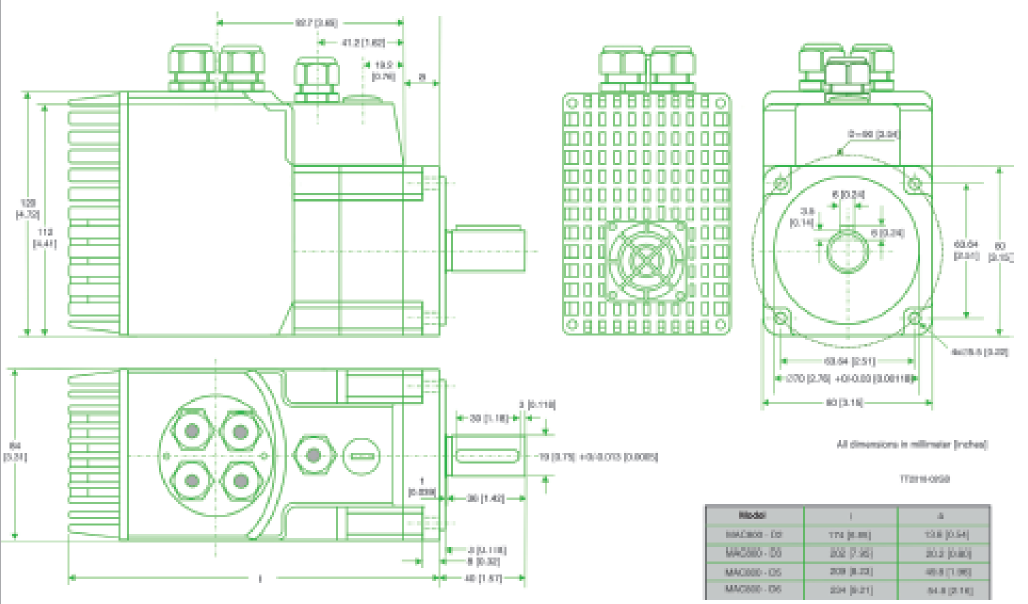

Model	l	A
MAC800 - D2	174 [6.85]	13.8 [0.54]
MAC800 - D3	202 [7.95]	20.2 [0.80]
MAC800 - D5	209 [8.23]	49.5 [1.95]
MAC800 - D6	234 [9.21]	54.8 [2.16]

Mechanical dimensions MAC1500 and 3000

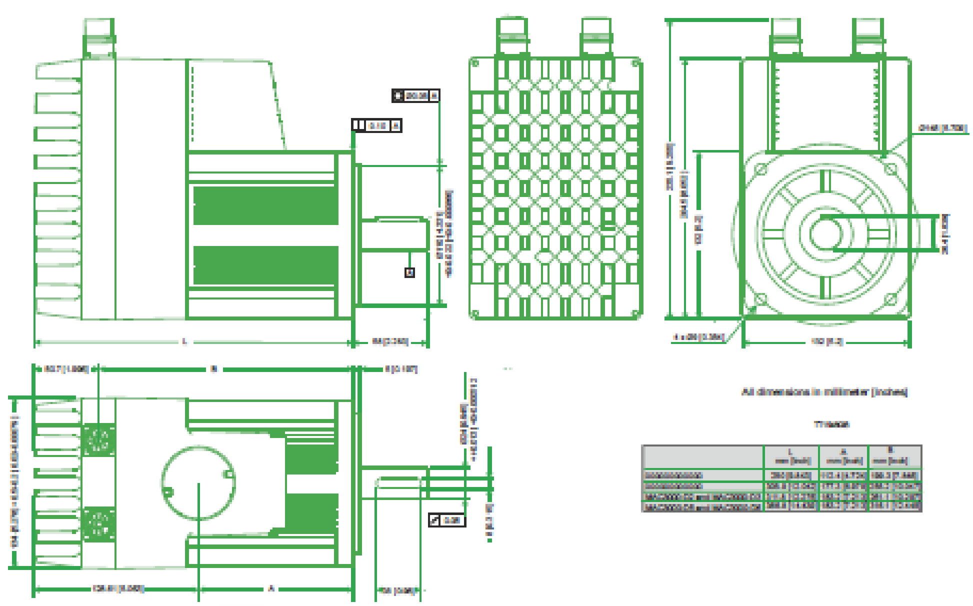

	L mm [inch]	A mm [inch]	B mm [inch]
[illegible]	[illegible]	[illegible]	[illegible]
[illegible]	[illegible]	[illegible]	[illegible]
[illegible]	[illegible]	[illegible]	[illegible]
[illegible]	[illegible]	[illegible]	[illegible]

13

Planetary and cycloidal (robot) gearheads

JVL offers a wide range of both worm, planetary and cycloidal (robot) gears. They fit either directly or by means of adaptors on the MAC motors. gear ratios can be from 1:3 to 1:1000. Se separate datasheets for detailed information on our website: www.jvl.dk

The advanges of using gearboxes:

- Sealed Ball Bearings
- High Reliability, High Efficiency Design
- Sealed Ball Bearings
- High Reliability, High Efficiency Design
- NEMA Mounting Standards
- High Shaft Loading Capacity
- Low Backlash Design
- Strong, Caged Roller Bearings
- Precision Input Pinion with Balanced Clamp Collar

MAC800 with HTRG gearbox

HTRG type gears:

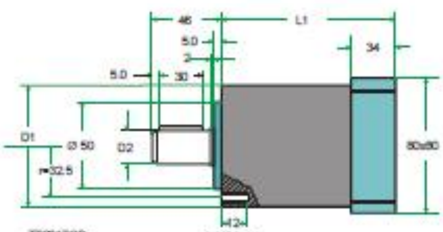

HSPG type gears:

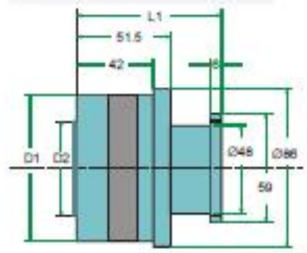

All dimensions in mm

Model. HTRG	Gear ratio	Efficiency	Rated torque	Emerg. Torque	Inertia at motor shaft	Noise	Radial load	Axial load	Weight	L1	D1	D2
MAC400		[%]	[Nm]	[Nm]	[kg*cm²]	[dB(A)]	[N]	[N]	[kg]	[mm]	[mm]	[mm]-(h7)
HTRG08N003MHP70119MC	3	97	18	70	0.11	<70	200	700	1.2	80,55	65	14
HTRG08N005MHP70119MC	5	97	25	90	0.37	<70	200	700	1.2	80,55	65	14
HTRG08N010MHP70119MC	10	97	25	90	0.29	<70	200	700	1.2	80,55	65	14
HTRG08N012MHP70119MC	12	94	30	100	0.56	<70	200	700	1.7	97,25	65	14
HTRG08N020MHP70119MC	20	94	70	250	0.36	<70	400	1400	4.6	142	85	19
MAC800												
HTRG08N003MHP70119MC	3	97	40	180	0.59	<70	400	1400	4	117.5	85	19
HTRG08N005MHP70119MC	5	97	50	200	0.37	<70	400	1400	4	117.5	85	19
HTRG08N010MHP70119MC	10	97	40	180	0.29	<70	400	1400	4	117.5	85	19
HTRG08N020MHP70119MC	20	94	70	250	0.36	<70	400	1400	4.6	142	85	19
HTRG08N100MHP70119MC	100	94	40	200	0.28	<70	400	1400	4.6	142	85	19
HTRG10N020MHP70119MC	20	94	170	600	0.93	<70	600	1600	6.5	180	106	25
HTRG13N100MHP70119MC	100	94	215	800	0.96	<70	800	6500	15.5	205	138	32
HTRG16N100MHP70119MC	100	94	350	1200	1.4	<70	1200	7500	21	229,5	155	40
HTRG19N100MHP70119MC	100	94	500	1400	3.3	<70	1400	15000	29	259.9	195	55
MAC1500-3000												
HTRG10N003MHS40224MC	3	97	100	360	2.2	<70	600	1600	6.5	167,5	106	25
HTRG10N005MHS40224MC	5	97	140	450	1.23	<70	600	1600	6.5	167,5	106	25
HTRG10N010MHS40224MC	10	97	100	360	0.85	<70	600	1600	6.5	167,5	106	25
HTRG13N100MHS40224MC	100	94	215	800	1.2	<70	800	6500	15.5	216	138	32
HTRG16N100MHS40224MC	100	94	350	1200	1.4	<70	1200	7500	21	229,5	155	40
HTRG19N100MHP70119MC	100	94	500	1400	3.3	<70	1400	15000	29	259,9	195	55

Backlash is 15 arcmin for all above HTRG gearboxes

Model. HSPG	Gear ratio	Efficiency	Rated torque	Emerg. Torque	Inertia at motor shaft	Noise	Radial load	Axial load	Weight	L1	D1	D2
		[%]	[Nm]	[Nm]	[kg*cm²]	[dB(A)]	[N]	[N]	[kg]	[mm]	[mm]	[mm]-(h7)
HSPG110 (MAC400)	33,67,89,119	<82	122	610	0,16	-	9300	13100	3,76	-	110	-
HSPG140 (MAC800)	33,57,87,115,139,175	<82	268	1340	0,67	-	11500	17000	6,45	-	140	-
HSPG170 (MAC1K5-3K0)	33,59,83,105,141	<82	495	2475	1,15	-	19200	27900	11,07	-	170	-
HSPG200 (MAC1K5-3K0)	63,83,125,169	<82	890	4450	2,6	-	21100	31700	17,23	-	200	-

Backlash is <1 arcmin for all above HSPG gearboxes

These gearboxes are some examples of the types we often use. For other requests please contact JVL.dk.

kulite

SOIL DYNAMICS

LQ-080U

The LQ-080U Series of soil stress gages is designed to meet the requirements of weapons test labs civil engineering field to make accurate measurements of blast induced soil reactions.

Insertion of a gage in soil disrupts the stress field and induces either stress concentrations or reliefs depending on gage thickness. This stress-transfer phenomenon can seriously affect gage accuracy. To overcome this problem, the LQ-080U employs a pair of extremely stiff diaphragms with a diameter-to-thickness ratio of greater than 5 and a diameter-to-deflection ratio of greater than 2000. This design together with good gage-medium matching ensures accuracy and repeatability of readings.

The DC energized sensing element of the LQ-080U comprises 4-active semiconductor strain gages directly bonded to the measuring diaphragms. The output may be conveniently monitored on most conventional instrument systems. During assembly, the entire unit is given a conformal coating to prevent any ingress of moisture after final on-site-installation.

The LQ-080U Series is available calibrated or uncalibrated, with or without mounting ring. No mounting ring available for 10K PSI.

SOIL STRESS GAGE

LQ-080U SERIES

Designed and developed in cooperation with the U.S. Army Corps of Engineers Waterways Experiment Station, Vicksburg, Mississippi.

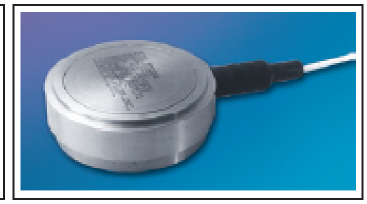

SOIL PRESSURE CELL

TYPE 0234

The BG Series of solid state load cells is designed to meet the demands of soil stress measurement. Being fluid filled the diaphragms exhibit virtually zero deflection under load and the active/total area ratio has been designed so that the intrusion of the cell into the material under study has the minimum effect on its properties. The transducer utilizes a solid state silicon pressure transducer as the basic sensing element coupling extreme robustness with high output. The unit is available with or without an additional reinforcing plate.

Range PSI (Nom.)	Diaphragm Thickness	Overpressure With No Change In Calibration
200	0.025"	300%
3000	0.075"	200%
10000	0.150"	130%

Range PSI	Overpressure
0-15	2 Times Rated Pressure Range
0-50	
0-100	

	LQ-080U Series	Type 0234
Deflection	NA	.0001" (0.0025mm) at Rated Pressure
Natural Frequency (KHz)	17 (Nom.) 200 PSI 80 (Nom.) 10000 PSI	2
Operational Mode	Compression	Compression
Pressure Media	Any Liquid, Solid or Gas Compatible With 17-4 SS (H 900 Condition)	Any Liquid, Solid or Gas Compatible With 17-4 SS (H 900 Condition)
Rated Electrical Excitation	10 VDC (Nom.)	10 VDC (Nom.)
Maximum Electrical Excitation	15 VDC (Max.)	15 VDC (Max.)
Input Impedance	2000 Ohms (Max.)	2000 Ohms (Max.)
Output Impedance	1000 Ohms (Nom.)	1000 Ohms (Nom.)
Full Scale Output	100mV (Nom.)	100mV (Nom.)
Residual Unbalance	± 5mV (Max.)	± 5mV (Max.)
Combined Non-Linearity, Hysteresis and Repeatability	± 0.1% FSO BFSL (Typ.) ± 0.5% FSO (Max.)	± 0.1% FSO BFSL (Typ.) ± 0.5% FSO (Max.)
Resolution	Infinitesimal	Infinitesimal
Operating Temperature Range	-40°F to +200°F (-40°C to +93°C)	0°F to 250°F (-18°C to 120°C)
Compensated Temperature Range	NA	0°F to 105°F (-18°C to 40°C)
Thermal Zero Shift	NA	± 0.01% FRO/°F
Thermal Sensitivity Shift	NA	± 0.01% /°F
Acceleration Sensitivity	Less Than .03 psi/G 200 PSI and 0.1 psi/G 10000 PSI	NA
Humidity	100% Relative Humidity	100% Relative Humidity
Response Time (To Step Input)	Less Than 6 x 10^{5} Sec	NA
Active/Total Area Ratio	NA	43%
Electrical Connection	10' #30 AWG 4 Conductor Shielded Polyurethane Cable	Sealed Cable Assembly In Lengths Up to 33' (10 Meters) 10 Foot Length Standard
Insulation Resistance	100 Megohms @ 50 VDC	100 Megohms @ 50 VDC
Case Material	17-4 PH (H 900) Stainless Steel	17-4 PH (H 900) Stainless Steel
Weight	8.75 Oz. (250 Grams Nom.) With 10' Cable	250 Grams
Sensing Principle	2 or 4 Arm Strain Gage Bridge	4 Arm Strain Gage Bridge

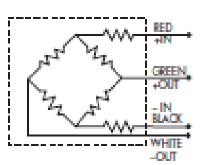

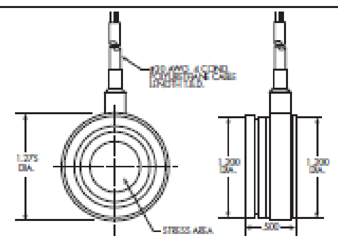

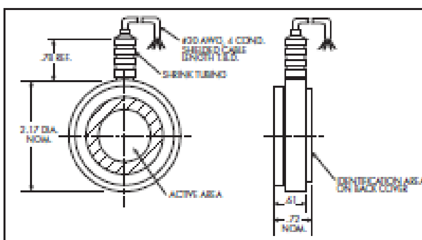

Note: Custom pressure ranges, accuracies and mechanical configurations available. Dimensions are in inches. Dimensions in parenthesis are in millimeters.
Continuous development and refinement of our products may result in specification changes without notice - all dimensions nominal. (D)

KULITE SEMICONDUCTOR PRODUCTS, INC. • One Willow Tree Road • Leonia, New Jersey 07605 • Tel: 201 461-0900 • Fax: 201 461-0990 • http://www.kulite.com

PS

Miniature Pressure Sensors

●For Pressure Distribution Measurement ●50 kPa to 7 MPa

Thin Compact Lightweight

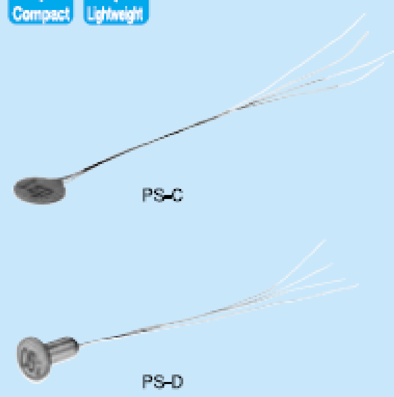

PS series is the strain gage pressure transducers having the bridge formed in the ultra-thin miniature structure. Installation is made with adhesive. Suitable for pressure distribution measurement by using multiple units.

Features

- Ultra-thin design
- Compact
- Wide range of rated capacities

Specifications

Performance

Rated Capacity:

Model (Cable Direction to Sensing Surface) Horizontal	Vertical	Rated Capacity	Natural Frequency (Approx.)
PS-05KC	PS-05KD	50 kPa	10 kHz
PS-1KC	PS-1KD	100 kPa	10 kHz
PS-2KC	PS-2KD	200 kPa	14 kHz
PS-5KC	PS-5KD	500 kPa	20 kHz
PS-10KC	PS-10KD	1 MPa	37 kHz
PS-20KC M2	PS-20KD M2	2 MPa	46 kHz
PS-30KC M2	PS-30KD M2	3 MPa	58 kHz
PS-50KC M2	PS-50KD M2	5 MPa	71 kHz
PS-70KC M2	PS-70KD M2	7 MPa	86 kHz

Measuring liquids of PS-20 to 70KC/D M2 are limited to oils.

Nonlinearity: Within ±1% RO
Hysteresis: Within ±1% RO
Rated Output:
0.25 mV/V (500 μm/m) or more (PS-05KC/D)
0.5 mV/V (1000 μm/m) or more (PS-1KC/D)
0.85 mV/V (1700 μm/m) ±30% (PS-2KC/D)
1 mV/V (2000 μm/m) ±20% (PS-5 to 70KC/D)
Note: Rated output is sorted to one of the classes divided by every 2% difference in output value. Since the rated output stated in the Test Data Sheet is the center value of the class, it may have a maximum error of ±1%.

Environmental Characteristics
Safe Temperature Range: –20 to 70°C
Compensated Temperature Range: 0 to 50°C
Temperature Effect on Zero Balance:
Within ±0.8% RO/°C (PS-05KC/D)
Within ±0.4% RO/°C (PS-1KC/D)
Within ±0.3% RO/°C (PS-2KC/D)
Within ±0.2% RO/°C (PS-5 to 70KC/D)
Temperature Effect on Output:
Within ±0.3%/°C (PS-05 to 2KC/D)
Within ±0.2%/°C (PS-5to 70KC/D)

Electrical Characteristics
Safe Excitation Voltage: 3 VAC or DC
Recommended Excitation Voltage: 1 to 2 VAC or DC
Input Resistance: 350 Ω ±10%
Output Resistance: 350 Ω ±10%
Cable: Polyurethane coated copper wires, 0.1 mm diameter (0.08 mm diameter with PS-05KD & 1KD) by 5 cm long, soldering finish at each tip (Shield wire is not connected to mainframe.)

Mechanical Properties
Safe Overload Rating: 150% (100% with PS-70KC/D M2)
Materials: Metallic finish
Weight: Approx. 0.5 g ±20% (including cable)
Dedicated Adhesive: RC-19 (Request when ordering, charge-free)

Dimensions

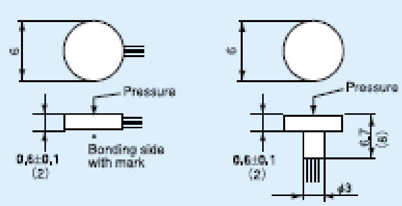

PS-C PS-D

Figures in parentheses are for PS-20 to 70KC/D M2.

2 TRANSDUCERS

AE Sensors B.V.
Jan Valsterweg 92
3315 LG Dordrecht
Tel.: +31 (0)78 6213152

AE-H3 "S"-type Loadcell

For Tension and Compression Loadcells

Short description:

- Nickel Plated alloy steel IP67 "S" type load cell.
- Tension and compression applications.
- Suitable for hanging, hopper and other weighing devices.
- Also available in imperial capacities and dimensions.

OIML test certificate no. D09-06.07
C of C no R60/2000-CNI-06.02

NTEP Certificate no. 06-099A1

Available models:

Capacity	Full article description	Accuracy
25 kg	AE-H3-C3-25kg-3B	C3
50 kg	AE-H3-C3-50kg-3B	C3
100 kg	AE-H3-C3/C4-100kg-3B	C3/C4
150 kg	AE-H3-C3/C4-150kg-3B	C3/C4
200 kg	AE-H3-C3/C4-200kg-3B	C3/C4
300 kg	AE-H3-C3/C4-300kg-3B	C3/C4
500 kg	AE-H3-C3/C4-500kg-3B	C3/C4
600 kg	AE-H3-C3/C4-600kg-3B	C3/C4
750 kg	AE-H3-C3/C4-750kg-3B	C3/C4
1 t	AE-H3-C3/C4-1t-3B	C3/C4
1,5 t	AE-H3-C3/C4-1,5t-3B	C3/C4
2 t	AE-H3-C3/C4-2t-6B	C3/C4
2,5 t	AE-H3-C3/C4-2,5t-6B	C3/C4
3 t	AE-H3-C3-3t-6B	C3 Excluded from OIML
5 t	AE-H3-C3-5t-6B	C3 Excluded from OIML
7,5 t	AE-H3-C3-7,5t-6B	C3 Excluded from OIML
10 t	AE-H3-C3-10t-6B	C3 Excluded from OIML
15 t	AE-H3-C3-15t-6B	C3 Excluded from OIML
20 t	AE-H3-C3-20t-6B	C3 Excluded from OIML
30 t	AE-H3-C3-30t-6B	C3 Excluded from OIML

Specifications and dimensions are subject to change without notice and do not constitute any liability whatsoever.

WWW.AESENSORS.NL

AE Sensors B.V.
Jan Valsterweg 92
3315 LG Dordrecht
Tel.: +31 (0)78 6213152

AE-H3 "S"-type Loadcell

For Tension and Compression Loadcells

Technical specifications:

Accuracy class		OIML R60 C3	OIML R60 C4	C3
Output sensitivity (= FS)	mV/V	2.0 ± 0.004		
Maximum capacity (Emax)	t	0.1, 0.15, 0.2, 0.25, 0.3, 0.5, 0.6, 0.75, 1, 1.5, 2, 2.5		0.025, 0.05, 3.0, 5.0, 7.5, 10, 15, 20, 30
Max. number of load cell intervals	n_{LC}	3000	4000	3000
Ratio of min. LC verification interval	Y = Emax / vmin	10000	20000	10000
Combined Error	%FS	≤± 0.020	≤± 0.018	≤± 0.020
Minimum dead load	of Emax	0%		
Safe overload	of Emax	150 %		
Ultimate overload	of Emax	300 %		
Zero balance	of FS	< ± 1.5 %		
Excitation, recommended voltage	V	5 ~ 12		
Excitation maximum	V	18		
Input resistance	Ω	350 ± 3.5		
Output resistance	Ω	351 ± 2.0		
Insulation resistance	MΩ	≥5000 (at 50VDC)		
Compensated temperature	°C	-10 ~+40		
Operating temperature	°C	-35 ~ +65		
Storage temperature	°C	-40 ~ +70		
Element material		Nickel plated alloy steel		
Ingress Protection (acc. to EN 60529)		IP67		
Recommended torque on fixation	Nm	M8:25 M10: 50 M12:75 M20:450 M33:750 M42:1450		
ATEX classification (optional)		II1G Ex ia II1C T4	II1D Ex iaD 20 T73°C	II3G nL IIC T4

Wiring:

- Shielded, 4 conductor cable.
- Cable diameter: Ø 5mm.
- Standard cable length for 25kg – 1.5t: 3m and for 2t – 30t: 6m.
- Shield not connected to element.

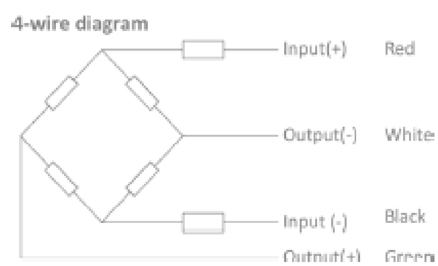

Specifications and dimensions are subject to change without notice and do not constitute any liability whatsoever.

WWW.AESENSORS.NL

AE Sensors B.V.
Jan Valsterweg 92
3315 LG Dordrecht
Tel.: +31 (0)78 6213152

AE-H3 "S"-type Loadcell

For Tension and Compression Loadcells

Dimensions in mm:

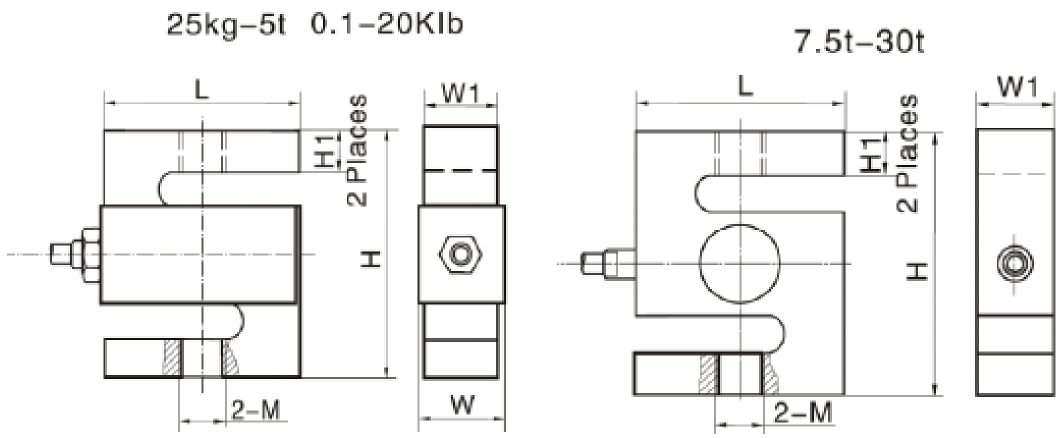

Dimension Capacity	L	H	W1	W	H1	M
25-50 kg	50,8	76,2	12,7	14,5	15,7	M8
100-150 kg	50,8	76,2	19,0	22,4	15,3	M10 x 1,5
200-750 kg	50,8	76,2	19,0	22,4	14,4	M12 x 1,75
1-1,5 t	50,8	76,2	25,4	28,8	12,5	M12 x 1,75
2-5 t	76,2	101,6	25,4	28,8	20	M20 x 1,5
7,5-10 t	125	175	50	-	40,2	M33 x 3
15-20 t	160	200	60	-	51	M45 x 3
30 t	190	230	80	-	57,5	M45 x 3

WWW.AESENSORS.NL

AE Sensors B.V.
Jan Valsterweg 92
3315 LG Dordrecht
Tel.: +31 (0)78 6213152

AE-H3 "S"-type Loadcell

For Tension and Compression Loadcells

Available accessories:

AE-HL-3-001-25Kg-5t hook • Alloy Steel • Suitable for hybrid scales, cranes scales, packaging scales and hopper scales	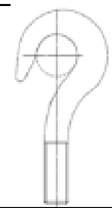
AE-HL-3-002-25Kg-5t eye • Alloy Steel • Suitable for hybrid scales, cranes scales, packaging scales and hopper scales	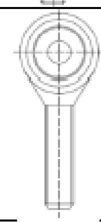
AE-HL-3-003-25Kg-5t rod end • Alloy Steel • Suitable for hybrid scales, cranes scales, packaging scales and hopper scales and other electronic weighing devices.	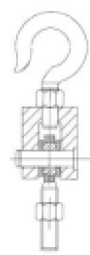
AE-HL-3-004-25Kg-5t hook assembly • Alloy Steel • Suitable for hybrid scales, cranes scales, packaging scales and hopper scales and other electronic weighing devices.	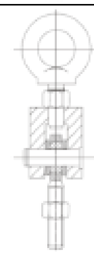
AE-HL-3-005-25Kg-5t eye assembly • Alloy Steel • Suitable for hybrid scales, cranes scales, packaging scales and hopper scales and other electronic weighing devices.	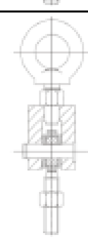

CONTROLE-FORMULIER TEMPOSONIC NIVO-OPNEMER.

Type: GHM0250MD601V3 **Datum:** 14-02-2018
Serienr.: 14403237 **Techn.:** F.M. de Vreede
Deltares-nr.: 01.11.240 **Eigendom:** HYE

Gebruikte apparatuur: De bij de verrichte kalibratie gebruikte meetmiddelen zijn herleidbaar naar primaire en/of (inter)nationaal erkende meetstandaarden.

Voeding 24Vdc	TTi EX354T	ID-nr. 07.00.248
Voltmeter uitg.spanning meetversterker	Agilent 34401A	ID-nr. 06.00.226
Meetlineaal	Sony SR1711	ID-nr. 01.11.173

Afregeling: [(Uuit +50N) + (|Uuit| −50N)] : 2 = 10 V ± 5 mV

Conversie: 12.5 mm / V (-10V…+10V ≡ -125mm…+125mm)

Bereik: 250 mm

IJKING:

Afstand (mm):	Uitgangs-spanning (Volt):
0	-9.994
25	-7.998
50	-5.996
75	-3.996
100	-1.998
125	0
150	1.999
175	3.998
200	5.998
225	7.997
250	9.993

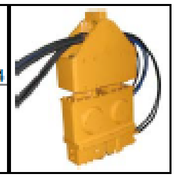

I. GENERAL DESCRIPTION

A. GENERAL

The APE J&M Model 23 is a low-frequency vibratory pile driver/extractor designed to drive and extract vinyl, aluminum and steel sheet piles.

The Model 23 operates in a frequency range of 800 to 1800 vibrations per minute to provide maximum pile penetration rates in a wide variety of soils. The unit has an eccentric moment of 2.6 kg-m (230 inch-pounds) and produces a maximum amplitude of 25 mm.

The vibratory driver unit consists of two major components. (1) The vibrator with attached clamp and (2) the hydraulic power unit with control pendant.

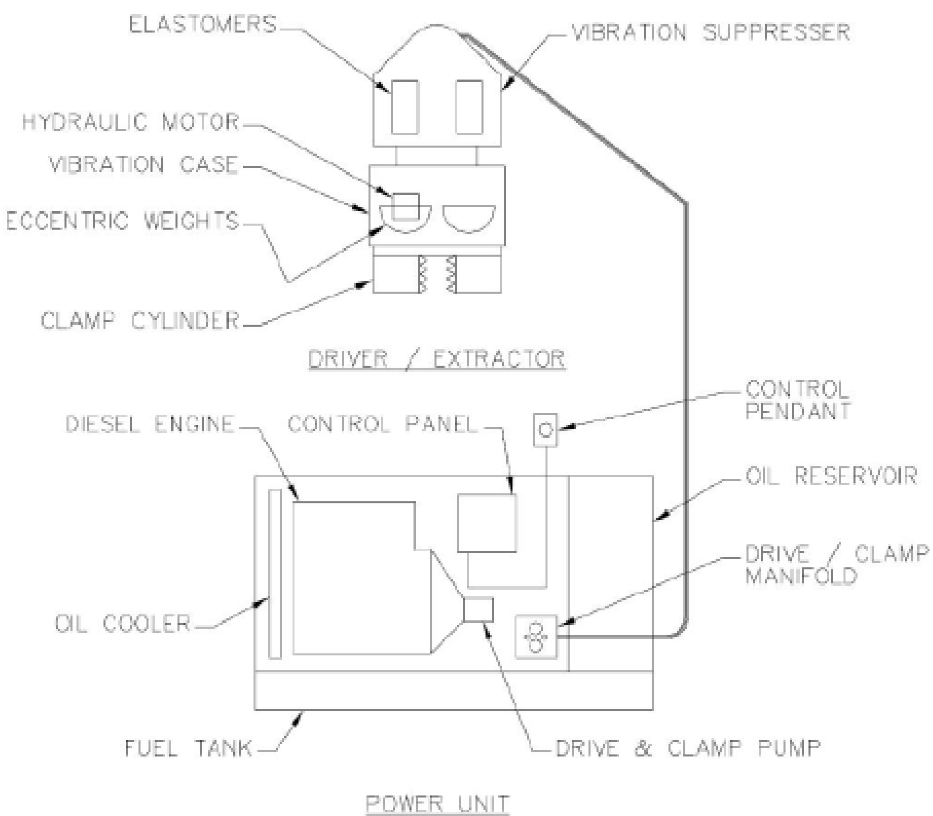

Figure 1 - GENERAL DESCRIPTION

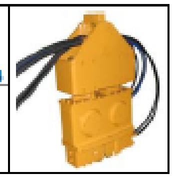

I. GENERAL DESCRIPTION

B. VIBRATOR

The vibrator consists of two major components; The vibration case and the vibration suppressor. The vibration case contains two eccentric weights which rotate in a vertical plane to create vibration. The eccentric weights are driven by a hydraulic motor. The vibration suppressor contains 4 rubber elastomers to isolate the vibration case from the crane line . The suppressor is designed for a maximum line pull of 13 tons (116kN) during extraction.

C. HYDRAULIC CLAMP

The hydraulic clamp attaches the vibrator to the pile, transmitting vibration to the piling. The hydraulic clamp contains two gripping jaws; one fixed and one moveable. A large hydraulic cylinder operates the moveable jaw with 20 tons (178kN) of force to grip the pile. Clamping and un-clamping occurs in a few seconds.

INFORMATION **Consult APE Holland in your area for any other clamp questions regarding other than what is stated herein.**

D. POWER UNIT

The Model 23 vibrator is powered by the APE J&M Model 51 Power pack. The 51 power pack is powered by a Caterpillar C-2.2 diesel engine. The engine develops 51 gross horsepower (38kW) at 3000 RPM, and is mounted on a tubular sub-base which serves as a fuel tank.
The Power Unit and Vibrator are operated from the control pendant.

E. HOSES

A hydraulic hose bundle (multiple hoses) connects the hydraulic power unit to the vibrator unit.

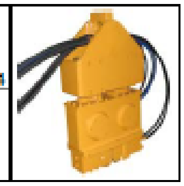

I. GENERAL DESCRIPTION

E. CONTROL PENDANT

The vibrator is operated by a hand-held control pendant. The control pendant has one, two-way switch. This switch (CLAMP OPEN-OFF-FWD) starts and stops the vibrator as well as opens and closes the clamp. Turning the swith to FWD first closes the clamp. When adequate clamp pressure is reached the vibrator will start. Turning the switch to off stops the vibrator. Turning the switch and holding it at CLAMP OPEN after the vibrator is stoped the clamp will open.

F. SPECIFICATIONS

1. Constant improvement and engineering progress make it necessary that we reserve the right to make specification changes without notice.

INFORMATION Always consult APE Holland in your area for current or additional information you may require.

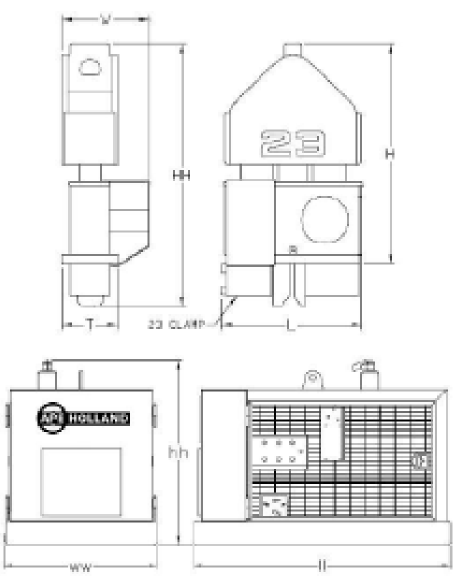

VIBRATOR	Model 23
Eccentric moment	2,65 kg-m (230 in-lbs)
Maximum frequency	2250 vpm (@ 125 l/min)
Centrifugal force	13 tons (115 kN)
Normal frequency	1600 vpm (@ 105 l/min)
Centrifugal force	7,6 tons (74 kN)
Pile clamping force	178 kN (18 tons)
Amplitude (free hanging)	15 mm (0.58 in)
Max pull for extraction	12 tons (116 kN)
Suspended weight (without clamps)	655 kg (1,440 lbs)
Weight with clamps	955 kg (2,100 lbs)
Height, with clamp & yoke (HH)	140 cm (55 in)
Height, without clamp (H)	119 cm (47 in)
Length (L)	67 cm (26,50 in)
Width (W)	56 cm (22 in)
Throat width (T)	26 cm (10.5 in)

POWER UNIT:	Model 51
Engine	Caterpillar C-2.2
Horsepower @ 2100 rpm	51 (38 kW)
Drive flow	106 l/min
Weight (w/ full fuel and fluids)	995 kg
Length (ll)	173 cm (68 in)
Width (ww)	103 cm (40.5 in)
Height (hh)	124 cm (48.75 in)

Figure 2 - EQUIPMENT DIMENSIONS

Appendix B: Sand specifications

Particle Size Distribution

Project id.	82839	Sample id.	MM1-x1
Project description	SIMOX – WP2D (1E) – Laboratory and centrifuge testing	Depth	from 0.00 to 1.00 m. gl. from +0.00 to -1.00 m. Ground level
Sample	S90_B4-1	Lab technician	AdV
Client	Deltares	Testing date	14-11-2022
		Soil type	SAND

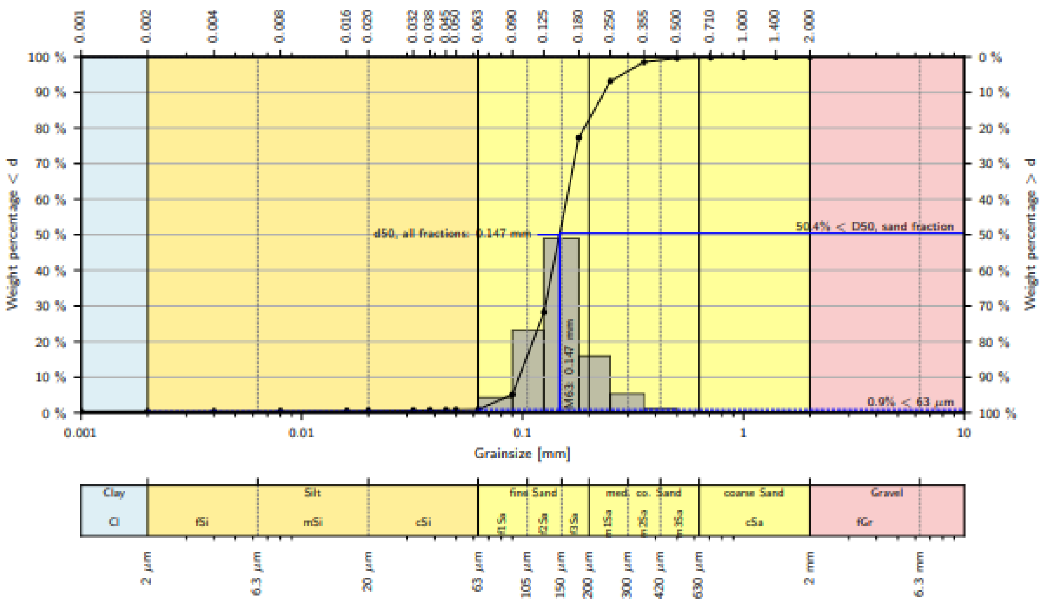

Particle Size Distribution	d [mm]	% < d
Sand	2.000	100.00
	1.400	99.95
	1.000	99.92
	0.710	99.81
	0.500	99.63
	0.355	98.55
	0.250	93.21
	0.180	77.30
	0.125	28.26
	0.090	5.13
Silt	0.063	0.88
	0.050	0.80
	0.045	0.75
	0.038	0.70
	0.032	0.65
	0.020	0.60
	0.016	0.55
	0.008	0.50
	0.004	0.45
Clay	0.002	0.40
	0.001	0.35

full range Number		Value
d10	[mm]	0.096
d15	[mm]	0.104
d20	[mm]	0.111
d30	[mm]	0.127
d40	[mm]	0.136
d50	[mm]	0.147
d60	[mm]	0.158
d70	[mm]	0.170
d80	[mm]	0.190
d85	[mm]	0.211
d90	[mm]	0.234
Cu	[-]	1.641
Cc	[-]	1.050
d90/d10	[-]	2.426

sand fraction Number		Value
D10	[mm]	0.098
D15	[mm]	0.105
D20	[mm]	0.112
D30	[mm]	0.127
D40	[mm]	0.137
D50	[mm]	0.147
D60	[mm]	0.159
D70	[mm]	0.171
D80	[mm]	0.191
D85	[mm]	0.212
D90	[mm]	0.234
Cu_{sand}	[-]	1.627
Cc_{sand}	[-]	1.045
D90/D10	[-]	2.403

Characteristics		
Gravel (2 mm - 63 mm)	[%]	-
Sand (63 μm - 2 mm)	[%]	99.1
Silt (2 μm - 63 μm)	[%]	0.5
Clay (< 2 μm)	[%]	0.4
Fines (< 63 μm)	[%]	0.9
M_{63} Sand median	[mm]	0.147
fine (105μm - 150μm)		
M_{2000} Gravel median	[mm]	-
M_{50}	[mm]	0.147
D_m Median grain	[mm]	0.152
U_{16} (16 μm - 2 mm)	[-]	71.48
U_{Sand} (63 μm - 2 mm)	[mm]	70.72
U-number according Zunker's formula		
F_m Fineness modulus	[-]	0.790

Geolab Wiertsema

SIMOX – WP2D (1E) – Laboratory and centrifuge testing

Particle Size Distribution including fines
(NEN-EN-ISO 17892-4(2014) & NEN-EN-ISO 13317-3(2001))

GEOLAB WIERTSEMA, THE NETHERLANDS

AKKOORD LAB

Appendix C: Installation results

Batch 2:

Penetration as a function of time

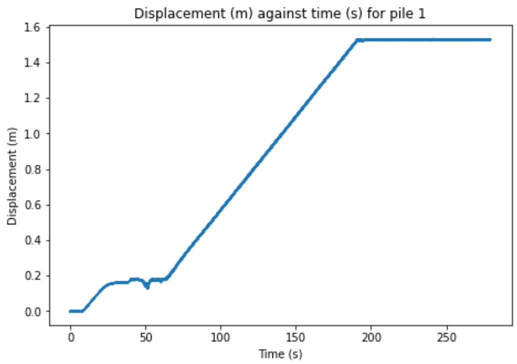

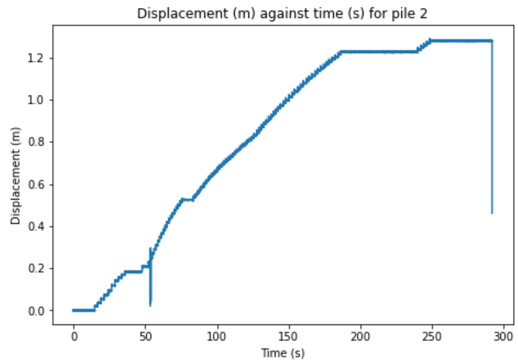

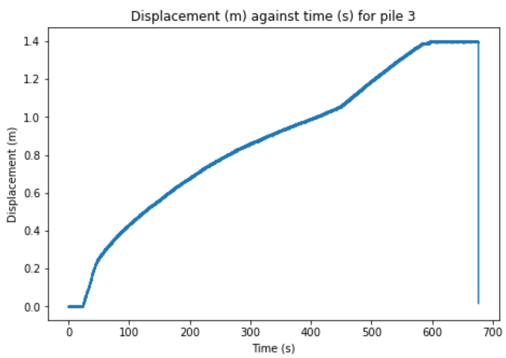

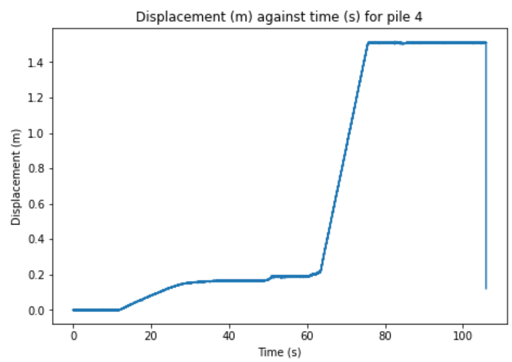

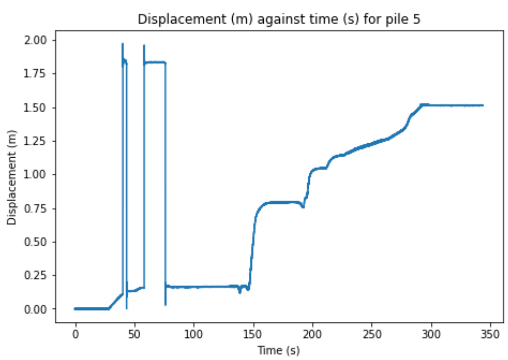

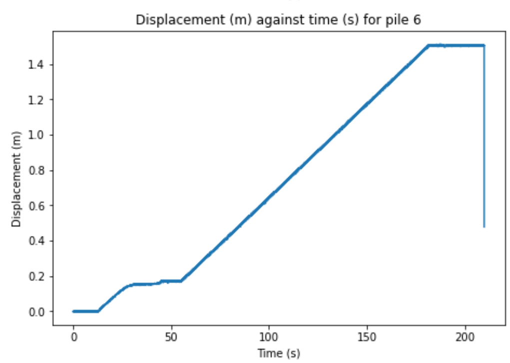

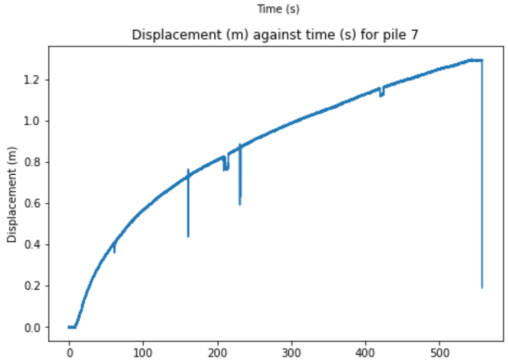

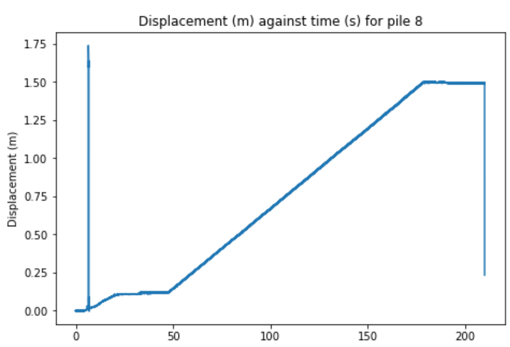

Pore water pressure:

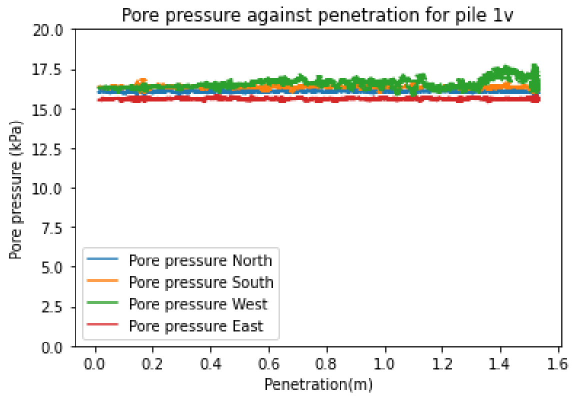

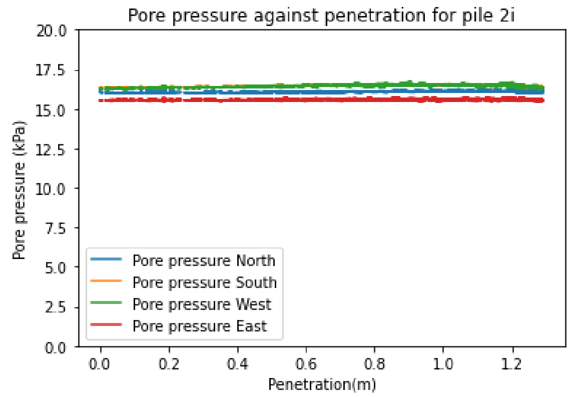

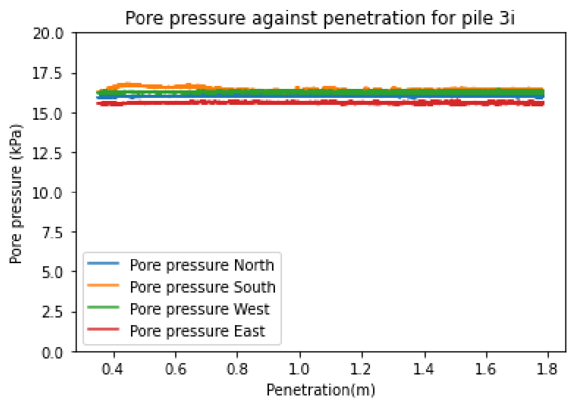

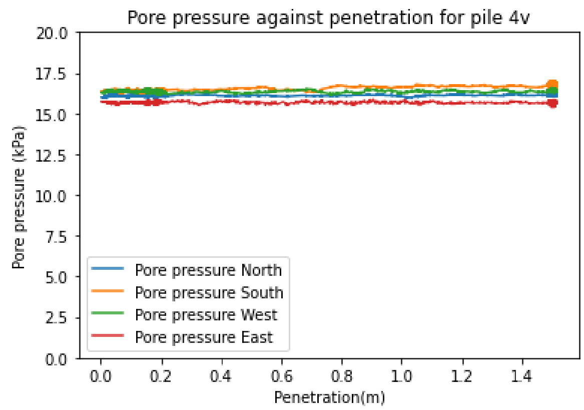

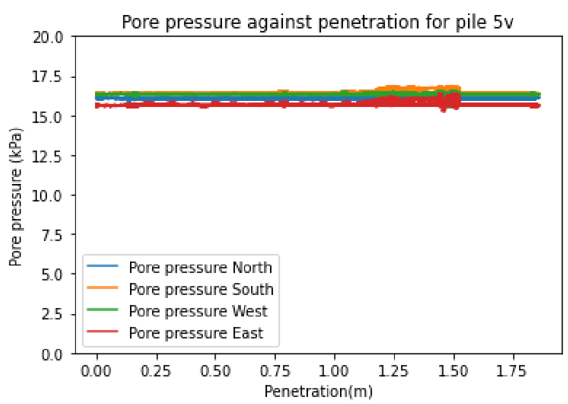

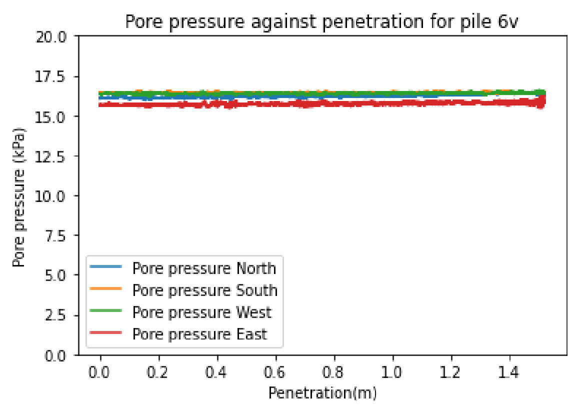

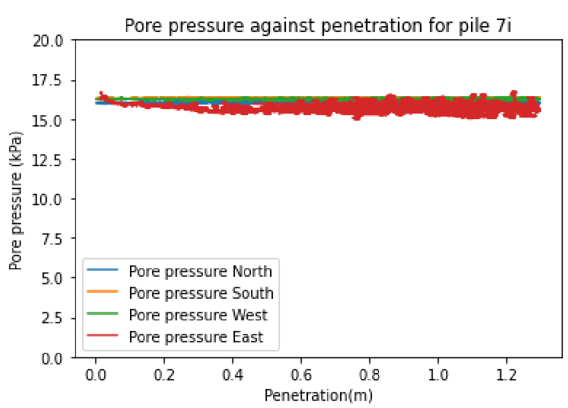

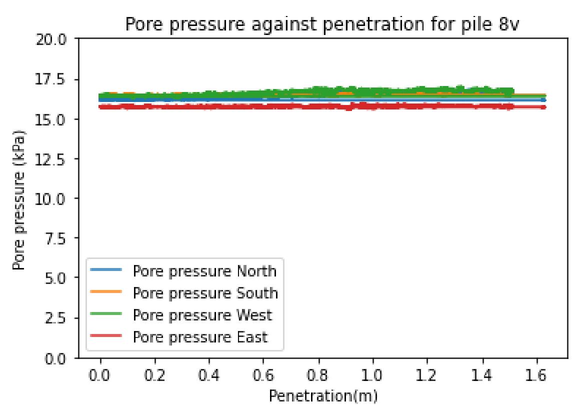

Crane loads:

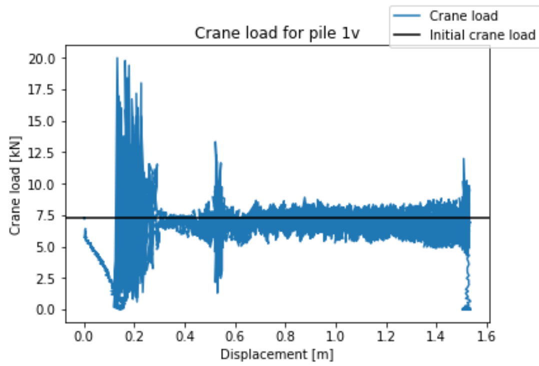

Crane load for pile 1v
Crane load
Initial crane load
Crane load [kN]
Displacement [m]

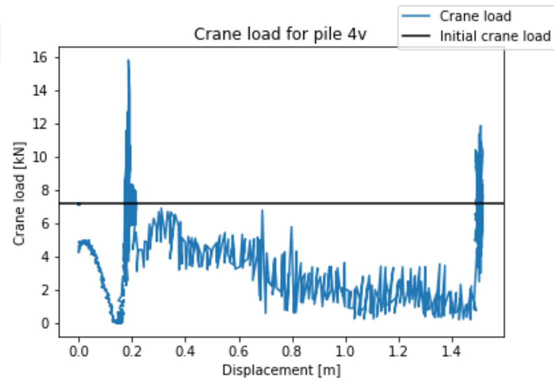

Crane load for pile 4v
Crane load
Initial crane load
Crane load [kN]
Displacement [m]

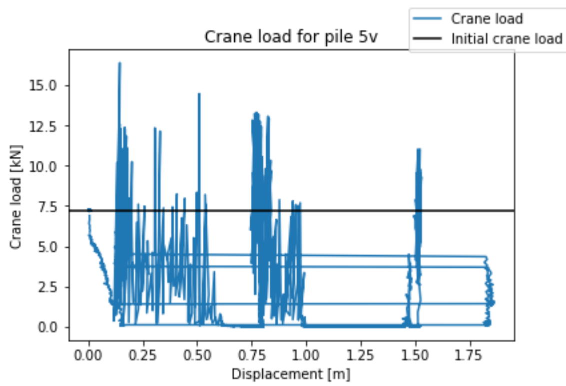

Crane load for pile 5v
Crane load
Initial crane load
Crane load [kN]
Displacement [m]

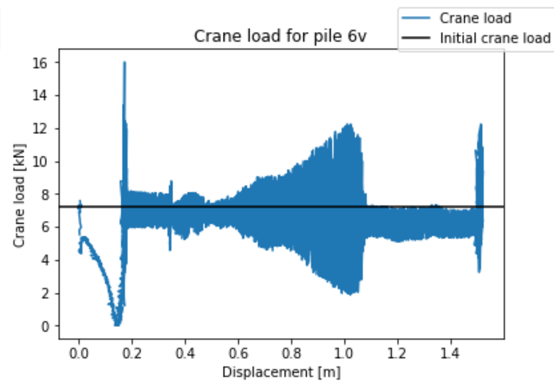

Crane load for pile 6v
Crane load
Initial crane load
Crane load [kN]
Displacement [m]

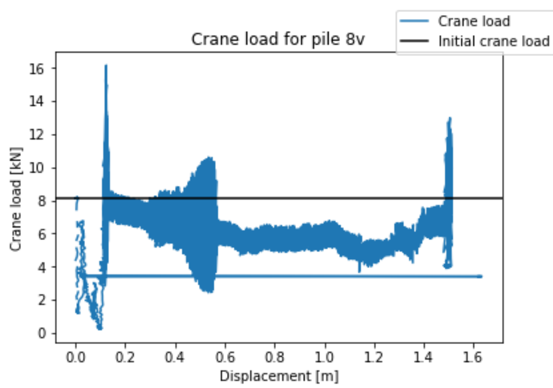

Crane load for pile 8v
Crane load
Initial crane load
Crane load [kN]
Displacement [m]

Batch 3

Penetration as a function of time

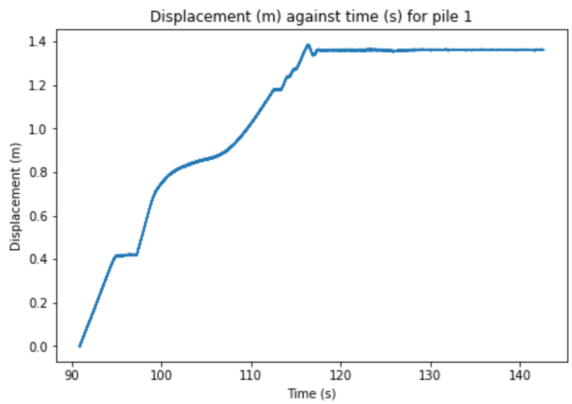

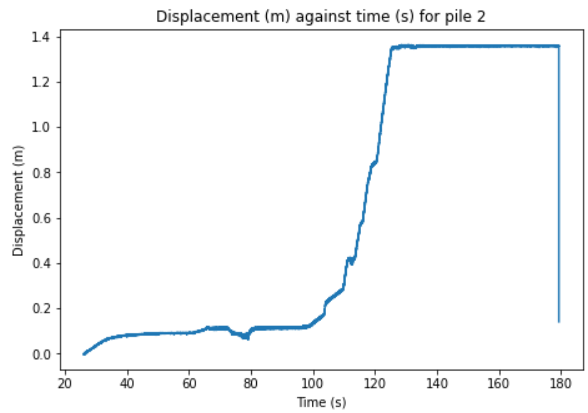

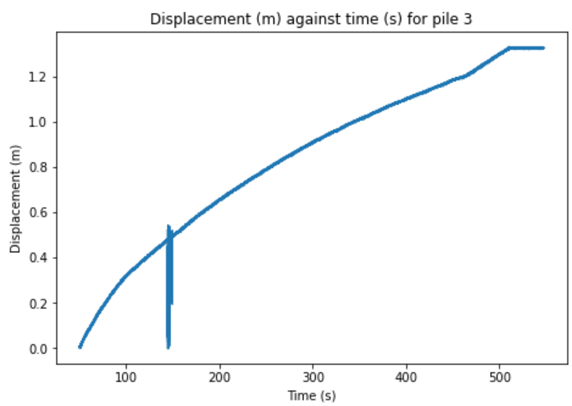

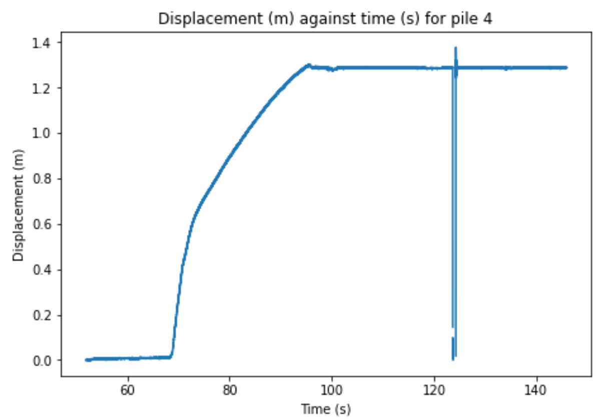

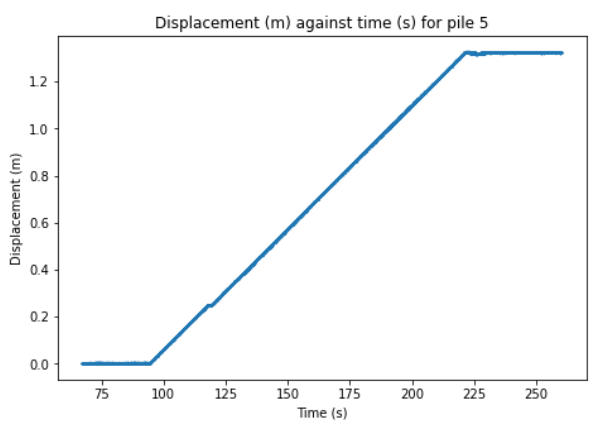

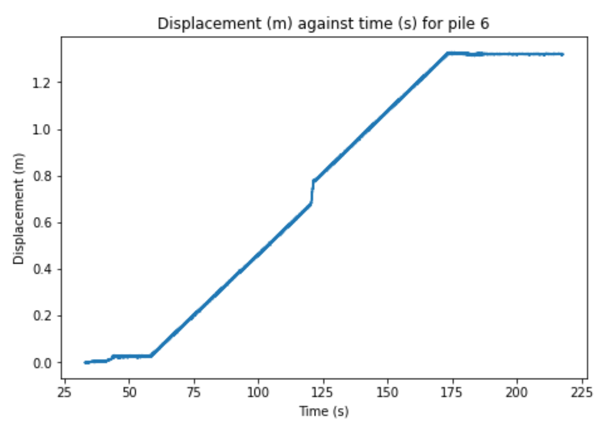

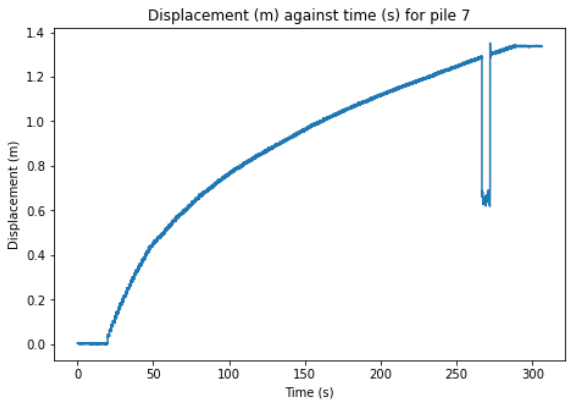

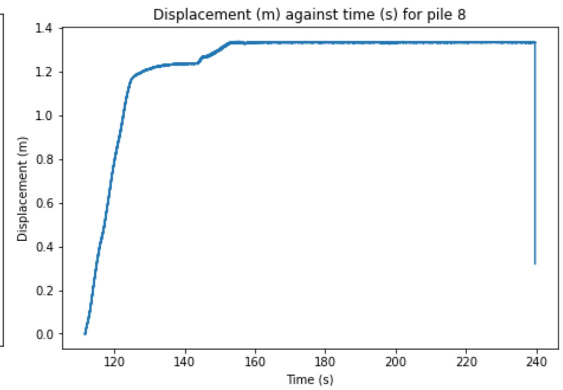

Pore water pressure:

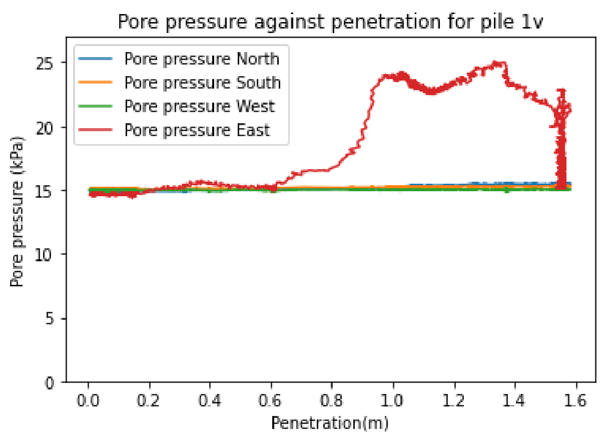

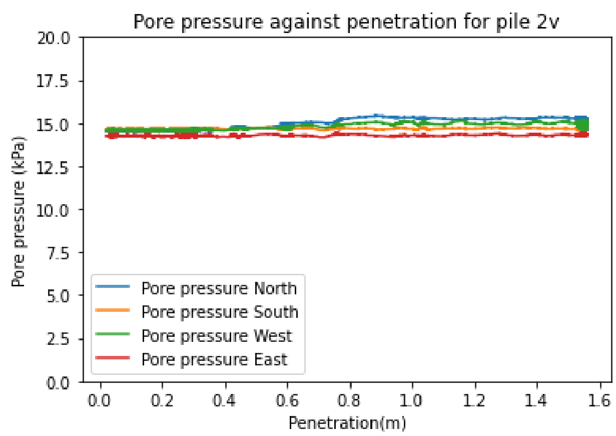

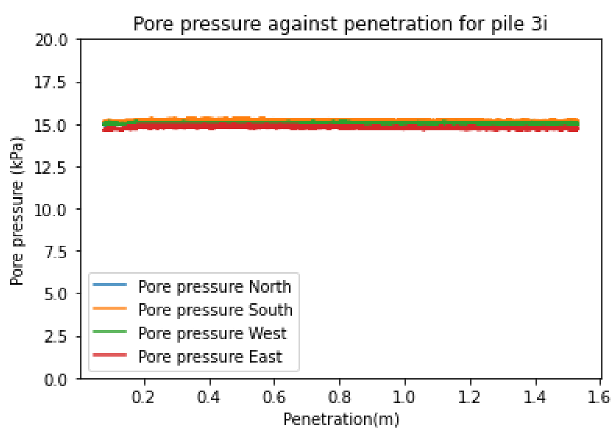

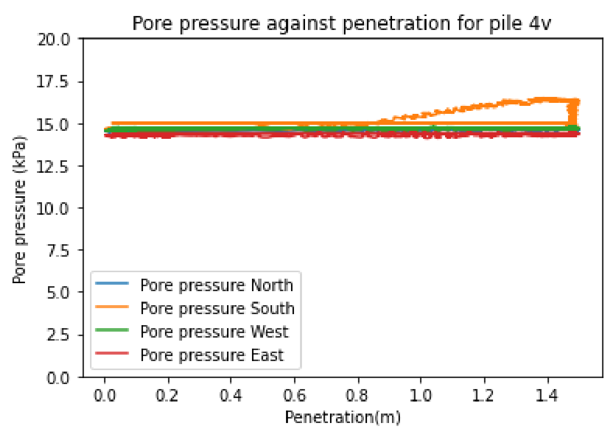

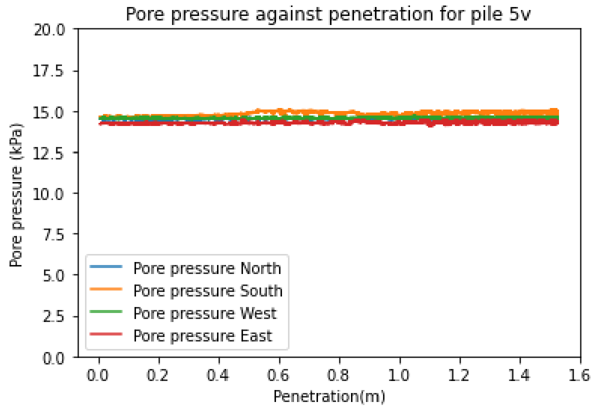

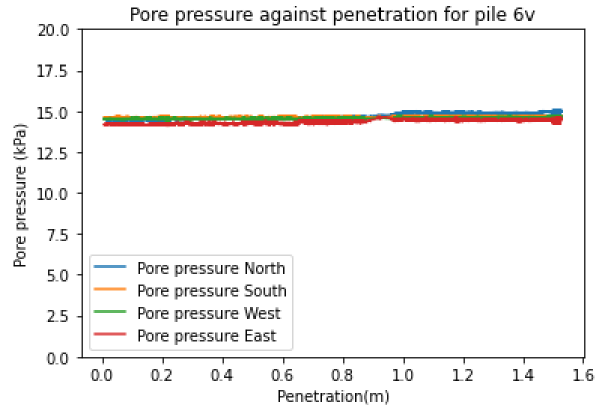

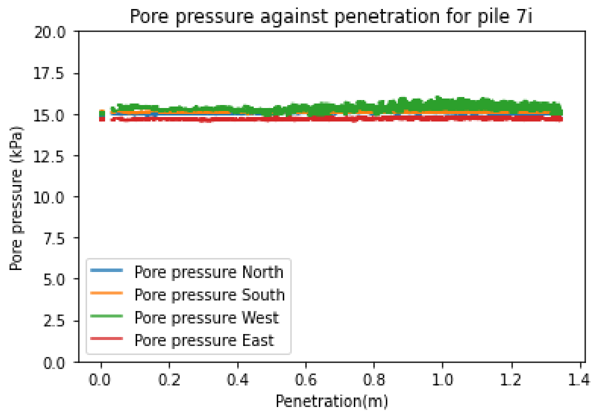

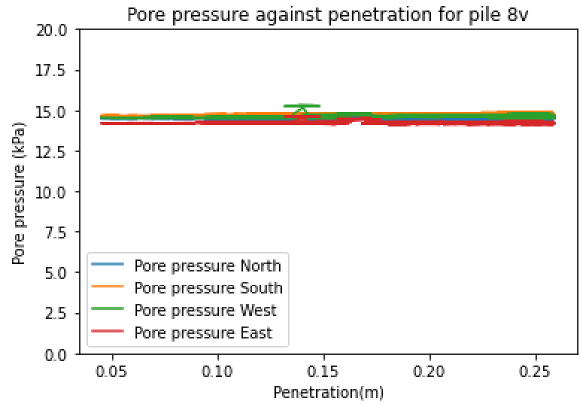

<u>Crane loads:</u>

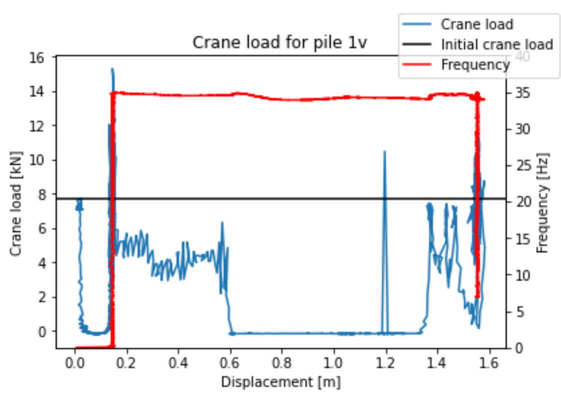

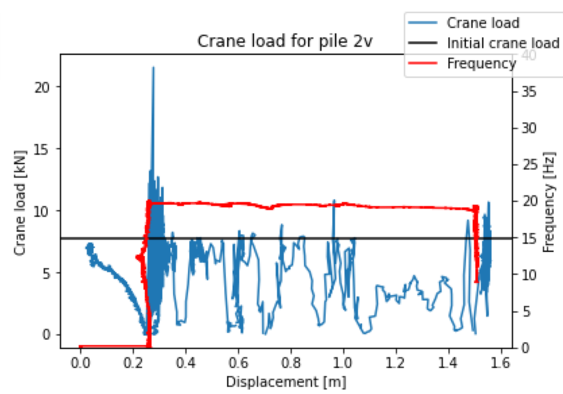

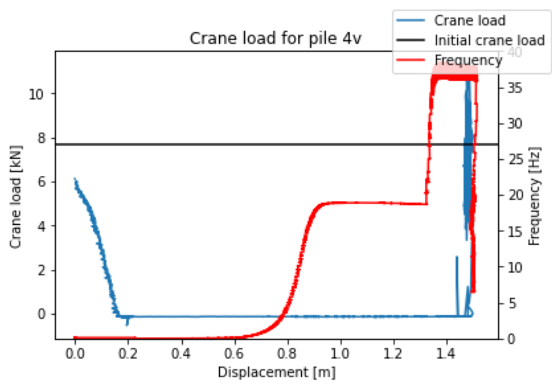

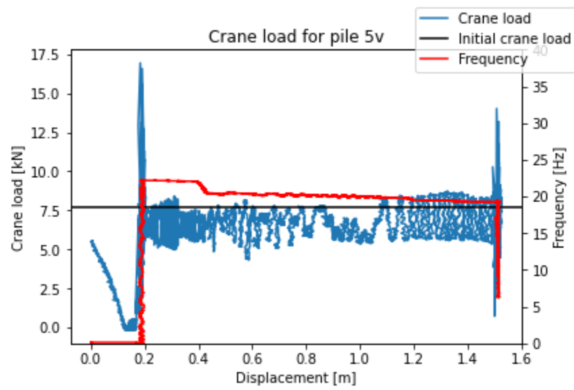

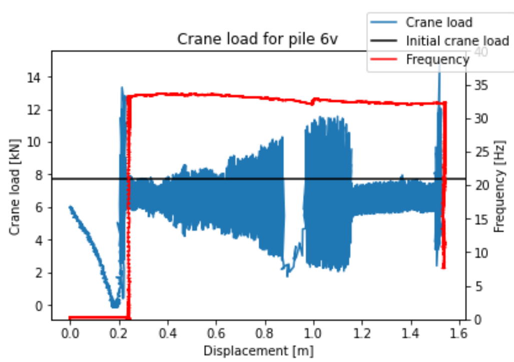

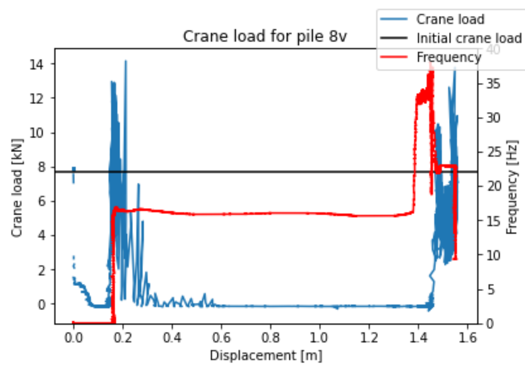

Batch 4

Penetration as a function of time

Pile 1v

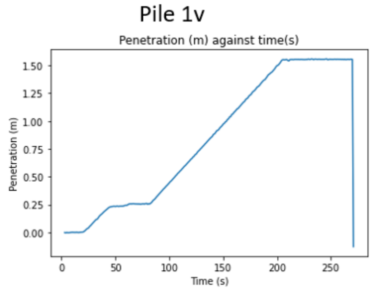

Pile 2v

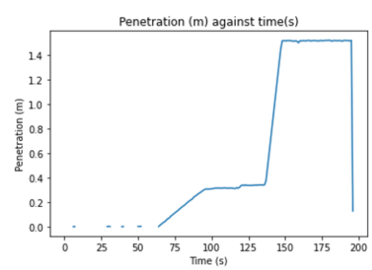

Pile 3i

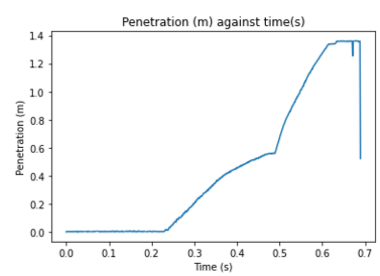

Pile 4v

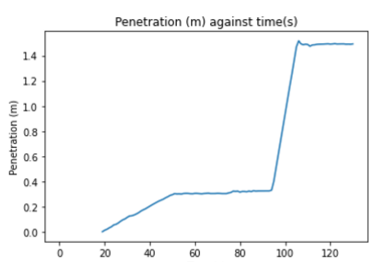

Pile 5v

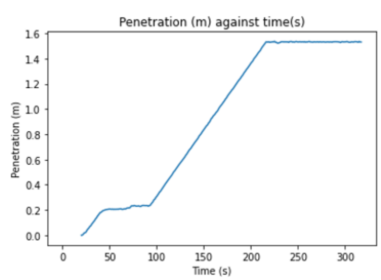

Pile 6i

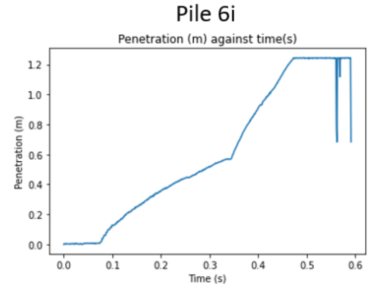

Pile 7i

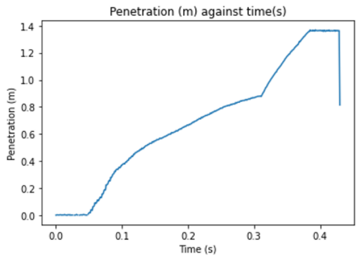

Pile 8v

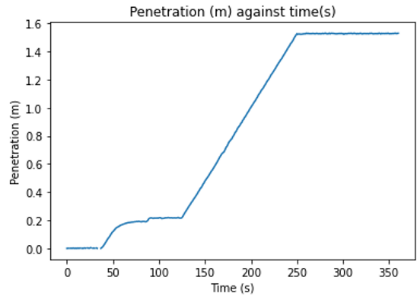

Pore water pressure:

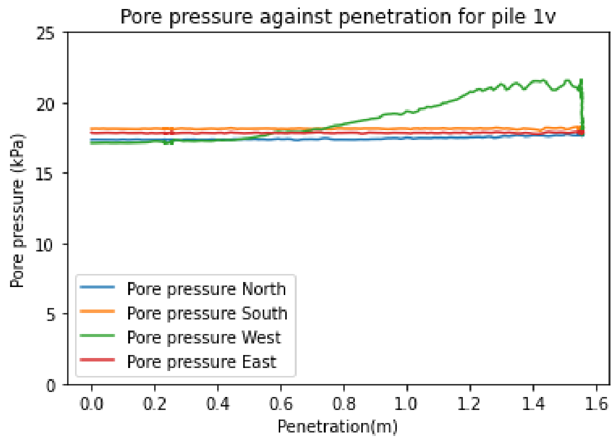

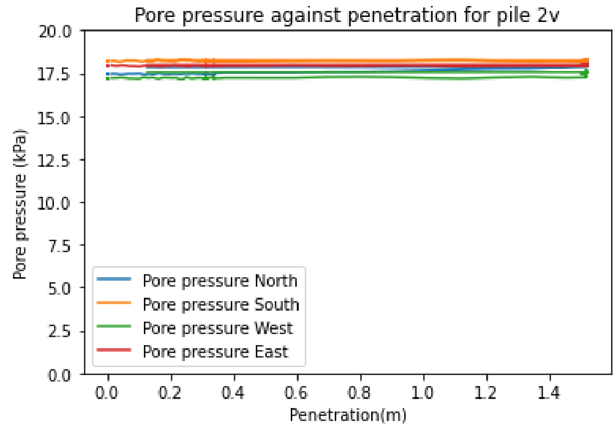

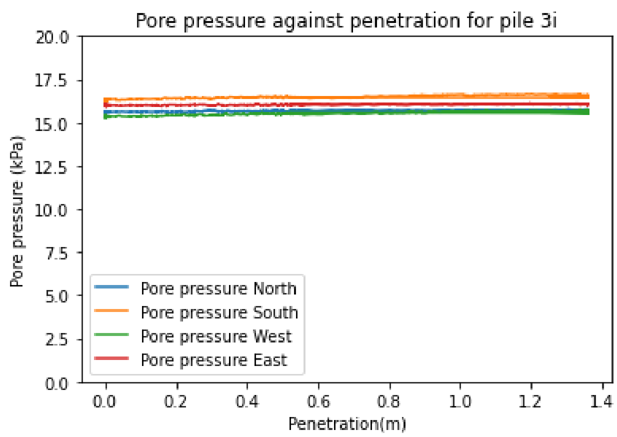

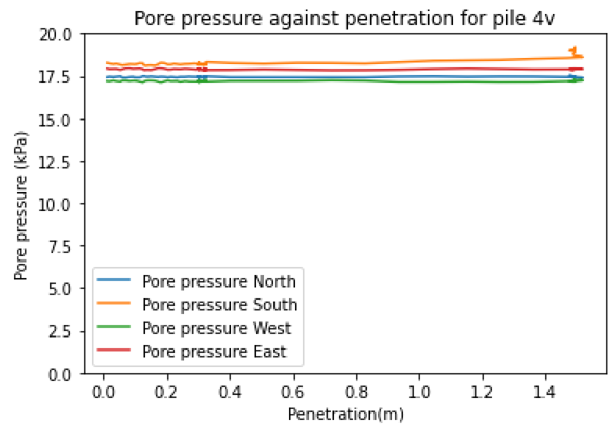

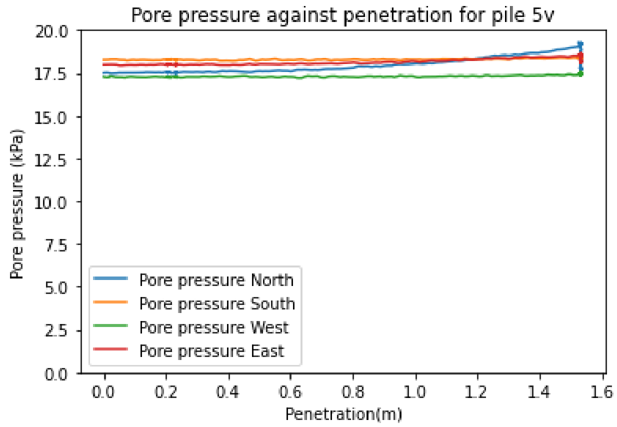
Pore pressure against penetration for pile 5v
Pore pressure (kPa)
Penetration(m)
Pore pressure North
Pore pressure South
Pore pressure West
Pore pressure East

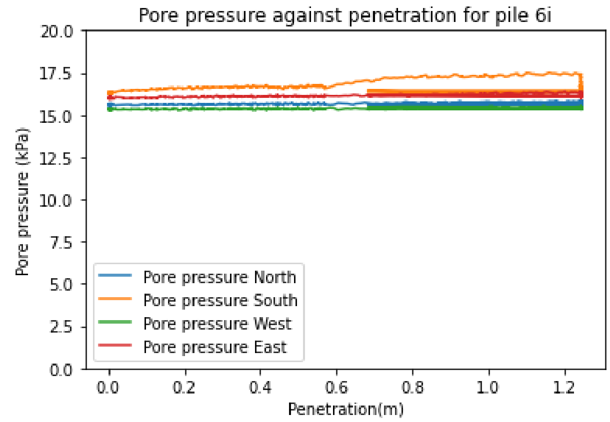
Pore pressure against penetration for pile 6i
Pore pressure (kPa)
Penetration(m)
Pore pressure North
Pore pressure South
Pore pressure West
Pore pressure East

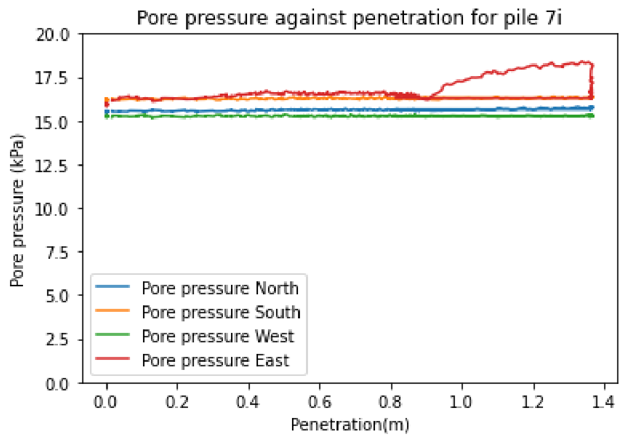
Pore pressure against penetration for pile 7i
Pore pressure (kPa)
Penetration(m)
Pore pressure North
Pore pressure South
Pore pressure West
Pore pressure East

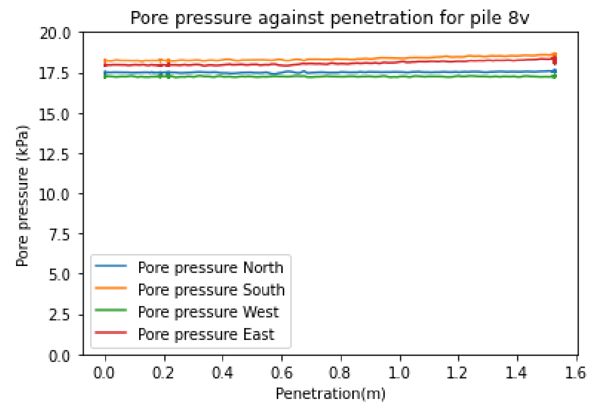
Pore pressure against penetration for pile 8v
Pore pressure (kPa)
Penetration(m)
Pore pressure North
Pore pressure South
Pore pressure West
Pore pressure East

Crane loads:

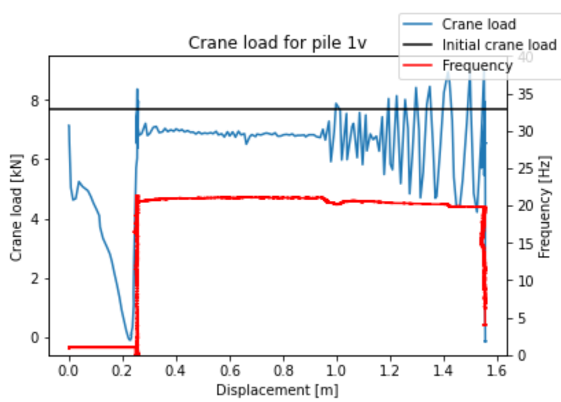
Crane load for pile 1v
Crane load
Initial crane load
Frequency
Crane load [kN]
Frequency [Hz]
Displacement [m]

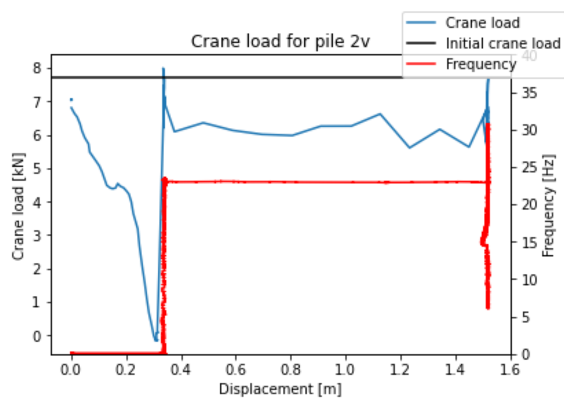
Crane load for pile 2v
Crane load
Initial crane load
Frequency
Crane load [kN]
Frequency [Hz]
Displacement [m]

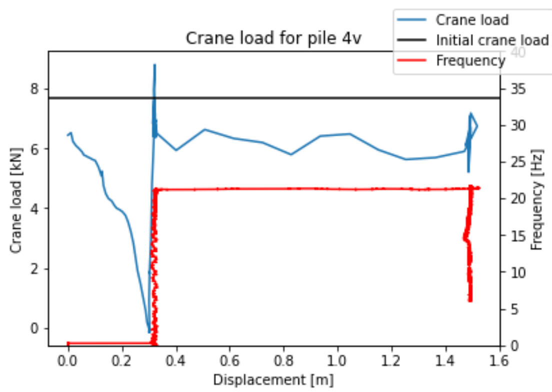
Crane load for pile 4v
Crane load
Initial crane load
Frequency
Crane load [kN]
Frequency [Hz]
Displacement [m]

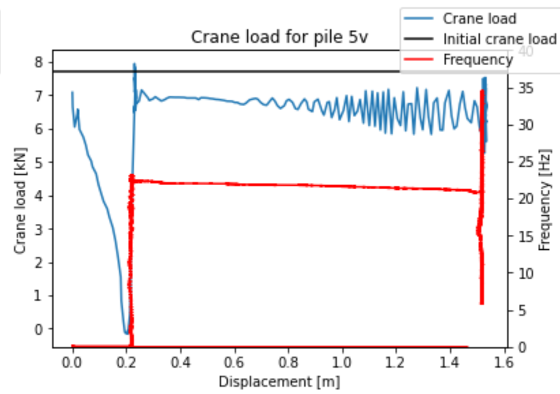
Crane load for pile 5v
Crane load
Initial crane load
Frequency
Crane load [kN]
Frequency [Hz]
Displacement [m]

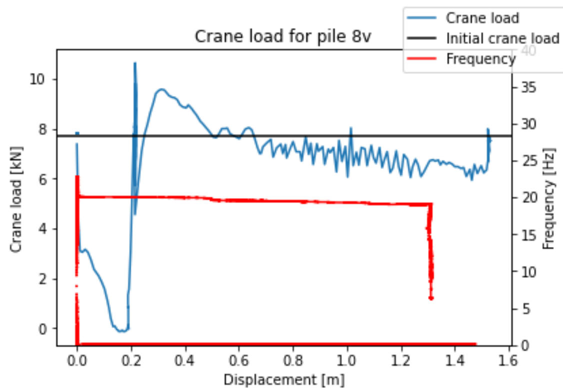
Crane load for pile 8v
Crane load
Initial crane load
Frequency
Crane load [kN]
Frequency [Hz]
Displacement [m]

Appendix D: CPT results

Batch 2: Before installation

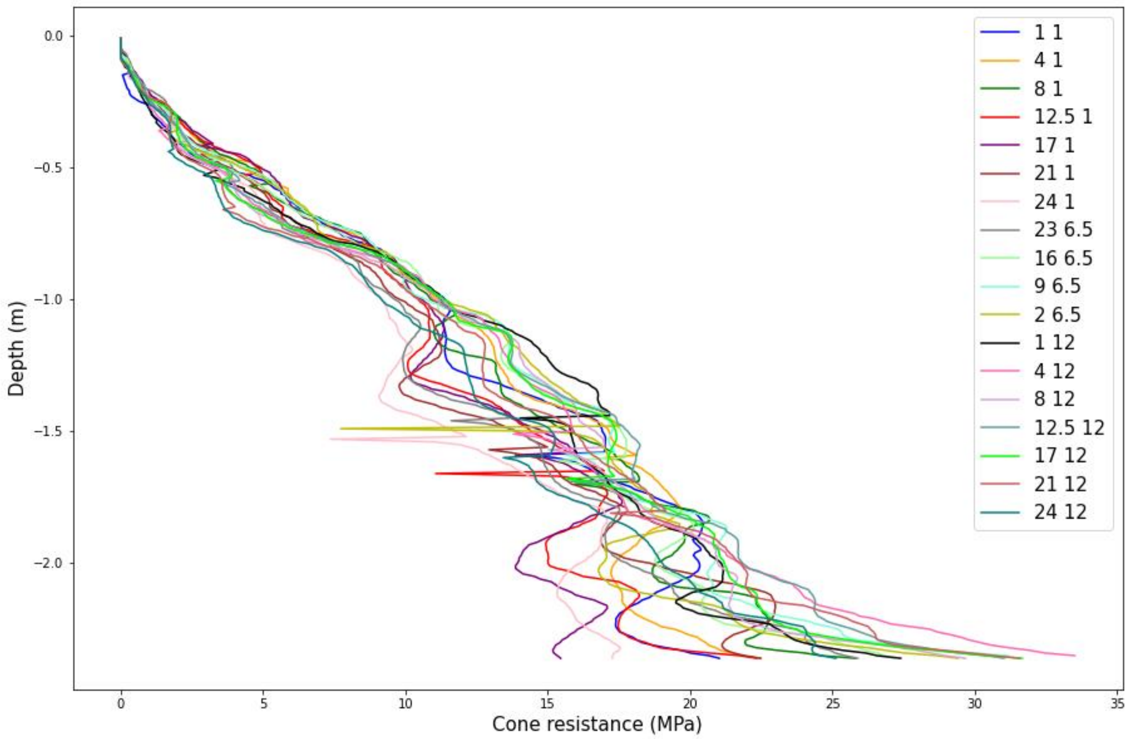

Batch 2: After installation

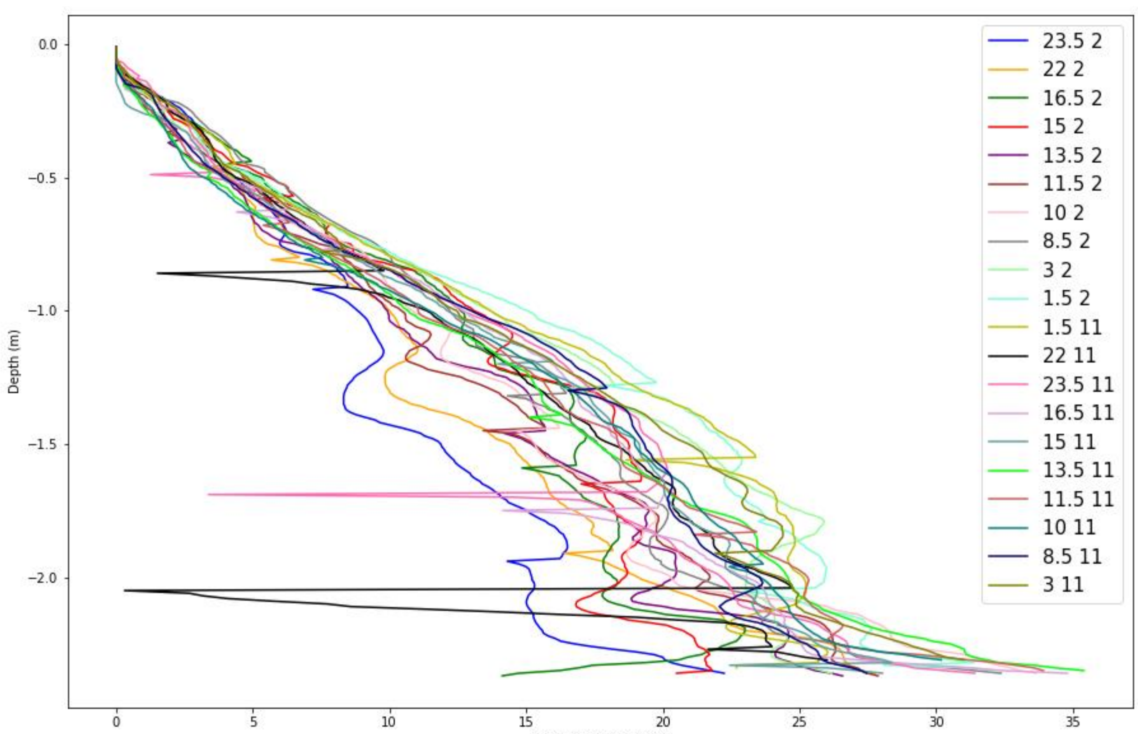

Batch 2: Comparison

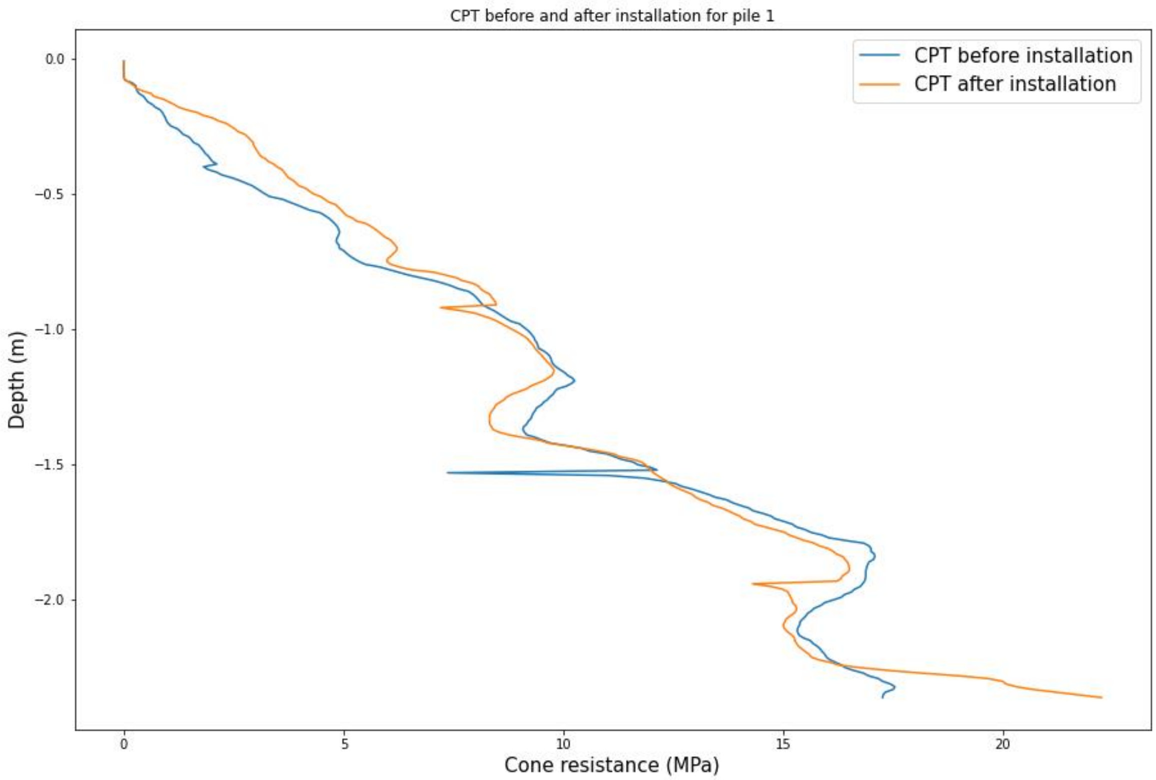

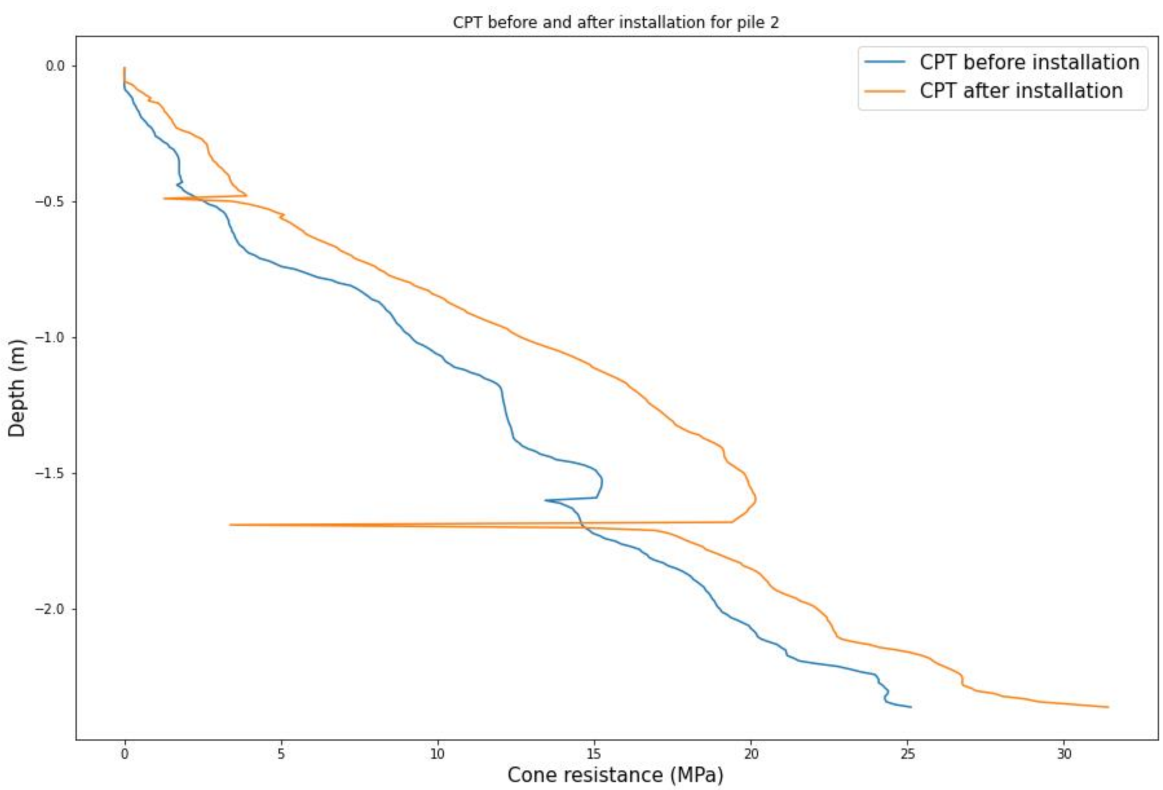

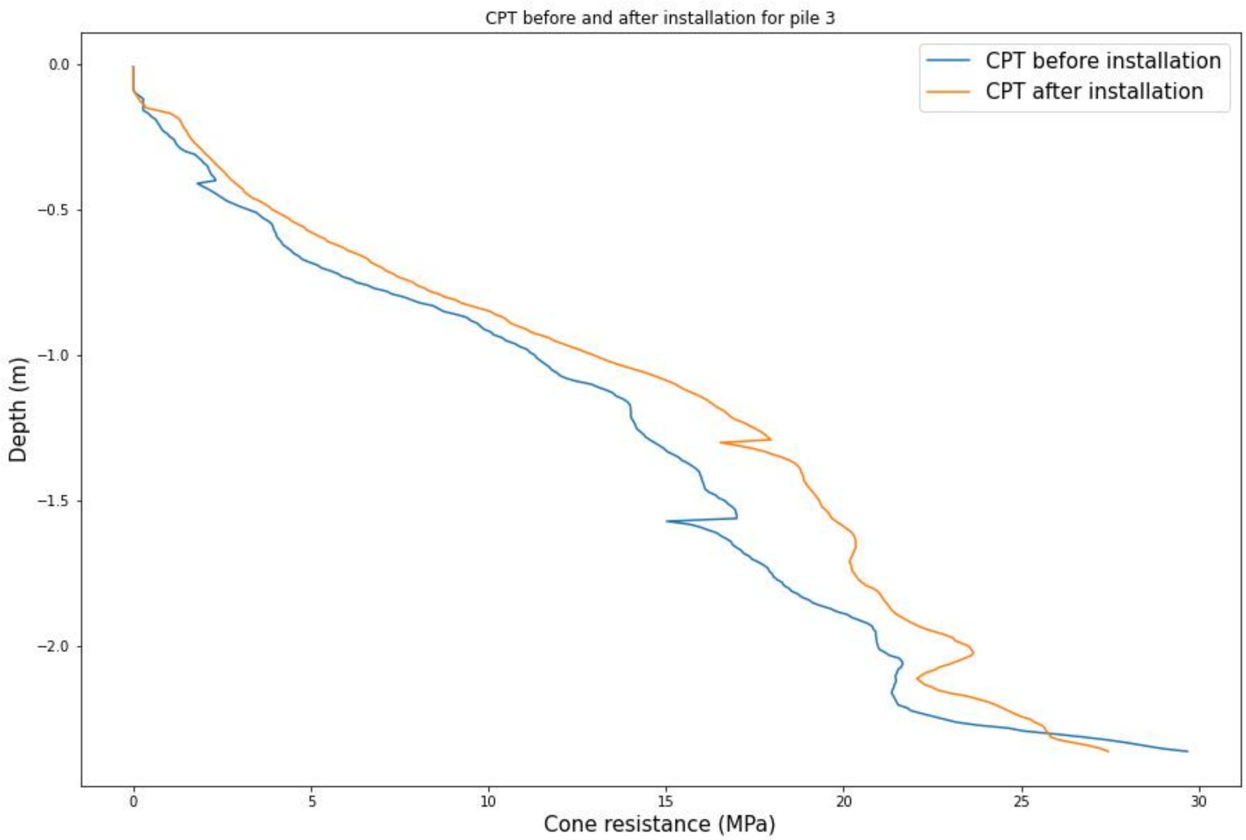
CPT before and after installation for pile 3
CPT before installation
CPT after installation
Depth (m)
0.0
−0.5
−1.0
−1.5
−2.0
0
5
10
15
20
25
30
Cone resistance (MPa)

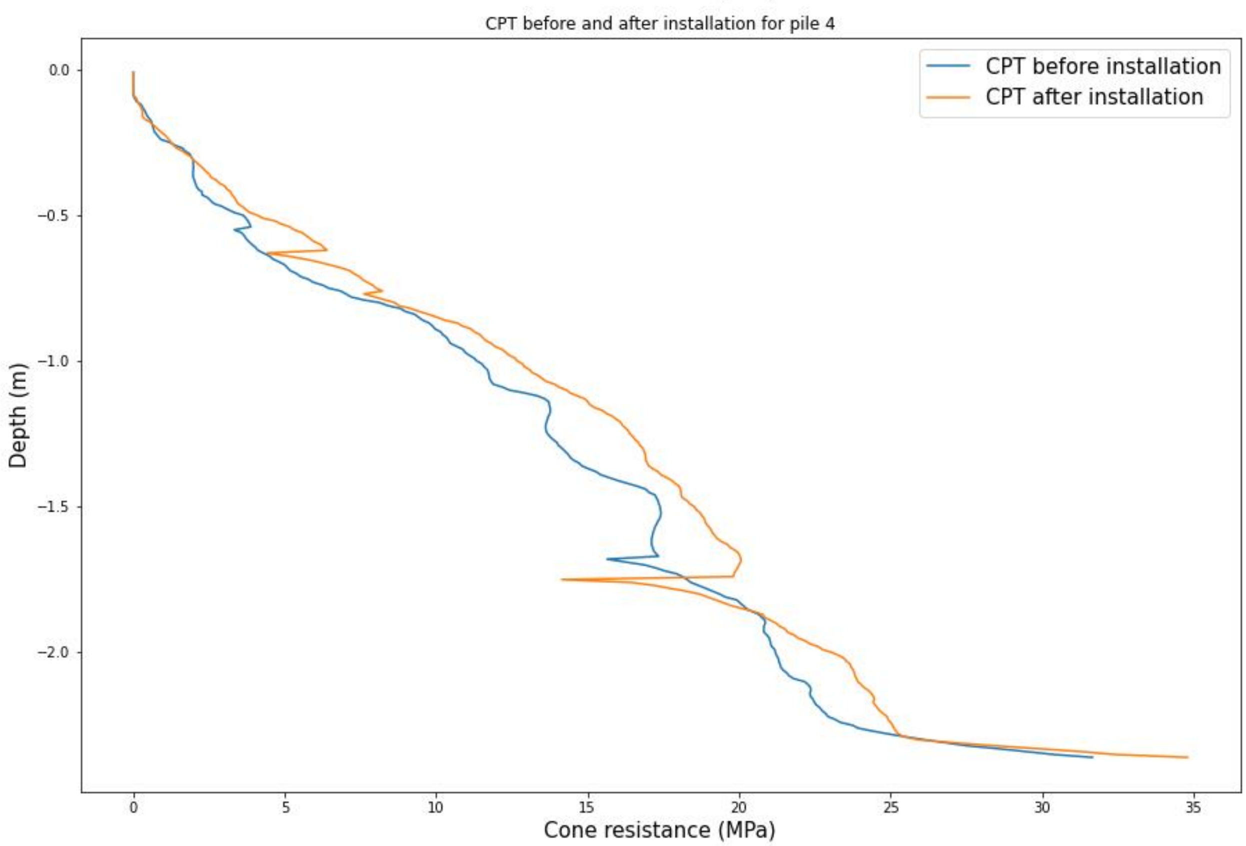
CPT before and after installation for pile 4
CPT before installation
CPT after installation
Depth (m)
0.0
−0.5
−1.0
−1.5
−2.0
0
5
10
15
20
25
30
35
Cone resistance (MPa)

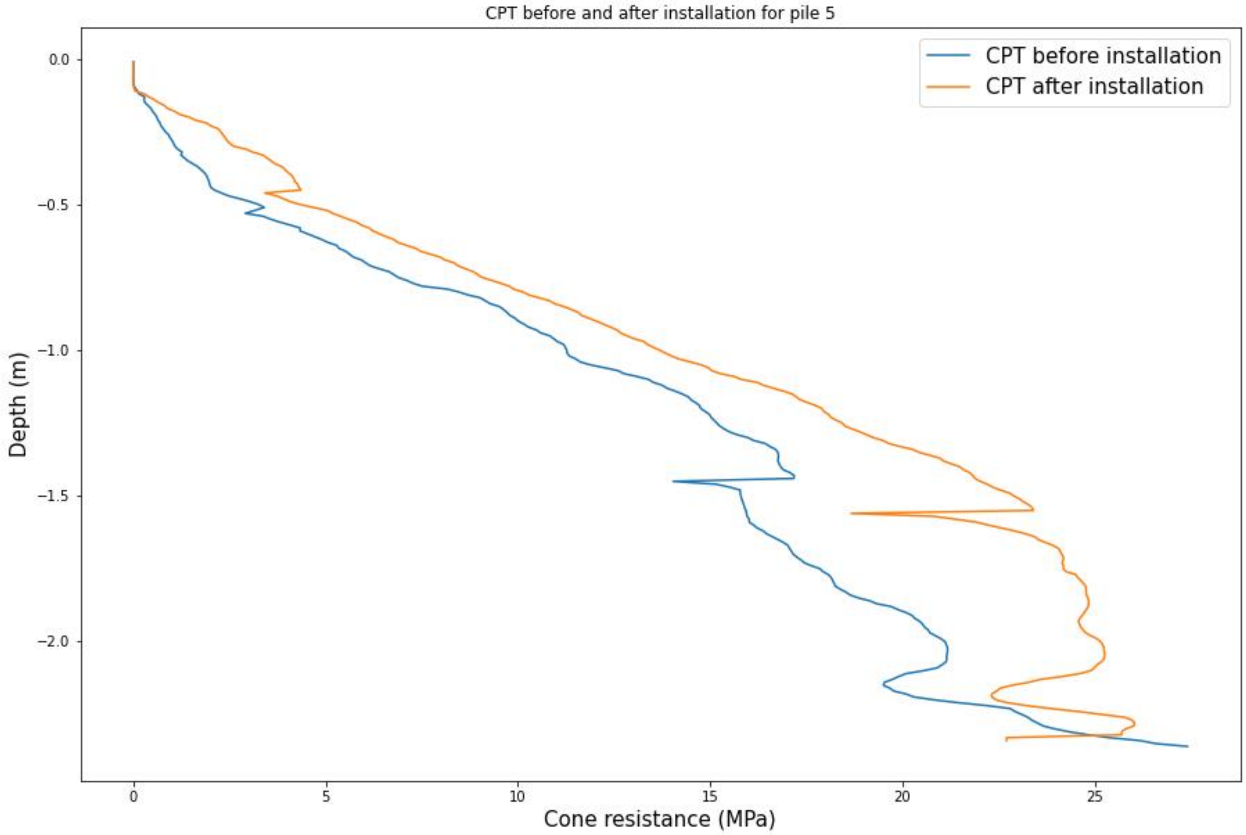
CPT before and after installation for pile 5
CPT before installation
CPT after installation
Depth (m)
0.0
−0.5
−1.0
−1.5
−2.0
0
5
10
15
20
25
Cone resistance (MPa)

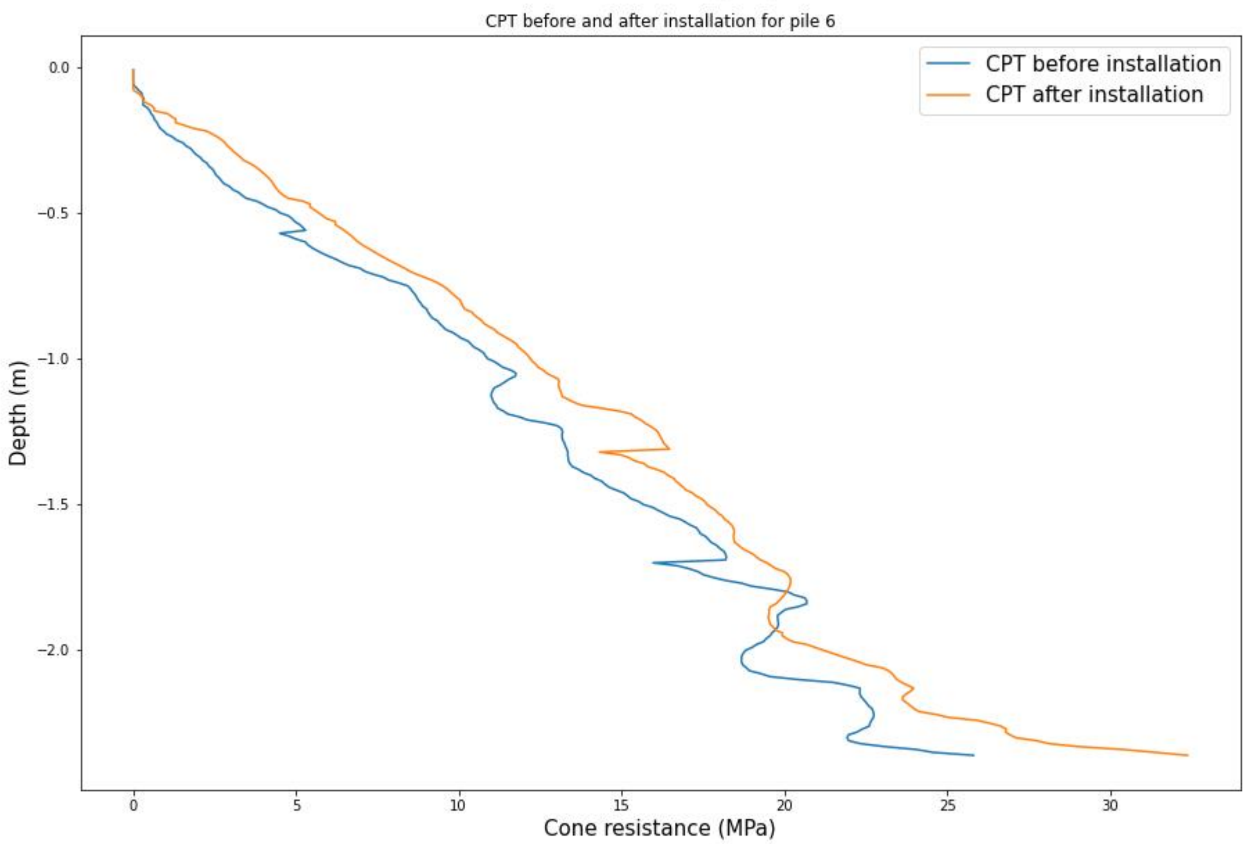
CPT before and after installation for pile 6
CPT before installation
CPT after installation
Depth (m)
0.0
−0.5
−1.0
−1.5
−2.0
0
5
10
15
20
25
30
Cone resistance (MPa)

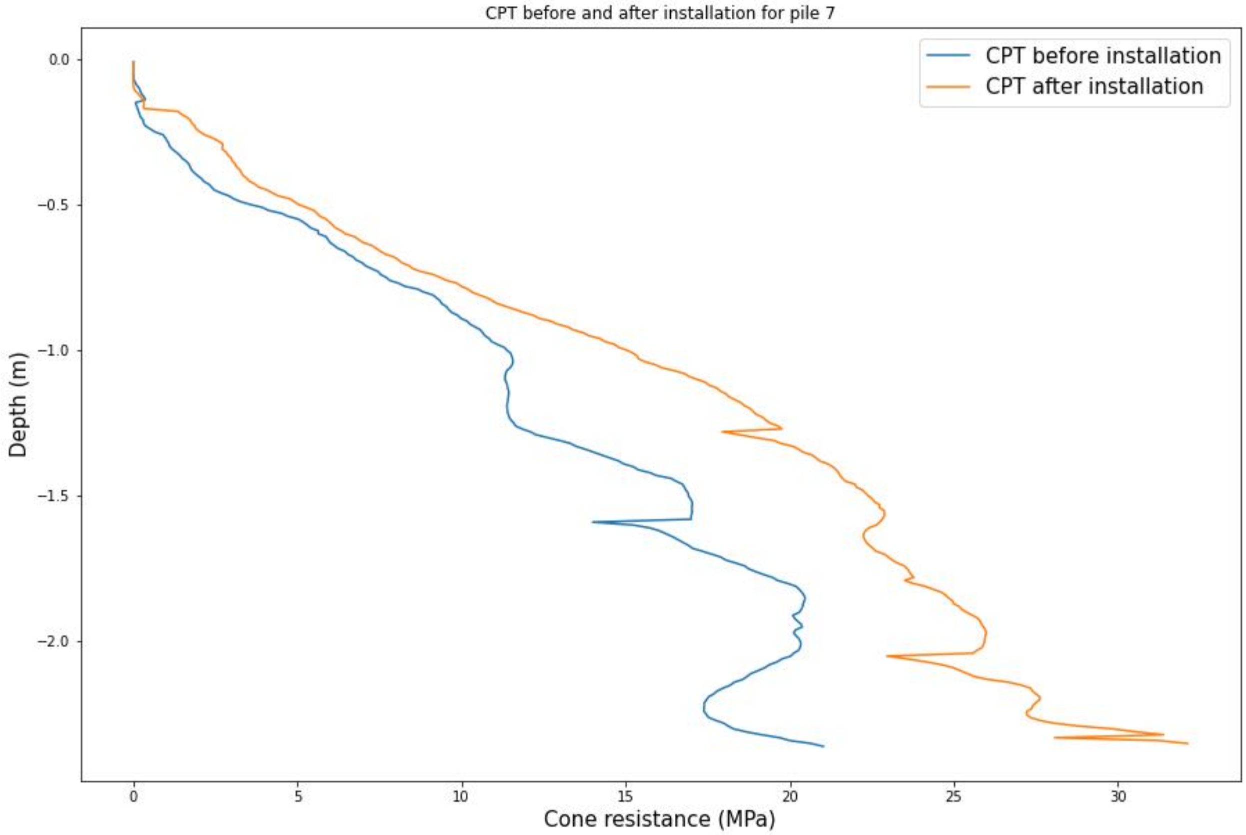

CPT before and after installation for pile 7
CPT before installation
CPT after installation
Depth (m)
Cone resistance (MPa)
0.0
−0.5
−1.0
−1.5
−2.0
0
5
10
15
20
25
30

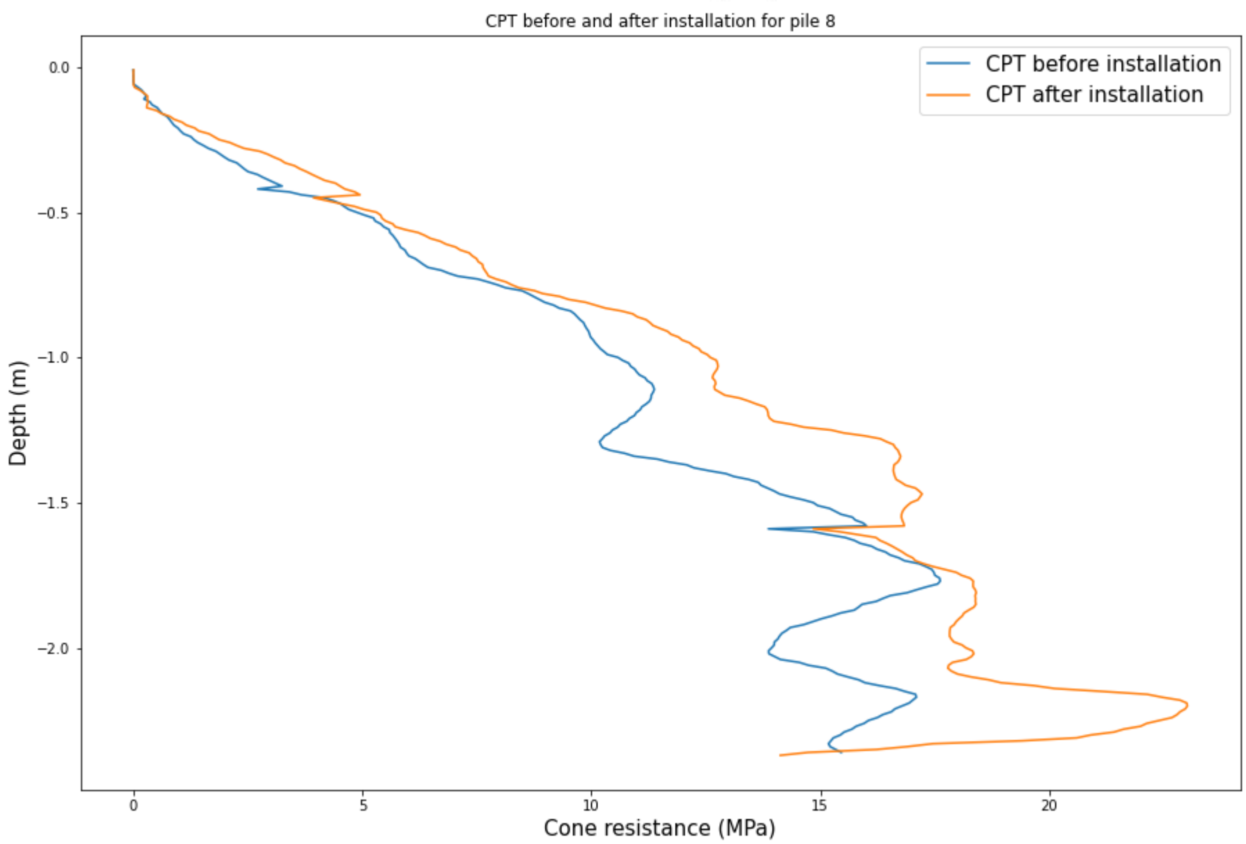

CPT before and after installation for pile 8
CPT before installation
CPT after installation
Depth (m)
Cone resistance (MPa)
0.0
−0.5
−1.0
−1.5
−2.0
0
5
10
15
20

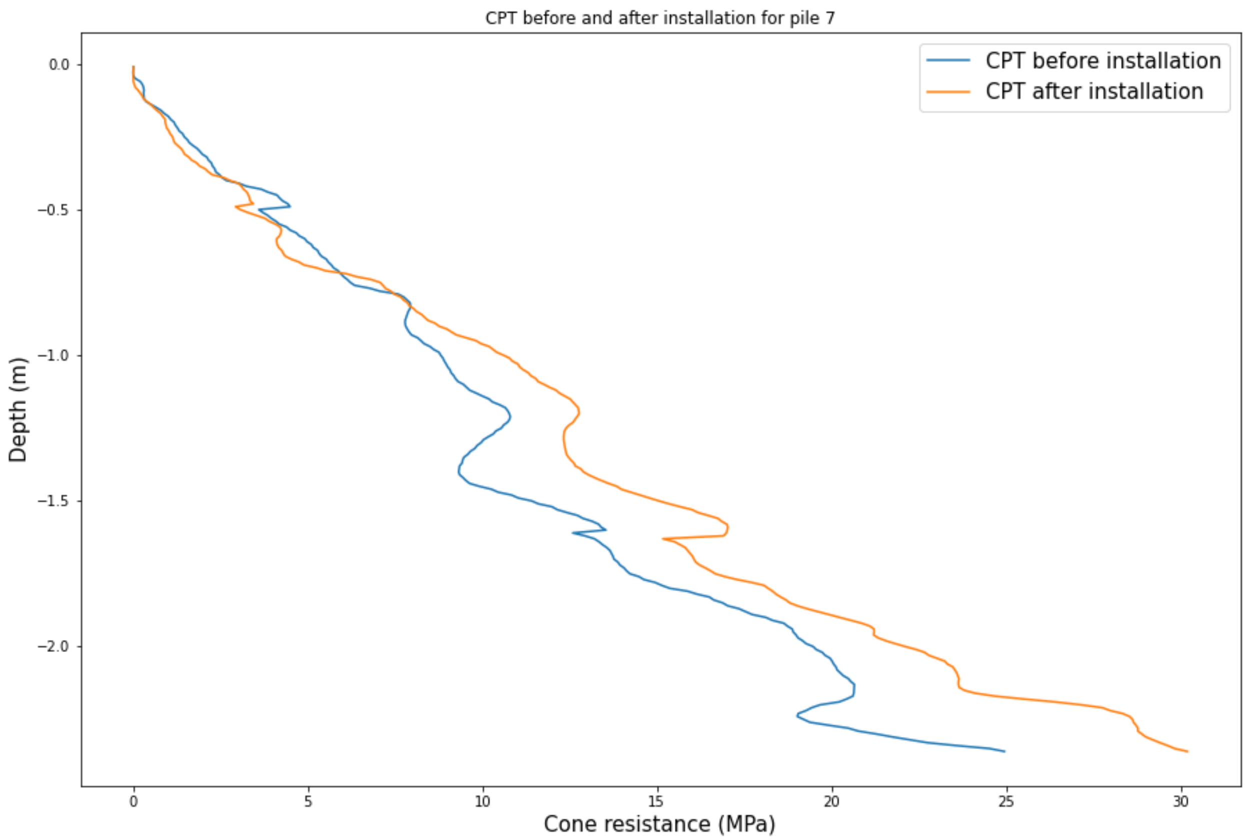

Batch 3: Before installation

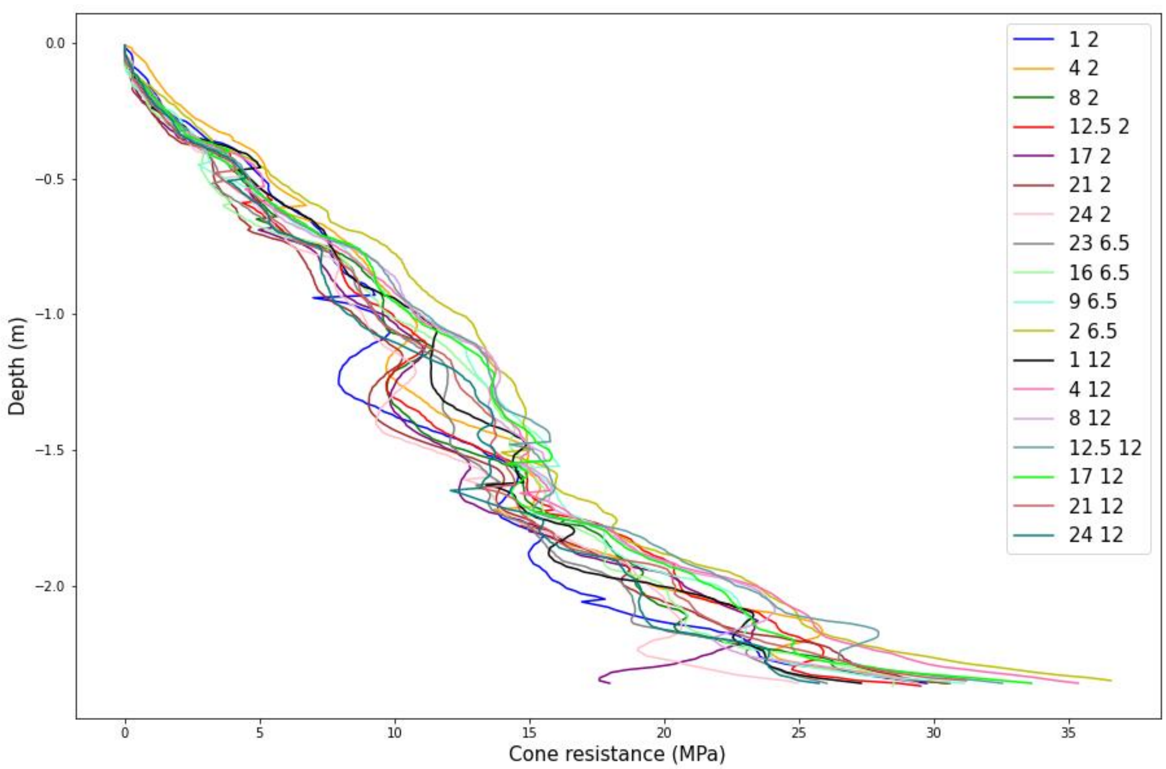

Batch 3: After installation

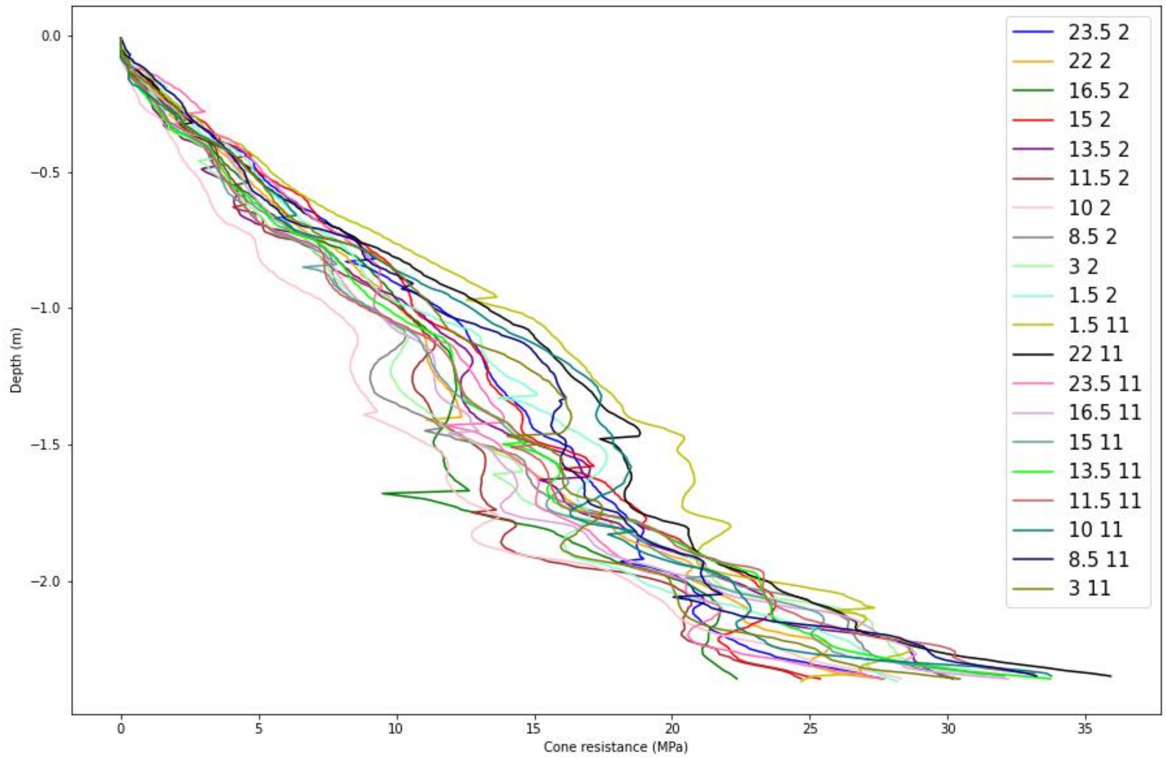

Batch 3: Comparison

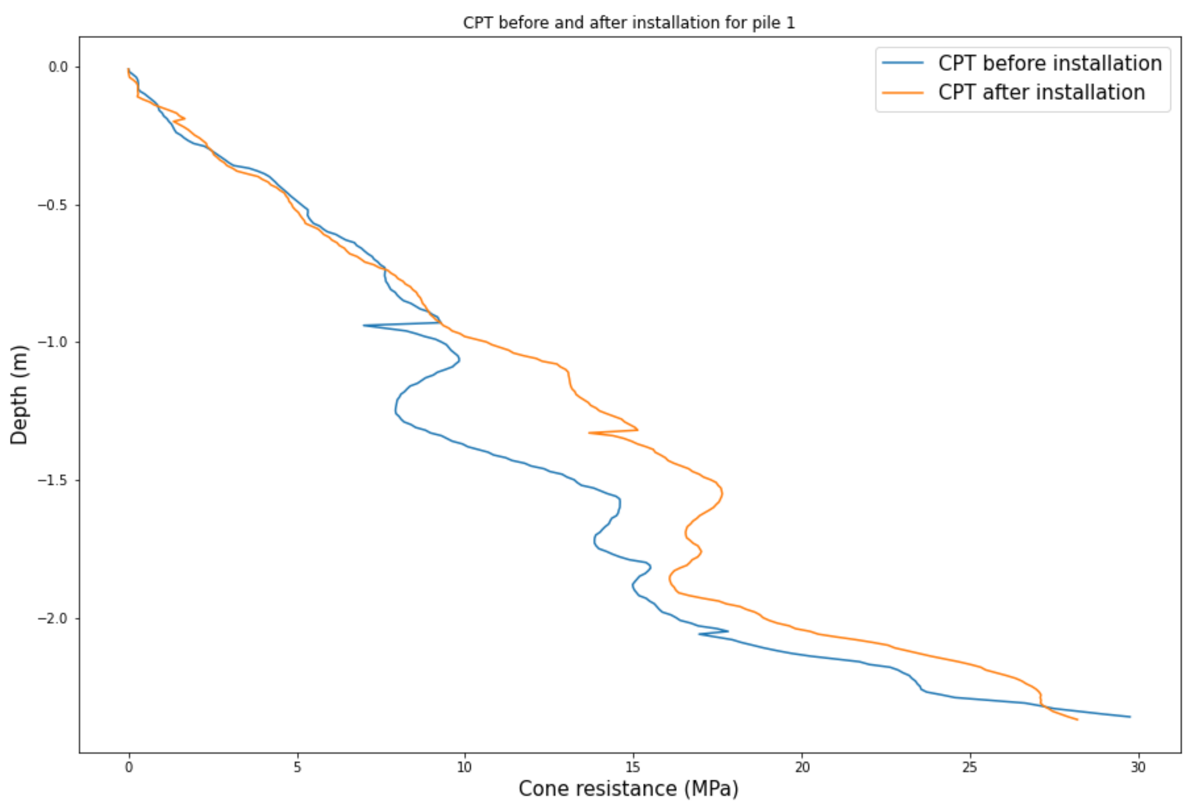

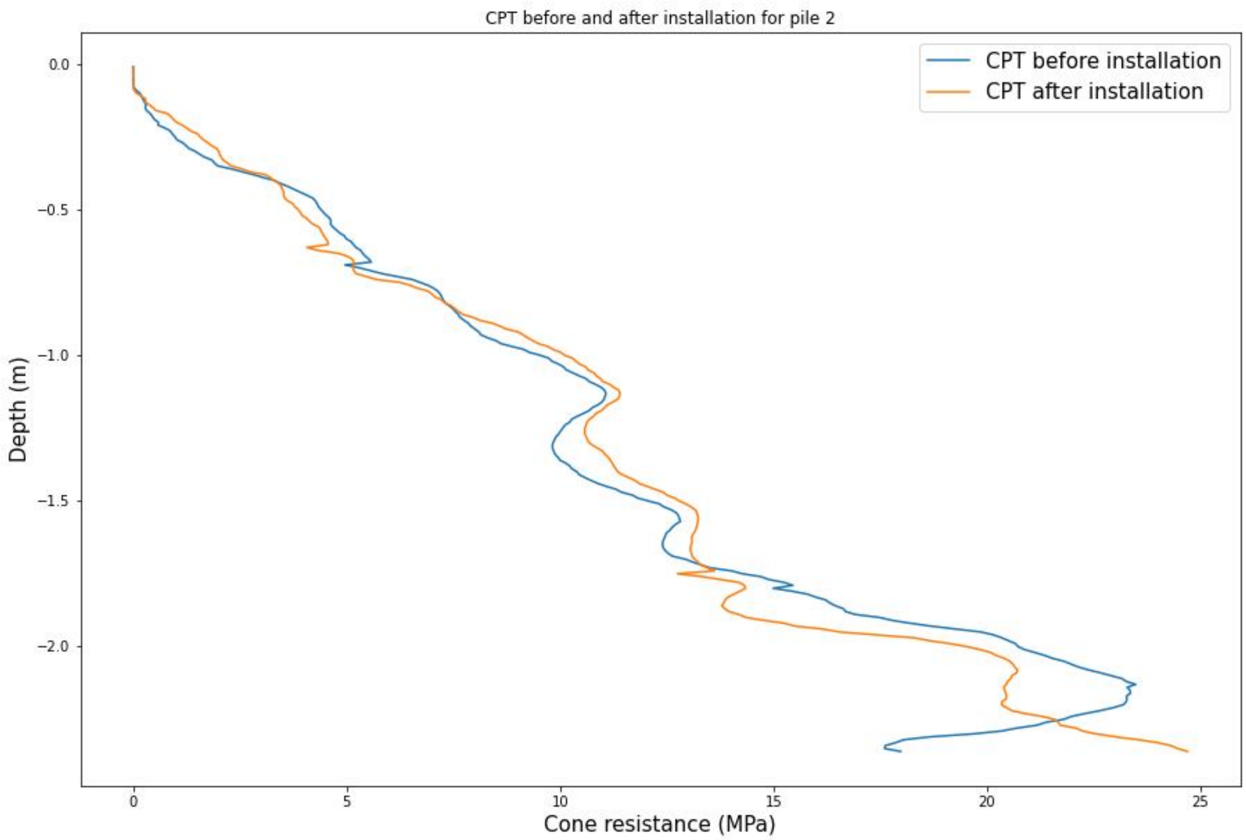

CPT before and after installation for pile 2
CPT before installation
CPT after installation
Depth (m)
Cone resistance (MPa)
0.0
−0.5
−1.0
−1.5
−2.0
0
5
10
15
20
25

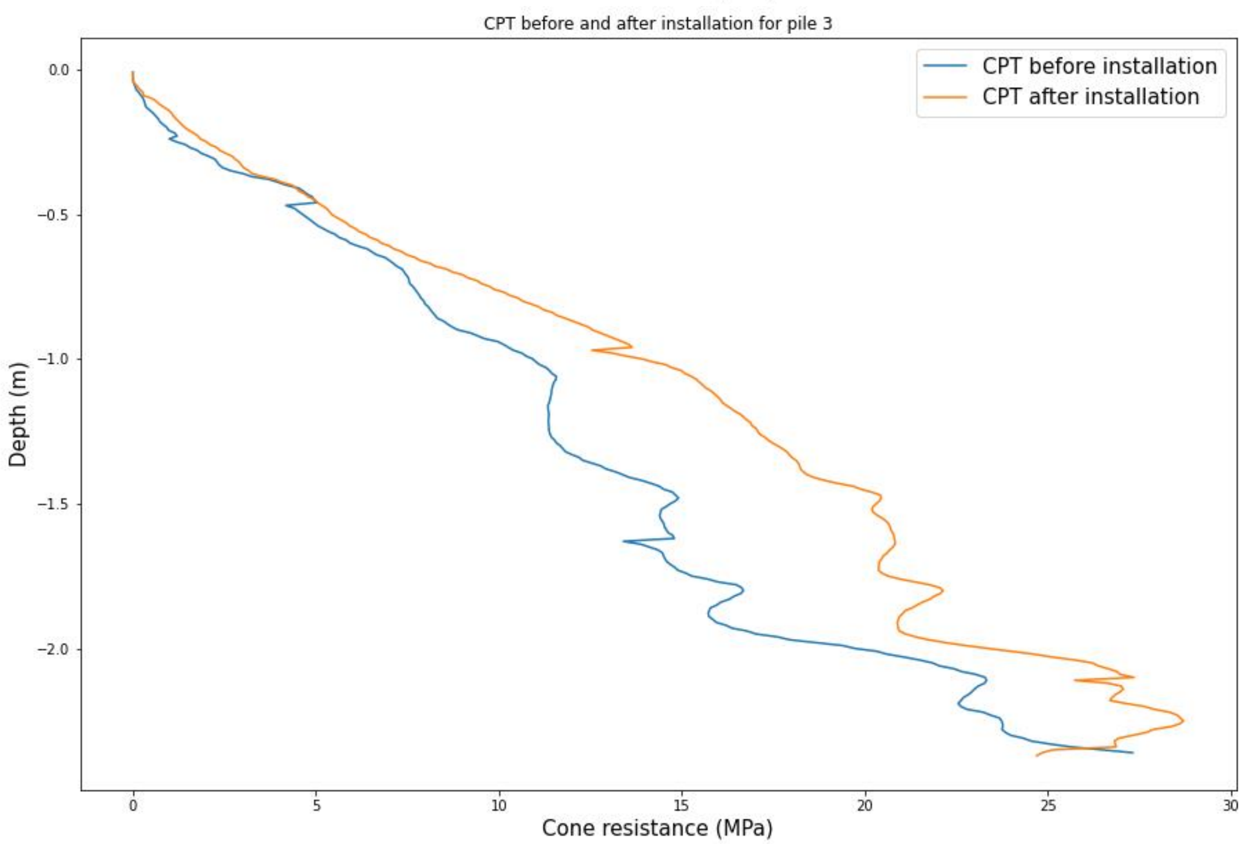

CPT before and after installation for pile 3
CPT before installation
CPT after installation
Depth (m)
Cone resistance (MPa)
0.0
−0.5
−1.0
−1.5
−2.0
0
5
10
15
20
25
30

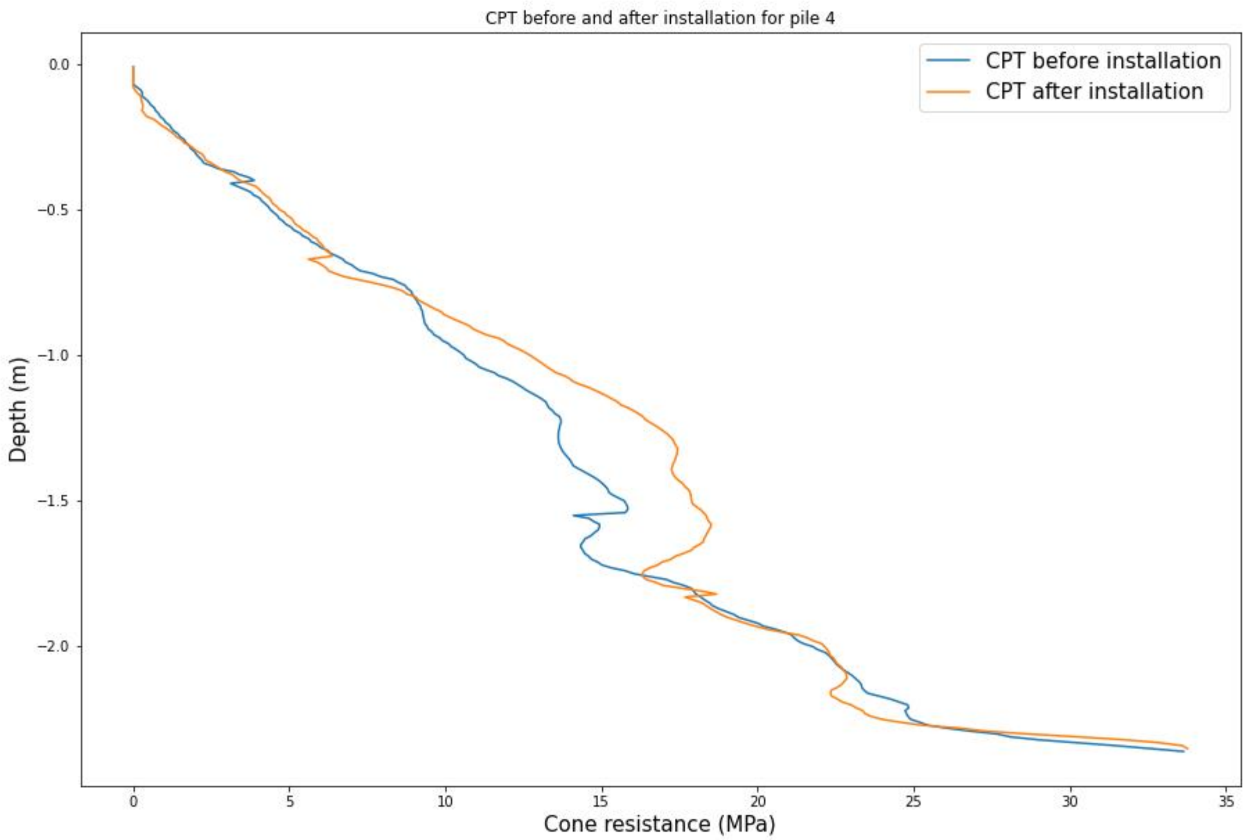
CPT before and after installation for pile 4
CPT before installation
CPT after installation
Depth (m)
0.0
−0.5
−1.0
−1.5
−2.0
0
5
10
15
20
25
30
35
Cone resistance (MPa)

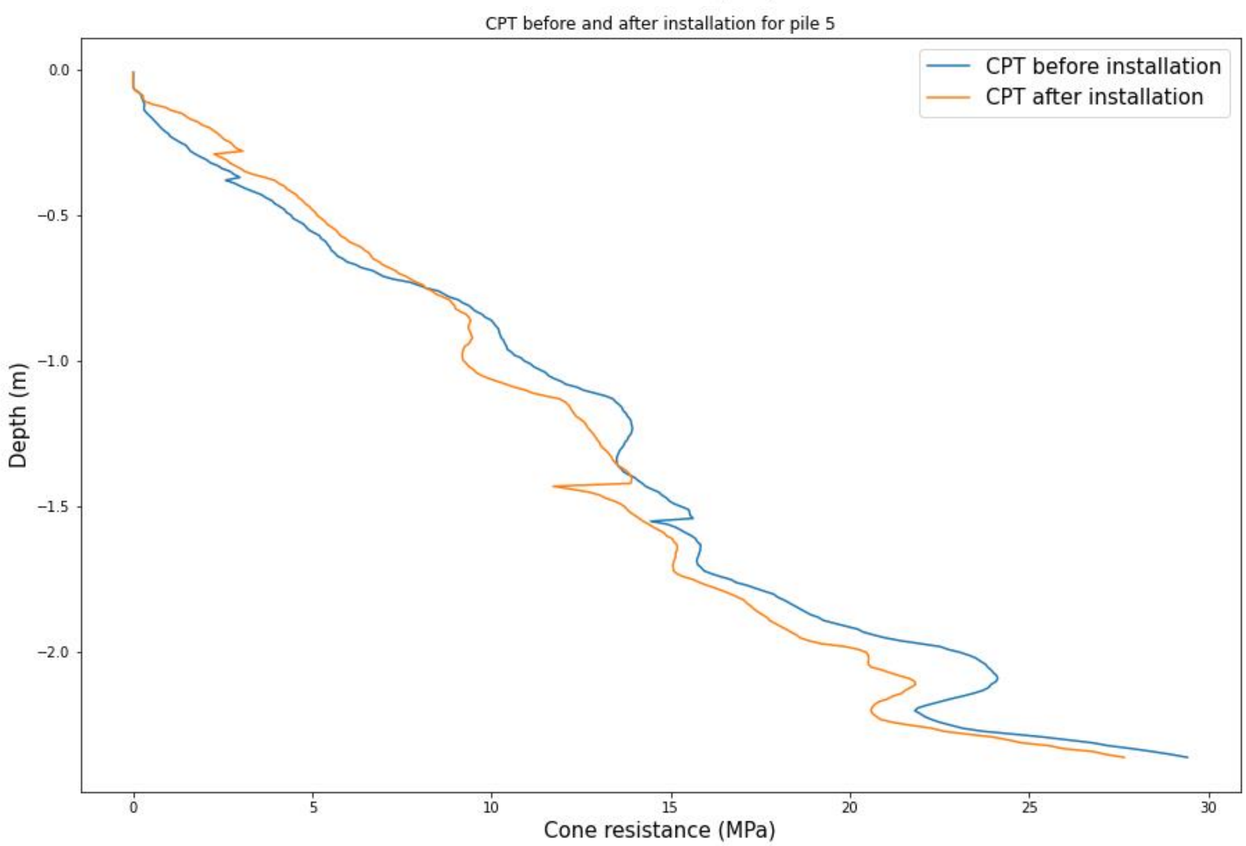
CPT before and after installation for pile 5
CPT before installation
CPT after installation
Depth (m)
0.0
−0.5
−1.0
−1.5
−2.0
0
5
10
15
20
25
30
Cone resistance (MPa)

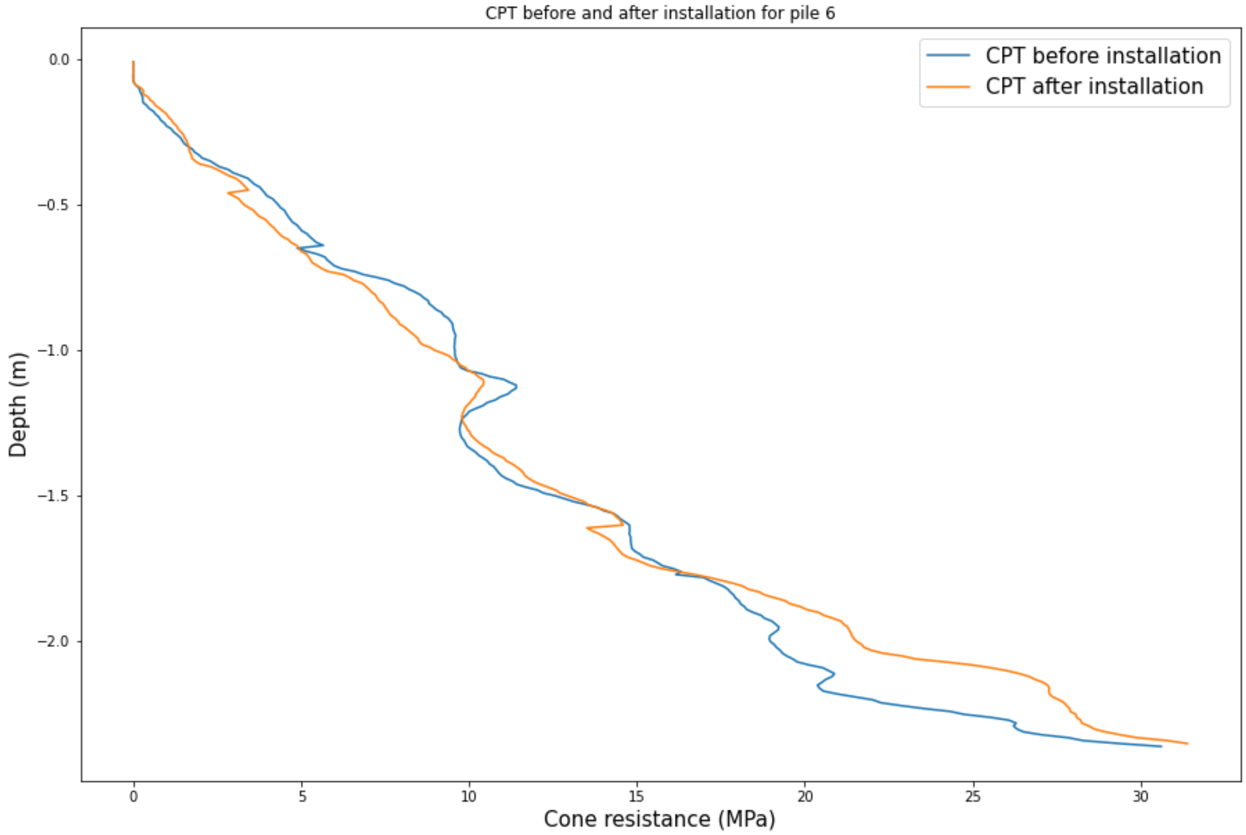
CPT before and after installation for pile 6
CPT before installation
CPT after installation
0.0
−0.5
−1.0
−1.5
−2.0
Depth (m)
0
5
10
15
20
25
30
Cone resistance (MPa)

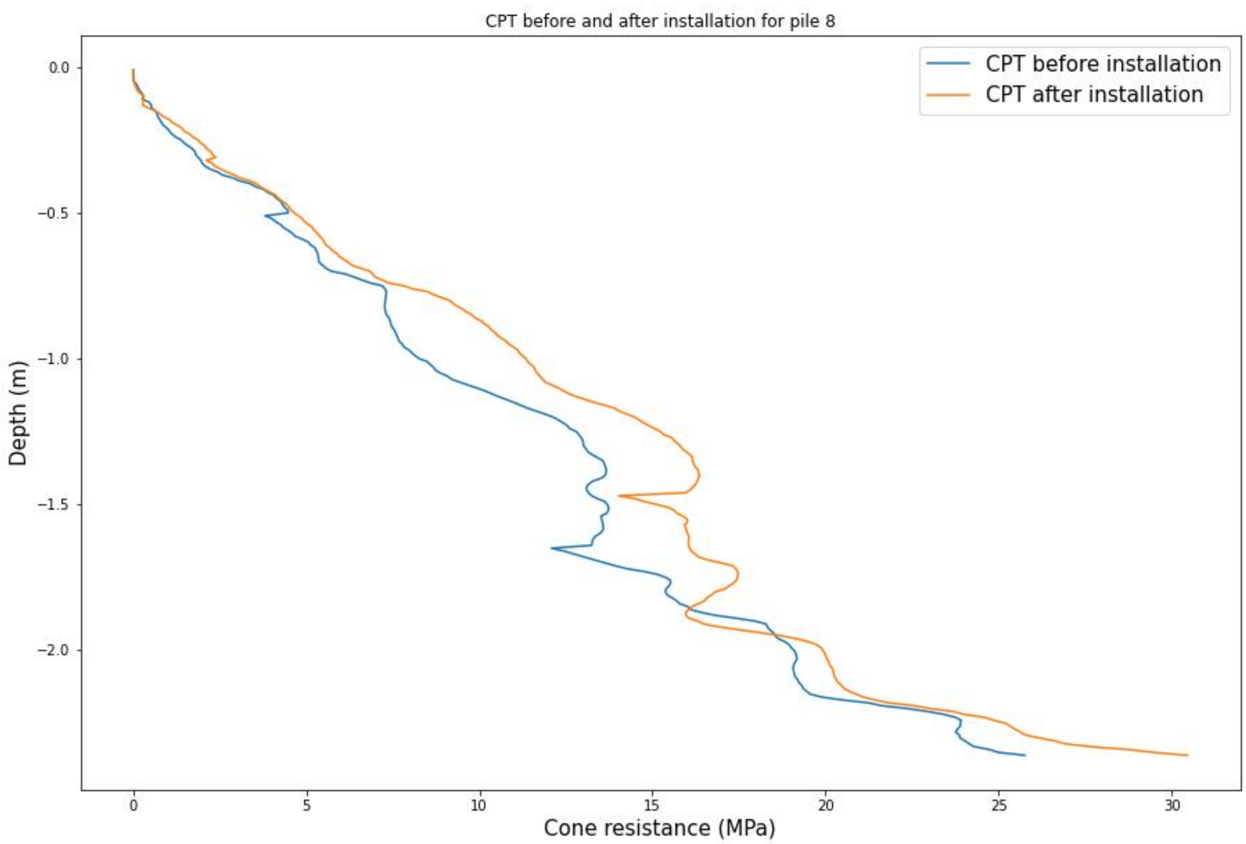
CPT before and after installation for pile 8
CPT before installation
CPT after installation
0.0
−0.5
−1.0
−1.5
−2.0
Depth (m)
0
5
10
15
20
25
30
Cone resistance (MPa)

Batch 4: Before installation

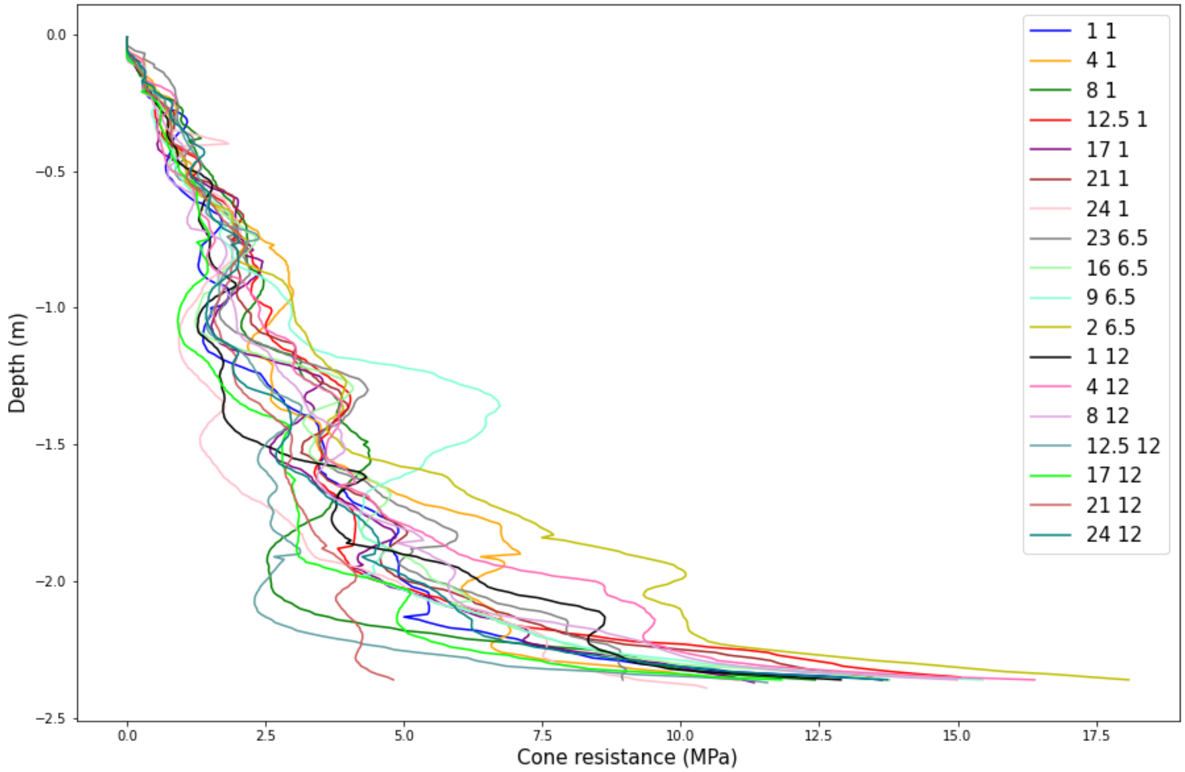

Batch 4: After installation

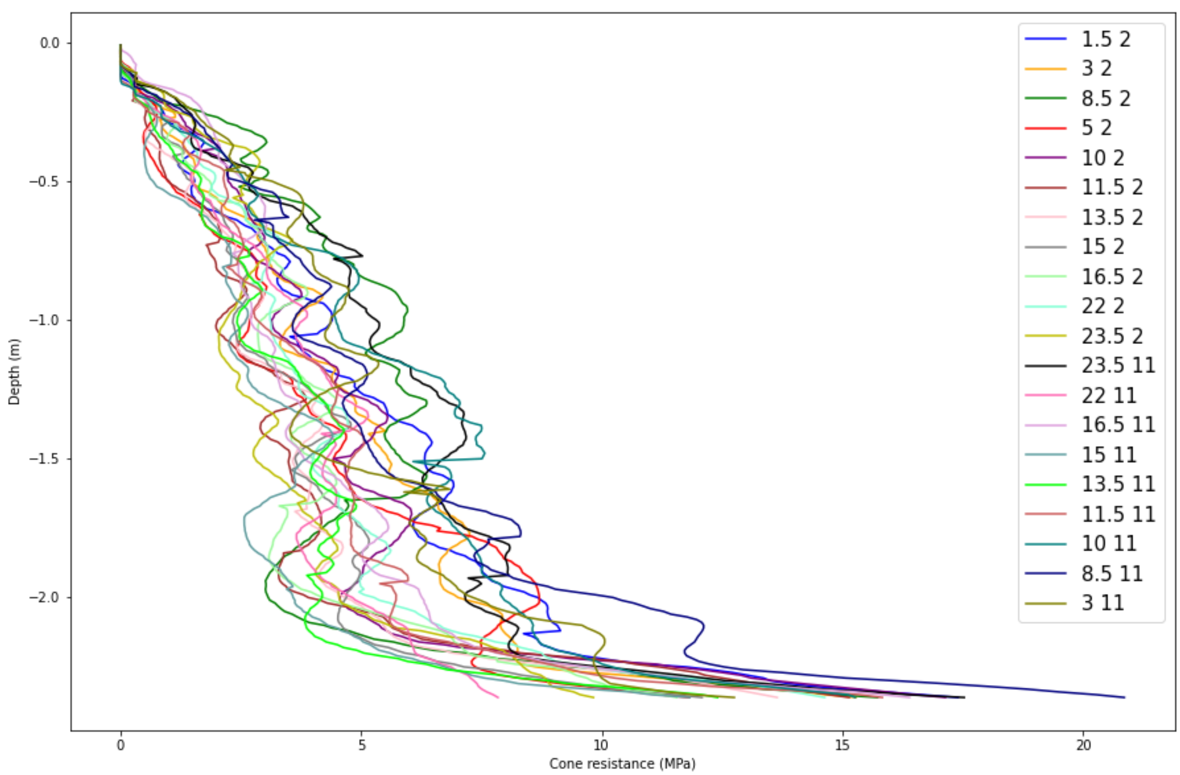

Batch 4: Comparison

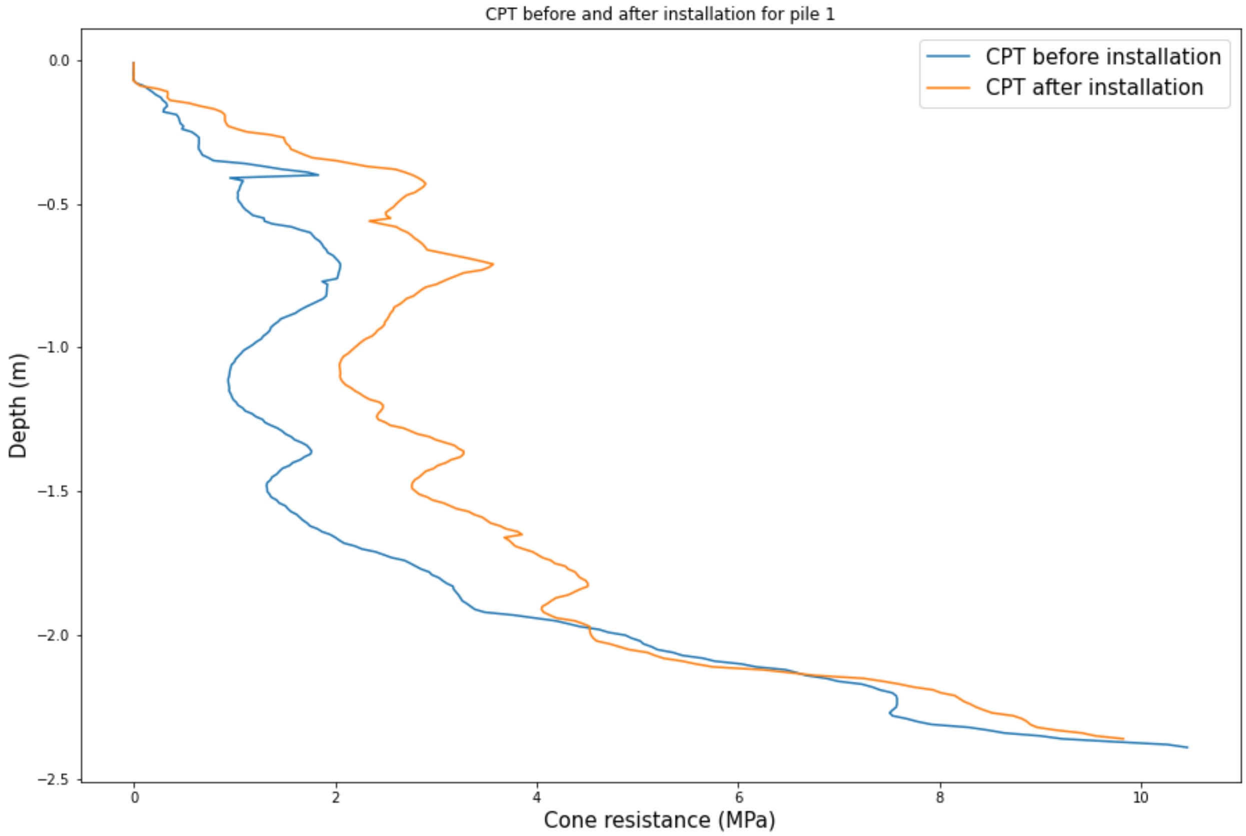

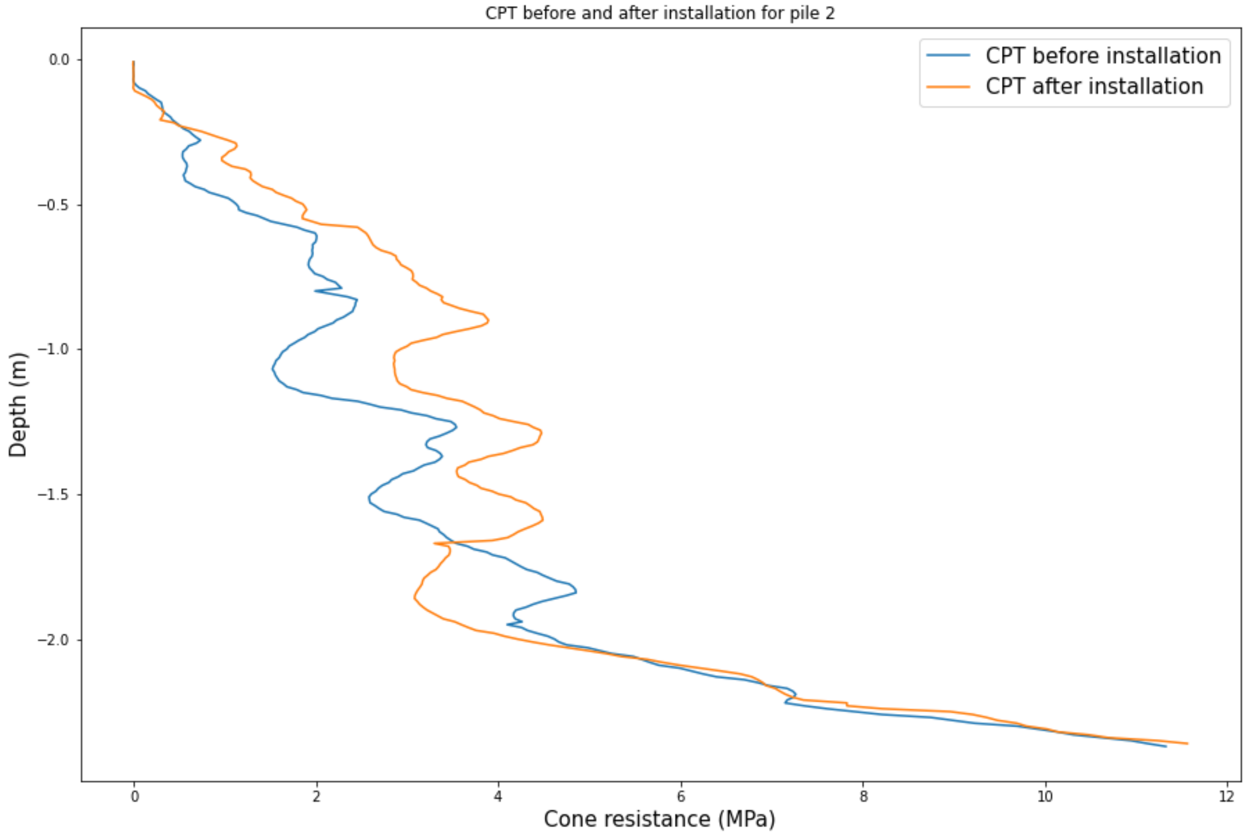
CPT before and after installation for pile 2
CPT before installation
CPT after installation
Depth (m)
0.0
−0.5
−1.0
−1.5
−2.0
0
2
4
6
8
10
12
Cone resistance (MPa)

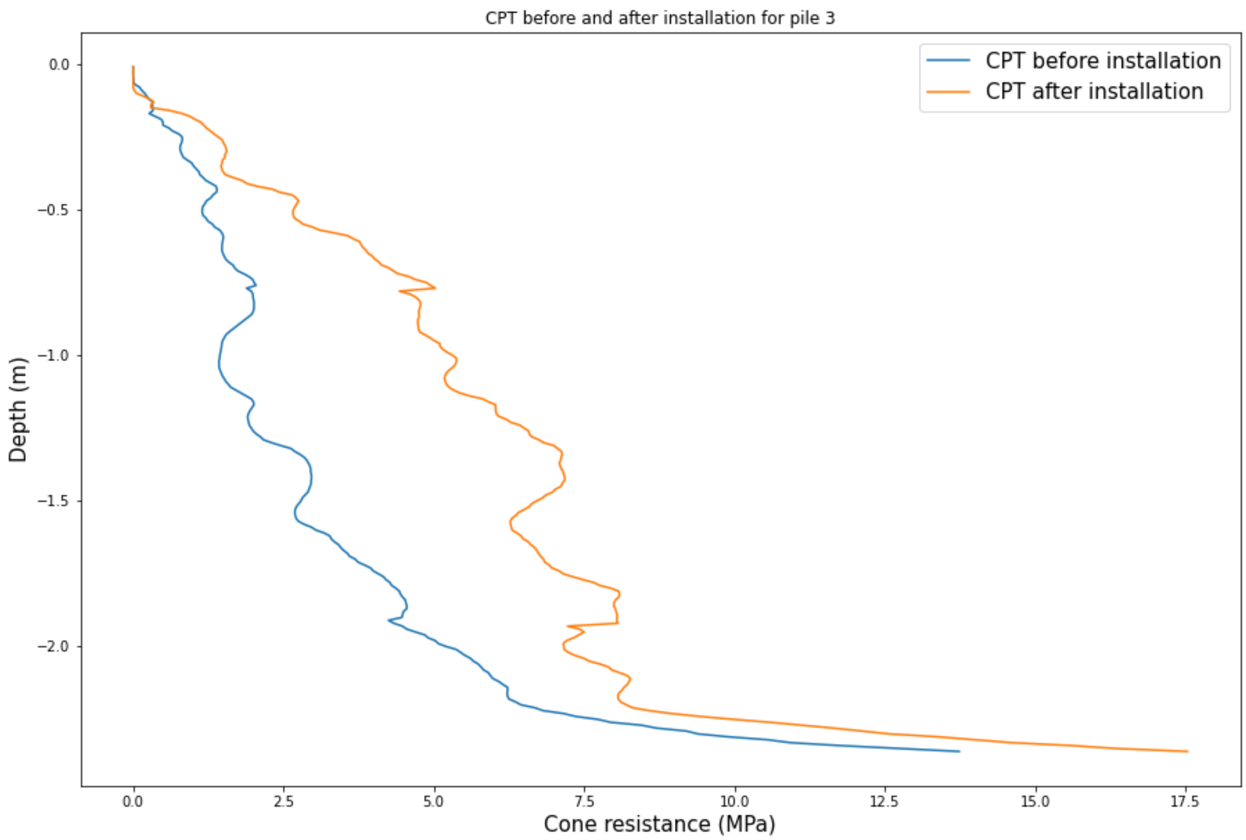
CPT before and after installation for pile 3
CPT before installation
CPT after installation
Depth (m)
Cone resistance (MPa)
0.0
−0.5
−1.0
−1.5
−2.0
0.0
2.5
5.0
7.5
10.0
12.5
15.0
17.5

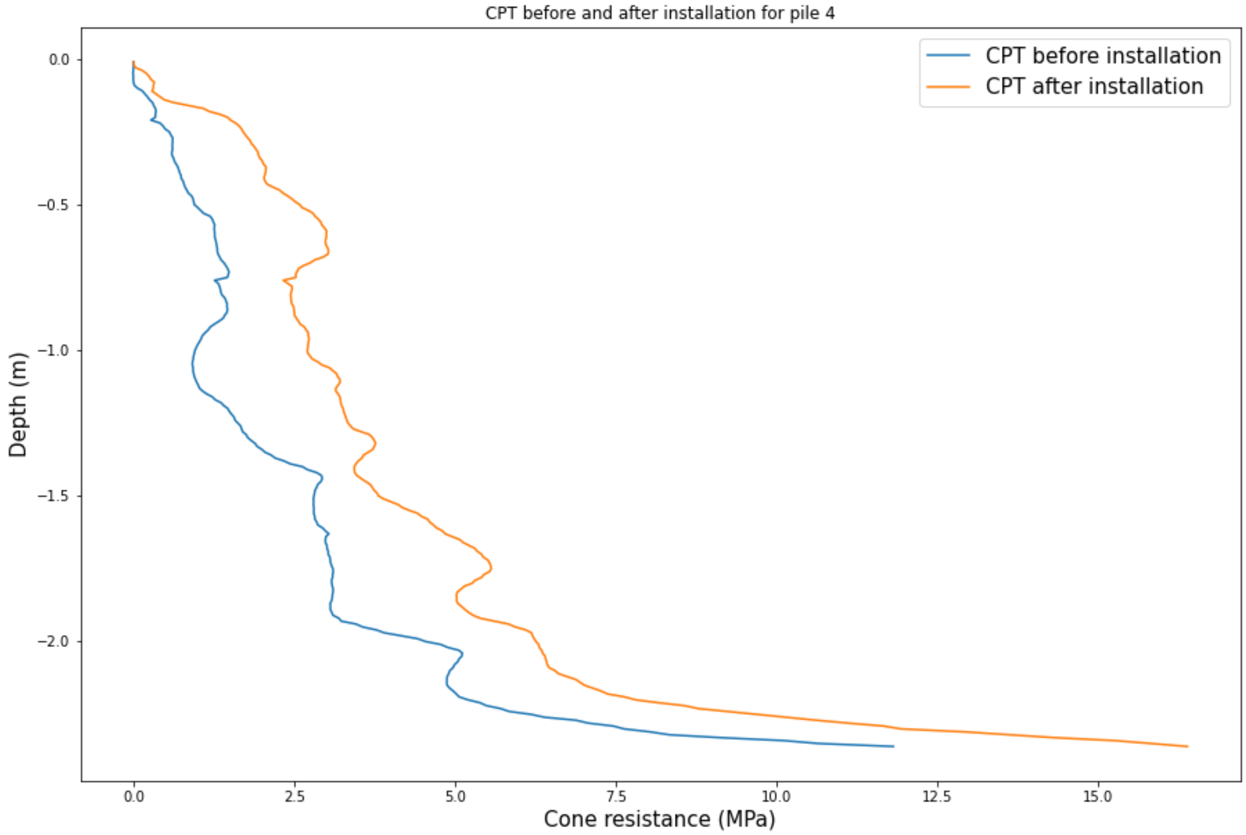
CPT before and after installation for pile 4
CPT before installation
CPT after installation
Depth (m)
0.0
−0.5
−1.0
−1.5
−2.0
0.0
2.5
5.0
7.5
10.0
12.5
15.0
Cone resistance (MPa)

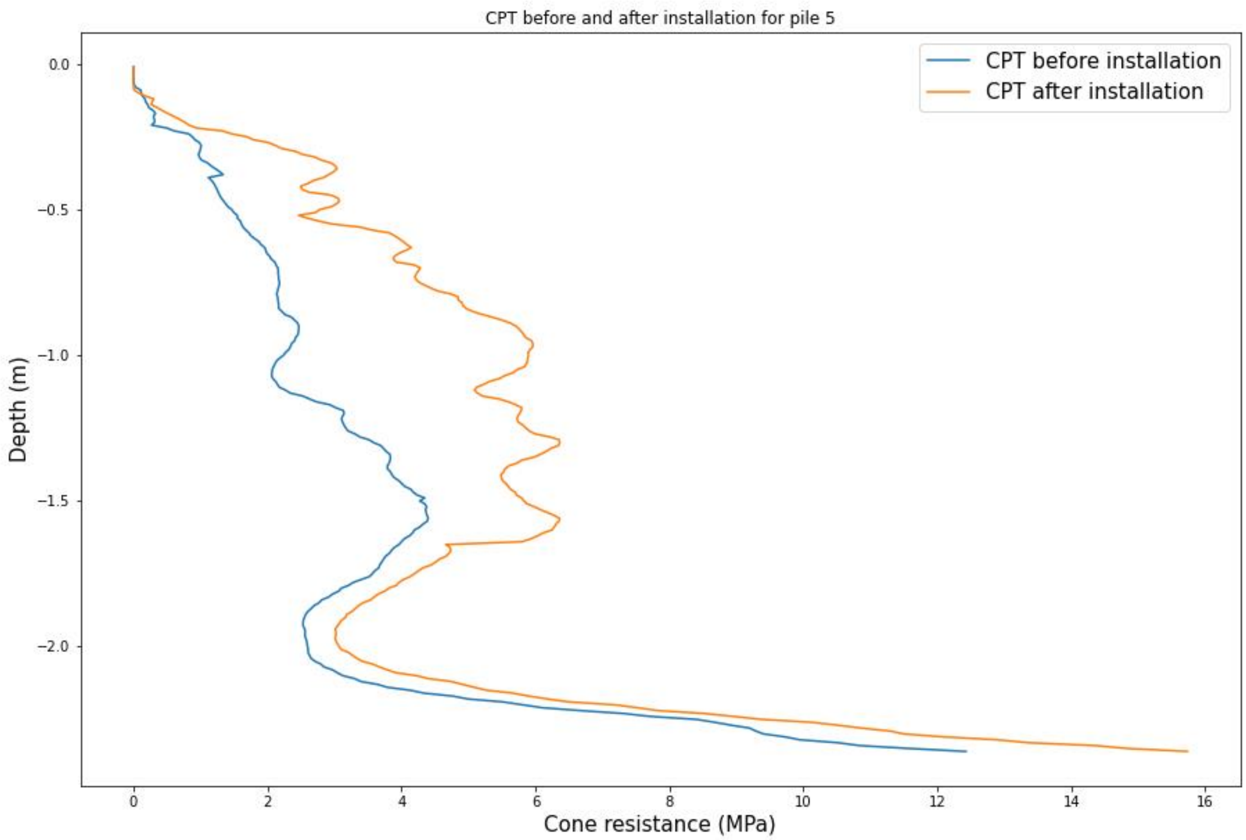
CPT before and after installation for pile 5
CPT before installation
CPT after installation
Depth (m)
0.0
−0.5
−1.0
−1.5
−2.0
Cone resistance (MPa)
0
2
4
6
8
10
12
14
16

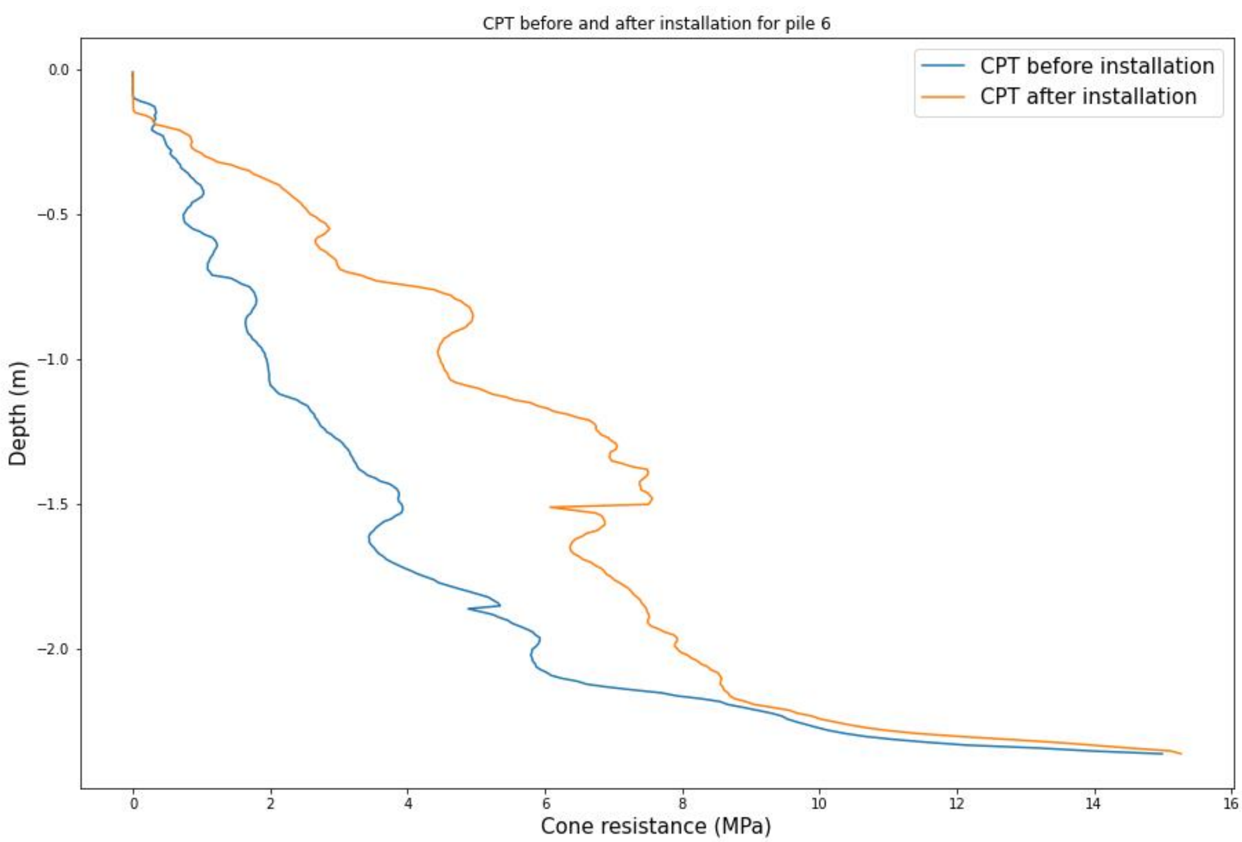
CPT before and after installation for pile 6
CPT before installation
CPT after installation
Depth (m)
0.0
−0.5
−1.0
−1.5
−2.0
Cone resistance (MPa)
0
2
4
6
8
10
12
14
16

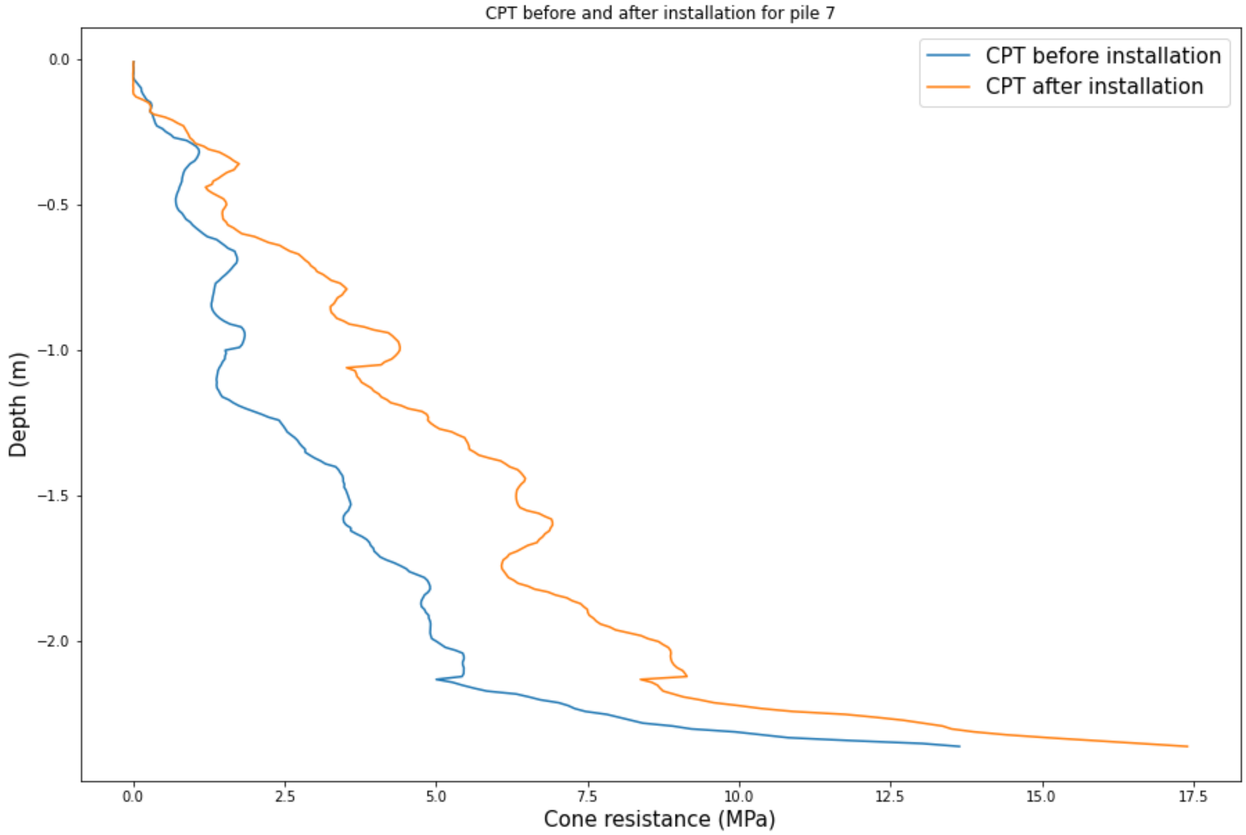
CPT before and after installation for pile 7
CPT before installation
CPT after installation
Depth (m)
Cone resistance (MPa)
0.0
−0.5
−1.0
−1.5
−2.0
0.0
2.5
5.0
7.5
10.0
12.5
15.0
17.5

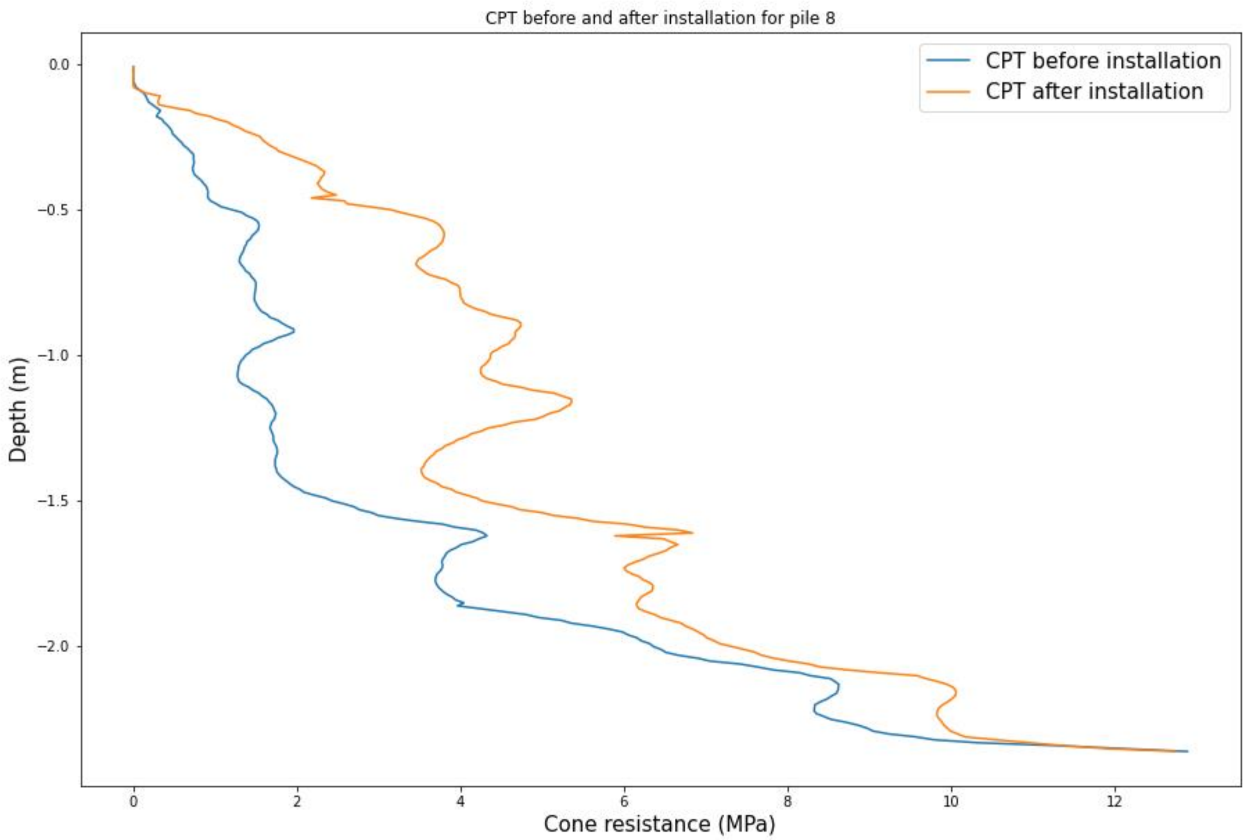

CPT before and after installation for pile 8
CPT before installation
CPT after installation
Depth (m)
Cone resistance (MPa)
0.0
−0.5
−1.0
−1.5
−2.0
0
2
4
6
8
10
12

Appendix E: Experiment logbook

Week	Date	Time	Batch	Description	Photos
23	15-Jun		1	Sensors installed	
24	20-Jun	14:00	1	Sand installation	783, 784
24	21-Jun	10:00	1	Vibrating with needles	781
24	22-Jun	10:30	1	Vibrating with needles	786 -> 791
24	22-Jun	12:00	1	Camera turned on	
24	23-Jun	9:30	1	Flume full	792
24	24-Jun	10:00	1	Equalizing, right side was 5cm higher than left side	793
24	24-Jun	15:00	1	Flat sand and marked piles with measuring equipment	794 -> 798
25	29-Jun	12:00	1	CPTs 1-12, no piles	799 -> 805
25	30-Jun	10:00	1	heigh measurments	
25	01-Jul	15:30	1	SIMOX steering committee lab visit	806
26	03-Jul	14:30	1	Plate, pile with sensors and vibro test drive	807 -> 810
26	05-Jul	10:00	1	Dragline sheets arrived	811
26	05-Jul	15:00	1	CPTS 13-24, test drive #1 of pile	812 -> 816
26	06-Jul	13:00	1	test drive #2 with guiding frame, filming + test drive #3,4,5	817

26	07-Jul	15:00		1	Set up frame for vibro test frequncy. Improved pressure on powerpack -> 36 Hz. Test drive #6,7		
26	08-Jul	10:30		1	Painting first piles		818
26	08-Jul	12:00		1	Rupture in power pack, mechanic repaired it by 14:00		
26	08-Jul	15:00		1	Full guiding frame + laser test		819
27	11-Jul	9:00		1	Start of batch 1 tests (x = 2, y = 2)	820 -> 830	
27	11-Jul	12:00		1	Second row (x=9), plug	831 -> 840	
27	11-Jul	16:00		1	Mounting of load frame	841, 842, 843	
27	12-Jul	9:00		1	Third row (x = 16)	844 -> 859	
27	12-Jul	13:00		1	Strain gauge broke		860
27	13-Jul	9:00		1	Last 2 pile positions	861 -> 869	
27	14-Jul	11:00		1	CPTs after installation		
27	14-Jul	16:00		1	Loading device test	870 -> 879	
27	15-Jul	11:00		1	Loading started	880 -> 884	
28	18-Jul	15:00		1	Loading instrumented pile. Cyclic 2-4 kN then up to 18.5 kN		
28	20-Jul	12:00		1	Piles removed. Tank emptied of water		
28	21-Jul			1	Manual measurement water level in tube 1.54 m. Pump stopped, measurements taken		
29	25-Jul			1	manual measurement water level in tuve 1.46 m. All pw sensors indicate -1.25 units (approx. 0 Volts)		

Week	Date	Time	Batch	Description	Photos
34	22-08		2	With coarse empty tank fill ~2m or so. Check sensors water pressure within 20 offset in all readings & witnessed effect of air in filters. Put filters in vacuum → [illegible]	895 → 898
34	22-08		2	Sensors on piles — Filters now put on under water to prevent air in filter	899 - 900
34	22-08		2	Refilling of tank	901 - 902
34	23-08		2	Total stress sensor West broke. → Decided not to replace and continue. Total stress sensor East replaced, works ok.	
34	23-08		2	During compaction of second layer (~m depth) noticed that third needle from south side was shifted. Marcel replaced needle to symmetrical position.	
34	24-08		2	Filling of tank and close up of needles	903 - 909
34	24-08		2	The vibro needle most south failed during compacting final or one extra run with compaction while second needle from south shifted to position 1.	
34	25-08		2	Building of [illegible] for [illegible]. This day used as 1 day consolidation.	910 - 911
34	26-08		2	CPT before installation (1-18) Height measurements	912, 913, 914, 915, 920
35	29-08		2	Prepare final things: pile numbering, etc.	937, 938
35	30-08		2	Start of pile driving, 3 impact piles	939 - 971
35	30-08		2	Pile 2: forgot geophone [illegible]	
35	31-08		2	Vibro piles, [illegible] frequency sensor not recording	972 - 987
35	01-09		2	CPT after driving	
35	01-09		2	Incident with Arco. [illegible] Stopped for the day	
35	02-09		2	CPTs (improved safety) + Height measurement, start loading pile 2.	
35	02-09		2	Fokus crack/hing pile 2. Detail [illegible]	
35	02-09		2	First 2 piles lateral loaded	
36	05-09		2	Continue lateral loading (3 piles)	
36	06-09		2	Continue lateral loading (3 piles) "Last piles" accidentally loaded Towards the wall	
				while adjusting position of spindle (~2kN).	
36	06-09		2	Extracting all piles by static pull. See notes in paperback [illegible].	Video recordings photos Anderson
36	07-09		2	Excavator emptying tank	
36	07-09		2	Compacting first layer: one vibro needle broke. Continue with 5 instead of 6 needles.	
36	08-09		2	Continuing filling the tank by excavator	some pictures
37	12-09		2	Started CPTs on y-row 2 instead of 1. Decided to finish on row 2, then continue as planned.	Two pictures
37	12-09		2	Kees (TUD) Rigging acc on vibro + install [illegible] on impact pile. Preparing dragline [illegible].	
37	13-09		3	2 Impact piles + 1 vibro. Pile 2U got stuck on the frame for a second during driving.	
37	14-09		3	Continue with vibro pile 3U: doubts about freq recording, Marcel used constant low freq of 20-23 Hz. TUD laptop shows differently —?	

Week	Date	Time	Batch	Description	Photos
37	15-09		B3	Perform CPTs after all pile installation. Height measurement on pile 2v only & started lateral load on this pile.	
37	16-09		B3	Height measurements. Lat loading pile 6v. Podcast & Demo day.	
37	16-9		B3	Lat test on pile 7. Put wire measurement on the wagon using aluminium frame.	
38	19-9		B3	Continue lateral loading.	
38	20-9		B3	Continue lateral loading. Pile 5v with a stiffer steel frame for wire measurement on wagon.	→ photo
38	20-09		B3	Pile 4v 1000 cycl was "jumped" (strong) a little bit at the end by activation of the clamp.	
38	21-09		B3	Pile 8V 1000 cycles CPTs after loading (nr. 45-56)	
38	22-09		B3	Falling Load tests ~~[illegible]~~ Measure exact pile position. Measure height water.	Photos
38	22-09		B3	Pile extraction with laser see separate comments in log book Mark	Videos Photos
38	23-09		B3	Tank excavation. Steelrings extracted by Marcel.	
39	26-09		B4	Tank fill. Stekerdoos bij proef sand nu nieuwe stekerdoos aangesloten. Gebr. net in data RK tender.	Video Photos
39	27-09		B4	No work	
39	28-09		B4	No work.	
39	29-09		B4	CPTs before installation. Height measurements. Height #7 had a local bump	
39	30-09		B4	Start impact driving. Note: updated settings for CPD west (?-5150). So [illegible] for falling but we used 1258 (need to adjust manually)	
39	30-09		B4	Kees came over to double check sensors. Total stress sensors B1_AL_020 and B2_A0_006 are working.	
39			B4	Order of work: install. Pile 7i. CPTs 18-12 and 15-12. Pile 6i	
39	30-09		B4	with Pile 6i also TUD laptop on, to measure geophone ID test 42.	
40	03-10		B4	Install vibropiles. Issue with TUD laptop, had to restart, as result ID 42 & 43 where used again. See notes Mark	
40	04-10		B4	CPTs after all installations (nr. 24-43) + height measurements.	
40	05-10		B4	Start lateral loading with pile 3i. Problem with lat. load device → see notes Mark.	
40	05-10		B4	Loaded Pile 4v with 0.4 mm/s instead of 0.2 mm/s.	
40	05-10		B4	Estimate of amount of sand that is not ~~[illegible]~~ put into medium dense bak (compared to dense) 3 m³	Photo of tank with re[illegible]
40	06-10		B4	Continue lateral loading. Using 0.4 mm/s instead of 0.2 mm/s for slow loading monotonic	Video phone Mark of lat loading pile 8
40	07-10		B4	Continue lateral loading	
41	10-10		B4	Continue lateral loading. End	
41	11-10		B4	CPT's "before" piles extraction. Steelrings to be done. 8 piles left in soil	
41	12-10		B4	No work on Silvex. But crane on top of sand for Gasunie project. Waterlevel lowered.	See photo.
41	13-10		B4	Steelringen. Extracted at pile 3i ring from -13 (Bakje B4S) then stopped, still to wet. Try again after holiday Marcel.	Photos phone Mark.